Development of a Solid-Phase Protein Labelling Method for The Synthesis of Peptide-Drug Conjugates

By
Manal Alanazi

A thesis submitted to the University of Birmingham for the degree of

DOCTOR OF PHILOSOPHY

College of Physical Sciences & Engineering

School of Chemistry

University of Birmingham

May 2020

UNIVERSITY OF
BIRMINGHAM

University of Birmingham Research Archive

e-theses repository

Acknowledgement

A great many thanks to my supervisor, Dr. Sam Butterworth for his continued and invaluable support, guidance, advice and inspiration during this project. I would like to say much thanks to you for invaluable discussions of my research and the exchange of valuable knowledge to me, I am very proud on everything I learned from you on my way to become a PhD.

I would like to thank all my supervisors, Dr. Francisco Fernandez-Trillo, Dr. Marie-Christine Jones and Dr. Anna Peacock for their invaluable support, discussions and advice with this project. I would like to thank my colleagues for their wonderful collaboration. I would like to thank the technical and support staff at the University of Birmingham chemistry school.

I would like to thank my parents (Muslih and Sabah Alanazi), my siblings and all my friends for the constant support and sympathy throughout my studies. A great many thanks to my husband (Hamdan Alanazi) for loving me and standing by my side; I love you.

I dedicate this thesis to my sweet daughters Netal and Alin and my new baby son Hattan, who have made me stronger and better than I could have ever imagined. I love you from the bottom of my heart.

Author's Declaration

This thesis has been written by Manal Alanazi and I declare I have performed all experiments.

This thesis has not been submitted for any other degree at the University of Birmingham or any other institution.

Abstract

Protein-drug conjugates are emerging as a powerful tool for the targeting of specific cell populations, as demonstrated by the emergence of approved antibody-drug conjugates. In common with the broader field of protein modification, the selective synthesis of these agents represents a significant chemical challenge, as the conjugation reaction must modify the targeted residue in the presence of other competing unprotected amino acid side chains. While the alkylation of cysteine thiols remains the most commonly utilized method for the selective modification of proteins, there remain significant issues with this approach in terms of controlling cysteine oxidation, separation of any unreacted protein, and reagent compatibility.

In order to address these issues, we have developed a novel system containing a thiol reactive group (iodoacetamide) attached to the standard solid support (agarose) via a linker that can be readily cleaved under mild conditions. Following initial studies an allyl carbamate linker was selected due to its general stability and relatively straightforward deprotection with optimised catalytic Pd systems. Based on this we have developed a synthesis of the completed catch-release linker system in 7 steps and demonstrated that this linker can be immobilised on agarose and cleaved on the solid phase.

This system was then combined with a second solid phase reducing agent to allow the direct reduction and alkylation/trapping of a standard protein (BSA). The protein was successfully alkylated and separated from the unreacted protein by simple filtration. Unfortunately, the release of alkylated BSA from the solid support by using catalytic Pd did not proceed as expected from the model system and this step is currently under investigation.

Table of Contents

List of Figures

List of Tables

Abbreviations

ADC	- antibody drug conjugates
alloHSCT	-allogeneic hematopoietic stem cell transplantation
AML	-acute myeloid leukemia
AP-2	-adaptin 2
Arg	- arginine
Asn	- asparagine
Asp	- aspartate
ASXL1	- additional sex combs like 1, transcriptional regulator
BCA	- bicinchoninic acid assay
BoC	- *tert*-butyloxycarbonyl protecting group
BSA	- bovine serum albumin
CCL2	- chemokine (C-C motif) ligand 2
CCR2	- C-C chemokine receptor type 2
CCR5	- C-C chemokine receptor type 5
CLP	- common lymphoid progenitors
CD	- cluster of differentiation
CD_3OD	- deuterated methanol
CH_3CN	- acetonitrile
CMML	- chronic myelomonocytic leukemia
CMP	- common myeloid progenitors

Cu	- copper
CuAAC	- copper-catalysed azide-alkyne cycloaddition
CXCR4	- C-X-C chemokine receptor type 4
Cys	- cysteine
DMF	- Dimethylformamide
DNA	- Deoxyribonucleic acid
D_2O	- deuterated water
DTBA	- dithiobutylamine
DTT	- dithiothreitol
Equiv.	- equivalent
ETA	- ethanolamine
Et_3N	- triethylamine
FAB	- french-American-British group
FLURAM	- fluorescamine
Fmoc	- fluorenylmethyloxycarbamate
Glu	- glutamate
GMP	- granulocyte/monocyte progenitor
GPCRs	- G-protein-coupled receptors
GRKs	- G protein-coupled receptor kinases

HepG2	- human liver cancer cell line
His	- histidine
HMA	- hypomethylating agents
HSCs	- hematopoietic stem cells
HPLC	- high performance liquid chromatography
IC_{50}	- half-maximal inhibitory concentration
K_2CO_3	- potassium carbonate
Lys	- lysine
MDS	- myelodysplastic syndrome
2-ME	- 2-mercaptoethanol
MEP	- megakaryocyte-erythrocyte progenitors
Met	- methionine
MPN	- myeloproliferative neoplasm
MPP	- multi-potent progenitors
MS	- mass spectrometry
MW	- molecular weight
NAD	- nicotinamide adenine dinucleotide
NAMPT	-nicotinamide phosphoribosyltransferase
NMR	- nuclear magnetic resonance
o-DANPHOS	- bis(3-sulfonatophenyl)(2-trifluoroMethylphenyl)phosphine

PBS   - phosphate buffer

Pd   - Palladium

PDC   - peptide drug conjugates

pH   - -log[H^+], hydrogen ion concentration

pKa   - - log(K_a)

Pro   - proline

PTM   - post-translational modifications

SA1   - shigella dysenteriae holotoxin

Ser   - serine

SRSF2   - serine and Arginine Rich Splicing Factor 2)

SSTR   - somatostatin Receptor

TCEP   - *tris*(2-carboxyethyl)phosphine

TET2   - tet methylcytosine dioxygenase 2

THF   - tetrahydrofuran

THPP   - tris(3-hydroxypropyl)phosphine

THPTA   - tris(3-hydroxypropyltriazolylmethyl)amine

Thr   - threonine

TNF   - tumor necrosis factor

Trp   - tryptophan

Tyr   - tyrosine

UAAs   - unnatural amino acids

UV   - ultra-violet

WBC   - white blood cell

WT   - wild-type

Chapter 1: Introduction

1.1 Chronic myelomonocytic leukemia (CMML)

Leukemia is a blood cancer that starts in the bone marrow and forms high numbers of abnormal blood cells called blasts or leukemia cells. Leukemia is classified according to the effected blood cells; lymphoblastic or lymphocytic leukemias where the cancer occurs in a cell lineage which normally forms lymphocytic cells, or the myeloid or myelogenous leukemia where the cancer occurs in bone marrow cells that normally forms red blood cells, monocyte/granulocyte-derived cells, and platelets. Each type of leukemia can be either acute (where levels of the immature blood cells increase rapidly) or chronic (sustained levels of elevates but typically lower levels of abnormal white blood cells).[1]

Chronic myelomonocytic leukemia (CMML) is the only subtype of chronic myelogenous leukemia.[1] It is a rare hematopoietic malignancy characterised by an increase in monocytes in the peripheral blood (monocytosis) and bone marrow, with a bone marrow dysplasia in at least one type of blood cell.[2] CMML is characterised as both a myelodysplastic syndrome (MDS) and a myeloproliferative neoplasm (MPN).[3] It was grouped with myelodysplastic syndrome (MDS) until 2002 because it shared several clinical and biological features, including bone marrow and cytopenia failure, risk of acute (AML) transformation and cytogenetic abnormality.[4] The first significant-size cohort of CMML was only identified in 1975, consisting of 18 elderly patients with unexplained monocytosis, cytopenias and splenomegaly.[5] The incidence rate of CMML is estimated to be 0.3 - 0.7 per 100000 person-years and the median age of CMML is 70 year at diagnosis.[6,7]

The French-American-British group (FAB) classified the CMML into two subtypes according to the white blood cell (WBC) count at patient diagnosis;[8] myelodysplastic CMML (MD-CMML) for patients that have WBC counts of $\leq 13 \times 10^9$ L^{-1}, or myeloproliferative CMML (MP-CMML)

for patients that have WBC counts of $>13 \times 10^9$ L^{-1}.[8] The World Health Organization (WHO) classifies CMML according to the blast percentage in the peripheral blood (PB) and bone marrow (BM).[9] The first category is CMML-1 for patients have blast percentage fewer than 5% in PB or 10% in BM, while the second category is CMML-2 for patients have blast percentage with 5%-19% in PB or 10%-19% in BM.[9]

Selimoglu-Buet *et al.* differentiated between CMML cases and other hematologic malignancies by the type of monocyte that accumulate in the peripheral blood of CMML patients compared to both healthy controls and patients with other hematologic malignancies.[10] They reported the accumulation of classical monocyte (MO1) with a cut off value of greater than 94% MO1s in comparison with intermediate (MO2) and non-classical monocytes (MO3) in the peripheral blood of CMML patients.[10] The increase in MO1% caused by the increase in the total number of MO1s and a decrease in the number of MO3s in the peripheral blood of CMML patients can be used to differentiate between CMML cases and MDS or MPN.[10]

These findings were supported by Hudson *et al.* who differentiated between CMML cases and non-CMML and non-atypical chronic myeloid leukemia (non-aCML) patients by quantification of the non-classical monocyte (MO3) percentage in both blood and bone marrow specimens.[11] They reported a significant decrease in MO3% in peripheral blood specimens in patients with CMML in comparison with non-CMML and non-aCML patients (0.5% ± 0.3% vs 5.8% ± 4.4%, *P* < .001),[11] while the percentage of the MO3 in the bone marrow specimens of CMML patients are decreased significantly in comparison with non-CMML and non-aCML patients (1.1% ± 0.5% vs 10.7% ± 8.6%, *P* = .002).[11] Moreover, Hudson reported the decrease of the intermediate monocytes MO2 percentage in peripheral blood specimens in CMML

patients in comparison with non-CMML and non-aCML patients (4.5% ± 6.8% vs 8.3% ± 4.6%, P = .014), while in the bone marrow specimens there was no significant difference the intermediate monocyte MO2 percentage.[11]

The blast count is one of the most important prognostic indicators in CMML. CMML-1 patients are likely to live longer than CMML-2 patients with median survival time of 20 months and they have an 18% risk of transforming to acute myeloid leukemia (AML) within 5 years of their CMML diagnosis.[12] The median survival time of CMML-2 patients was 15 months and they have an 63% risk of transforming to AML within 5 years.[12] However, some CMML-1 (about 20%) and CMML-2 (about 10%) patients survived much longer than 5 years.[12]

At present, the intensive chemotherapy followed by allogeneic hematopoietic stem cell transplantation (alloHSCT) is the only known curative treatment for CMML.[6] However, HSCT is limited to a minority of CMML patients, generally younger patients with good performance status, due to the toxicity of the alloHSCT.[6] Therefore, for the majority of patients there is no curative treatment for CMML and the therapeutic options are cytotoxic hypomethylating agents (HMA) (such as 5-azacitidine (AZA) or decitabine (DEC)) to delay progression used in combination with hydroxyurea for myeloproliferation and erythropoiesis-stimulating agents for anemia.[6]

There are relatively few on going clinical studies investigating new therapies for CMML, with recent commercial trials failing to deliver improved therapeutic options. For example, Tefinostat (CHR-2845) is a cell permeant ester which is converted into an active acid histone deacetylase (HDAC) inhibitor (CHR-2847) by the human carboxylesterase 1 (hCE-1) enzyme, which is highly expressed in cells of monocyte lineage.[13] The selective toxicity of tefinostat

towards monocytic cells and tolerability were confirmed in pre-clinical and phase 1 studies.[13]

However, the minimum number of clinical responses to tefinostat (CHR-2845) and targeting monocyte in CMML were not achieved in a phase 2 study.[13]

The strongest prognostic factor in CMML is gene mutation. The most frequent genetic events in CMML are TET2, SRSF2 and ASXL1 mutations.[14] The study of genetic lesions in 28 cases of CMML confirmed the gene mutations are found early in hematopoiesis, during myeloid differentiation to the granulocyte/monocyte progenitor (GMP) stage, resulting in accumulation of monocytes and decrease in erythrocytes (figure 1 and 2).[14] Therefore, to improve disease control there is a need to find therapeutic strategies that target the disease at the earliest hematopoiesis stages in bone marrow.[14]
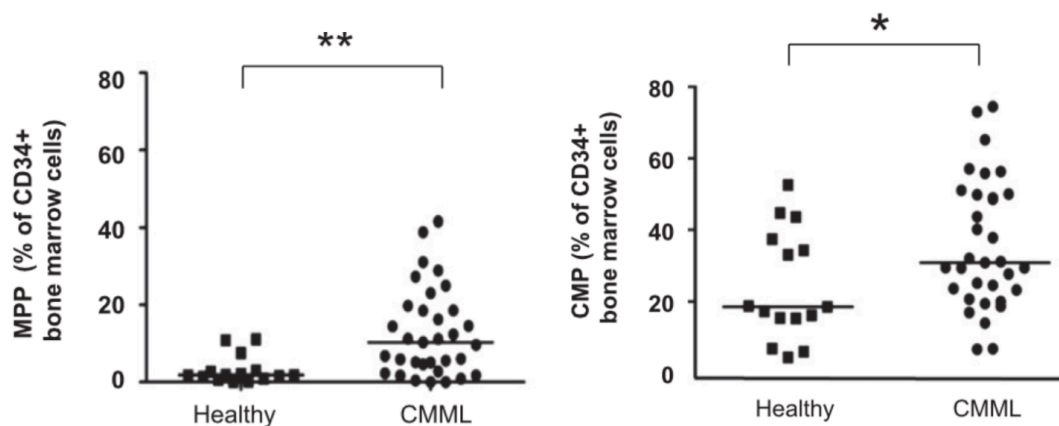
Figure 1: Immature CMP and MPP in CMML. MPP: multipotent progenitor (left hand side), CMP, common myeloid progenitor (right hand side). Proportion of MPP and CMP by flow cytometry among total BM CD34[1] cells from patients with CMML (n = 33) or aged-matched healthy control participants (n = 15).[14]
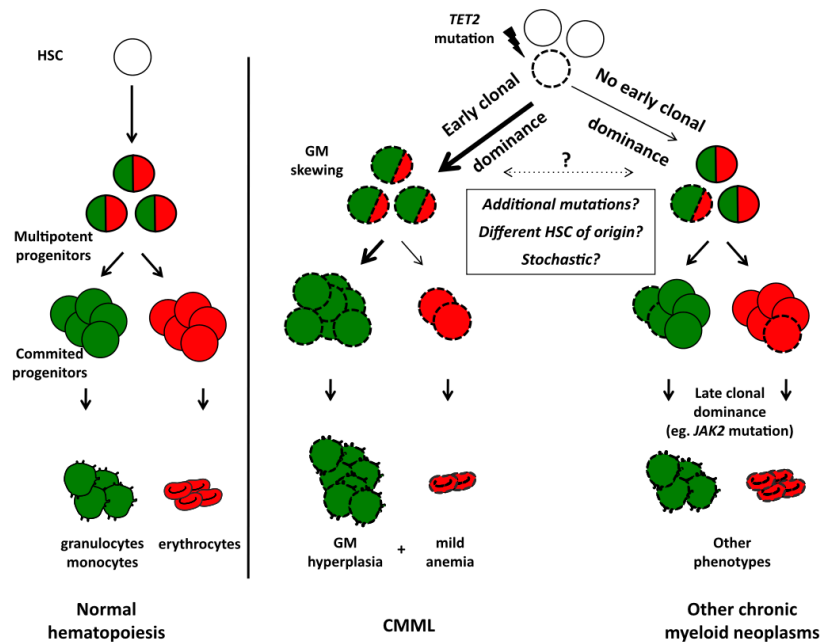
Figure 2: Proposed model linking early clonal dominance with granulomonocytic skewing of immature progenitors in CMML and later clonal dominance in other chronic myeloid neoplasms, dashed lines represent the mutated cells, green represents granulomonocytic differentiation potential, red represents erythroid potential.[14]

1.2 Monocytes

All blood cells originate from hematopoietic stem cells (HSCs) in bone marrow in a process called hematopoiesis. Hematopoietic stem cells (HSCs) differentiate into multi-potent progenitors (MPP) and then to common lymphoid progenitors (CLP) and common myeloid progenitors (CMP), with each lineage further differentiating to produce one or more specific types of blood cell. The common myeloid progenitors (CMP) differentiate to produce granulocyte-macrophage progenitors (GMP) and megakaryocyte-erythrocyte progenitors (MEP) which further differentiate to more specific types of blood cells; monocytes, granulocytes, megakaryocytes and erythrocytes (figure 3).[15]
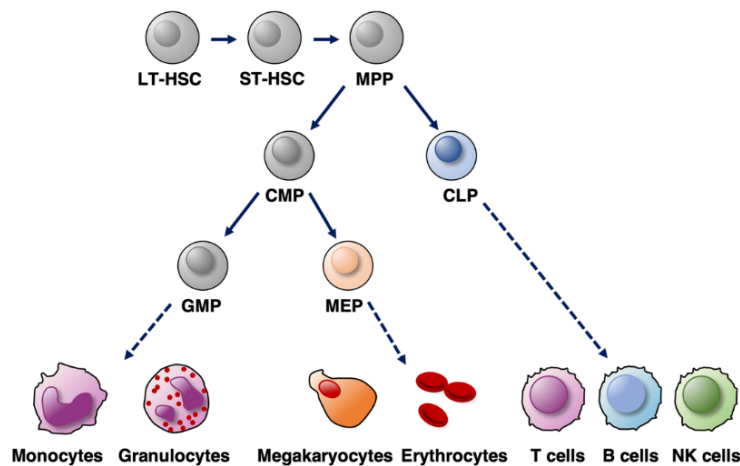
Figure 3: Differentiation of hematopoietic stem cells (HSCs) into blood cells in bone marrow (hematopoiesis).[16]

Monocytes are a subset of the white blood cells (leukocytes), which typically represent around 10% of the circulating white blood cells in humans.[17] Monocytes originate from hematopoietic stem cells (HSCs) in bone marrow then are released to the bloodstream,[18,19] where they circulate in the blood for up to a few days before differentiating into macrophages, dendritic cells and osteoclasts.[18,19] The main functions of the monocytes are homeostasis, immune defence and tissue repair.[20,19]

Human peripheral-blood monocytes are variable in size, receptor expression, trafficking and ability to differentiate after stimulation by cytokines or microbial molecules.[21] The CD14 surface receptor is used to mark human monocytes due to its abundant expression on the cell surface.[22] Monocytes are divided into three subsets according the CD and chemokine receptor expression, which are classical, intermediate and non-classical monocytes.[19,22,23]

The classical monocytes MO1 (CD14^{++}CD16^{-}) are the most abundant subset of human monocytes.[24] They express high level of the CCR2 receptor, which is a chemokine receptor that mediates chemotaxis of the monocytes during inflammation, and express low levels of the CX3CR1 receptor which is a chemokine receptor that mediates accumulation of tissue-resident monocytes (table 1).[17] Phagocytosis is considered to be the major function of classical monocytes MO1 (CD14^{++}CD16^{-}).[22] In addition classical monocytes MO1 (CD14^{++}CD16^{-}) are pro-inflammatory in part due to expression CD62L, which plays role in migration into lymph nodes, where they can differentiate into macrophages and dendritic cells that help control the adaptive immune response.[22]

In contrast, the intermediate and non-classical monocytes (which are called CD16^{+} monocytes due to co-expression of CD16 with CD14) have lower phagocytic capacity and express more MHC class II complex for antigen presentation (table 1).[18] The non-classical human monocytes MO3 (CD14^{+}CD16^{+}) produce low level of the CCR2 receptors and high level of the CX3CR1 receptors.[22,23] The intermediate human monocytes MO2 (CD14^{++}CD16^{+}) express CCR2 receptors and have inflammatory function and low peroxidase activity.[22] During inflammation, the classical monocytes MO1 (CD14^{++}CD16^{-}) and the intermediate monocytes MO2 (CD14^{++}CD16^{+}) invade tissue, mediated predominantly by CCL2/CCR2 signalling.[22]

	Classical CD14^{+}CD16^{-}	Intermediate CD14^{++}CD16^{+}	Non-classical CD14^{+}CD16^{+}
Endothelium patrolling	no	no	yes
Phagocytose beads	high	high	low
ROS production	high	none	none
TNF-æ	none	high	low
IL-1ß	low	high	high
CCR2	high	med	low
IL-10	high	med	none
IL-8	high	med	low
IL-6	high	high	low
CCL3	high	high	low
IL-1 receptor antagonist	none	low	high

Table 1: Comparison between the three monocyte subsets in production of

cytokines/chemokines.[25]

The differentiation of the classical human monocyte MO1 into non-classical monocyte is now

widely accepted.[26] CCR2 mediates migration of the classical human monocyte from bone

marrow to the blood stream after maturation. In the blood, classical human monocytes MO1

differentiate into intermediate monocytes MO2 then non-classical human monocytes

MO3.[20,27]

1.3 Chemokines and their receptors

Chemokines are small heparin-binding proteins containing 60-100 amino acids that control

cell trafficking (chemotaxis). More than 50 human chemokines and 20 chemokine receptors

have been discovered since 1977. The molecular mass of chemokines is about 8 - 12 kDa and

they contain 1–3 disulfide bonds. The four subfamilies of chemokines are classified according

to the number and location of the cysteine residues at the N-terminus of the molecule,

resulting in the classification CXC-, CC-, CX_3C-, and C-.[28,29]

Despite having limited secondary structure the chemokines contain three distinct domains. The first domain is N-terminal region, which is highly flexible and is the region that binds to and activates receptors. The disulfide bond between the N-terminal cysteine constrains the N-terminal region in place relative to the second domain, which is a long loop that enters the triple-stranded antiparallel β-sheet. The final domain is C-terminal α-helix region which overlies the sheets (figure 4).[30,31,32]
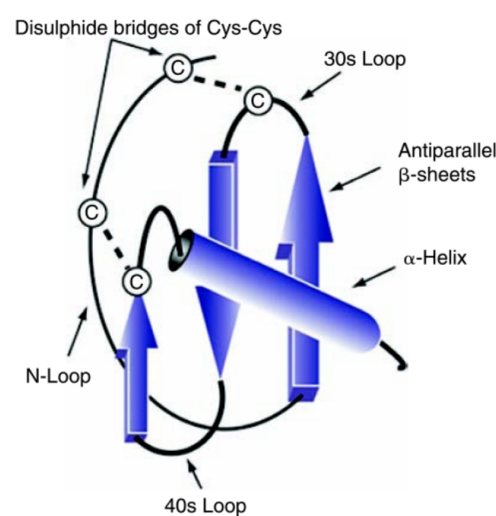
Figure 4: The structure of chemokines.[28]

The chemokine ligands are secreted by many cell types in response to signals such as proinflammatory cytokines, and specifically recruit subsets of monocytes, neutrophils and lymphocytes. As a result, their receptors are generally found only on the surface of leukocytes. The chemotaxis process is induced by binding of the chemokines ligands to G-protein-coupled receptors (GPCRs) on the specific cell surface. The resulting activation of intracellular signalling cascades leads to migration toward the chemokine source.[28]

1.3.1 CCL2-CCR2 Signalling Axis

CCL2, also called monocyte chemoattractant protein-1 (MCP-1), belongs the C-C chemokine family and is composed from four members (MCP-1, -2, -3, and -4). CCL2 contains 76 amino acids and the molecular mass of the mature protein is about 9 kDa. The principle receptor for CCL2 is CCR2, a helical seven-transmembrane G protein-coupled receptor (GPCR) found on the cell membrane of a large proportion of monocytic cells. CCL2 acts as a chemoattractant chemokine which is responsible for monocyte recruitment from bone marrow into peripheral blood then into tissue; CCL2 is expressed by many cells in response to pro-inflammatory cytokines or microbial molecules, leading to increased CCL2 concentration in serum and within inflamed tissue followed by migration of the monocytes to the site of the infection.[28,33,34]

G protein-coupled receptors (GPCR) consist of two regions, intracellular and extracellular. The extracellular region is composed of the N-terminus and three extracellular loops, while the intracellular region is composed of C terminus and three intracellular loops. The extracellular domain is important for binding with chemokines ligand and the intracellular domain collaborate to transduce the chemokine signal. Changes in the seven-transmembrane conformation lead to receptor activation.[32,33,35]

The binding of the chemokine ligands to the G protein-coupled receptor (GPCR) enhances internalisation and trafficking of the receptor. There are two different mechanisms for internalisation, clathrin-mediated endocytosis and lipid raft/caveolae-dependent internalization. Most ligand-induced internalisation of the receptors occurs through the clathrin-mediated endocytosis mechanism, while the research in the lipid raft/caveolae-dependent pathways is limited with only CCR5 and CXCR4 being identified in lipid rafts. Lipid

rafts are glycosphingolipid-enriched microdomains and caveolae is a protein that is highly enriched in cholesterol and glycosphingolipids. Once internalised GPCRs enter caveosomes, followed by fusing with early endosomes and join the clathrin-mediated endocytosis pathway.[36]

The clathrin-mediated endocytosis mechanism starts with binding of chemokine ligands with GPCR, causing conformational changes that result in phosphorylation of the chemokine receptor in serine and threonine residues in the intracellular loops and carboxyl-terminus by G protein-coupled receptor kinases (GRKs). Phosphorylation of the chemokine receptor leads to G protein subunits uncoupling from the receptor and migration of the adaptor molecules which link the receptor to a lattice of clathrin to facilitate receptor internalization. Adaptin 2 (AP-2) and ß-arrestin are adaptor molecules have critical role in internalization of the chemokine receptor. The endocytosis is mediated by binding of ß-arrestin to the phosphorylated receptors and adaptin 2 (AP-2) then binds to clathrin to form a clathrin-coated pit. This is followed by internalization of the receptor in a clathrin-coated vesicle through cleavage from the membrane by the action of dynamin. Following uncoating of the clathrin-coated vesicle the receptor-ligand complex progresses into an early endosome, from which the chemokine receptor can be either recycled back to the surface for further ligand binding or degraded by entering the late endosome then to lysosomes (figure 5).[36,32]
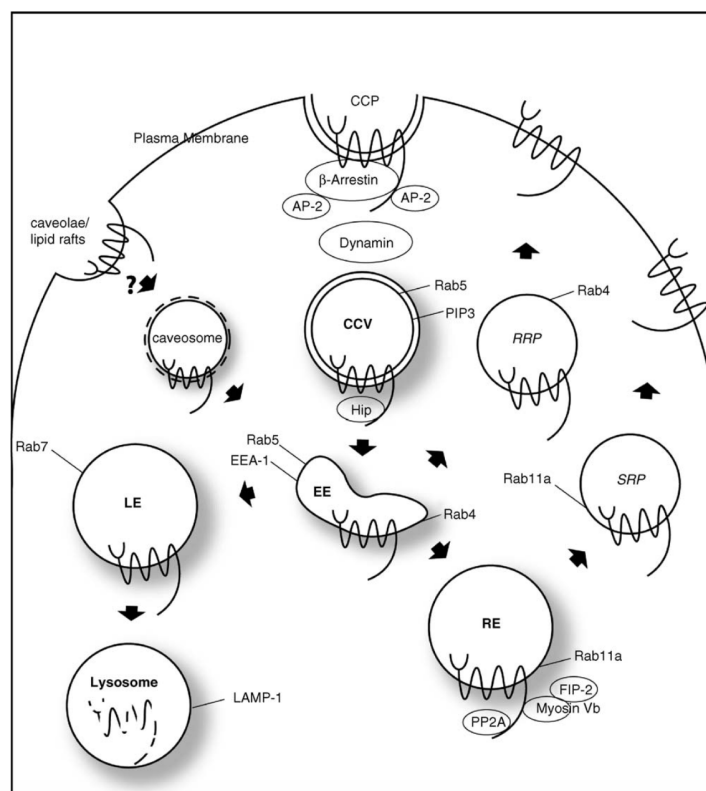
Figure 5. Endocytosis scheme. CCP: clathrin-coated pit, CCV: clathrin-coated vesicle, EE: early endosome, LE: late endosome, RE: recycling endosome, RRP: rapid recycling pathway, SRP: slow recycling pathway, EEA-1: early endosomal antigen-1, FIP-2: Rab11-family interacting protein-2, LAMP-1: lysosomal-associated membrane protein-1.[36]

Although CCL2 attracts mature monocyte/macrophages to migrate to the area of inflammation and injury by activation of CCR2, it has been demonstrated that CCR2 also mediates hematopoietic stem and progenitor cells trafficking from BM to areas of inflammation and injury in mice in response to CCR2 ligands.[37] While the role of the hematopoietic stem and progenitor cells in the inflammation site is unclear, it has been suggested to contribute in the repair and regeneration of damaged tissue by *in situ* hematopoiesis and differentiation.[37] CCR2 expression can be observed on the surface of a portion of primitive hematopoietic cells in mice, with the proportion of cells expressing CCR2

increasing as differentiation proceeds toewards monocytes.[37] The expression of CCR2 in the myeloid lineages (CMPs and GMPs) is more than self-renewing HSCs and MPPs (figure 6) and expression increases further in fully differentiated monocytes.[37]
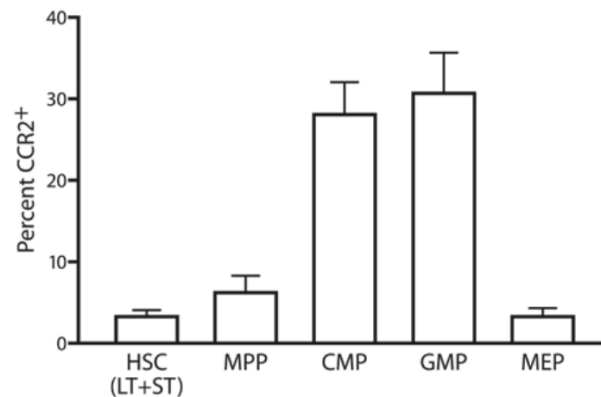
Figure 6: CCR2 expression on cells. HSC: hematopoietic stem cells, MPP: multipotent progenitor, CMP: common myeloid progenitor, GMP: granulocyte-macrophage progenitor, MEP: megakaryocyte-erythroid progenitor.[37]

1.3.2 CCL2/CCR2 Therapies and CCL2 Conjugates

Several CCL2 conjugates have been used to investigate the functional behaviour of CCL2-CCR2 signalling axis or towards development of novel therapeutics agents. Volpe and co-workers developed a fluorescent protein tagged CCL2 by fusing mCherry fluorescent protein at the C-terminus of CCL2,[1] which they used to investigate the migration of the human monocytes mediated by CCL2/CCR2.[38] It was shown that the potency of the CCL2-mCherry conjugate to initiate chemotaxis is similar to the wild-type CCL2.[38] The time-lapse video microscopy showed the CCR2 mediated the efficient and selective internalization of the CCL2 during migration and the rapid processing of CCR2 from the plasma membrane to the endosomal structure for CCL2 degradation, with CCR2 recycled to the surface for further chemotaxis and

ligand internalisation.[38] The uptake of the fluorescent CCL2–mCherry demonstrates that the CCR2 which expressed on the surface of monocytes can act as scavenger for CCL2.[38]

CCL2 conjugates have also been used to deliver therapeutics inside cells; the CCL2-SA1 toxin was prepared as a fusion protein containing the Shigella dysenteriae holotoxin (SA1) with CCL2 through recombinant protein expression.[39] The CCL2 binds to CCR2 that is expressed on the cell surface, where the fusion protein enters the cells then the SA1 toxin causes cell death by inhibition of protein synthesis.[39] It has been shown that the CCR2 mediates the internalization of CCL2-SA1 conjugate in monocytes that caused a reduction in protein synthesis and subsequent cell death.[39] In the kidney nephropathy model, the CCL2-SA1 conjugate caused decrease in infiltrating monocytes/macrophages, decrease glomerular lesions and proteinuria.[39] However, no chemotactic migration was observed when non-native CCL2 variant was used this was in line with previous reports that CCL2-variants can reduce the chemotactic potency relative to wild-type CCL2.[39]

In the previous work of our group, novel CCL2-fluorophore conjugates have been prepared to investigate the CCL2 uptake by primary human immune cells that express CCR2 and chemotactic activity of CCL2 conjugate. The CCL2-fluorophore conjugate is prepared by copper catalysed azide alkyne cycloaddition reaction (CuAAC) between an azido-bearing fluorophore and synthetic CCL2 that is modified by propargyl glycine at C-terminus (scheme 1). In order to study the impact of changes in the protein the conjugates were prepared using wild-type CCL2 as well as a P8A mutant which was reported to be chemotactically inactive *in vivo*.[40]
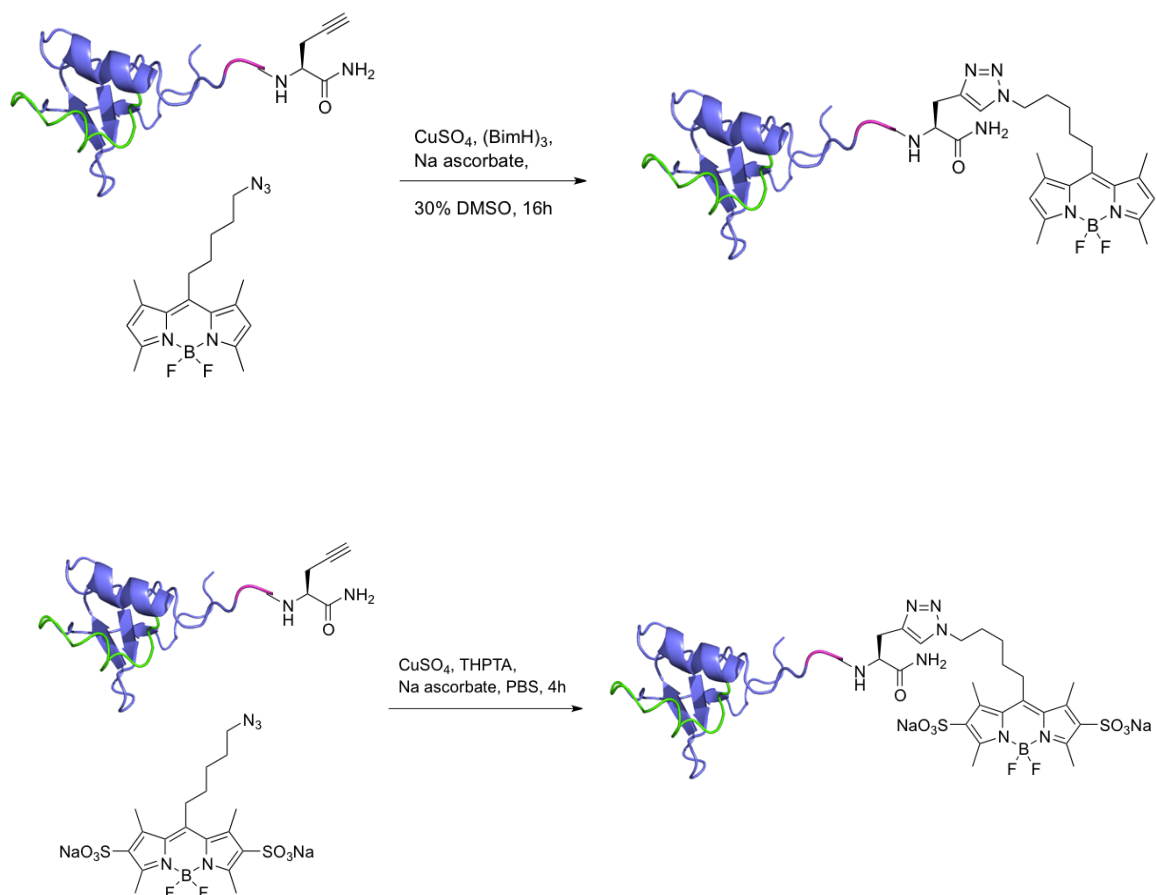
Scheme 1: Synthesis CCL2 fluorophore conjugates by CuAAC reaction between azido-bearing fluorophore and alkyne modified CCL2.

The transwell Chemotaxis assay was used to characterise the chemotactic activity of the CCL2-fluorophore conjugates. This assay is composed from an upper chamber where the immortal monocytic THP-1 cells are placed and a lower chamber where the chemoattractant is placed. The two chambers are separated by a porous membrane to facilitate cell migration from the upper chamber towards the chemoattractant in the lower chamber. The chemotactic activity of the conjugates was clearly observed with maximum migration response at 10 nM (figure 7). However, fewer cells migrated at higher concentrations because the highly concentrated chemokine saturates the receptors, thus blocking the cell's ability to detect the direction of

concentration gradient (figure 7) with the cells movement therefore switched from chemotaxis to chemokinesis, where cells move in a random motion. The migrated cells showed a concentration-dependant increase in fluorescence, which appears to plateau at around 30 nM which would be consistent with this being a saturating concentration in this model.
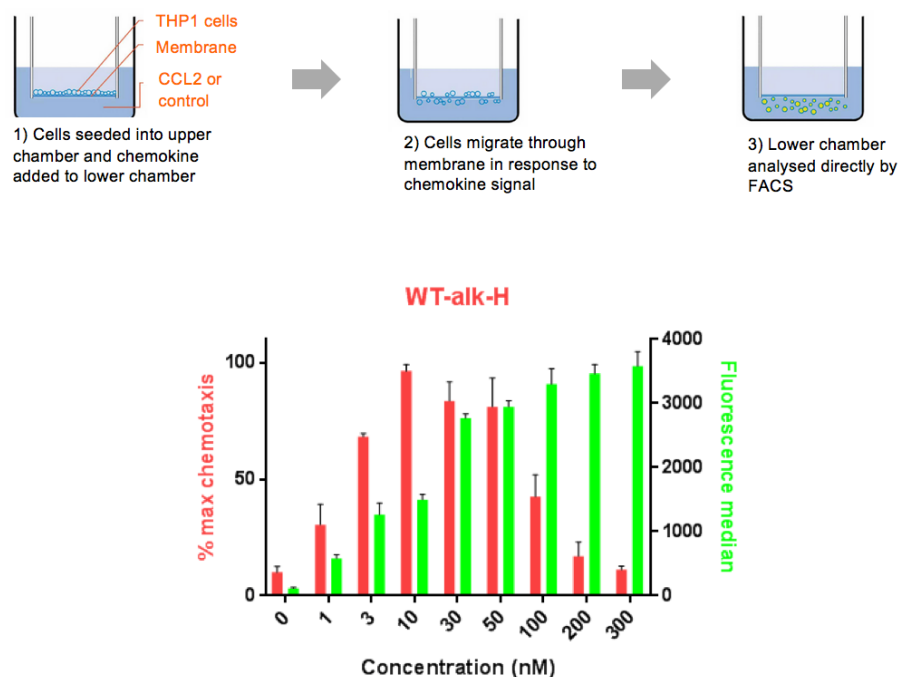
Figure 7: Transwell Chemotaxis assay for CCL2 fluorophore conjugate and THP1 cells. The maximum migration response at 10 nm of CCL2 fluorophore conjugate, few cells were migrated at higher concentrations.

Fluorescence microscopy was used to determine the behaviour of the CCL2 fluorophore conjugate inside cells. Either THP-1 cells or peripheral blood mononuclear cells (PBMCs) from healthy volunteers were incubated with CCL2 fluorophore conjugate for 2 hours then 4',6-diamidino-2-phenylindole (DAPI) was used to stain the nuclei. The Zeiss Axio Observer was

then used to capture the images using LED illumination at 405 and 495 nm with Apotome

optical sectioning (figure 8). The images demonstrate that the PBMCs internalise the CCL2

fluorophore conjugate, with the fluorophore distributed throughout the cytosol even at early

time points (2 hr), with similar results observed for THP-1 cells and/or WT CCL2.
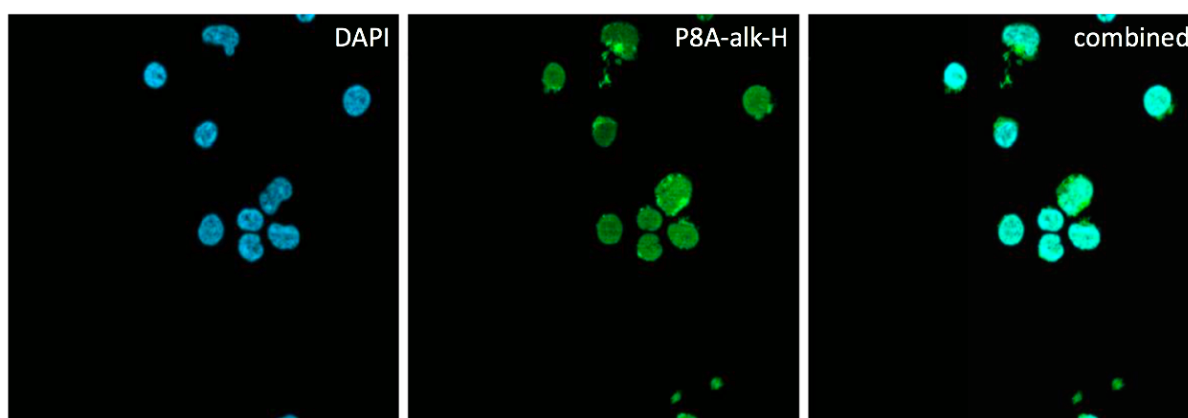
Figure 8: The fluorescence microscopy of PBMCs incubated with P8A CCL2 fluorophore

conjugate for 2 hours.

1.3.3 CCL2-NAMPTi Conjugates

FK866 is an experimental anticancer drug that acts as a highly specific inhibitor for

nicotinamide phosphoribosyltransferase (NAMPT), which is an essential enzyme regulating

the biosynthesis of the intracellular coenzyme NAD^+ from the natural precursor nicotinamide

(figure 9).[41] FK866 effectively inhibits NAMPT in HepG2 human liver carcinoma cells in an IC_{50}

of ~1 nM leading to gradual depletion in NAD^+ that results in cell death by apoptosis.[41] The

metabolic mechanism of action makes this an interesting class of anticancer drug in

comparison to the traditional cell-cycle cytotoxins, however unfortunately to date there have

been no successful late-stage clinical trails with NAMPT inhibitors such as FK-866,

predominantly due to their poor selectivity for cancerous cells. In order to investigate if this

poor selectivity can be overcome by use of a targeting peptide, our group have prepared a CCL2-FK866 conjugate and evaluated its function using THP1 cells that express CCR2 and Jurkat cells that do not have CCR2. While FK-866 was toxic to both cell types, the CCL2-FK866 conjugate induced cell death in THP1 cells with an IC_{50} of 2 nM, while Jurkat cells were not affected up to concentrations of 100 nM (figure 10).
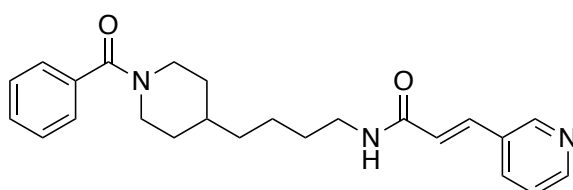
Figure 9: Chemical structure of FK866, NADPRT inhibitor.[41]
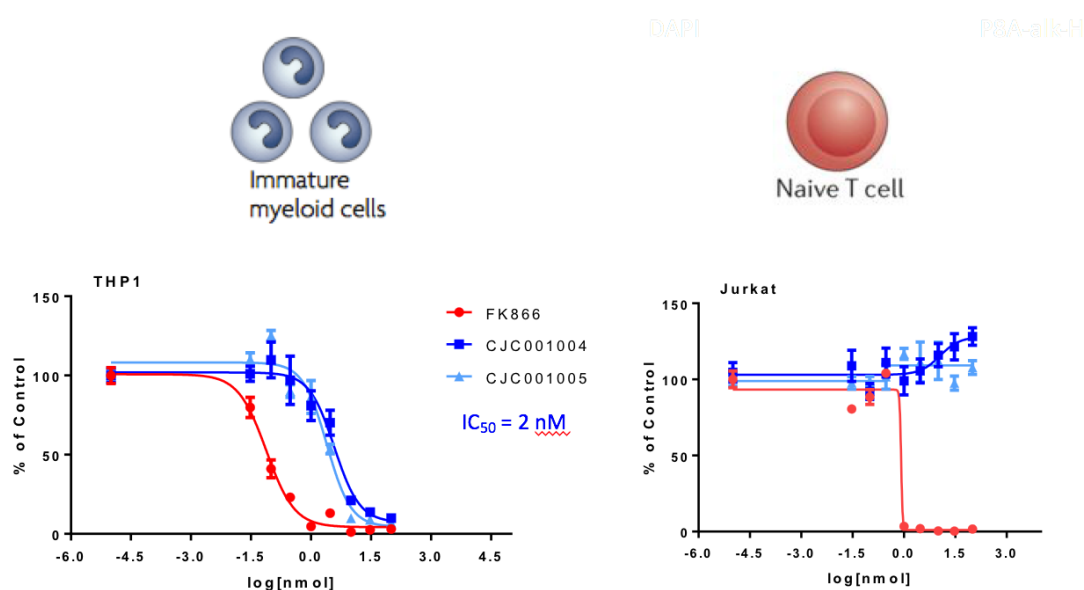
Figure 10: Investigation of CCR2-cytotoxin conjugates in THP1 cells and Jurkat cells.

We have successfully confirmed the chemotactic activity of the CCL2 fluorophore conjugate by using the transwell Chemotaxis assay and cellular internalising the CCL2 fluorophore conjugate. In addition, the induction of cell death in THP1 cells due to CCL2-FK866 conjugate

has been confirmed in compare with control cell. However, we faced issues in the scaling the CCL2 synthesis as just a few milligrams are available, therefore, we decided to move to the recombinant system by targeting a nucleophilic thiol introduced at the C-terminus of the CCL2. The FK866 will be attached to a thiol alkylation reagent then reacted with cysteine in order to form the CCL2-FK866 conjugate.

1.4 Peptide -drug conjugate (PDCs)

Antibody-drug conjugates (ADCs) and peptide-drug conjugate (PDCs) are targeted therapies that have been extensively studied in recent years. They contain three components; a monoclonal antibody or peptides, one or more (toxic) payloads and linker to connect the active components (figure 11). PDCs and ADCs are generally designed to reduce the adverse effects of typical therapy as they combined the advantages of both cytotoxic payloads and highly specific monoclonal antibodies/peptides ligands. ADCs are generally more stable and selective in comparison with PDCs, however PDCs composed of linear or cyclic peptides have lower molecule weight than ADCs, which can allow higher drug loading and enhanced penetration into solid tissues. Moreover, the short peptide nature of PDC make their structure more flexible and modification and conjugation much easier, allowing rational development of agents with improved targeting specificity and/or stability.[42]
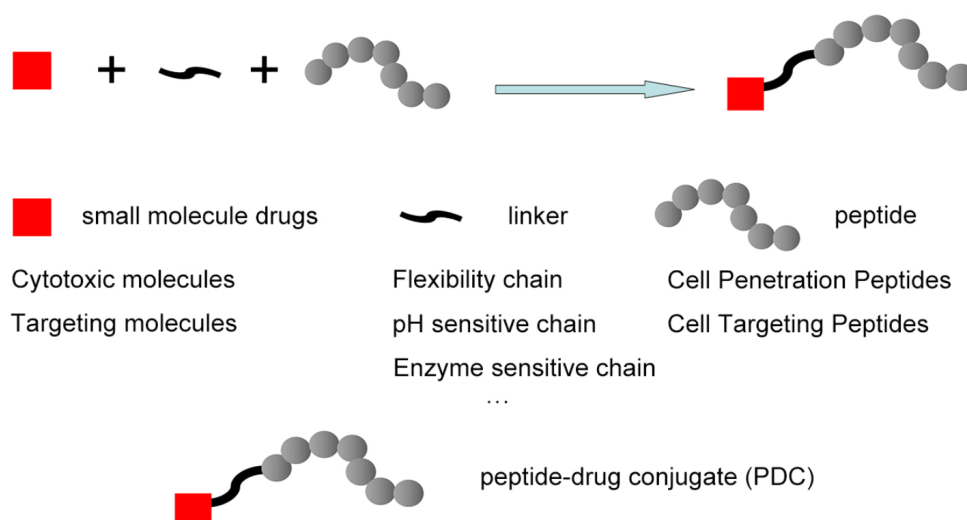
Figure 11: The basic structure of PDCs.[42]

While there are several approved ADCs and a much larger number under development, there are relatively few PDCs in late stage trials and only approved drug. GHIH-177Lu conjugate is a peptide-drug conjugate that has recently been approved for treatment of gastroenteropancreatic neuroendocrine tumours. The GHIH-177Lu conjugate is a conjugation of a somatostatin-derived peptide with beta-emitter 177 Lu that acts as a radioactive chemotherapeutic agent (figure 12). Somatostatin is a growth hormone-inhibiting hormone (GHIH) that inhibits secretion of different hormones such as growth hormone, thyroid stimulating hormone, and other pituitary-derived hormones. Therefore, Somatostatin analogues are used clinically to treat acromegaly and hormone-dependent tumours such as pancreatic and vasoactive intestinal peptide-secreting tumours. Somatostatin has five receptors subtypes (SSTR1-5) that are expressed by many cells, with SSTR2 in particular expressed by many tumour cells. Somatostatin is has higher affinity for SSTR2 (IC_{50} 1.5 nM) in comparison with other receptor such as SSTR5 (IC_{50} 547 nM) and SSTR3 (IC_{50} >1000 nM), therefore, GHIH-177Lu is able to target SSTR2 in tumour cells to selectively induce internalization of the cytotoxic component.[43]

The combination of the anticancer pharmacology of somatostatin and radioisotope therapy leads to tumour death by process called peptide receptor radionuclide therapy (PRRT). A clinical study in 310 patients with gastroenteropancreatic cancer showed the GHIH-177Lu conjugate provided 28% partial tumour remission and 2% complete tumour remission.[43]
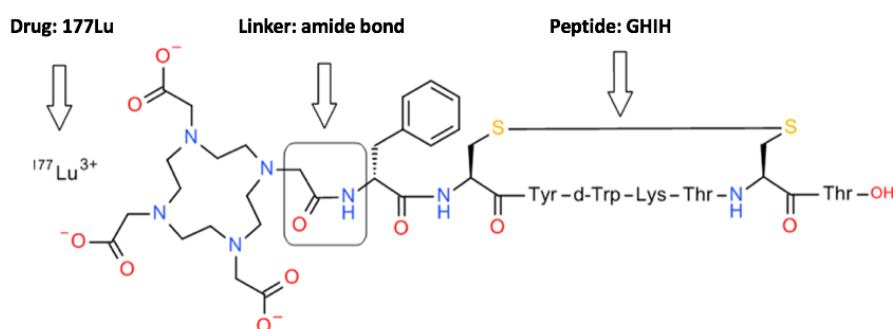
Figure 12: chemical structure of GHIH-177Lu conjugate.[43]

1.5 Protein modification

1.5.1 Background

Proteins are responsible for a wide range of critical functions in living organisms, including for example DNA replication, catalysis of metabolic reactions, stimulation response (cell signalling) and transport of molecules. Because of the broad array of roles conducted by proteins, the control of protein behaviour provides a huge number of opportunities to study and exploit their function in the fields of biology, medicine and enzymatic catalysis.[44]

Many chemical species are added to proteins during and after synthesis on the ribosome to modify their structure. This is can explain the complexity of the human proteome over the human genome; It is estimated that the human genome comprises about 20,000 to 25,000 genes but the human proteome is estimated to comprise over 1 million proteins.[45] This demonstrates that a single gene can encode multiple proteins, as a single gene generates

different mRNA transcripts due to transcription initiation at alternative promoters, differential transcription termination, and alternative splicing of the transcript. The Post-translational modifications (PTM) play a key role in further increasing the complexity from level of the genome to the proteome (figure 13).[46]
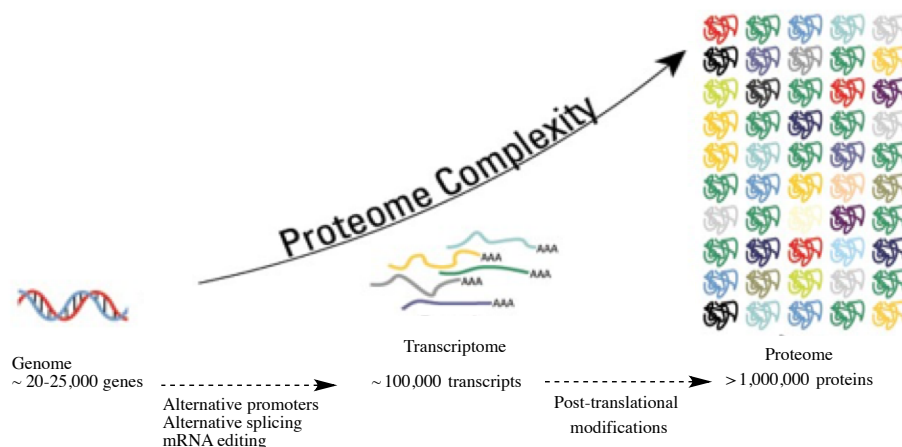
Figure 13: The role of post-translation modifications in increasing proteomic diversity.[46]

Post-translational modifications (PTM) are the natural modification of proteins after synthesis in the ribosome. A large set of reactions have been developed by chemists to mimic natural protein modification in order to determine the exact biological roles of PTMs.[47] Such protein modifications have many applications in biology and therapeutic discovery. For example as previously discussed protein conjugation with fluorophores allows optical measurement of physiological parameters of cells and tissues, while the conjugation of cytotoxic medicines to antibodies can improve the efficacy and reduce the side effects of anti-cancer drugs.[48,49,50]

The ideal chemical modification of protein should be chemoselective to one amino acid side chain among other reactive amino acid side chains on the protein surface. While nature can achieve this through secondary recognition in enzymatic catalysis, synthetic protein

modification typically relies on targeting amino acids with low abundance on the protein surface, such as cysteine. Another method for site-selective protein modification is incorporation of unnatural amino acids (UAAs) to form proteins that have functional groups that are normally not present in living cells, such as an azide, alkyne, ketone, alkene or tetrazine. The reactions with these functional groups are highly chemoselective over all other amino acid side chains that are present in cells.[51,52]

1.5.2 Natural post-translation modification

The post-translational modification of proteins (PTMs) can lead to changes in the structure, localisation and activity of proteins and plays a critical role in the vast biodiversity of proteins found in nature.[46,53] In addition, PTMs play an important role in many cellular processes such as protein degradation, cellular differentiation, cellular signaling, protein-protein interactions and gene expression regulation.[46,53,47] These modifications can cause very simple chemical changes of proteins such as phosphate and acetate addition or more significant chemical changes such as proteoglycans.[53]

PTMs occur at any step in the protein life cycle. For instance, some proteins are modified directly after completion of translation in order to provide a proper protein folding or stability, such as in proteins glycosylation and lipidation. Other proteins are modified after completion of folding and localisation in order to activate or inactivate their biological activity, such as phosphorylation of proteins and methylation.[46] PTMs can be classified into four categories, which are addition of proteins or peptides, an addition of functional groups, changes protein structure and changes to the chemical nature of an amino acid, some common PTMs are listed in table 2 and some of common PTMs are discussed briefly below. Proteins can have single modification or combinations of these modifications.[54]

Modification	Function	Residue
Phosphorylation	Control of cellular function and signalling	Ser, Thr, Tyr, Asp, His, Cys
N-Acetylation N-Methylation	Transcriptional regulation	Arg, Lys, His
Glycosylation	Cellular differentiation, fertilization, Immune response	Ser, Thr, Asn, Trp
Oxidation	Protein stability, Redox regulation	Cys, Met
Polyprenylation	Membrane localisation, Protein-protein interaction	Cys
Hydroxylation	Oxygen sensing, Collagen maturation	Lys, Pro, Asn
Sulfation	Control of protein-protein interactions	Tyr

Table 2: Examples of post-translational protein modifications (PTM).[54]

1.5.2.1 Glycosylated proteins

The most common PTM in eukaryotic cells is glycosylation, it is estimated that 50% to 70% of human proteins are glycosylated.[55] Glycosylated proteins are the most clinically useful proteins, which include in over 40% of the approved protein therapeutics such as activase (thrombolytic), avastin (antibody) and gonal F (hormone).[56,57] The glycosylation pathway is an important pathway for proteins, as defects in a number of genes in this pathway cause congenital disorders with serious medical consequences and the change of glycosylation profiles of specific proteins is recognized as disease marker.[55] For example, the alteration of glycosylation is among the best methods for characterisation of cancer,[58] and can aid in the understanding, diagnosis and treatment of several disease such as heart disease, cancer, diabetes and immune disorders.[55]

Glycoproteins are categorized according to the type of the linkage between protein and the complex oligosaccharide chains (glycans) such as *N*-linked glycoprotein, *O*-linked glycoprotein or glycosylphosphatidylinositol (GPI) anchored.[59,60] However, some glycoproteins have more than one type of saccharide side chain.[61] The attachment of glycans to the polypeptide backbone highly influences the physicochemical properties of protein, such as protein folding, solubilize and sorting of protein within the cell.[62] Glycan can be very large and bulky that can affect protein-protein interactions by either facilitating or preventing proteins from binding to cognate interaction domains. In addition, the hydrophilic property of sugar can also change the solubility of a protein.[63]

N-glycosylation is the covalent attachment of glycans to the amide nitrogen on the side chain of asparagine (Asn) residues, which presents as a part of Asn-X-Ser/Thr consensus sequence (X is any amino acid except proline (Pro)) (figure 14).[63] *N*-glycosylation can change the essential biological functions, such as the immunogenicity, clearance rate, specific activity and ligand–receptor interactions.[63] *O*-glycosylation is the attachment of oligosaccharide to oxygen atom at serine or threonine residues (figure 14).[59,63] It is started by protein mannosyltransferases, which transfer mannose to serine or threonine residues in the endoplasmic reticulum, then completed in the Golgi by mannosyltransferases.[63,64]

A glycosylphosphatidylinositol (GPI)-anchor is the attachment of phosphatidylinositol to the tri-amannosyl core attached to a non-acetylated glucosamine through a glycosidic linkage.[65] During transfer GPIs to the rough endoplasmic reticulum, GPIs are attached to the polypeptide chain with cleavage and removing of a hydrophobic carboxy-terminal signal peptide. GPIs-anchor linked over a hundred different membrane proteins to the membrane.[65]
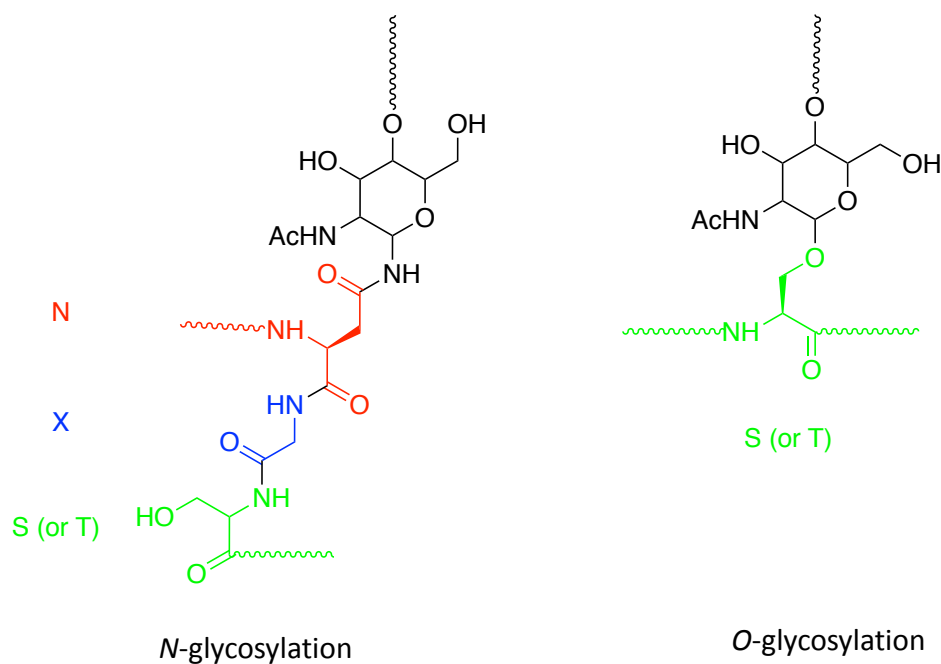
Figure 14: The attachment of N-acetylglucosamine to protein through *N*- linked glycosylation and *O*- linked glycosylation.

1.5.2.2 Protein Lipidation

Lipids are covalently attached to protein for regulation of protein functions and localisation. The most common outcome of lipid attachment is an increased affinity for membranes and enabling of protein-protein interactions. However, the study of protein lipidation is considered challenging due to hydrophobic character of lipid modifications.[66,67,68]

In cells, five types of lipids are used to modify about 1000 proteins; sterols, fatty acids, isoprenoids and glycosylphosphatidyl inositol (GPI) anchors. These lipids are attached to proteins covalently and more than one type of lipid can bind with protein such as palmitate + myristate, palmitate + cholesterol or palmitate + farnesyl. Different lipid transferases are used to attach different lipid with proteins and each type of lipid provide different properties to the modified protein.[69,70]

The major classes of lipid modification of protein are N-myristylation, palmitoylation and prenylation, which occur in the cytoplasm. Palmitoylation is the attachment of the saturated long chain fatty acid to the cysteine residue through thioester bond (figure 15). In the N-myristylated protein, the saturated fatty acid myristate is attached to an N-terminal glycine residue by a stable amide bond. In the prenylated protein, the 15-carbon isoprenes farnesyl and 20-carbon geranylgeranyl are attached to the C-terminal end of cysteine residue by thioether bond. The attachment glycosylphosphatidylinositol (GPI) anchors is another type of lipid modification, which occur in the lumen of the secretory pathway. In this lipid modification, the phosphatidylinositol attached to the protein through a carbohydrate linker.[71,72]
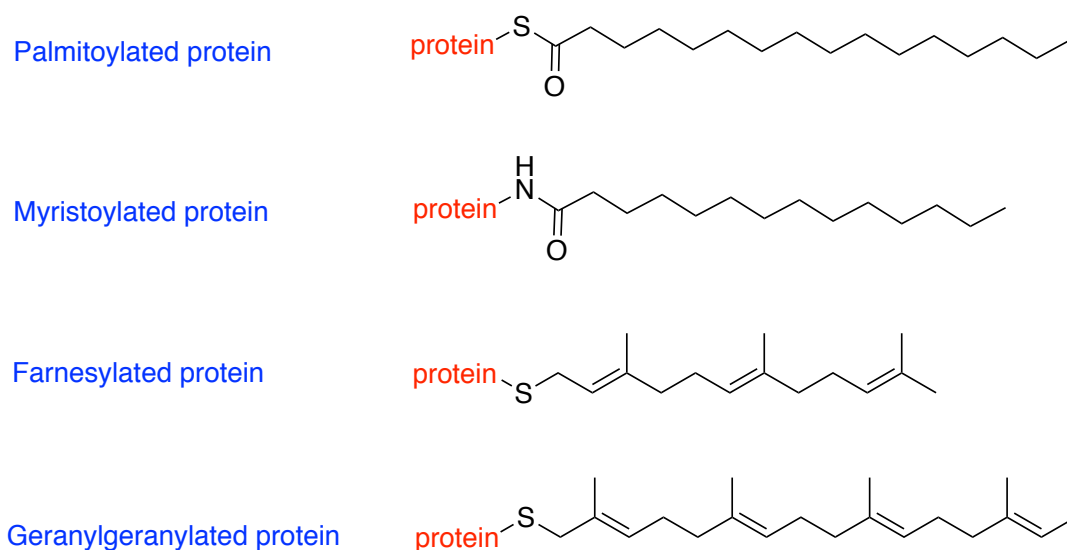
Figure 15: Examples of lipid modifications of protein.[72]

1.5.2.3 Protein Phosphorylation

Protein phosphorylation is one of the most important and well-studied areas of post-translational modification. It is estimated that one-third of mammalian proteins are substrates for phosphorylation. Protein phosphorylation plays a significant role in the regulation of many cellular processes such as cell cycle, growth, apoptosis, differentiation, transformation, development, peptide hormone response, adaptation and signal transduction pathways.[73] It is considered the most common mechanism for regulation of transmission of signals throughout the cell, where kinase-catalysed phosphorylation of downstream proteins results in conformational changes that can regulate, for example, catalytic activity.[74,75]

Although protein phosphorylation is the most common post-translational modification for regulating protein function, only three amino acid side chains (in eukaryotic cells) are stably phosphorylated, which are serine, threonine and tyrosine. It is a reversible modification that is mediated by kinases for phosphorylation of substrates and phosphatases for dephosphorylation of substrates. During phosphorylation the nucleophilic hydroxyl groups of these three amino acids attack the terminal phosphate group (γ-PO_3^{2-}) on the universal phosphoryl donor adenosine triphosphate (ATP) causing transfer phosphate group to the amino acid side chain (figure 16). Magnesium (Mg^{2+}) facilitates this transfer by chelating the γ- and β-phosphate groups to lower the threshold for phosphoryl transfer to the nucleophilic ($^-$OH) group.[74,76]
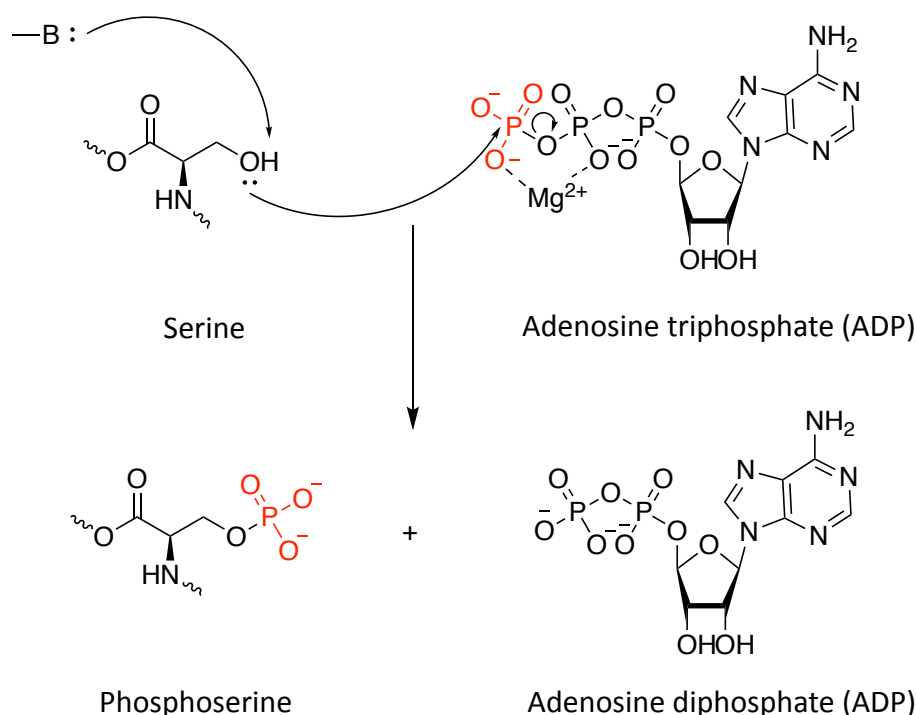
Figure 16: Mechanism of protein phosphorylation.[74]

1.5.2.4 Protein Tyrosine Sulfation

The sulfation of tyrosine residues is a common post-translational modification that was first discovered in bovine fibrinogen, with the estimated level of tyrosine sulfation in eukaryotic proteins being about 1% of total tyrosines.[77,78] The sulfation of tyrosine residues is catalyzed by tyrosylprotein sulfotransferase (TPST) and takes place in the Golgi apparatus. The tyrosylprotein sulfotransferase (TPST) catalyses protein tyrosine sulfation by transfer of an activated sulfate from 3'-phosphoadenosine-5'-phosphosulfate (PAPS) to the hydroxyl group of tyrosine residues in proteins or peptides to form a tyrosine O-sulfate ester and 3'-phosphoadenosine-5'-phosphate (PAP) (figure 17). There are two TPST isoforms in human, TPST1 and TPST2, which share 64% amino acid sequence identity and some common enzymatic characteristics.[79,80,81,82]
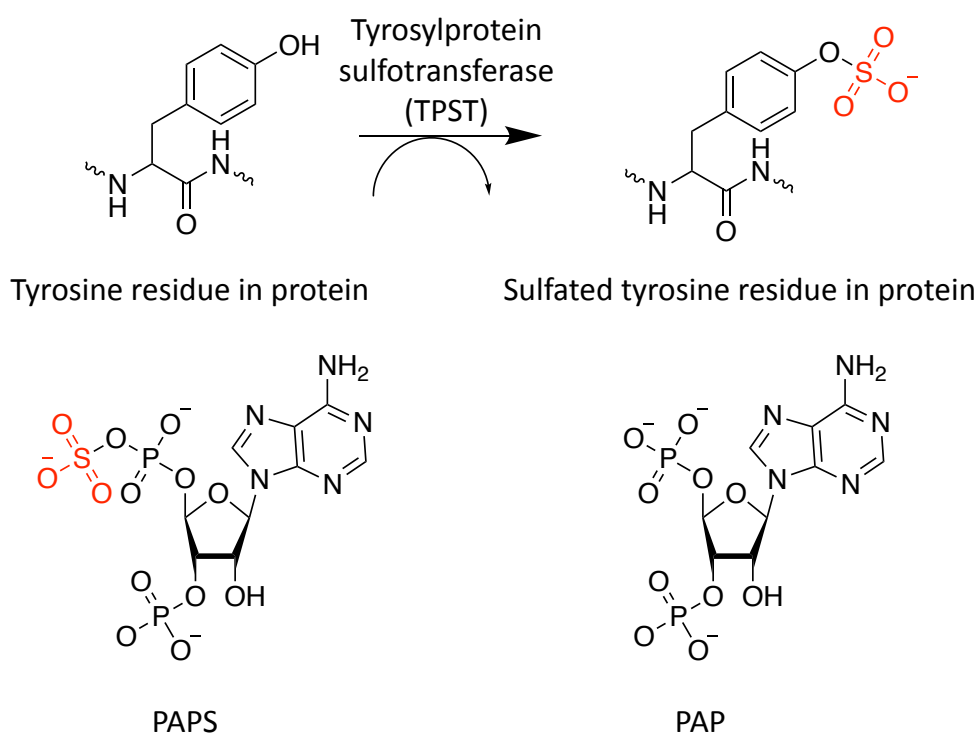
Figure 17: Protein tyrosine sulfation, catalyzed by tyrosylprotein sulfotransferase (TPST).[80]

The sulfation of tyrosine residues often occurs in secreted and transmembrane proteins that and plays important roles in the regulation of intracellular trafficking and proteolytic processing of secreted proteins. It is a key modulator of protein-protein interactions that plays important roles in some biological process include hemostasis, inflammation, viral entry into cells, leukocyte rolling on endothelial cells, visual functions, and binding of several chemokine receptors with the chemokine ligands by recognising sulfated proteins.[83,84,85] As a result protein tyrosine sulfation plays important roles in several diseases such as HIV infection, lung diseases, autoimmune response, multiple sclerosis and cellular enzyme regulation.[86] For example, tyrosine sulfation of chemokine receptor CCR5 leads to viral attachment and invasion in HIV-1 infection of T cells, therefore it suggested that the inhibition of protein tyrosine sulfation of CCR5 can block the HIV-1 cellular entry.[86]

1.5.3 Synthetic approaches to protein post-translation modification

The usage of both genetic and chemical methods allows the preparation of an almost unlimited number of protein constructs with either natural or synthetically modified residues. The natural modifications of proteins (by introducing natural PTMs) are highly efficient and controlled, which allow studying the specific protein functions, however they are generally undertaken by enzymes with high substrate specificity, limiting the application of these biological processes to a broader range of systems. The synthetic modification of proteins provides a key tool to study the specific proteins functions and intervening biological systems both *in vitro* and *in vivo*. The introduction of bio-orthogonal unnatural amino acids improves the properties of unnatural PTMs during isolation, analysis, and processing and provides site-selective modification of proteins.[87]

The different methods of chemical modification provide an opportunity to decide which residue to target and which type of modification, in order to provide a desired protein properties and functions such as affinity probes, fluorophores, reactive tags.[24] For instance, the attachment of single chain or branched chains of polyethylene glycol (PEG) groups to therapeutic proteins in process called pegylation leads to increased circulation half-life of a therapeutic protein. However, there are still many challenges in the chemical modification field including synthesis, processing, manufacturing, stability and safety.[54,88]

The selective synthetic modification of complex proteins represents a significant chemical challenge because the reaction must modify the targeted residue selectively in the presence of other competing unprotected polypeptide side chains (carboxylic acids, amides, amines, alcohols and thiols). This selectivity needs to occur under specific conditions (aqueous media,

low temperature and neutral pH) in order to prevent denaturation of the protein. Furthermore, salts and surfactants must be tolerated during the reaction in order to maintain the stability of the protein. In addition, the reactions have to be rapid in order to achieve full conversion of protein due to the likely low concentration of protein.[54,88,89]

1.5.4 Selective modification of natural amino acids and unnatural amino acids

The abundance of functional groups in natural amino acids play a critical role in determination selectivity and hence precision. Strategies of site-selective reaction may be possible by targeting functional groups with low abundance on the protein surface. Nucleophilic amino acids (mainly cysteine (Cys) or lysine (Lys) residues) are usually targeted by classical protein bioconjugation methods (figure 18).[54] However, the selectivity in natural amino acids is limited because many of the functional groups in proteins are nucleophilic. In addition, the high abundance of functional groups can generate mixtures of many products.[90]
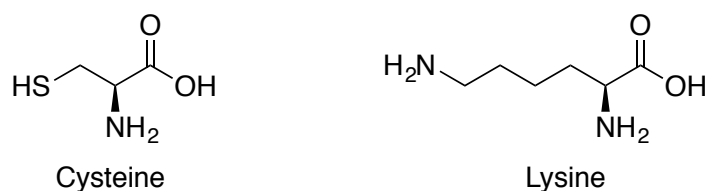
Figure 18: Cysteine and lysine structures.

Limitations of selective modification of natural amino acids can be addressed *via* inclusion of unnatural amino acids into the peptide sequence. This approach can solve the selectivity issue because it can allow the introduction of unique bio-orthogonal functional groups, for example, azide-, arylhalide-, alkyne-, and alkene-containing amino acids, which can be modified selectively under biocompatible reaction conditions. These reactions typically depend on metal catalysts such as copper catalysed alkyne-azide cycloaddition (CuAAC), Ru-catalysed olefin metathesis, and Pd-catalysed cross-coupling. However, unnatural amino acid

modification is limited by methods of the installation of these bio-orthogonal functional groups.[91,92]

1.5.5 Cysteine modification

Despite the growing body of methods for modification of a range of natural amino acid side chains including tyrosine,[93] tryptophan,[94,95] lysine[96] and methionine,[97] cysteine remains the most commonly targeted residue for selective modification.[87,98] This is due to the presence of the sulfhydryl side chain, which is a strong nucleophile, and because of the low abundance of cysteine on peptide surfaces in comparison with other reactive amino acids such as lysine.[99,100] There are different reactions of cysteine that are widely used for protein modification, which are alkylation, oxidation, disulphide formation, desulfurization, oxidative elimination and metal-mediated modification at cysteine, which generally exploit the 'soft' nucelophilic nature of thiols to enhance selectivity over 'hard' nucleophiles such as the amine side chain of lysine.[54] A nucleophile is a chemical moiety that donates a pair of electrons to form a new covalent bond with its reaction partner (the electrophile). They are molecules like NH_3 or ions like OH^- that have at least one lone pair of electrons or one σ-bond. Because nucleophilicity is defined as the affinity of nucleophile to nuclei, they are regarded as Lewies bases. Therefore, nucleophilicity represents the capacity of Lewis base to take part in a nucleophilic substitution reaction and differs from basicity which is measured by monitoring the position of an equilibrium reaction with a proton donor (usually water). Nucleophilicity describes rates of substitution reaction trends that are ascribed to nucleophile properties, however there is no unified scale to measure nucleophilicity as the relative nucleophilicity of any species varies toward different electrophiles. However, some indication can be given about the structural features that control nucleophilicity and the relationship between

nucleophilicity and basicity to get a better understanding about how the structure of the nucleophile (base) and reactant affect the two competing reactions.[101,102] The most important factors influencing nucleophilicity are those measured regarding an S_N2 mechanism in which the properties of the nucleophile are very important, as the rate of an S_N2 reaction is directly linked to the nucleophilic displacement of the leaving group, whereas the rate of an S_N1 reaction is not affected by relative nucleophilicity.[103] There are many factors that influence the behaviour of nucleophiles, the most significant factors amoung these are listed below.[104]

(1) nucleophile solvation energy: Nucleophiles with strong solvation means the anionic nucleophile have lower energy compared to the TS, in which the Ea is increased due to greater diffusion of the charge. The two different obtained trends depend on the type of solvent. In polar protic solvents (table 3) nucleophilicity increases as we go down the periodic table (table 3). This, because at the top of periodic table the capacity of hydrogen bonding is the highest hence the nucleophile is more hindered during solvation.[105]
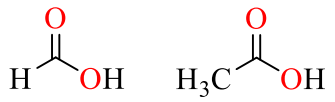
Nucleophiles	Polar protic solvents
I⁻ > Br⁻ > Cl⁻ > F⁻ Strongest weakest ⁻SeH > ⁻SH > ⁻OH	H_2O CH_3OH CH_3CH_2OH

Table 3: Strength of some nucleophiles in polar protic solvents.

In polar aprotic solvents (table 4), hydrogen bond formation with the nucleophile is insignificant. As a result, nucleophiles have more freedom to attack and nucleophilicity increases up the periodic table (table 4).[106]

Nucleophiles	Polar aprotic solvents
I⁻ < Br⁻ < Cl⁻ < F⁻ weakest Strongest ⁻SeH < ⁻SH < ⁻OH	$H_3C-C\equiv N$ (dimethyl sulfoxide) (acetone) (N-methylformamide)

Table 4: Strength of some nucleophiles in polar aprotic solvents.

(2) The strength of the bond formed with carbon: Since S$_N$2 is regarded more important, the strength of the partially formed new bond with carbon results in lower Ea and more stable TS.[101]

(3) Electronegativity of the attacking atom: High electronegativity is unfavorable because the SN2 process requires donation of electrons to an antibonding orbital of the electrophile (figure 19).[101]

$$CH_3^- > NH_2^- > OH^- > F^-$$

$$NH_3 > H_2O > HF$$
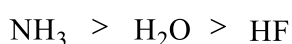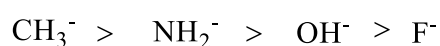
Figure 19: Strength of some nucleophiles according to their electronegativity.

(4) Polarizability of the attacking atom: Polarizability explains how the electron density of the nucleophile is easily distorted. Since bond formation by an electron pair from the nucleophile is required by S$_N$2 reaction, therefore better nucleophilicity is achieved by easier distorted the attacking atom. This means nucleophilicity increases with increasing electron density on the attacking atom (figure 20).[101]

$$OH^- > H_2O \qquad NH_2^- > NH_3 \qquad HS^- > H_2S$$

$$H_3C\text{-}CO\text{-}O^- > H_3C\text{-}CO\text{-}OH \qquad C_6H_5\text{-}O^- > C_6H_5\text{-}OH$$
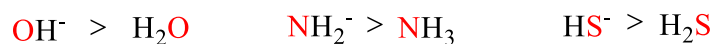
Figure 20: Strength of some nucleophiles according to electron density.

(5) Steric bulk of the nucleophile: less hindered nucleophile is more reactive than sterically congested one because in the TS nonbonded repulsions are developed. In the TS the trigonal bipyramidal geometry is sterically more demanding than the tetrahedral reactant in S_N2. The bulkier the nucleophile is the slower the rate of the reaction (figure 21).[101]

$$H_3C\text{-}O^- > H_3C\text{-}CH_2\text{-}O^- > (H_3C)_2CH\text{-}O^- > (H_3C)_3C\text{-}O^-$$

Least bulky   Most bulky
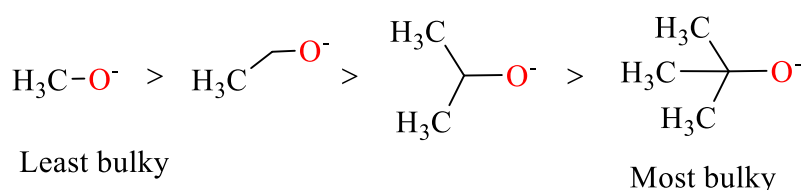
Figure 21: strength of nucleophiles according to their bulkiness.

While this aids understanding of relative reactivity and demonstrates some contrasting properties that can result in increased or decreased reactivity, as mentioned above the nature of the relative nucleophiles and electrophiles also influence the rate, and therefore the selectivity, of such reactions. The most effective qualitative method for making predictions about reactivity is based on the observation that reactions occurs most readily between species that have equivalent strength of 'hardness' and 'softness', although these terms are not firmly defined (see table 5). Hard nucleophiles have their reactive electron pair in smaller orbitals in the lower shells of more electronegative atoms, and are often highly charged or more basic in nature. These nucleophiles interact most readily with smaller and are more

reactive towards more positively charged electrophiles, for example smaller metal ions or highly δ-positive carbon electrophiles. Soft nucleophiles have their reactive electron pair in larger orbitals in the higher shells of less electronegative atoms, and are likely to be less charged charged or less basic in nature. Soft nucleophiles interact most readily with larger metal ions and favourably react with less δ-positive carbon electrophiles and π systems.[101,107]

Strength	Nucleophiles (Bases)	Electrophiles (Acids)
Soft	CO, C_2H_4, R_2S, RSH, CN^-, I^-, $(CH_3CH_2)_3P$, $RCH=CHR$, benzene	I_2, Br_2, $RS\text{-}X$, $RSe\text{-}X$, $RCH_2\text{-}X$ $Cu(I)$, $Ag(I)$, $Pd(II)$, $Hg(II)$ Zero valent metal complexes
Intermediate	$ArNH_2$, C_5N_5N, NO_2, Br^-, N_3^-, Pyridine	$Cu(II)$, $Zn(II)$, $Sn(II)$ R_3C^+, R_3B^+
Hard	H_2O, RNH_2, OH^-, SO_4^{-2}, R_2O, F^-, Cl^-, RO^-, RCO_2^-, NH_3, NO_3^-	$H\text{-}X$, Li^+, Na^+, $R_3Si\text{-}X$ $Mg(II)$, $Ca(II)$, $Al(III)$, $Sn(IV)$ $Ti(IV)$, H^+

Table 5: List of some nucleophiles according to their strength with their corresponding electrophiles.

1.5.6 Cysteine alkylation

The most common technique for cysteine modification is the direct alkylation of its nucleophilic thiol with suitable electrophiles. The selective reaction of cysteine with electrophiles such as α-halocarbonyls (e.g., iodoacetamide or chloroacetamide) and Michael acceptors (e.g., maleimides or vinyl sulfones) has been known for almost a century.[88] If

surface cysteines are not present in the natural protein or are not found in the region of the protein that is to be labelled they can be readily introduced via expression of recombinant DNA in standard expressions systems.[54, 44]

1.5.6.1 α-halocarbonyls

The alkylation of cysteine with iodoacetamide (scheme 2) has been widely used in protein analysis by mass spectrum, peptide mapping of cysteine containing proteins and protein modification.[108,109,110,111,112] Although iodoacetamide reacts more rapidly with the cysteine thiol than lysine amine, undesired reaction with lysine has been noticed when the pH >7-8, which can be resolved by adjusting the pH and reaction time or using less reactive chloroacetamide.[108] The undesired reaction with lysine N terminal can be avoided by reducing the reaction pH to less than 7-8 in order to protonate the nucleophilic amine.[108,110]
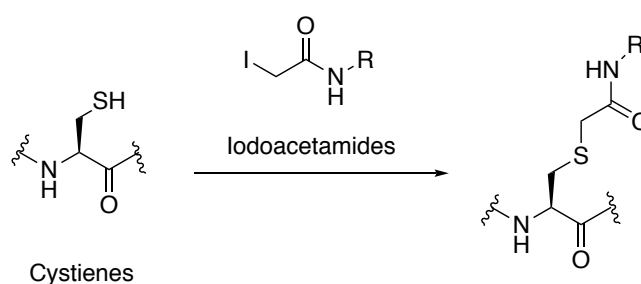
Scheme 2: Alkylation of cysteine using iodoacetamides.

Robinson and his co-workers compared the selectively of iodoacetamide and chloroacetamide to alkylate cysteine in the presence of another nucleophilic amino acids.[113] They demonstrated that both iodoacetamide and chloroacetamide are able to alkylate cysteine, however chloroacetamide is more specific than iodoacetamide, which showed low level of off-target modifications to the N-terminus along, Asp, Glu, His, Lys, Ser, Thr, and Tyr residues (figure 22). [113] For example, the off-target modification of chloroacetamide at the

N-terminus alone is about 0.05% while the off-target modification of the iodoacetamide at the N-terminus is about 0.5 %. However, the average overall level of off-target alkylation with both alkylation reagents was <0.5% which is relatively low.[113] Although there was a minor difference between the two alkylation reagent in the off-target alkylation, there was a significant differences in levels of oxidation between the two alkylation reagents. The oxidation level of the methionine and tryptophan was greatly increased with chloroacetamide in comparison with iodoacetamide (figure 23). For example, the average of the oxidised methionine in all peptides containing methionine in the presence of chloroacetamide is about 28.7 %, while the average of the oxidised methionine in the presence of iodoacetamide is about 3.4 %.[113]
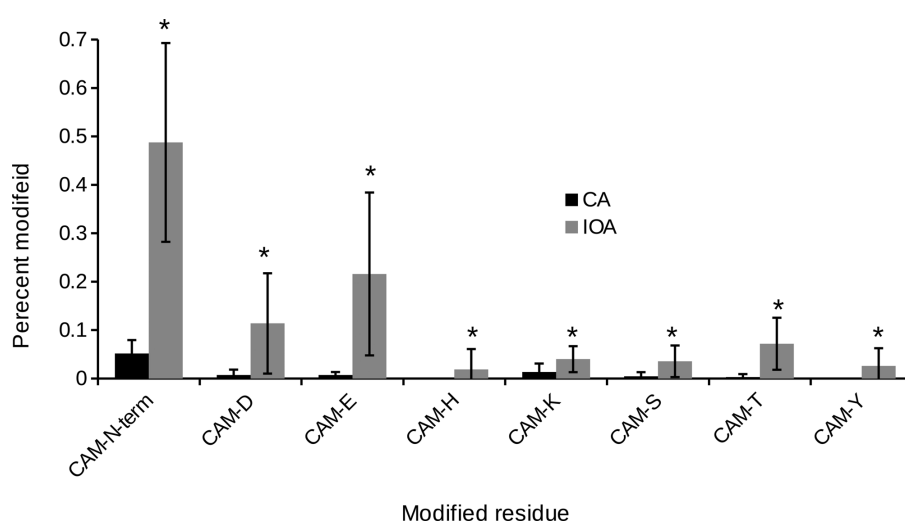
Figure 22: The comparison between iodoacetamide (IOA) and chloroacetamide (CA) off-target modification.[113]
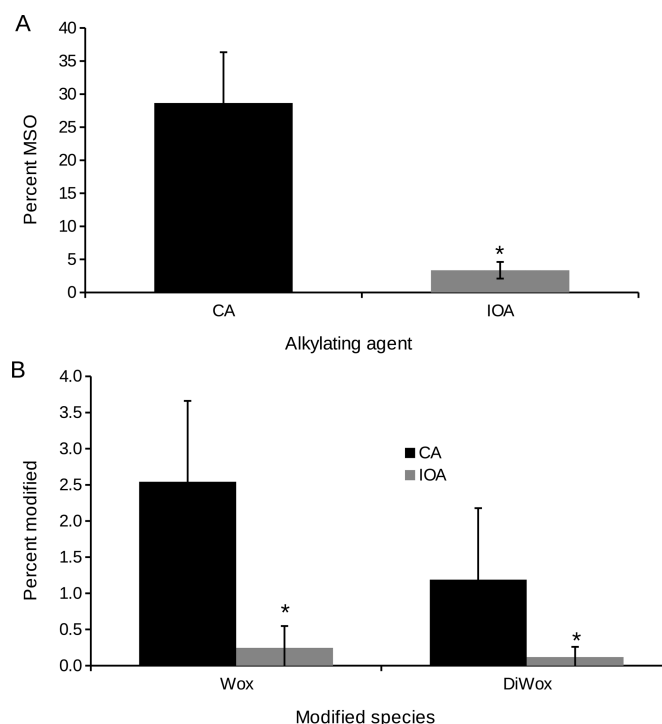
Figure 23: The comparison between iodoacetamide (IOA) and chloroacetamide (CA) oxidation level. (A) the percent of oxidised methionine (MSO). (B) the percent of singly oxidised Tryptophan (Wox), and the dioxidised form of Tryptophan (DiWox).[113]

Carbohydrate-tethered iodoacetamides can be used to glycosylate protein selectively by reaction with cysteine side chains to offer the cysteine-sugar linkages, which mimics to the natural asparagine-linked glycoproteins.[114] This methodology has been used to investigate the glycosylation effect on the thermal stability of dihydrofolate reductase (DHFR) which is naturally non-glycosylated enzyme.[115] In addition, ß-N-glycosyl iodoacetamides have been used to glycosylate human erythropoietin to study the effect of the glycosylation on the structure and function of the human erythropoietin.[116]

Sunbul and co-workers alkylated proteins with a chloroacetamide-appended fluorophore in order to study the target proteins role in biological systems by fluorescence microscopy.[117]

The TR512 peptide attached to two cysteine residues to offer a Reactive Texas Red binding (ReacTR) tag was conjugated to the maltose binding protein (MBP),[117] using fluoresence to quantify the formation of a covalent bond between the N-α-chloroacetamide-Texas Red fluorophore and cysteine of MBP-ReacTR.[117]

Cysteine alkylation with α-halocarbonyl electrophiles has been used to introduce ester carbonyls as infrared (IR) probes in peptides and BSA to study peptide structure integrity and ligand binding that induce changes in the local hydration status of BSA.[118] Although the ester moiety can be introduced simply in the protein by using solid-phase synthesis, the cysteine alkylation methodology used to introduce ester moiety in the specific site of the large protein.[118] Therefore, methyl bromoacetate was used to alkylate cysteine in peptides and proteins under mild conditions to introduce methyl ester in high yield (scheme 3).[118]
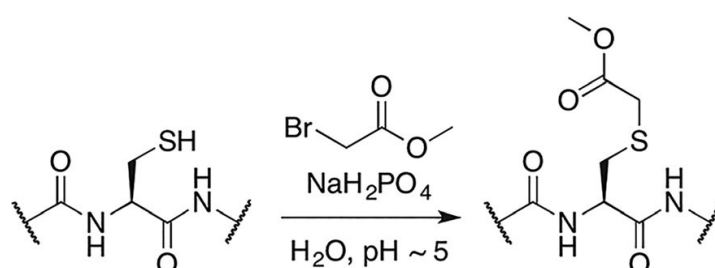
Scheme 3: Installation the ester carbonyl (IR probe) into proteins at cysteine.[118]

1.5.6.2 Michael Acceptors

The chemoselective cysteine alkylation by Michael acceptors has been used widely.[54] The most used Michael acceptors used for cysteine alkylation are maleimides and vinyl sulfones. Maleimide reagents are used in protein analysis by blocking the sulfhydryl groups, peptide mapping of cysteine containing proteins and protein modification in various applications, including the preparation of approved ADCs.[119,120] Maleimide reagents are used in chemical

protein modification because they are highly selective towards thiol groups with lack of side products (scheme 4). Moreover, the nitrogen atom of maleimide moiety can be functionalised with different groups such as fluorophores, polymer moieties and lipids. Some of the antibody-containing therapeutics that are already on the market are formed by maleimide–thiol conjugation. For example, certolizumab pegol (Cimzia) is an anti-TNF antibody fragment which is conjugated to polyethylene glycol through succinamide thioether linkages to extend in vivo half-life.[121] Cimzia has been approved by FDA for Crohn's disease and rheumatoid arthritis treatment.[121]
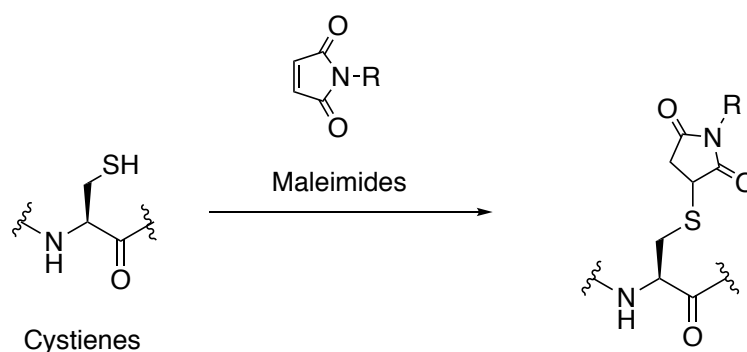
Scheme 4: Alkylation of cysteine using maleimides.

Although the succinimide thioethers are stable, they are sensitive to oxidative/reductive environments under near-physiological conditions. The potential for cleavage by retro-Michael addition is the main disadvantage of the succinimide thioethers, which leads to formation of the free maleimide in solution (scheme 5) followed by thiol exchange by endogenous thiol in blood plasma (GSH).[122] Hydrolysis is another side reaction that can occur to the succinimide thioethers, leading to ring opening. However, the ring opening after conjugation is in fact a preferred outcome in therapeutic applications because it provides stable adducts. The substituents on the ring effect on the hydrolysis of the succinimide

thioethers, the electron-withdrawing N substituents increase the hydrolysis, while the electron-donating N substituents minimise the hydrolysis process.[99]
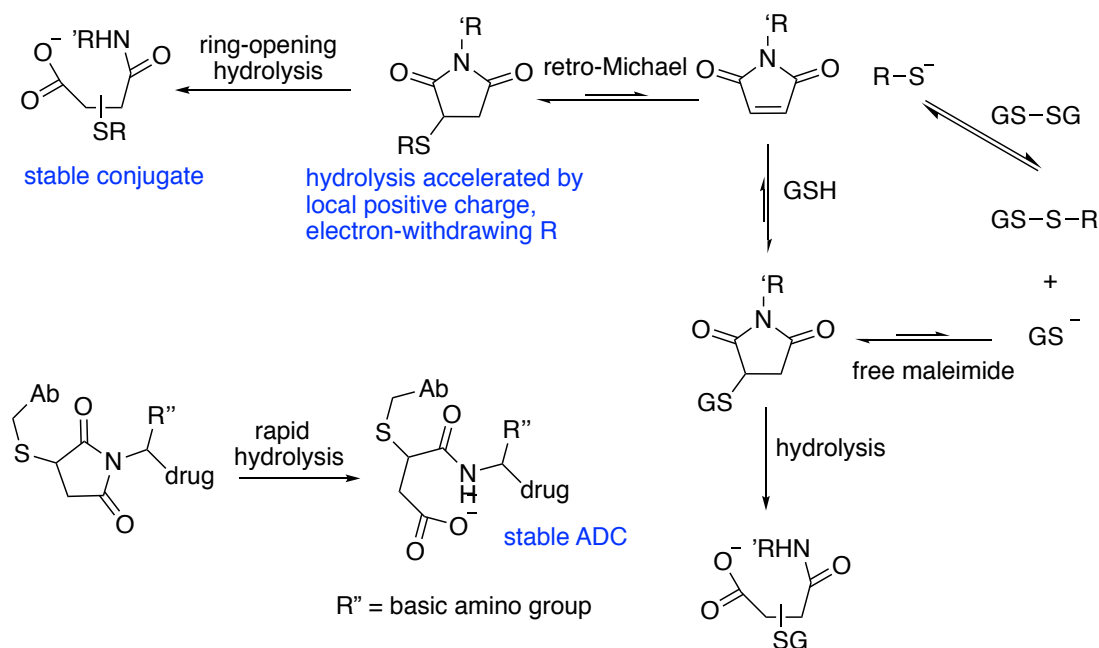
Scheme 5: The thiol exchange of maleimide- thiol conjugates with GSH and the ring opening by hydrolysis.[99]

Another limitation of maleimides in protein modification is that while conjugation is partly reversible, regeneration of the unmodified protein by controlled disassembly of the conjugate is impossible.[123] That can be solved by using of bromomaleimide derivatives which provide selective and reversible conjugation with cysteine.[123] They allow formation of stable conjugates of thiolates, which can be easily cleaved upon reaction with phosphines (e.g. TCEP) or a large excess of a thiol (scheme 6).[123] In addition, further attachment of functional groups to the protein-maleimide adducts is possible by using (di-)bromomaleimide derivatives, the second thiol reacts with the protein-maleimide adducts to form succinimide conjugates

(scheme 6).[123] In addition to the N substituents on the maleimide ring, the bromomaleimide derivatives provide three points of protein conjugation.[123]
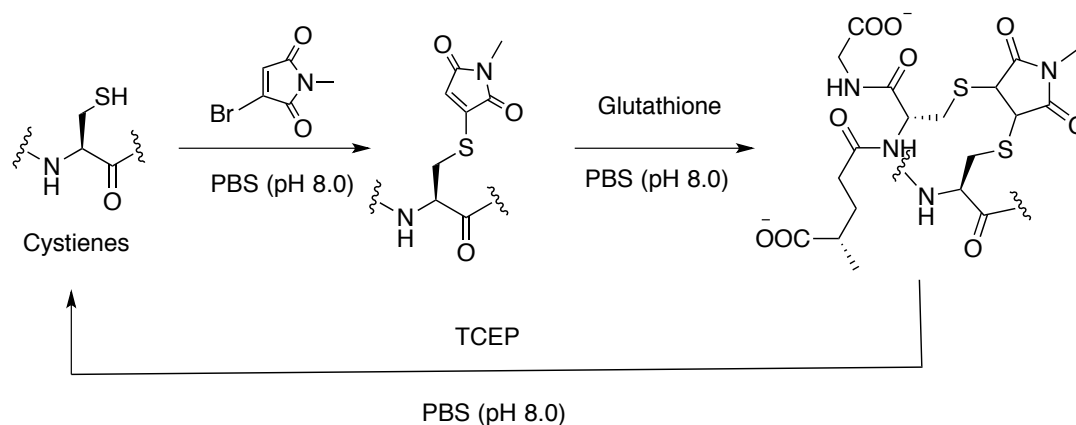
Scheme 6: Conjugation of bromomaleimide with cysteine.

The first example of using maleimide for cysteine alkylation in proteins was introduced by Moore and Ward where the disulfide bonds were reduced then bis-maleimides were used to cross-link cysteine in proteins.[124] The chemoselective cysteine alkylation with maleimides have been used to glycosylate hemoglobin (Hb) which provide higher oxygen affinity.[125] In addition, the maleimide conjugation was used in synthesis of cancer vaccines.[126] Haralampiev et al. recruited sulfhydryl-containing biomolecules to membranes by using palmitic acid functionalized with a maleimide moiety (PAEM) and applied to recruit proteins to lipid vesicles and biological membranes.[127] Inclusion of a rhodamine-label allowed detection and monitoring of certain membrane processes (figure 24).[127]
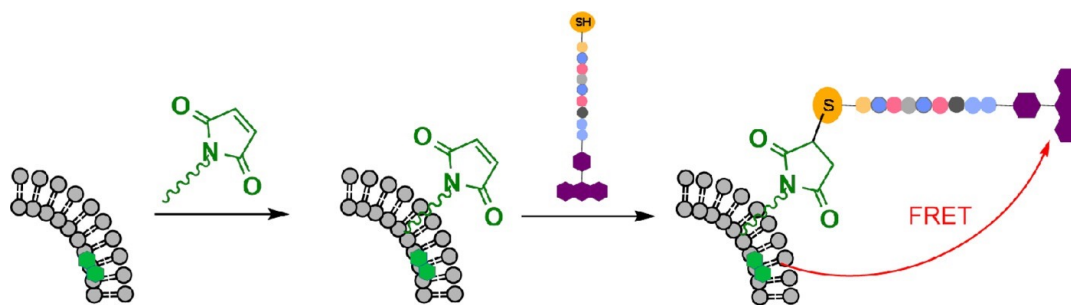
Figure 24: Recruitment of rhodamine-labeled peptide RLP to membranes using palmitic acid functionalized with a maleimide moiety (PAEM). The lipid membrane was prepared to contain a donor fluorophore then the Forster Resonance Energy Transfer (FRET) between two fluorophores used to determine the binding of PAEM and RLP.[99]

Oxytocin is a peptide hormone that is used to prevent postpartum haemorrhaging (PPH) after childbirth.[128] Oxytocin prevent blood loss post-birth by causing contraction of the uterus, however, it is degraded at higher temperature, causing a loss of drug activity.[128] The degradation of oxytocin occurs through several processes, the most significant of which is cleavage of its disulfide bond.[128] It has been found that reduction of the disulfide bond in oxytocin followed by disulphide 're-bridging' using dithiophenol maleimide, (that was further functionalised with a polymer) significantly increased the stability of the oxytocin at elevated temperatures (scheme 7).[128]
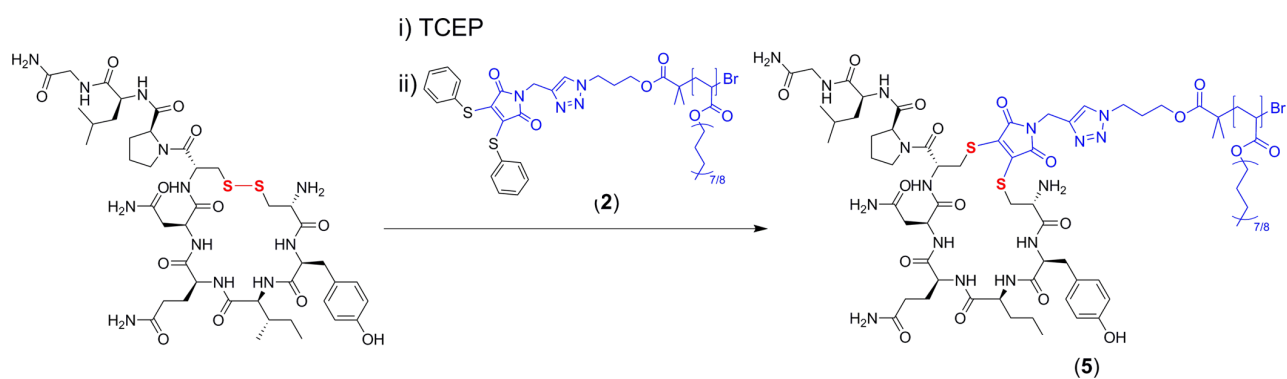
Scheme 7: The reduction and conjugation of the therapeutic oxytocin peptide with maleimide functional polymer.[128]

1.5.6.3 Aminoethylation

Cysteine aminoethylation can be used to convert cysteine to lysine mimics, allowing controlled investigation of the role of lysine in protein function.[129] Mecinovic and co-workers installed trimethyl lysine analogs into histone proteins by cysteine alkylation, leading to cysteine-trimethyllysine analogs that are close to the natural methylated lysine (scheme 8).[130]
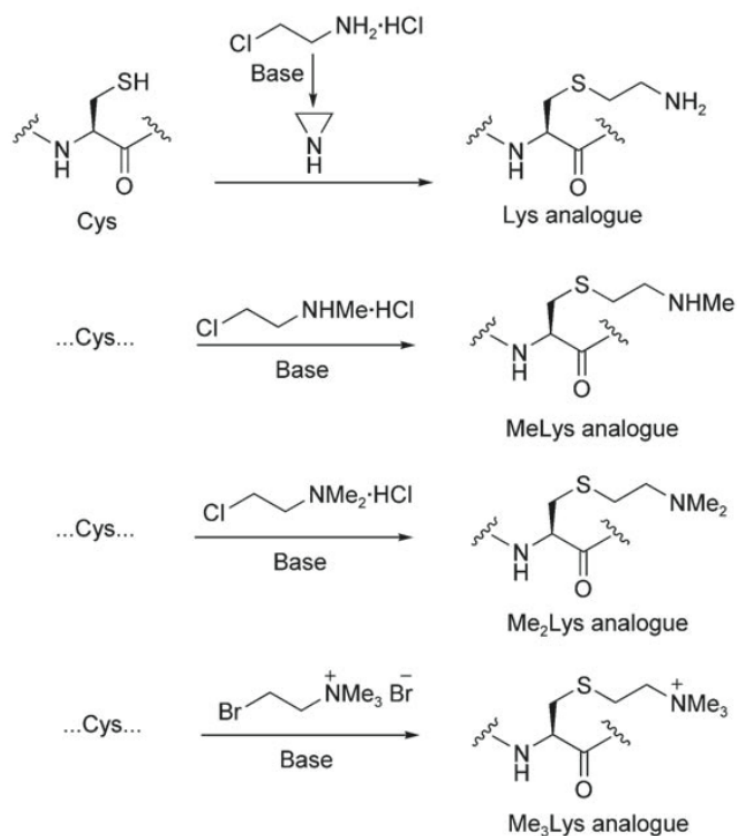
Scheme 8: Cysteine aminoethylation to prepare lysine mimics.

The cysteine alkylation can also be used to install acetyl-Lys mimics at specific sites of peptides and proteins as a model of protein acylation.[131,132] Methylthiocarbonyl-aziridine (MTCA) reacts selectively with the cysteine thiol to offer methylthiocarbonyl-thiaLys (MTCTK) which close to natural acylated lysine (scheme 9).[131] The mass spectrometric analysis confirmed that six different cysteine-containing peptides were completely converted to MTCTK, while no modification was observed in the Cysteine free peptide control which confirmed the high selectivity of MTCA to the cysteine thiol.[131]
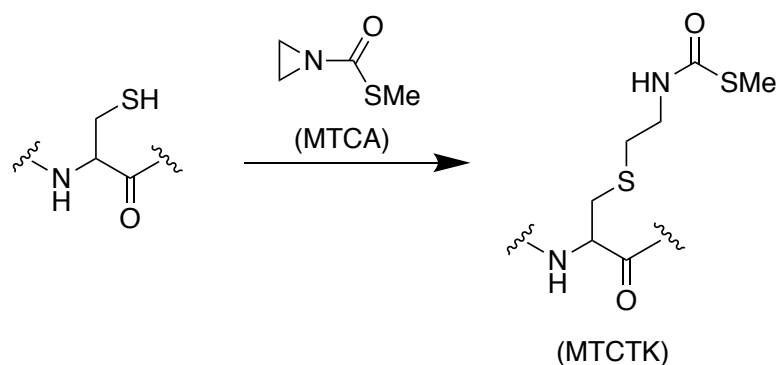
Scheme 9: Alkylation of cysteine with methylthiocarbonyl-aziridine (MTCA) to form

methylthiocarbonyl-thiaLys (MTCTK).[131]

1.5.7 Other Cysteine modification

1.5.7.1 Site-Selective formation of disulfides

Disulfides are essential in structure and stability of proteins and disulfide formation is one of

the most common natural cysteine modifications. Due to the critical role of glycoproteins in

mediating a variety of cellular processes, disulfide-linked glycoproteins provide an

opportunity to assess glycoprotein function. Although a mixed disulfide can be formed by air

oxidation of a mixture of a thiol and a cysteine-tagged protein, the reaction will also form

unwanted symmetrical disulfides.[133] However, cysteine reacts with methanethiosulfonate

(MTS), phenylthiosulfonate (PTS), or phenylselenenylsulfide (SeS) rapidly and specifically to

form mixed disulfides (or more stable SeS- linked conjugates) (figure 25).[134,135,136]
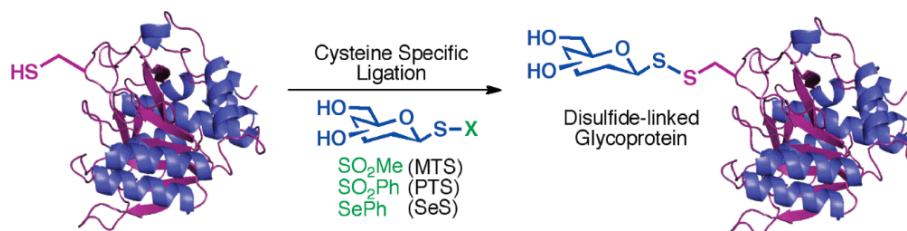
Figure 25: Disulfide-linked glycoproteins formed by site-specific cysteine modification. [133]

These reactions are used widely for the synthesis of glycoproteins due to highly efficiency of these reactions, which do not need a large excess of reagent. For example, glycodendriproteins and delicate trisulfide-linked glycoproteins are synthesised by this chemistry.[137,138] In addition, the selenenylsulfide method can be used to conjugate up to seven saccharide units in size at protein, which is a synthetic glycan attached to a protein.[136]

1.5.7.2 Formation of Stable Thioethers

Although disulfides are often stable *in vivo*, they are typically labile under reducing conditions. The conversion of the disulfide into stable thioether derivative facilitates the combination between the convenience of the disulfide modification and the benefit of the thioether stability. The reaction of electron-rich phosphines (e.g hexamethylphosphorus triamide (HMPT)) with disulfide glycoconjugates provides stable thioether derivatives (figure 26 A). The mechanism of the transformation of the disulfide to the stable thioethers proceeds by attack of the cysteine sulfur onto the aminophosphine, followed by elimination of the thiophosphonium ion to produce dehydroalanine. The liberated thiol can then add to dehydroalanine to give the thioether (figure 26 B).[133]
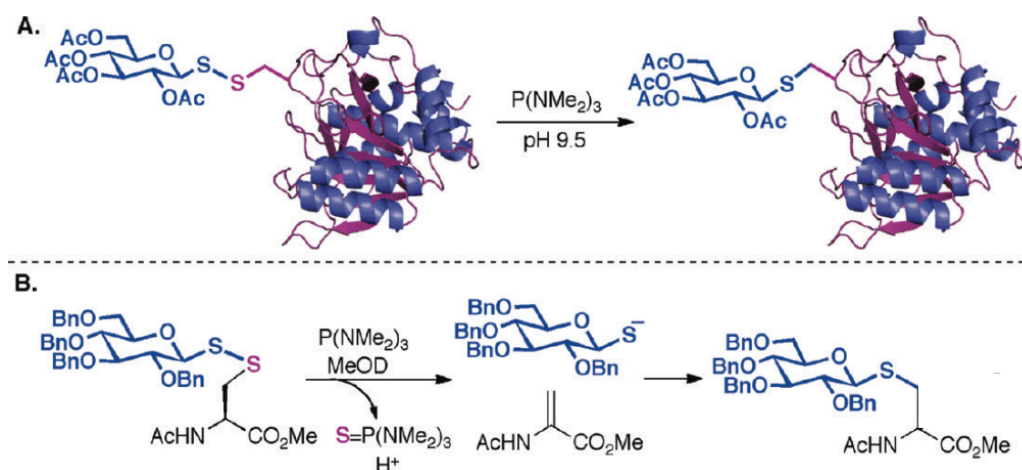
Figure 26: A- Disulfide conversion to the thioether-linked glycoprotein. B- A model for the transformation mechanism of the the disulfide into stable thioether derivative.[133]

Dehydroalanine also can be rapidly formed by treatment of cysteine with the electrophilic nitrogen source O-mesitylsulfonylhydroxylamine (MSH) (figure 27).[139] The use of dehydroalanine tag provides rapid and selective incorporation of a high range of post-translational modifications and their mimics, for example these methods can also be applied to introduce ^{18}F-fluorosugars as potential imaging labels.[140] In addition, these methods allowed preparation of PEGylated proteins, homogeneous glycoconjugate vaccine candidates, and histone mimetics.[141,142,143] On the other hand, the potential racemization at the site of modification and formation of D/L diastereoisomers limits the dehydroalanine tag approach.[144]
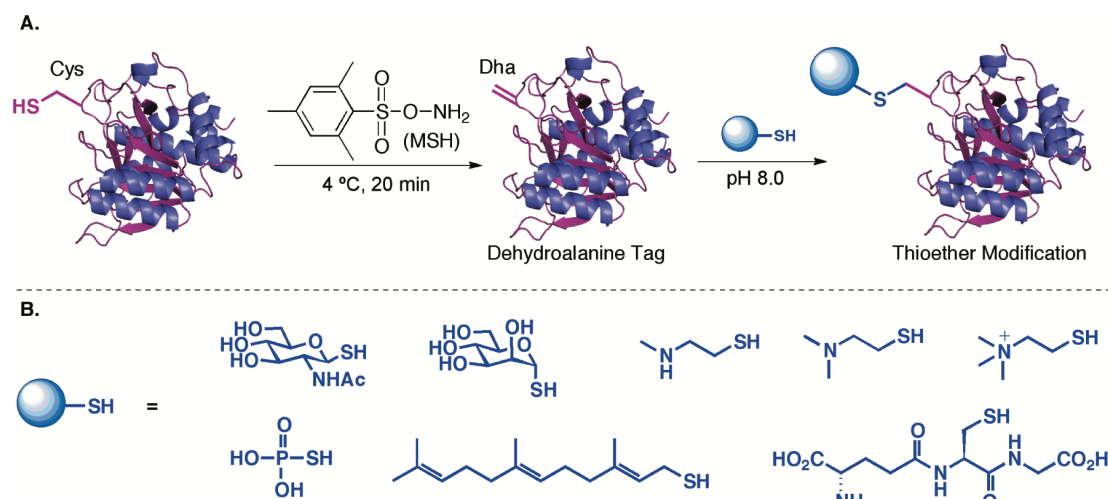
Figure 27: A- Conversion of cysteine to dehydroalanine by treatment of cysteine with O-mesitylsulfonylhydroxylamine (MSH) and use in synthesis of post-translational modifications and their mimics. B- different thiol groups for post-translational modifications.[133]

1.5.7.3 Metal-mediated natural modification at cysteine

One of the critical advances in synthetic protein modification allowed use of organometallic transformations in site-selective protein modification. These new approaches attracted synthetic chemist interest in protein modification because these reactions provide excellent functional group tolerance and high yields under mild conditions. On the other hand, there are several limitations of using these reactions for site-specific protein modification. It should be suitable for protein reaction conditions (aqueous media, high efficiency, and chemoselectivity at or near room temperature and over a narrow pH range). In addition, it should tolerate potential nonspecific binding to the Lewis-basic residues on protein surfaces.[90]

The gold-mediated oxidative allene–thiol coupling reaction is a new approach for selective cysteine modification in aqueous media, which is the first gold-mediated reaction use allenes for cysteine modification of peptides. In this reaction, gold complexes are used to activate

allenes diversity followed by coupling with the thiol group of cysteine-containing peptides that provides a novel hydroxy vinyl thioethers instead of 1,2/1,3-adducts, which is commonly observed (scheme 10). The highest conversion of allene is achieved by using AuCl/AgOTf as a catalytic system at room temperature. This method provides a direct functionalization of N-terminal, internal and C-terminal cysteine residues.[145]

Nucleophilic addition of allenes
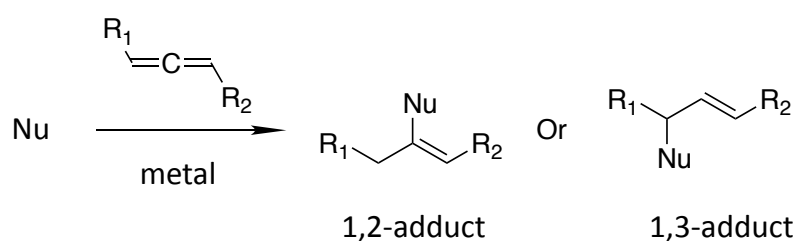
Gold-mediated selective cysteine modification of peptides using allenes
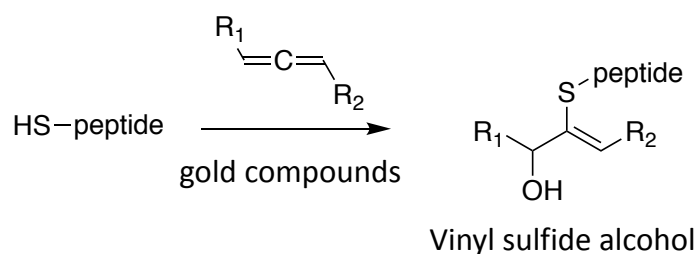
Scheme 10: Nucleophilic addition to allenes and Gold-mediated selective cysteine modification of peptides using allenes.

1.5.8 Cysteine modification in the preparation of therapeutic protein conjugates

The conjugation of cytotoxic drugs to antibodies in ADC preparation is typically achieved through modification of lysine side-chain amines or cysteine thiols, that are activated by reduction of interchain disulfide bonds.[146] However, these procedures leading to formation of heterogenous ADCs that contain a mixture of drug to antibody ratio (DAR) with linkages at different sites, which may impact on the efficacy and stability of ADCs profile.[146] The incorporation of engineered cysteine residues into specific site in the antibody can be used to produce a new ADC format with precise DAR.[147] Potent cytotoxic drugs can be attached to recombinant antibodies engineered with cysteine residues by using strategies of site-selective modification, typically based on those developed for the selective reduction of disulfides present in the natural antibody structure.[147] N-substituted maleimide linkers with a cleavable site for drug release are usually used to build antibody–drug conjugates (ADCs).[147] however, these methods are limited by the high cost and low expression yield.[148]

Chudasama and co-workers demonstrated that the insertion of the next generation maleimides NGMs (dithiomaleimide) into antibody disulfide bonds provide site-selective conjugation (figure 28).[148] In a comparison between the stability of the classical maleimide conjugate and NGM conjugates, neither were stable in blood serum due to the retro-Michael reaction that lead to transfer the payloads to serum albumin (figure 28).[148] However, the hydrolysis of the NGM conjugate to form a maleamic acid conjugate provides complete stability in blood serum (figure 28).[148]
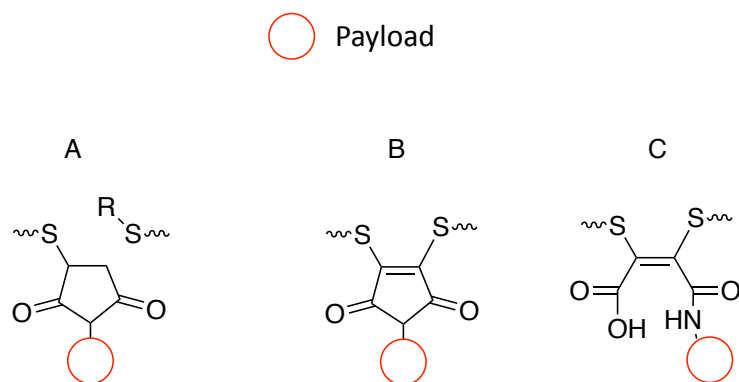
Figure 28: A- Classical maleimide with payload conjugate to antibody. B- NGM with payload conjugate to antibody. C- maleamic acid with payload conjugate to antibody.[148]

Spring and co-workers developed a novel divinylpyrimidine (DVP) linker to conjugate cytotoxics drugs to the native antibody by reduction of the disulfide bond followed by re-bridge of the cysteine residue (figure 29).[149] DVP conjugates provide highly stable ADCs with precise DAR and drug distribution at native antibody.[149]
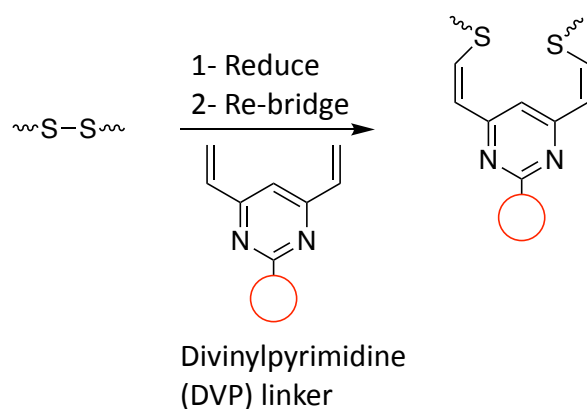
Figure 29: Antibody-drug conjugate ADC with divinylpyrimidine (DVP) linker.[149]

1.6 Disulfide reduction

The alkylation of cysteine thiols is complicated by the fact that free cysteines are isolated as mixtures of the reactive thiol alongside disulfides (as dimers or conjugates with other native thiols such as cysteine) and sulfinic/sulfonic acids (figure 30).[150] Therefore, reducing agents are used to selectively reduce these mixtures to the thiol form for alkylation. Reducing agents can be phosphines, such as *tris*(2-carboxyethyl)phosphine (TCEP) and tris(3-hydroxypropyl)phosphine (THPP) or thiols, such as dithiothreitol (DTT), dithiobutylamine (DTBA) and 2-mercaptoethanol (2-ME) (Figure 31).[151,91] The disulfide bonds are reduced by thiol–disulfide exchange in the thiol-containing reagent, while the phosphine reagent forms phosphine oxide after disulfide reduction (Figure 31).
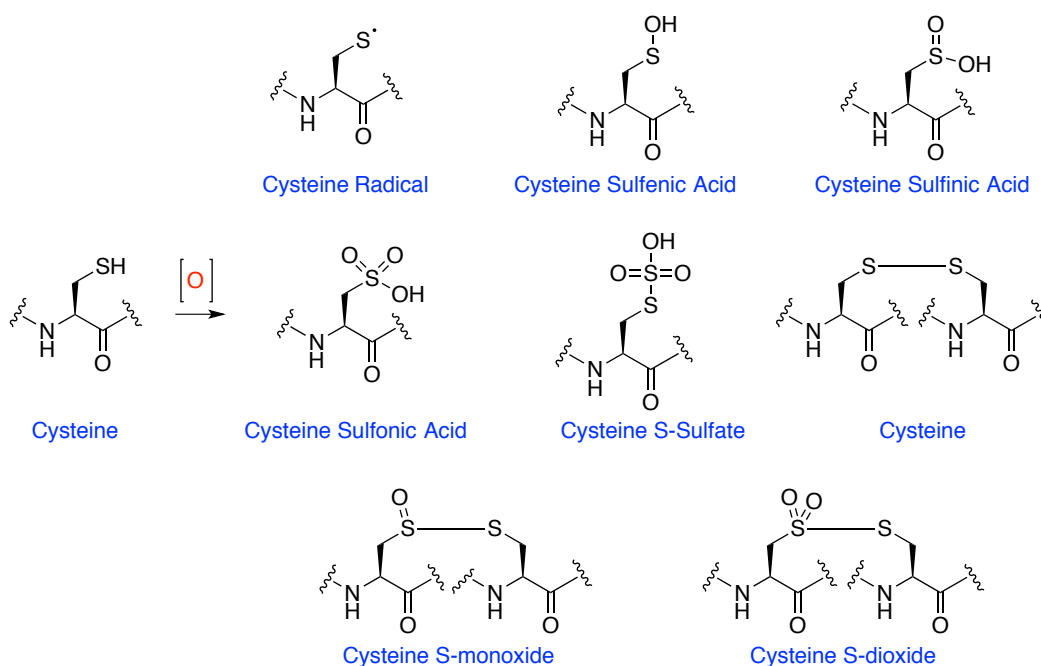
Figure 30: Common oxidised forms of cysteine.

2-ME   DTT   DTBA

TCEP   THPP

$$HS-R-SH + R`SSR` \longrightarrow HS-R-SSR` + R`SH \quad (1)$$

$$R_3P + R`SSR` + H_2O \longrightarrow R_3P=O + 2R`SH \quad (2)$$
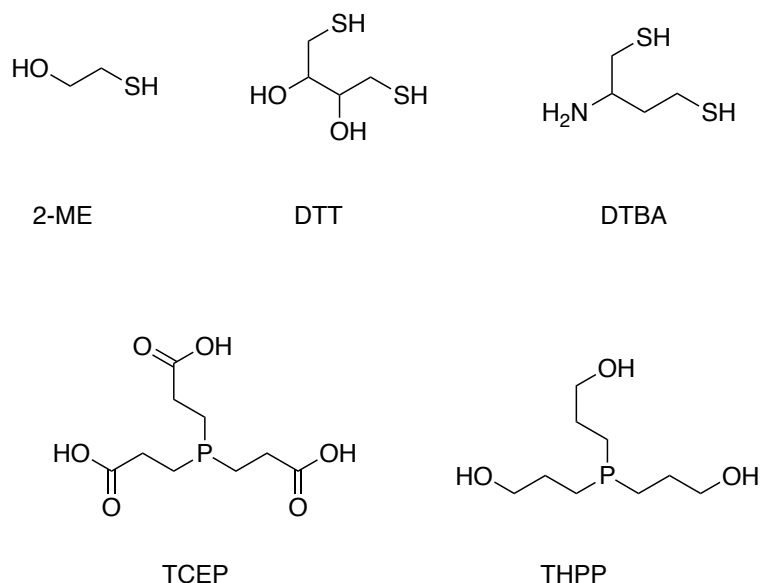
Figure 31: Structure of some thiol and phosphine reducing agents.

Suttapitugsakul and coworkers evaluated the reduction step of the cysteine disulfide with commonly used reducing agents; DTT, 2-ME, TCEP and THPP.[111] Peptides were incubated with the same concentration of each of these reducing reagents at 56 °C for 25 minutes, under these somewhat harsh conditions all four reducing reagents have the same efficacy to reduce disulfide bonds.[111]

The majority of thiol-reducing agents contain either nucleophilic phosphines or free thiols (DTT and DTBA), which can compete directly with the cysteine thiol for attachment of thiol-reactive labels such as maleimide and iodoacetamide derivatives. In addition, as they are used in excess this completing reaction will degrade both the alkylation agent and the reducing agent.[152] Although DTT is the standard reagent for reducing disulfide bonds between and within biological molecules, it's thiol groups are protonated at neutral pH and thus poorly

reactive. On the other hand, the pKa value of DTBA thiol is lower than DTT by about 1 unit, and this resides as the reactive thiolate at pH 7.0. As a result DTBA reduces disulfide bonds 3.5- fold faster than DTT in oxidised β-mercaptoethanol (βME) and 14- fold faster than does DTT in papain at pH 7.0.[151]

The trialkylphosphines derivatives reduce the disulfide bonds irreversibly due to the strength of the phosphorus-oxygen bond.[153] The low solubility of some of simple trialkylphosphines in water limited their usage, however, TCEP is a water-soluble phosphine agent that efficiently cleaves the disulfide linkage.[153] TCEP has been used extensively for disulfide reduction before cysteine alkylation for example Getz and his co-workers reported the using of TCEP in the attachment of maleimide to mysin.[154] In addition, TCEP has been used to study protein structure, for example, TCEP has been used to break the disulfide bond in the hen egg-white lysozyme (HEWL) model in order to study the folding and unfolding mechanism of protein.[155]

Although TCEP is normal used to break the disulfide bonds for protein analysis, the excess of TCEP can interfere with these methods. In addition, there are several reports proved that the presence of TCEP in the reaction medium can prevent the labelling of cysteine thiol because it can react with maleimide and iodoacetamide derivatives.[156] It has been reported the exposure to TCEP over prolonged time can cause cleavage in the protein backbone.[157] Therefore, TCEP is normally removed before any modification reaction, by using dialysis or gel filtration but these are time-consuming and can result in re-oxidation of the protein if oxygen cannot be excluded during this process. There are different alternative methods to separate TCEP such as immobilisation of TCEP on polyethylene glycol (PEG) beads, but it is effective just for small peptides.[156] Zwyssig and his co-workers developed a novel method to

separate TCEP by immobilization of the phosphine on magnetic nanoparticles with reduction capacity of 70 mmol per gram of particles.[156]

1.7 The aim of project

The aim of this project is to develop a robust system to reliably provide clean products of nucleophilic cysteine thiol alkylation, to allow us to synthesise CCL2-FK866 conjugates by utilising a recombinant CCL2-Cys construct. Alkylation of protein thiols is complicated by the free cysteine typically being isolated as mixtures of the reactive thiol alongside disulfides.[150] Therefore, reducing agents are used to selectively reduce these mixtures to the thiol form for alkylation, however prolonged exposure of CCL2 to phosphines such as TCEP will result in reduction of the functionally essential disulfides in CCL2.

Thiol-based reducing reagents are mild but must be removed before selective alkylation of cysteine otherwise they will compete with the target thiols in proteins. Unfortunately, this process is complicated by difficulties in monitoring the progress of reduction and the fact that the cysteine unless the reaction is conducted in oxygen-free conditions the cysteine will begin to re-oxidise as soon as the reducing agent is removed. Consequently, the alkylation is likely to be conducted on a mixture of free and oxidised thiol, resulting in mixtures of alkylated and non-reactive proteins that are hard to separate. This is an issue for the purity of the final alkylated protein as in most instances the difference between the species is too small to allow further purification and both of them are in the solution phase (figure 32).[158]
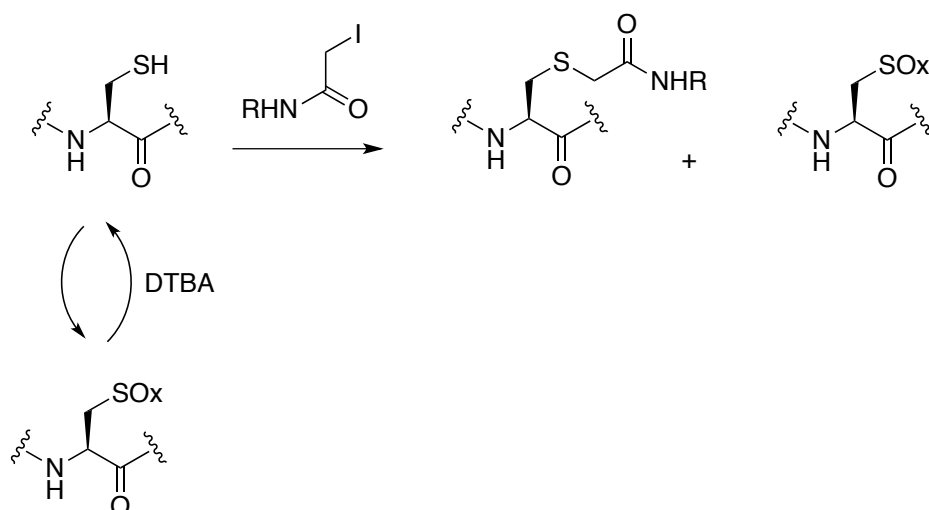
Figure 32: Issues in cysteine alkylation. Iodoacetamide is used as alkylation agent, SOx are undefined oxidised thiol species.

Developing a solid phase catch-release alkylation system can help to address both the incompatibly of the reducing and alkylation agents and the purification of alkylated protein. In this approach the cysteine oxidation that occurs in the solution phase approach can be avoided in the solid-phase system by attaching the reducing and alkylation agents to separate solid phases.[159] The protein should therefore be able to access the reducing agent and alkylation agent *in situ*, in order to overcome the re-oxidation of cysteine residue, while avoiding reaction of the alkylation agent with the reducing agent (DTBA) as shown in figure 33. In comparison to the solution-phase approach, the solid-phase purification of the immobilsed S-alkylated protein should then be easily and quickly performed by simple filtration. Finally, following cleavage from the solid phase the protein should be readily separated from any unreacted alkylation agent and/or cleavage reagents by size exclusion chromatography.
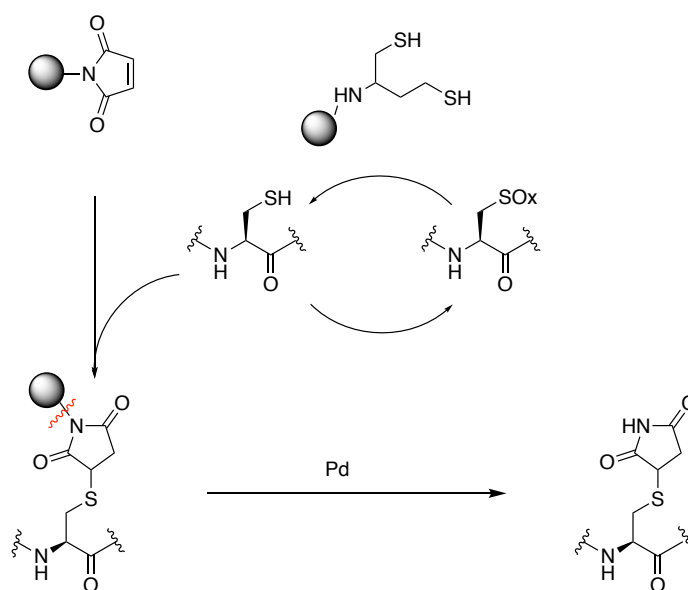
Figure 33: Proposed reaction utilising solid phase alkylation and reducing agents.

The aims of the project are therefore as follows:

1- Synthesise azide-containing alkylation linkers and immobilize onto solid phase by copper (I)-catalysed alkyne-azide cycloaddition (CuAAC) reaction.

2- Prepare a solid phase alkylation linker containing a cleavable group that can release the alkylated protein after purification.

3- Investigate the cleavage reaction in solution phase.

4- Investigate the CuAAC reaction in solution phase.

5- Investigate the selectivity of the alkylation reagent toward thiol in solution phase.

6- Evaluate the use of catch-release methodology to selectively alkylate cysteine in combination with a second solid phase by using BSA (which is well studied in the context of cysteine alkylation methodology and readily available).

7- Apply the methodology developed to the synthesis of CCL2-FK866 conjugates.

Chapter 2: Result and Discussion

2.1 First generation solid phase alkylation system with a cleavable linker

This project has focused on the synthesis of a solid phase protein-alkylation system, containing a cleavable linker that will allow liberation of the alkylated protein under mild conditions. The alkylation linker **1** was initially designed to include an azide group to allow immobilisation onto the solid phase through a copper (I)-catalysed alkyne-azide cycloaddition (CuAAC) reaction between the azide and alkyne groups immobilised onto agarose gel (figure 34). An allyl ester was included as a cleavable group and a chloroacetamide as the thiol alkylation agent (figure 34). In this first model system we plan to use a simple glycine linker as the modifying agent (figure 34). This will allow us to minimise the complexity of the system but could be replaced by alternative amino acids or related systems with increased functionality once the basic aims of the project have been achieved.
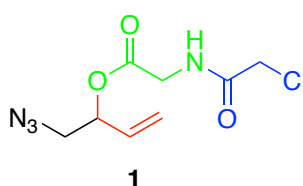
Figure 34: The thiol alkylation system containing an allyl cleavable linker and azide to immobilise onto solid support.

Although the maleimide is more selective towards cysteine, the iodoacetamide has been selected as the alkylation agent in our project due to its easy chemical synthesis and the fact it can be carried through the synthetic sequence as a less-reactive chloroacetamide and activated by S_N2 displacement with excess iodide once immobilised. The allyl group was selected to be used as the linker due to its general stability and straightforward deprotection with catalytic Pd (5 mol%), which can be made compatible with aqueous conditions through

utilising water-soluble phosphine ligands. The biocompatibility of this process has been highlighted by the use of this system in cells by Chen *et al.*,[160] who demonstrated that allyl group is biocompatible with cell integrity.

Aldehyde-modified agarose gel **2** was selected as the solid phase because it is readily available, and agarose gel has been used extensively in the immobilisation, purification and transformation of proteins. The aldehyde-modified agarose gel **2** can be used to attach a commercially available alkyne **3** to the solid phase via well-establish reductive amination conditions in aqueous media, to provide the alkyne immobilised onto solid phase **4** (scheme 11). We tried to attach a long chain alkyne to the agarose in order to minimise any impact that could result when the protein interacted with the solid phase (agarose gel).[161] The preparation of the target solid phase alkylation agent system with a cleavable linker **5** should be achievable by CuAAC reaction of azide **1** with alkyne **4** (scheme 11)
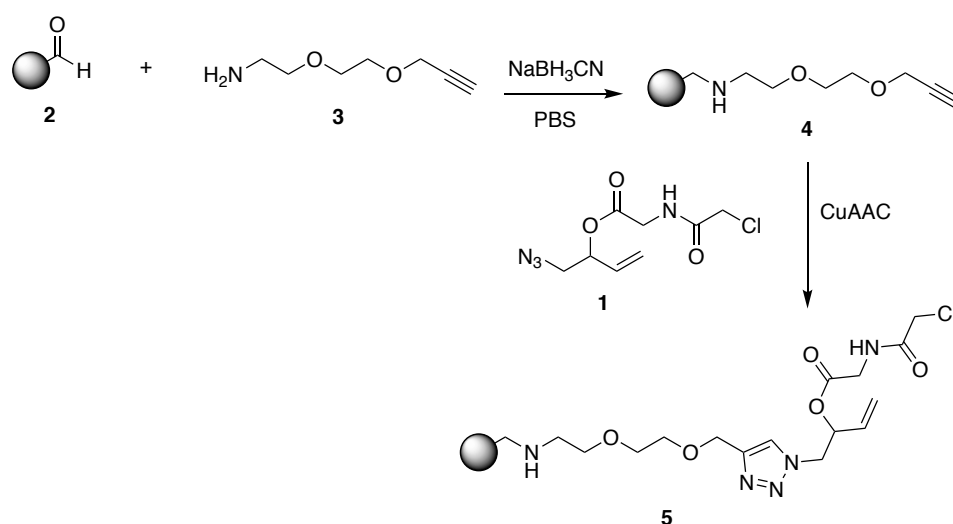
Scheme 11: Proposed synthetic route for the solid phase alkylation linker with allyl ester as the cleavable group.

2.1.1 Synthesis of the alkylation linker

Alkylation linker **1** was prepared by acylation of compound **6** (figure 35), compound **6** prepared by using a commercially available allyl compound **8** followed by selective activation of the primary alcohol with a tosyl group **9** (scheme 12).[162,163] The p-toluenesulfonyl chloride selectively activates the primary alcohol due to the higher steric hinderance of the secondary alcohol, and it is a good leaving group that facilitates the next substitution reaction.[163] Although the selective activation of the primary alcohol with a p-toluenesulfonyl chloride was a straightforward step, it took several days to complete the reaction, yielding 68% of the desired compound **9**, as confirmed by mass spectrometry, ^{13}C NMR and ^{1}H NMR.
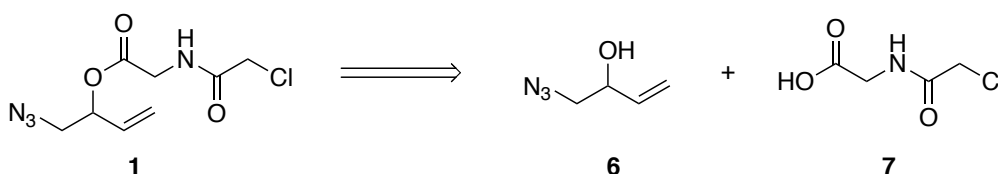
Figure 35: Retrosynthesis of the alkylation linker with azide to use in CuAAC reaction.
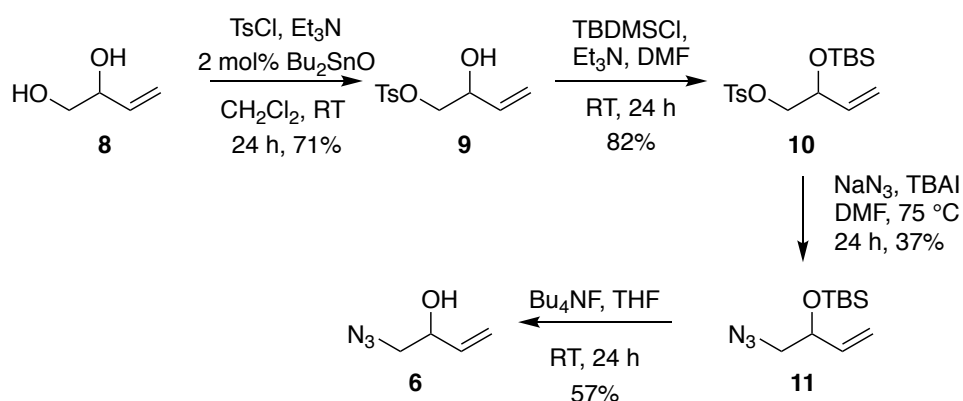
Scheme 12: Synthesis of compound **6**.

It has been demonstrated that the Sn-derivative-catalysed diol tosylation reaction provides higher yield and better selectivity than the uncatalysed diol tosylation reaction.[162] in our hands using the catalytic dibutyl tin oxide (Bu$_2$SnO) helped improve the tosylation of the primary alcohol, thus providing a better yield (71% of compound **9**) in 24 hours. The Bu$_2$SnO is thought to accelerate the tosylation reaction due to the formation of the reactive tin acetal intermediate **12** followed by the fast selective addition of TsCl and the metal exchange (scheme 13).[162]
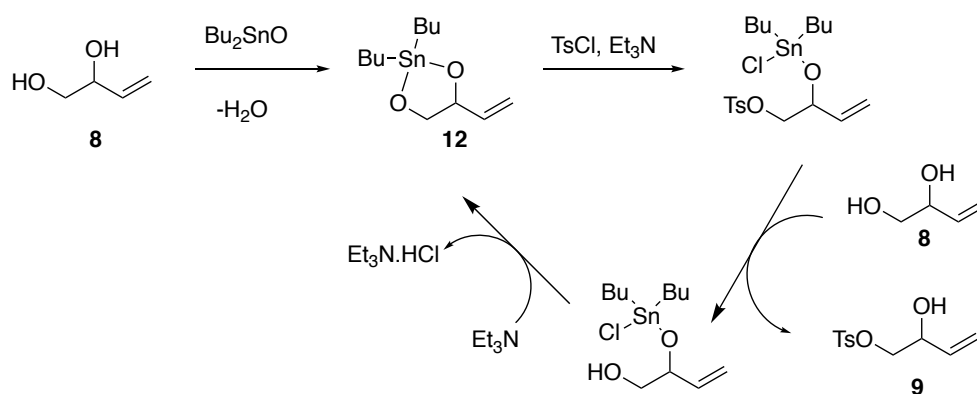
Scheme 13: Bu$_2$SnO-catalysed monotosylation of a diol **8**.[162]

After the successful synthesis of compound **9**, this intermediate subjected to the published synthetic procedure for protecting a secondary alcohol with silyl ether before azide displacement, followed by a deprotection step to yield compound **6** (scheme 12).[164] The published synthetic procedure showed the protection of the secondary alcohol with tert-butyldimethylsilyl chloride (TBDMSCl) using imidazole and dichloromethane, however these conditions did not protect the secondary alcohol even when the equiv.s of TBDMSCl were increased.[164] In order to optimise the reaction conditions, dimethylformamide (DMF) was used instead of dichloromethane in order to improve the solubility of the reagents, and the temperature of the reaction mixture was increased to 75 °C.

However, changing the reaction solvent and heating the reaction did not help improve the protection step. Therefore, we tried to determine the effect that the base had on the reaction, so we used pyridine instead of imidazole. The reaction with pyridine took seven days to complete, and it yielded 68% of the desired compound **10**, as confirmed by mass spectrometry, ^{1}H NMR and ^{13}C NMR.

A simpler form of silyl ether (trimethylsilyl chloride, TMSCl) was also used instead of TBDMSCl to help speed up the protection reaction (scheme 14).[165] In this silylation, all the starting material was consumed in just 24 hours, and yielded 78% of the desired compound **13**. Although this silylation reaction was rapid and provided a better yield in comparison to the reaction that used TBDMSCl, compound **13** was not stable in the next step (azide displacement) due to the cleavage of the bond between silicon and oxygen, presumably resulting from nucleophilic attack at the unhindered TMS (scheme 14).
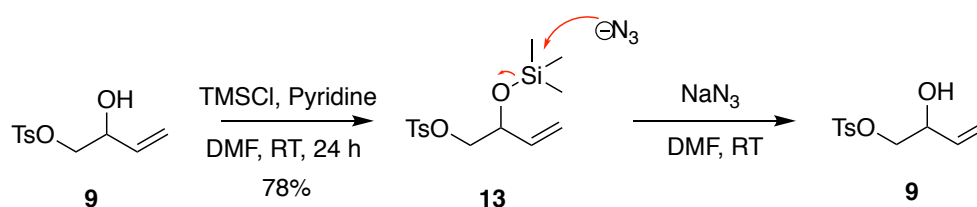
Scheme 14: Use of TMSCl for secondary alcohol protection of compound **9**.

After the disappointing result for TMSCl protection, we decided to return to TBDMSCl and use a base that is stronger than pyridine, such as triethylamine. We found that triethylamine was very helpful in accelerating the protection reaction in 12 hours at room temperature to yield 82% of the desired compound **10**. This effect appears to relate to difference in the pK_a of these three bases as shown in table 6, although the exact role of the base in this reaction is not clear given none are able to significantly deprotonate the alcohol starting material and all

should be sufficiently basic to neutralise the HCl formed.

Base	pK_a
Triethylamine	10.75
Imidazole	7.05
Pyridine	5.5
Alcohol	16

Table 6: The pKa values of different bases used in the protection of compound **9**.

The next step in the synthesis of compound **6** is the displacement of the tosyl group with azide.[166] Initially the reaction was carried out using NaN$_3$ and DMF at room temperature, but it took a long time (more than 7 days). Therefore, the reaction temperature was increased to 75 °C in order to speed up the reaction; however, it took seven days until all the starting material was consumed, and the yield was very low. Surprisingly, the ^{1}H NMR did not show any signals for the desired compound **11** or even the starting material **10**. In order to understand this situation and to optimise this displacement reaction condition, different conditions were investigated (table 7).

Towards that end, DMF is the best solvent for this reaction, and tetrabutylammonium iodide (TBAI) accelerates the displacement reaction, because iodine is able to displace the OTs and then act as a better leaving group than tosyl.[150] The displacement reaction was carried out using NaN$_3$, TBAI and DMF at 75 °C and all the staring material was consumed within 24 hours. However, the ^{1}H NMR did not show any signals for the desired compound **11** or the starting material **10**. The low recovery after simple extraction led us to suspect that the product was volatile, and therefore lost by evaporation when concentrating the solvent.[167] This is in line

with previous report, where compound **6** was lost during the work up due to its low boiling point.[167]

Solvent	Catalyst	Temperature	Comment
DMF	TBAI	RT	Reaction completed within three days.
DMF	TBAI	75 °C	Reaction completed within 24 hours.
DMF	-	RT	No reaction
DMF	-	75 °C	Reaction completed within seven days.
DMF and H_2O	TBAI	RT	No reaction
DMF and H_2O	TBAI	75 °C	Reaction completed within three days.
DMF and H_2O	-	RT	No reaction
DMF and H_2O	-	75 °C	No reaction
DMF and H_2O	NaI	RT	No reaction
DMF and H_2O	NaI	75 °C	No reaction
Methanol	TBAI	60 °C	No reaction
Wet Methanol	TBAI	60 °C	No reaction

Table 7: Summary of different reaction conditions to synthesis compound **11**.

Consequently, deuterated dimethyl sulfoxide (DMSO) was used to check the reaction mixture by ^1H NMR before doing the extraction and concentration. Proof of a successful reaction was provided by the NMR of compound **11**, this is confirmed the volatility of compound **11**. Keeping the volatility of compound **11** in mind we prepared it by using DMF, which is easier to remove than DMSO and, this time, we avoided using high vacuum. However, only 37% of the desired compound **11** was recovered (accounting for residual DMF not removed by

extraction, which was quantified by relative peak integrals in the NMR spectra). Moreover, after conducting the deprotection step using tetra-n-butylammonium fluoride (TBAF), only 57% of compound **6** was isolated. Our conclusion from these studies was that the published route did not describe an optimal synthesis of compound **6**.[168]

In order to resolve the volatility issue, we used the bulkier silyl ether (tert-butyldiphenylsilyl, TBDPS) for secondary alcohol protection instead of TBDMSCl (scheme 15). When using this bulkier group, the protection reaction took longer until the reaction reached completion and yielded just 28% of the desired compound **14**. Moreover, the azide displacement was more difficult because TBDPS makes the molecule less reactive.
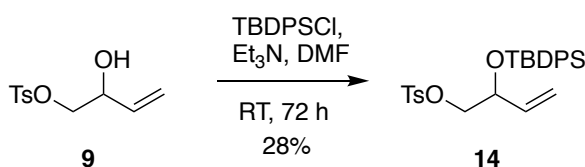
Scheme 15: Protection of compound **9** with tert-Butyldiphenylsilyl (TBDPS).

After understanding that following the published routes for the synthesis of compound **6** does not provide a good yield, and after finding the best reaction conditions, we decided to attempt the synthesis of the azide allyl alcohol by direct azide displacement of compound **9**, as this approach allowed to synthesise compound **6** in one step instead of three steps in previous procedure (scheme 16). The displacement reaction was carried out using NaN$_3$, TBAI and DMF at 75 °C and under these conditions all starting material was consumed within 24 hours to yield compound **6** (scheme 16). The higher aqueous solubility of compound **6** necessitated extracting the product eight times with diethyl ether to take it from the aqueous phase to the organic phase. After optimisation it was found that, compound **6** can be isolated in 82% with some DMF (yield accounting for residual DMF not removed by extraction, which

was quantified by relative peak integrals in the NMR spectra); in contrast when DMF was completely removed, the yield decreased to 26%. Therefore, this product was used in the next step (acylation) without fully removing DMF, and after the acylation reaction we could easily purify the product of interest.
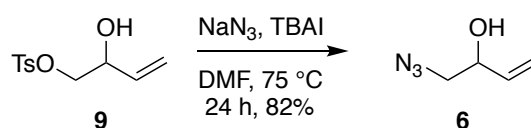
Scheme 16: Synthesis of compound **6** by direct azide displacement of compound **9.**

With compound **6** in hand, compound **7** was prepared in order to carry out the acylation reaction to afford compound **1**. Although compound **7** is commercially available, we were interested in preparing it.[169,170] compound **7** was prepared by following the published preparation (scheme 17).[169] Although this reaction was expected to be extremely rapid due to the high reactivity of chlorine, it took three days to yield only 40% of compound **7**, as confirmed by mass spectrometry, ^{13}C NMR and ^{1}H NMR.
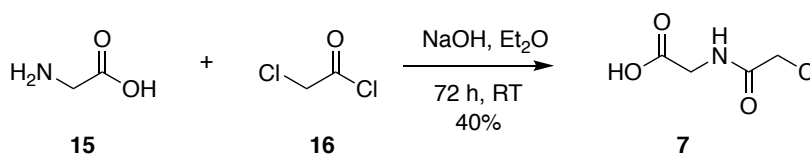
Scheme 17: Preparation of compound **7**.

The acylation reaction (scheme 18) was first carried out using 4-dimethylaminopyridine (DMAP), 1-ethyl-3-(3-dimethylaminopropyl (EDC) and DMF (DMF was used as a reaction solvent because compound **6** was isolated with some DMF) at room temperature to afford

only 12% of compound **1**.[171] This low yield might be due to the possibility of the nucleophilic

attack from DMAP lone pair on compound **7** as shown in figure 36.
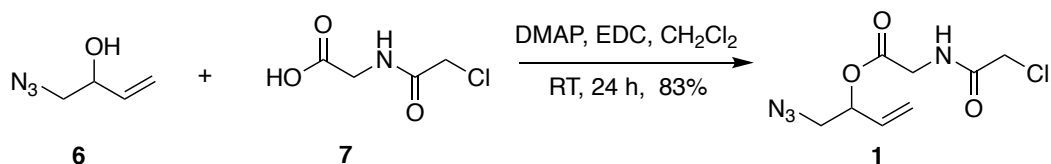
Scheme 18: Optimised acylation reaction to form compound **1**.
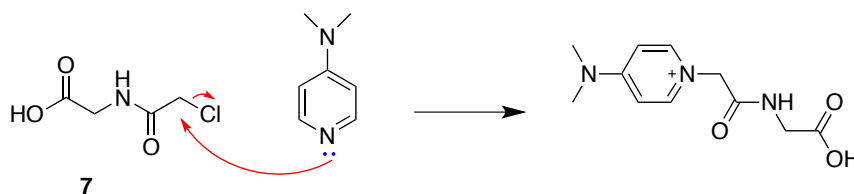
Figure 36: Mechanism of the DMAP nucleophilic attack.

To investigate this possibility, we conducted an acylation reaction with a commercially

available acetylglycine **17**, which does not contain a chlorine atom (scheme 19). This acylation

reaction produces a low yield (12%), similar to the previous reaction. This low yield invalidates

our expectation that chlorine would have an effect on the reaction yield.
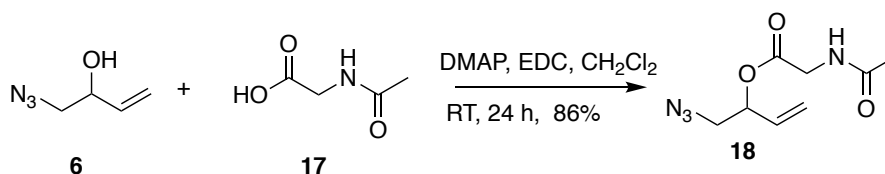
Scheme 19: Acylation reaction using acetylglycine **17**.

In terms of optimising the reaction conditions (table 8), it is not enough to use an equiv. amount of amino acid; rather, an excess amount of amino acid should be used. Using dichloromethane as a reaction solvent increased the reaction yield from 12% to 86% (compound **18**) and 83% (compound **1**) at room temperature in 24 hours, while the reaction that used DMF needed to be heated, and it took three days to yield 70%. In addition, it is necessary to use an equiv. amount of DMAP for the base, while triethylamine does not improve the reaction. Proof of the successful preparation of compound **1** and compound **18** was provided by the NMR of the compounds.

Solvent	Base	Catalyst	Temperature	Equiv. amino acid	Yield, Time
DMF	DMAP		RT	1 equiv.	12%, 48 hours
DMF	DMAP		RT	6 equiv.	39%, 7 days
DMF	DMAP		65 °C	6 equiv.	70%, 72 hours
DMF	Et$_3$N		65 °C	6 equiv.	10%, 72 hours
DMF	Et$_3$N	DMAP	65 °C	6 equiv.	39%, 72 hours
CH$_2$Cl$_2$	DMAP		RT	4 equiv.	86%, 24 hours
CH$_2$Cl$_2$	DMAP		RT	2 equiv.	50%, 72 hours

Table 8: Different acylation reaction conditions.

2.1.2 Investigation CuAAC reactions in the solution phase

After the successful synthesis of the alkylation agent containing an allyl ester cleavable linker (compound **1**), we were interested in investigating the CuAAC reaction and the Pd catalysed allyl deprotection in the solution phase in order to find efficient reactions conditions before going to the solid phase. Moreover, we were interested in investigating the iodine

displacement reaction and the thiol alkylation by the alkylation linker that we prepared in solution phase.

For the CuAAC reaction in solution phase, the commercially available simple alkyne **19** was coupled to compound **18** (Scheme 20).[172] A CuAAC reaction can be conducted under aqueous conditions at room temperature, and it should specifically yield the 1,4-disubstituted 1,2,3-triazoles regioisomer, in contrast to the Huisgen 1,3-dipolar cycloaddition (uncatalysed), which requires an elevated temperature and provides a mixture of 1,4-triazoles and 1,5-triazoles regioisomers (figure 37).[173]
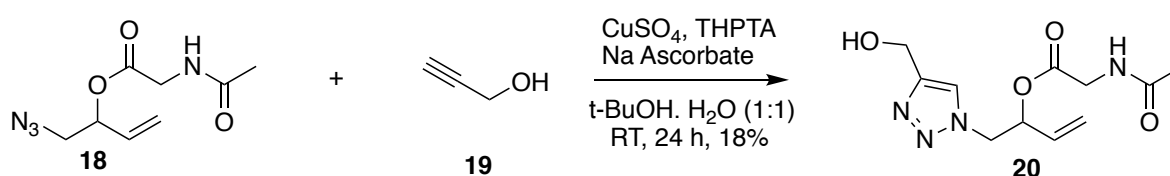
Scheme 20: The copper (I)-catalysed alkyne-azide cycloaddition (CuAAC) reaction using alkyne **19**.
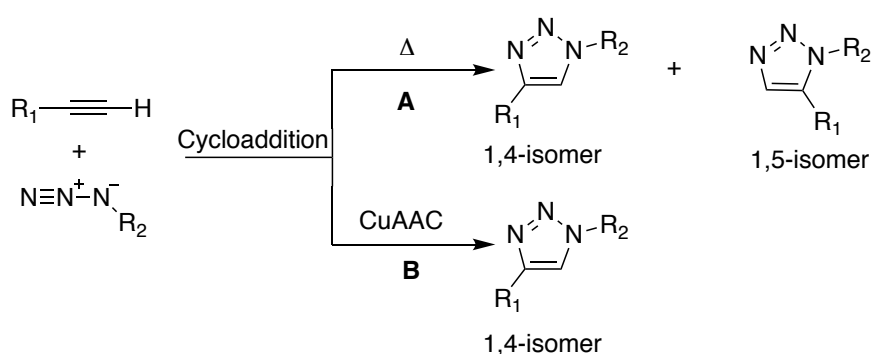
Figure 37: Azide-Alkyne cycloaddition reaction, (A) uncatalysed thermal Azide-Alkyne cycloaddition reaction, (B) copper catalysed Azide-Alkyne cycloaddition reaction.

The CuAAC reaction mechanism is complicated due to the number of copper ions that are involved in the reaction.[174] It is started by the reduction of the copper (II) salt into copper (I) followed by coordination of the terminal alkyne to the copper to form π alkyne-copper intermediate. This coordination increases the acidity of the terminal alkyne hydrogen leading to deprotonation of the terminal alkyne to form copper (I) acetylide.[175] After formation of the copper (I) acetylide intermediate, the azide could attack the same copper centre that binds to alkyne, which is the oldest proposed mechanism of the CuAAC reaction called the mono-copper pathway (figure 38).[176, 177,178] In the reviewed mechanism of the CuAAC reaction, the copper (I) acetylide intermediate binds to a second copper ion to form bis-Cu acetylide complex, and then the azide can attack the second copper centre, which is called the bis-copper pathway (figure 39).[176, 177,178]

Regardless of the mono/bis mechanism, the azide binds to the copper (I) acetylide through the proximal nitrogen to the carbon to form azide-copper intermediate.[179,180] The distal nitrogen of the azide then attacks the C2 carbon of the acetylide to form a six-membered copper containing intermediate,[179] followed by reductive elimination and formation the second C-N bound to form the 1,4-disubstituted 1,2,3-triazoles. Finally, the 1,4-disubstituted 1,2,3-triazole product is released and the active copper species catalyst regenerated by fast protonation of the copper (Figure 38, 39).[181,182]
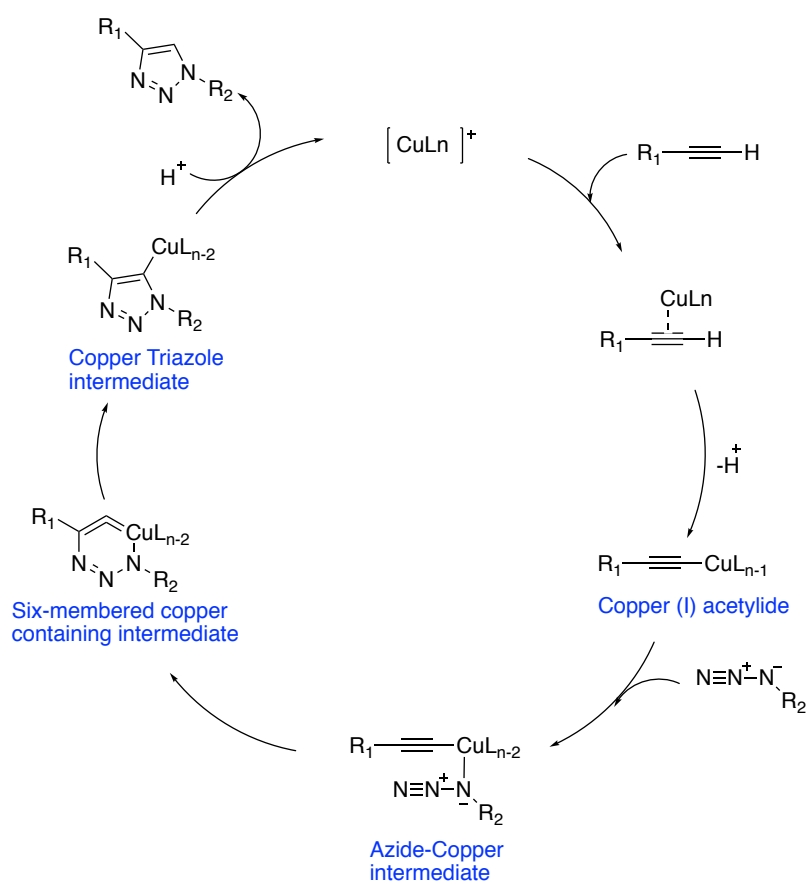
Figure 38: Mono-copper mechanism for the copper (I)-catalysed alkyne-azide cycloaddition (CuAAC).
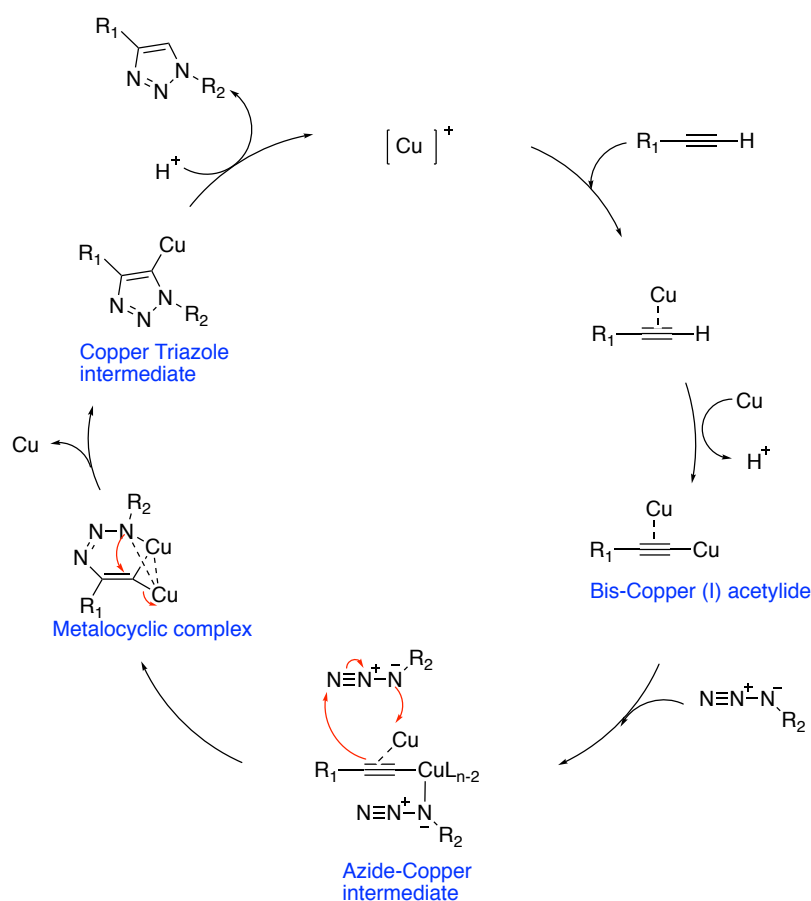
Figure 39: Bis- copper mechanism for the copper (I)-catalysed alkyne-azide cycloaddition (CuAAC).

Tris(3-hydroxypropyltriazolylmethyl)amine (THPTA) is a water soluble amine ligand that is used to avoid the oxidation of catalytic Cu(I) by dissolved oxygen and to accelerate the reaction rate by facilitating the coordination of the azide to the copper center.[175,183] It is a water-soluble ligand that provides further simplification for the click chemistry by allowing the entire reaction to be run in water, thereby affording biological compatibility for these CuAAC reactions (figure 40).[184,175]
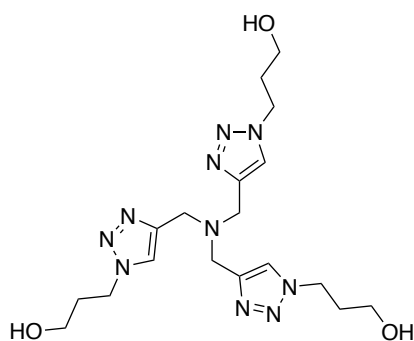
Figure 40: The tris(3-hydroxypropyltriazolylmethyl)amine (THPTA) structure.

Although the CuAAC is a click reaction that should provide a high yield, in our hands the reaction only provided a low yield of the triazole compound **20** (Scheme 20).[182] The product identity was confirmed by mass spectrometry and ^{1}H NMR, however, ^{1}H NMR showed a mixture of product and impurities that was hard to purify, in part due to the low yield of the reaction.

In order to investigate the low yield of CuAAC, alkyne **21** was used for the CuAAC reaction (Scheme 21). Using alkyne **21** with compound **18** yielded 86% of the desired product **22**, as confirmed by mass spectrometry, ^{1}H NMR and ^{13}C NMR, suggesting that the poor reaction profile observed when using propargyl alcohol **19** is due to some specific side reactions with this compound.
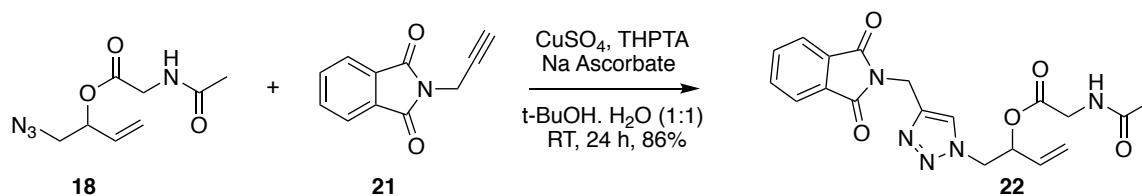
Scheme 21: The copper (I)-catalysed alkyne-azide cycloaddition (CuAAC) reaction using alkyne **21**.

2.1.3 Investigation of the cleavage reactions in the solution phase

To investigate the Pd-catalysed allyl deprotection in solution phase, different allyl esters (compounds **1**, **18**, **22**) were used to investigate the cleavage of the linker in the solution phase based on the reported strategy of the mild deprotection of allyl ethers in the presence of Pd(0) catalyst (1 mol%) under basic conditions.[185] These studies showed the deprotection of allyl aryl ethers with 1 mol% of tetrakis(triphenylphosphine)Pd(0) (Pd(PPh$_3$)$_4$) and 3 equiv. of potassium carbonate (K$_2$CO$_3$) in methanol was faster than deprotection of the allyl alkyl ether in the same reaction conditions.[185] Here we were interested in the allyl ester deprotection, where the pKa value of the acid is lower than phenolic OH, which makes it much less basic and better leaving group than allyl aryl ether. Therefore, the compounds **1, 18** and **22** were treated with Pd (PPh$_3$)$_4$ in methanol in order to investigate the ability of Pd to undergo deallylation in the presence of azide (compounds **1**, **18**) and triazole (compound **22**). If this chemistry worked, we planned to investigate allyl deprotection using water-soluble phosphine ligands.

The mechanism of allyl deprotection is closely related to the more studied Pd-catalysed allyl alkylation, which was first introduced by Tsuji 1965 then further developed by Trost in 1973 through inclusion of phosphine ligands.[186,187] The Pd-catalysed deallylation occurs in two steps; the first step is the coordination of the Pd(0)-catalyst to the double bond, to give the η^2 π-allyl complex, followed by expelling the leaving group (with inversion) to give the η^3 π-allyl complex. The Pd(0) is oxidised to Pd(II) in this process, which is also called the ionization step (Figure 41, Path A). The second step is the nucleophilic substitution step, which results in reduction to Pd(0), followed by decomplexation of the η^2 π-allyl complex to produce the allylation product and recover the active Pd(0) species (Figure 41, Path A).[188,189,190,191,192,193,194,195,196]
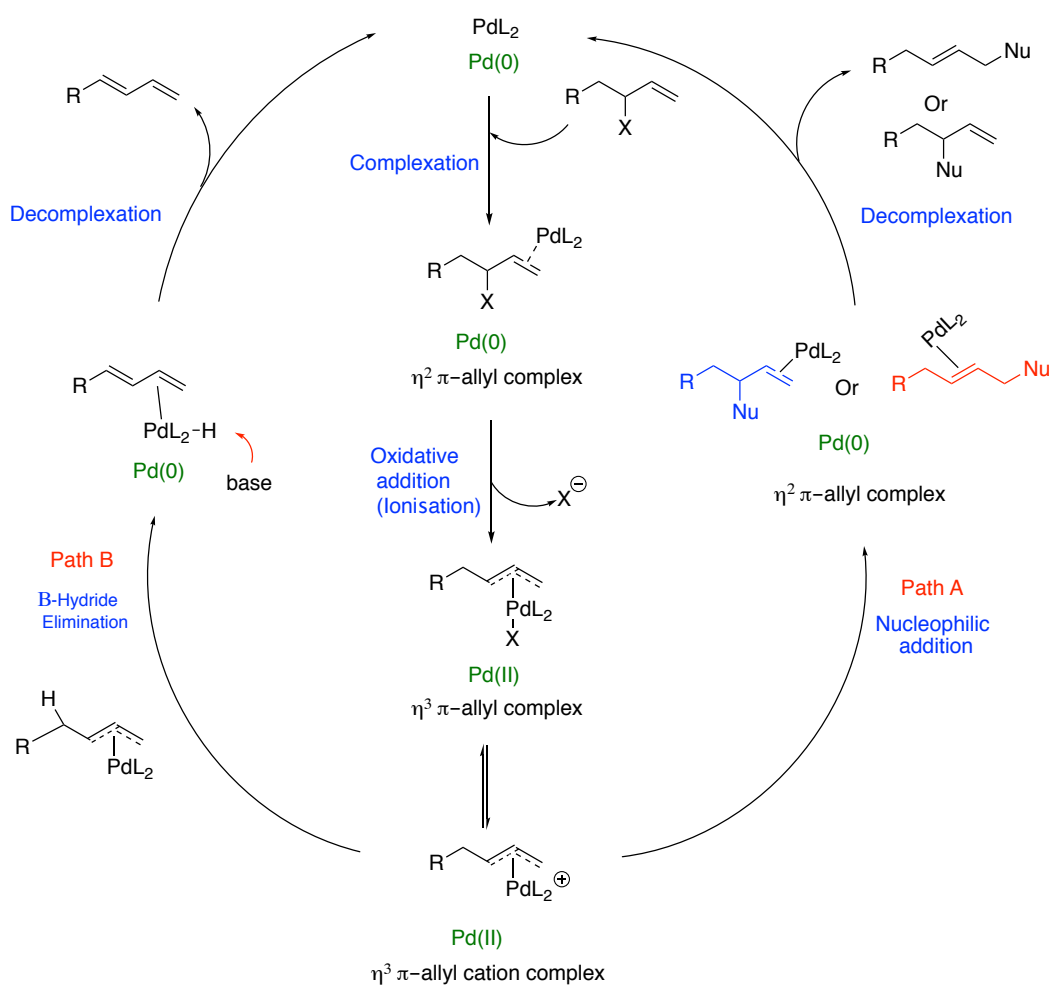
Figure 41: Pd catalysed the reactions of allylic compounds (the nucleophilic pathway and the β-hydride elimination pathway).

The addition of the nucleophile can occur through two different pathways depending on the nature of the nucleophile. Soft nucleophiles attack directly the allylic moiety on carbon, opposite from the face where the Pd resides (leading to net retention of stereochemistry from the leaving group).[192,190,193,188] The nucleophile can attack either terminal allyl carbon to produce regioisomers, however reaction at the less hindered terminus is preferred, which

increases the regioselectivity of the reaction (Figure 42, Type A).[192] In contrast, hard nucleophiles attack the metal center first, with the allylation product produced by reductive elimination (Figure 42, Type B).[192,190,193,188,194] In line with this hard/soft principle carbon nucleophiles prefer to attack the η^3 π-allyl complex directly, while heteroatom nucleophiles attack the Pd center followed by migration to the allyl unit.[188,193]
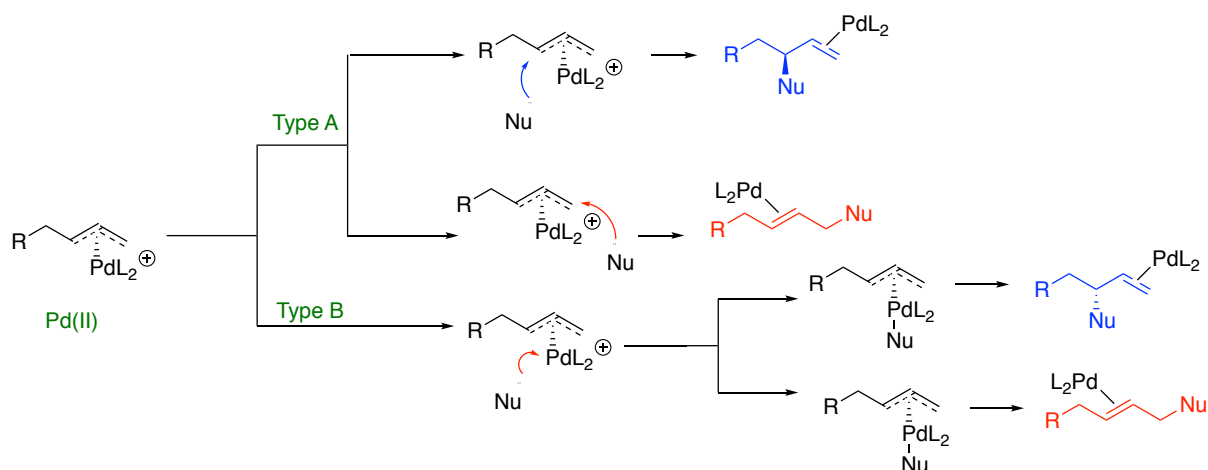
Figure 42: Soft (type A) and hard (type B) nucleophile addition to the η^3 π-allyl Pd complex.

On the other hand, if the ligand has hydrogens on β-carbon of the alkyl, an alternative β-hydride elimination reaction pathway can theoretically occur. The hydride on β-carbon of the η^3 π-allyl complex is transferred to the Pd center, followed by the reductive elimination to regenerate the Pd(0) in the presence of a base. Based on other Pd-catalysed reactions it was expected that the β-hydride elimination pathway is rapid in comparison to the nucleophilic pathway (Figure 41, Path B).[197,198]

The allyl ester was cleaved in all compounds (**1**, **18** and **22**) when the reaction was carried out in deuterated methanol (CD$_3$OD) in the presence of Pd(0) catalyst (1 mol%) under basic conditions (3 equiv. of K$_2$CO$_3$) (scheme 22). This was confirmed by ^{1}H NMR, which showed the absence of the signal of the C-H environment that was adjacent to the ester at 5.45 ppm

(Figure 43) and appearance of a proton peak at 4.20 ppm, which is similar to the signal of the C-H adjacent to the alcohol in compound **6** (Figure 43). The peak of the methylene protons that are adjacent to amine are also completely lost under these conditions, which can be attributed to exchange with deuterium. Although this result was initially promising, control experiments demonstrated that the allyl ester is unstable in the basic conditions leading to direct hydrolysis of the molecule independently of the Pd deprotection pathway. This hypothesis was confirmed by ^{1}H NMR when the reaction was carried out in CD_3OD and K_2CO_3 in the absence of the Pd(0) catalyst. Again, the disappearance of the adjacent amine methylene protons is most likely due to the use of base in deuterated methanol leading to exchange of these acidic protons (Figure 44).
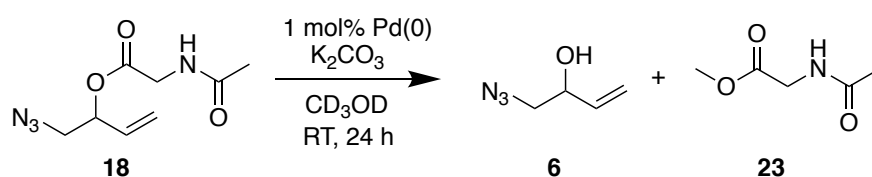
Scheme 22: The cleavage reaction of compound **18** by catalyst Pd(0) in the presence of base, leading to hydrolysis of compound **18** independently of the Pd deprotection pathway.
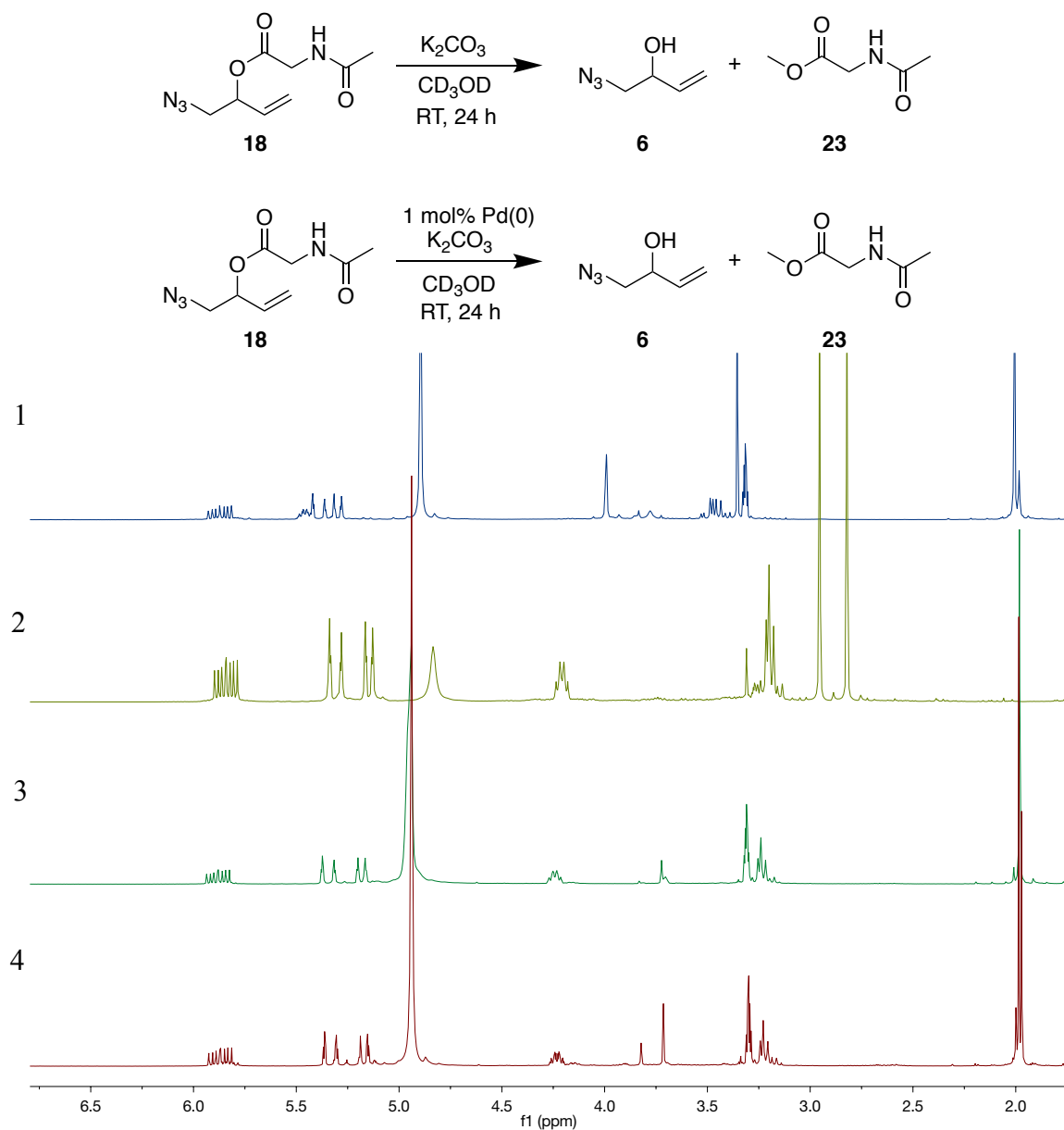
Figure 43: Comparison between ^{1}H NMR spectrum for: 1- compound **18** in CD$_3$OD, 2-

compound **6** in CD$_3$OD, 3- compound **18** with potassium carbonate in CD$_3$OD without Pd(0)

and 4- Pd catalysed cleavage of the allyl ester of compound **18** under basic conditions in

CD$_3$OD.
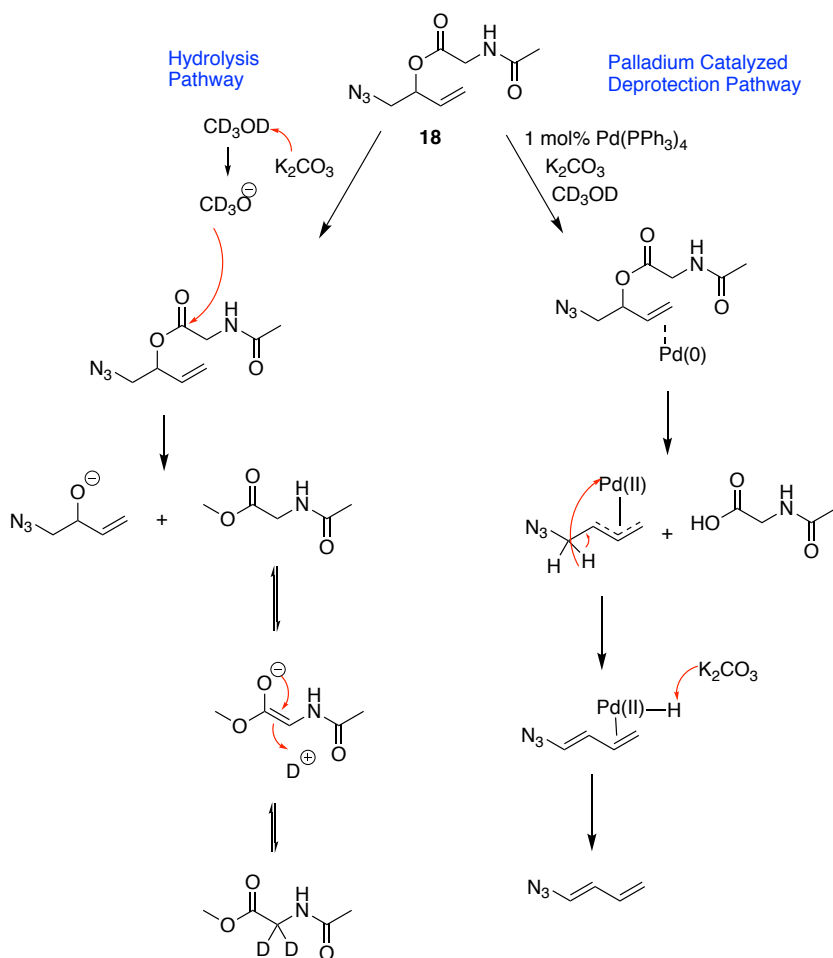
Figure 44: Hydrolysis and Pd deallylation pathways of compound **18**.

We optimised the reaction conditions and found that the allyl ester compounds (**1**, **18** and **22**) were hydrolyzed under basic conditions even when deuterated water (D_2O) is used instead of CD_3OD (Table 9). Also, we note that no deprotection product was observed when the reaction was carried out in CD_3OD in the presence of Pd(0) catalyst but without base, consistent with literature reports that the absence of the base slowed the reaction process in the deprotection of allyl ether in CD_3OD in the presence of a Pd(0) catalyst.[185] However, the deprotection of the allyl ester was achieved when the reaction was carried out in CD_3OD or D_2O in the presence of 100 mol% Pd(0),

without base (Table 9). We therefore conclude that the failure of catalytic Pd deprotection under neutral conditions is due to trapping of a stable catalytic intermediate that forms following the oxidative addition. This could be the Pd hydride species (Figure 41, path B), as base is generally required to recycle Pd(0) during e.g. Heck reactions, it is also possible that the η^3 π-allyl complex itself is stable in the absence of a good nucleophile. It was also noted that the presence of agarose prevented the cleavage when the reaction was carried out in DMSO, however there was no effect when the reactions were carried out in D_2O and CD_3OD.

Solvents	Pd(0) catalyst (5 mol%)	Pd(0) (100 mol%)
$CD_3OD + K_2CO_3$	Hydrolysis	NA
CD_3OD	No reaction	Complete conversion at 3 hours
CD_3OD + Agarose	No reaction	Complete conversion at 3 hours
$D_2O + K_2CO_3$	Hydrolysis	NA
D_2O	No reaction	Complete conversion at 3 hours
D_2O + Agarose	NA	Complete conversion at 3 hours
DMSO	No reaction	Complete conversion at 3 hours
DMSO + Agarose	NA	No reaction

Table 9: Different reaction conditions to optimise the deallylation of the allyl ester.

2.1.4 Investigation of the iodine displacement and the thiol alkylation reactions in the solution phase

To investigate the iodine displacement reaction in solution phase, compound **1** was treated with sodium iodide (NaI) in acetone for 24 hours to provide compound **24** in 76% yield as confirmed by mass spectrometry, ^{13}C NMR and ^{1}H NMR (scheme 23). To investigate the thiol alkylation reaction in solution phase, compound **27** was prepared by the CuAAC reaction between compound **1** and a commercially available N-Boc propargylamine **25** followed by Boc deprotection under acidic conditions (scheme 24). Compound **27** was designed to be close

to our thiol alkylation linker which has chloroacetamide, allyl ester and triazole group. Compound **27** was treated with different amounts of cysteamine **28** (4, 2, 1 and 0.5 equiv.) in PBS at room temperature and 60 °C with and without sodium iodide (NaI) in order to find efficient reaction conditions.
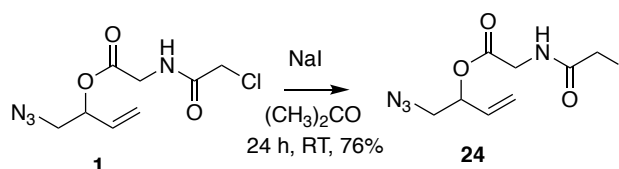
Scheme 23: Iodine displacement to chlorine of compound **1**.
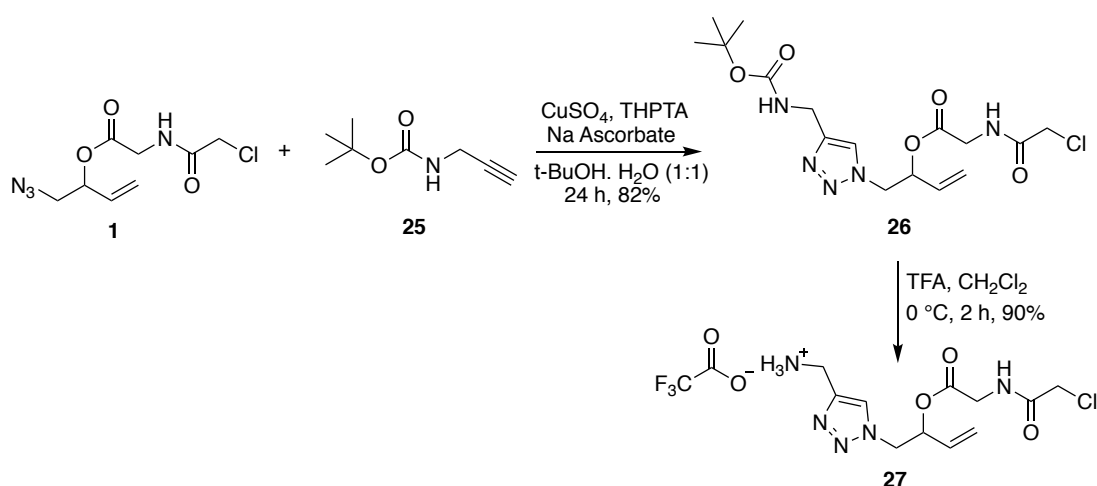
Scheme 24: Preparation of the compound **27**.

The thiol alkylation reaction of the cysteamine **28** resulted in a mixture of products in the ^{1}H NMR spectra and ES$^+$MS (scheme 25). As expected the ^{1}H NMR showed a shift of the two protons that were next to chlorine from 4.1 ppm into 3.4 ppm, however we also observed loss of the signal of the methylene proton that was adjacent to the ester at 5.75 ppm and appearance of a new proton peak at 4.60 ppm. One hypothesis for this side reaction was that the cystemine **28** caused an increase in the pH of the reaction mixture that led to hydrolysis

of the ester, although this occurred even when small amount of cysteamine **28** was added

(0.5 equiv.). Therefore, we used thioglycolic acid **30** instead of cysteamine **28** and found that

the ester of compound **27** was still hydrolysed.
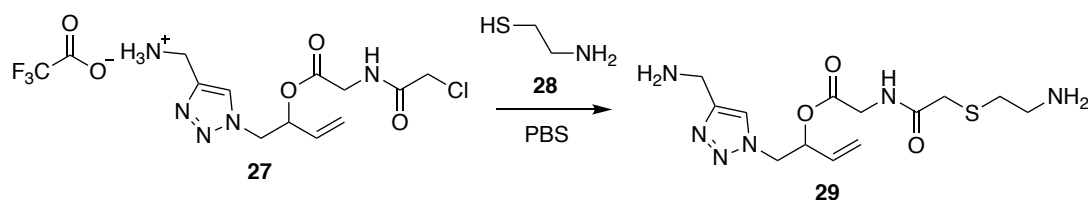
Scheme 25: alkylation of Cysteamine **28** by compound **27**.

By this stage it was clear that the ester system was unlikely to be sufficiently stable for longer-

term use in the project, therefore, we attempted to investigate the thiol alkylation by using

simple molecules that do not have ester, in order to avoid hydrolysis. The (2-

chloroacetyl)glycine **7** was treated with cysteamine **28**, thioglycolic acid **30** or

mercaptoethanol **31** (figure 45) in PBS for 24 hours in presence or absence of NaI (table 10).

We also prepared (2-iodoacetyl)glycine **32** to investigate the efficiency of thiol alkylation

reaction by using iodine instead of chlorine (table 10). When the (2-chloroacetyl)glycine **7** was

treated with different thiol molecules in PBS for 24 hours, no change was observed in the ^{1}H

NMR. However, the presence of NaI in the reaction mixture provided ~100% alkylation when

thiol was used in excess. The iodine is a good leaving group due to the weakness of the

carbon-iodine bond in comparison with other carbon-halogen bonds. The bond dissociation

energy of carbon-iodine bond is 57.6 kcal/mol while the bond dissociation energy of carbon-

chlorine bond is 83.7 kcal/mol. The large atomic radius of the iodine and the long carbon-

iodine bond make the bond easy to break in comparison with the carbon-chlorine bond.[199]

HS–CH₂CH₂–NH₂ **28** HS–CH₂–C(=O)OH **30** HS–CH₂CH₂–OH **31**
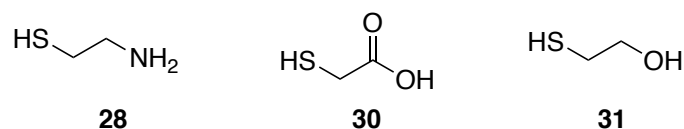
Figure 45: Cysteamine **28**, thioglycolic acid **30** and mercaptoethanol **31**.

(Reaction scheme: (2-chloroacetyl)glycine **7** + HS~ , (+/ -) NaI, PBS, 24 h, RT / 60 °C → thioether product)

(Reaction scheme: (2-iodoacetyl)glycine **32** + HS~ , PBS, 24 h, 60 °C → thioether product)
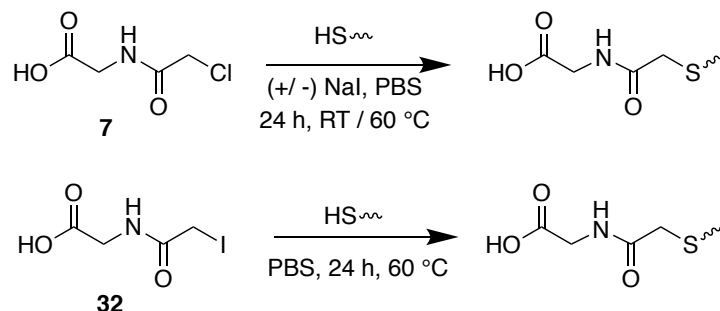
	Alkylation reagent	Thiol Compound	Thiol equiv.	Iodine equiv.	Temp.	Comments
1	(2-chloroacetyl)glycine **7**	Cysteamine **28**	2	-	RT	0% conversion
2	(2-chloroacetyl)glycine **7**	Cysteamine **28**	4	4	60 °C	100% conversion
3	(2-chloroacetyl)glycine **7**	Thioglycolic acid **30**	2	-	40 °C	0% conversion
4	(2-chloroacetyl)glycine **7**	Thioglycolic acid **30**	2	2	40 °C	100% conversion
5	(2-chloroacetyl)glycine **7**	Mercaptoethanol **31**	2	-	40 °C	0% conversion
6	(2-chloroacetyl)glycine **7**	mercaptoethanol**31**	2	2	40 °C	59% conversion
7	(2-iodoacetyl)glycine **32**	Thioglycolic acid **30**	2	-	60 °C	100% conversion

Table 10: Different reaction conditions for thiol alkylation.

2.1.5 Investigation of the immobilisation of the alkylation linker onto agarose and cleavage reaction in the solid phase

Investigation of the loading of the alkylation linker into agarose and cleavage efficiency of the allyl ester from the solid phase was expected to be complicated by challenges with directly quantifying the degree of loading on the solid phase. To address this question, we therefore focussed our efforts on accurately quantifying the amount of recovered linker following the immobilisation step and considering the mass balance when the immobilised material is isolated following cleavage. In order to facilitate these studies a model system was developed based on the strongly absorbing and fluorescent rhodamine scaffold (scheme 26). The

rhodamine azide **34** was prepared by the acylation of compound **6** with a commercially available rhodamine B **33** (scheme 26). Then, the rhodamine azide **34** was immobilised onto agarose by the copper (I)-catalysed alkyne-azide cycloaddition (CuAAC) reaction of azide **34** with alkyne **4** (scheme 26). The extent of labelling of the commercial aldehyde-agarose gel **2** is approximately 45 µmole/mL, though the precise amount of gel used in reactions (scheme 27). None the less by varying equiv. the recovery of free rhodamine **33** following the CuAAC reaction to form the solid model system **35** can be used estimate both the loading of the agarose with alkyne and efficiency of the CuAAC reaction.
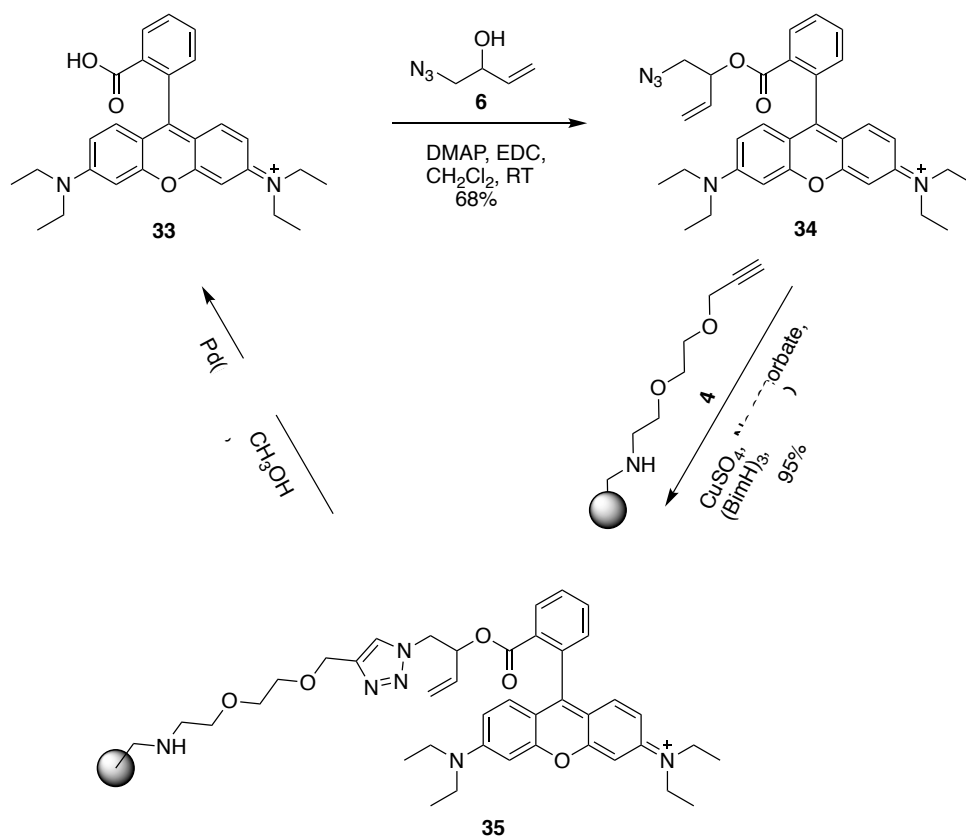
Scheme 26: The loading of the fluorophore Rhodamine Azide **35** on the resin **4** and the cleavage to form Rhodamine B **33**.
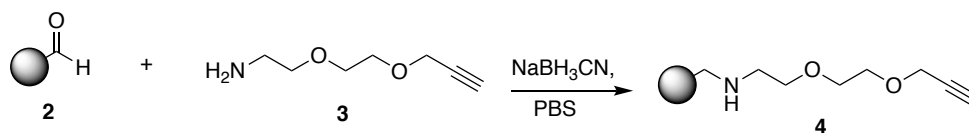
Scheme 27: alkyne immobilisation onto solid phase by reductive amination reaction.

In order to find the best condition for the CuAAC reaction, varying equiv. of the rhodamine azide **34** were reacted with the solid phase alkyne **4** (table 11). The data supports an alkyne loading close to that expected, with high loading efficiency for the rhodamine azide **34** when excess azide is used. However, only 55% of rhodamine azide **34** was recovered after using 4 equiv. of the azide relative to the alkyne, which theoretically should be 75%. This suggests that either the alkyne loading is higher than expected, or we are seeing incomplete recovery of the free Rhodamine following the CuAAC reaction.

Amount of Rhodamine Azide	Loading Efficiency
0.25 equiv.	11%
1 equiv.	77%
4 equiv.	164%

Table 11: The loading efficiency of the Rhodamine azide **34** on the resin.

Unfortunately, the cleavage conditions developed off-agarose gave very poor recovery of the rhodamine B **33** in the solid model system **35** (0.4 %) when the reaction was carried out in CD$_3$OD in the presence of 100 mol% Pd(0) (scheme 26). It became apparent at this stage that the low yield of the cleavage reaction of the solid model system **35** may be due to an expected known effect of the copper on the agarose

during the CuAAC reaction.[200] It has been reported that, the Cu(I) decreased the MW of polysaccharides, likely through formation of reactive intermediates, and changed the colour of the agarose from colourless to dark brown.[200] We could not notice these effects of the Cu(I) during the ligand immobilisation due to the purple colour of rhodamine azide **34**. It is therefore possible that the agarose products and/or retained copper leads to degradation of the rhodamine at this stage. The Cu(I) side effects on the agarose may be avoided by doing the CuAAC reaction before the attachment to the agarose, however given the concerns about the stability of the allyl ester in the actual linker system we instead chose to redesign the linker system in full to allow alternative immobilisation approaches.

In the first attempt toward the solid phase alkylation linker, the alkylation linker **1** had been successfully synthesised and the CuAAC reaction in the solution phase and solid phase confirmed the formation of the triazole product in good yield when the reaction was carried out under aqueous conditions at room temperature. In addition, the deprotection of the allyl ester was achieved when the reaction was carried out in the presence of 100 mol% Pd(0), without base. However, the cleavage reaction of the rhodamine solid model system gave very low yield when the reaction was carried out in the presence of 100 mol% Pd(0). Moreover, the allyl ester linker was unstable under basic conditions, leading to direct hydrolysis of the allyl ester system which complicates understanding of the cleavage reaction. In a comparison between a simple iodoacetamide molecule and the chloroacetamide, it was demonstrated that the iodoacetamide molecule is more efficient for thiol alkylation than the chloroacetamide molecule.

2.2 Development of the cleavable linker and cleavage conditions

2.2.1 Optimisation of linker Stability

It is essential that the solid phase alkylation linker is stable under the conditions needed to prepare the solid phase system and conduct the immobilisation reactions. After the disappointing finding that hydrolysis of the allyl ester linker occurs under basic conditions, we turned our attention to improve the stability of the linker. We expected that changing this component of the linker to a carbamate or carbonate would improve the stability as the carbonyl group in the carbamate and carbonate is conjugated to two electron donating groups (amine and oxygen in carbamates, oxygen and oxygen in carbonates) therefore the carbonyl group is more electron rich and thereby protected from nucleophilic attack.

Changing the allyl ester into allyl carbamate or allyl carbonate should not affect the cleavage of the linker as it is still good leaving group (their pK_a are close to the carboxylic acid of the ester) (figure 46).[201,202] This approach has been used by other groups looking at biocompatible Pd activated prodrugs, for example Unciti-Broceta and co-workers showed the gemcitabine carbamate prodrugs are more stable than the gemcitabine carbonate prodrugs in human cancer cell lines.[203]
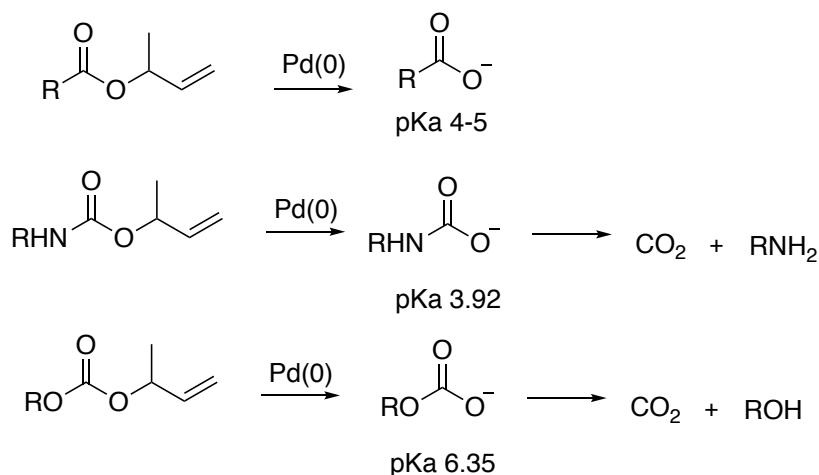
Figure 46: Ester, carbamate and carbonate leaving group.

2.2.2 Carbamate to improve the linker stability

Bearing in mind the importance of the stability of linkers in basic conditions, two different allyl carbamate derivatives **37** and **39** were prepared by the reaction of commercially available 1-bromo-4-isocyanatobenzene **36** and (isocyanatomethyl)benzene **38** with compound **6** (scheme 28).[204] These derivatives were synthesised to make the carbonyl group more resistant to nucleophilic attack, therefore, the stability these derivatives were studied under basic conditions.
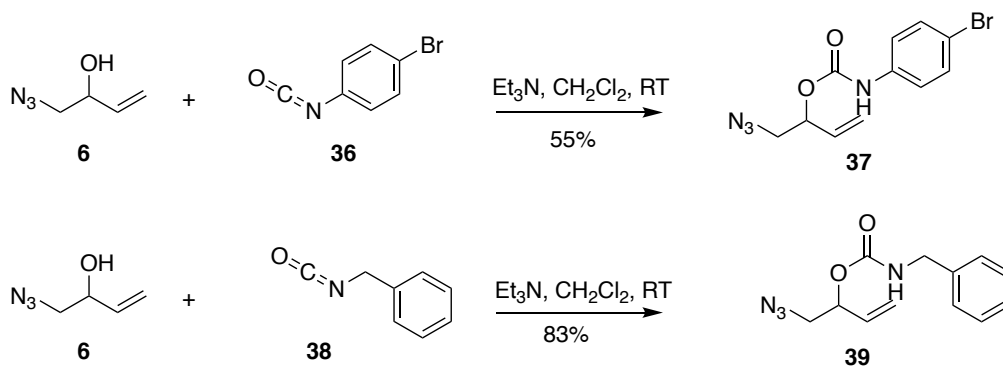
Scheme 28: Preparation of the carbamate derivatives.

Allyl carbamate **37** was found to undergo hydrolysis in methanol under basic conditions using 3 equiv. of K_2CO_3. The instability of allyl carbamate **37** in basic conditions is most likely due to the amine lone pair being delocalised into the phenyl ring, reducing the stabilisation of the carbonyl group. However, the ^1H NMR confirmed that the carbamate molecule **39** was stable under basic conditions. The deallylation reaction of the carbamate molecule **39** resulted in a complex mixture of products in the ^1H NMR spectra when the reaction was carried out in methanol in the presence of $Pd(PPh_3)_4$ catalyst under basic conditions. This could be due to the high reactivity of azide towards phosphines, as seen in the Staudinger reaction. Therefore, the allyl carbamate molecule **39** was not used for further investigation in order to avoid any unwanted reactivity between the azide and phosphine ligands.

2.2.3 Propargyl carbamate as a cleavable group

After Optimisation of the linker stability by using carbamates instead of esters, we turned our attention to investigating a wider range of functional groups that can be cleaved by catalytic Pd under mild conditions. It has been reported that the Pd catalyses the depropargylation reactions more efficiently than the deallylation reactions without any additional reagents, potentially because the depropargylation reactions can be catalysed by Pd(0) or Pd(II) forms with little dependence on phosphine ligands, while the deallylation reaction needs a Pd(0)-active species and is greatly accelerated by phosphine ligands.[203,160,205,206] Therefore, depropargylation can reduce the need for strong reducing agents and phosphine ligands and may therefore prove more compatible with peptides.[207]

Chen and co-workers investigated propargyl/allyl carbamate lysine protecting/blocking groups and the Pd complexes that can catalyse uncaging reactions under living conditions (figure 47). They found allyl$_2$Pd$_2$Cl$_2$ and Pd(dba)$_2$ were the most efficient simple Pd complexes

that catalysed the uncaging reactions.[160] They reported the cleavage reaction of the propargyloxycarbonyl (Proc)-caged rhodamine was more efficient than the allyloxycarbonyl (Aloc)-caged rhodamine.[160] Moreover, neither of the simple Pd species catalyse the deallyation reaction of the Aloc-protected lysine amino acid in the absence of a reducing agent.[160] However, they showed the addition of the water-soluble phosphine ligand (TPPS) increased the deallyation reaction of the allyloxycarbonyl (Aloc)-caged rhodamine without any noticeable effect on the depropargylation reaction of the propargyloxycarbonyl (Proc)-caged rhodamine.[160]
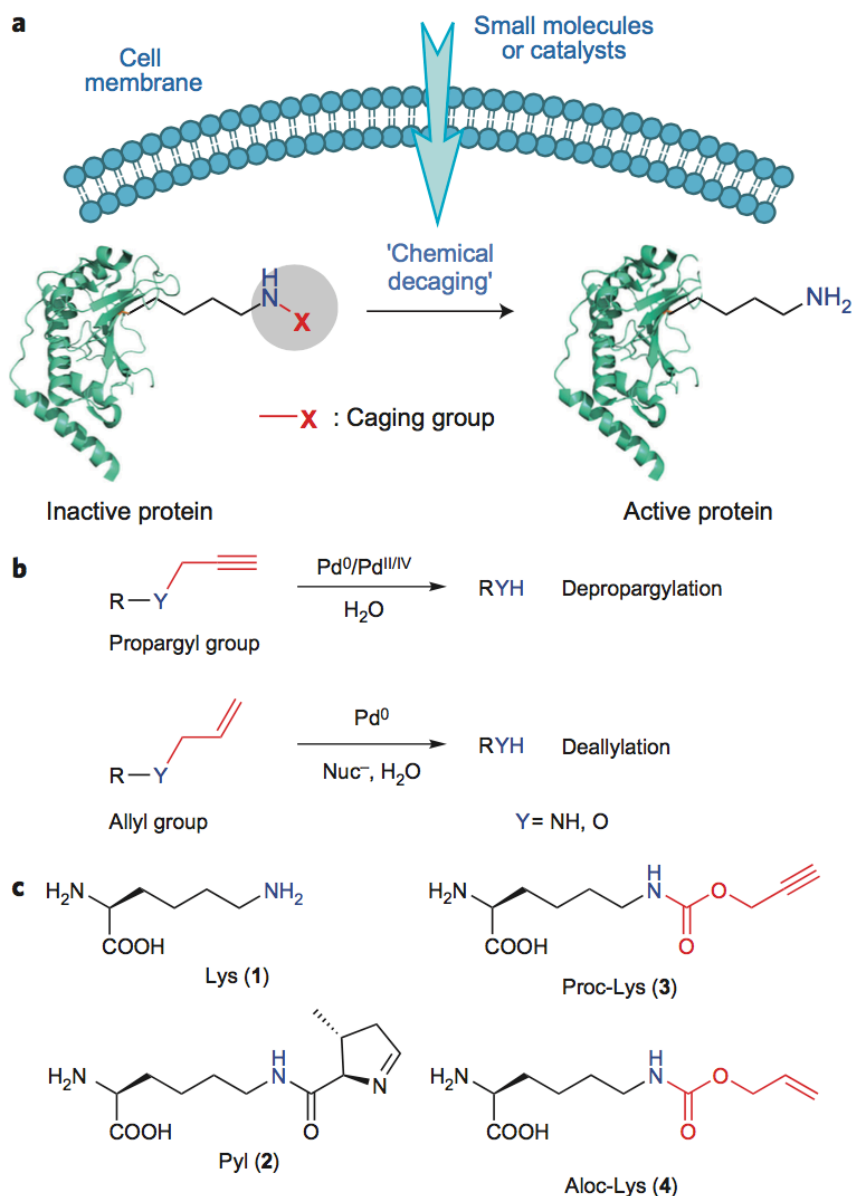
Figure 47: A chemical decaging strategy for protein activation in living cells. **a,** a lysine residue caged on a protein of interest, showing how a biocompatible catalyst triggers the decaging reaction to activate protein inside living cells. **b,** decaging conditions for propargyl and allyl group. **c,** Structures of lysine (Lys, 1), pyrrolysine (Pyl, 2), N- propargyloxycarbonyl-L-lysine (Proc-Lys, 3) and N-allyloxycarbonyl-L-lysine (Aloc-Lys, 4).

Unciti-Broceta and co-workers tested Pd catalysed deprotection reactions under biological conditions, with HPLC used to analyse the deprotection reactions at different time points.[203,205] They reported that Pd(0)-resin mediated the activation of 5-fluoro-1-propargyl-uracil (Pro-5FU) to release the cytotoxic 5-fluorouracil (5FU),and that this reaction was more efficient and faster than the activation of the 5-fluoro-1-allyl-uracil (All-5FU).[205] The same authors reported the activation of gemcitabine prodrugs was faster when the proc-protected gemcitabine was treated with Pd(0)-resin at 37 °C (reaction half-life < 6 hours) than the Alloc-protected gemcitabine.[203]

In contrast, Weissleder and co-workers tested different Pd(0) and Pd(II) catalysts under biological conditions. They reported the deallylation reaction of the Alloc-caged rhodamine was 37% more efficient than the deproprargylation reaction of the Proc-caged rhodamine. The addition of the electron deficient ligands (tri-2-furylphosphine (TFP)) increased the efficiency of the deprotection reaction due to the generation of a more reactive Pd(0) species.[208]

Wood and his co-workers investigated the cleavage of allyl carbamate attached to a Halo Tag labelled with tetramethylrhodamine (TAMRA) fluorophore to monitor the cleavage efficiency by loss of fluorescence. They screened a set of water-soluble phosphine ligands in combination with various nucleophiles and showed that the allyl carbamate cleavage conducted using sodium tetrachloropalladate (Na_2PdCl_4) in combination with o-DANPHOS (which is an electron-deficient sulfonated phosphine ligand) and the nucleophilic morpholine in amine-based buffer MOPS was nearly complete within 30 minutes in a protein-rich environment.[209]

Interestingly, despite the commonly observed poisoning of Pd(0) catalysts by thiols it was reported that the presence of glutathione increased the efficiency of the deallylation reaction. In this context glutathione was hypothesised to act as both nucleophile (to recycle Pd from the π-allyl complex) and reducing agent for the Pd.[210,211] In agreement with this finding, Bradley and his co-workers reported that Pd(0) microspheres catalysed the deallylation reactions of the Aloc-caged-rhodamine and that catalytic activity was increased 7 fold in the presence of 5 mM glutathione.[211]

2.2.4 Pd catalysed depropargylation

The Pd-catalysed reactions of allylic compounds have been extensively studied as discussed earlier in this chapter, while the reactions of propargylic compounds are more complex and less studied, although the propargylic carbonates are highly reactive.[212]

The Pd catalysed depropargylation reactions begin with oxidative addition of the Pd(0) to the propargyl compound to give the η^1-σ-propargyl Pd(II) intermediate complex, which is in equilibrium with η^1-σ-allenyl Pd(II) complex and η^3-π-propargyl Pd(II) cation complex (figure 48). The η^3-π-propargyl Pd(II) cation complex displays different reactivity towards nucleophiles, dependant on the nature of the nucleophile. Hard nucleophiles typically prefer to attack the C1 to form allenylated product or attack C3 to form the propargylated product (figure 48).[212,213,214]

In contrast, two equiv. of soft nucleophiles typically react with the η^3-π-propargyl Pd (II) cation complex in different mechanism. One equiv. of nucleophile undergoes the alkenylation reaction and another nucleophile undergoes the allyl alkylation reaction. The first equiv. of the nucleophile attacks the central position (C2) of the η^3-π-propargyl Pd (II) cation complex

followed by immediate protonation by the second equiv. of the nucleophile to produce η^3-π-allyl Pd (II) intermediate. This is followed by addition of the nucleophile to the η^3-π-allyl Pd (II) intermediate at one of the terminal positions to produce the alkene product (figure 48).[212,213,214,215,216]
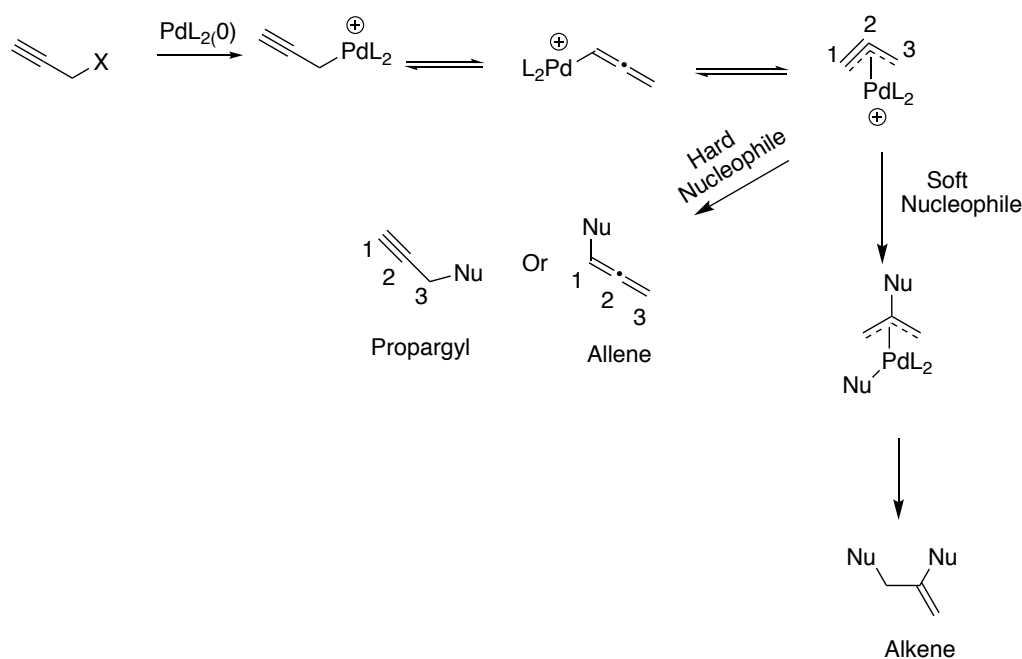
Figure 48: Pd catalysed reactions of propargyl compounds.

2.2.5 Design of a second cleavable group and Pd catalyst system

In order to investigate the Pd catalysed cleavage reaction under mild conditions, we synthesised a set of allyl and propargyl carbamates (scheme 29).[204] Different Pd(0) and Pd(II) catalysts were used to study the reactivity of these systems, including Pd(PPh$_3$)$_4$ and simple air stable Pd species (figure 49) that had been reported as useful catalysts for deprotection reactions at mild temperature.[160] The efficiency of the cleavage catalysed by each Pd species was evaluated by ^{1}H NMR and mass spectrometry. The stability of the carbamate derivatives in the basic conditions was initially tested by mixing them with potassium carbonate (K$_2$CO$_3$)

in CD$_3$OD for 24 hours, with ^{1}H NMR confirming that all carbamates **41**, **43**, **45**, **47** and **49** were

stable.
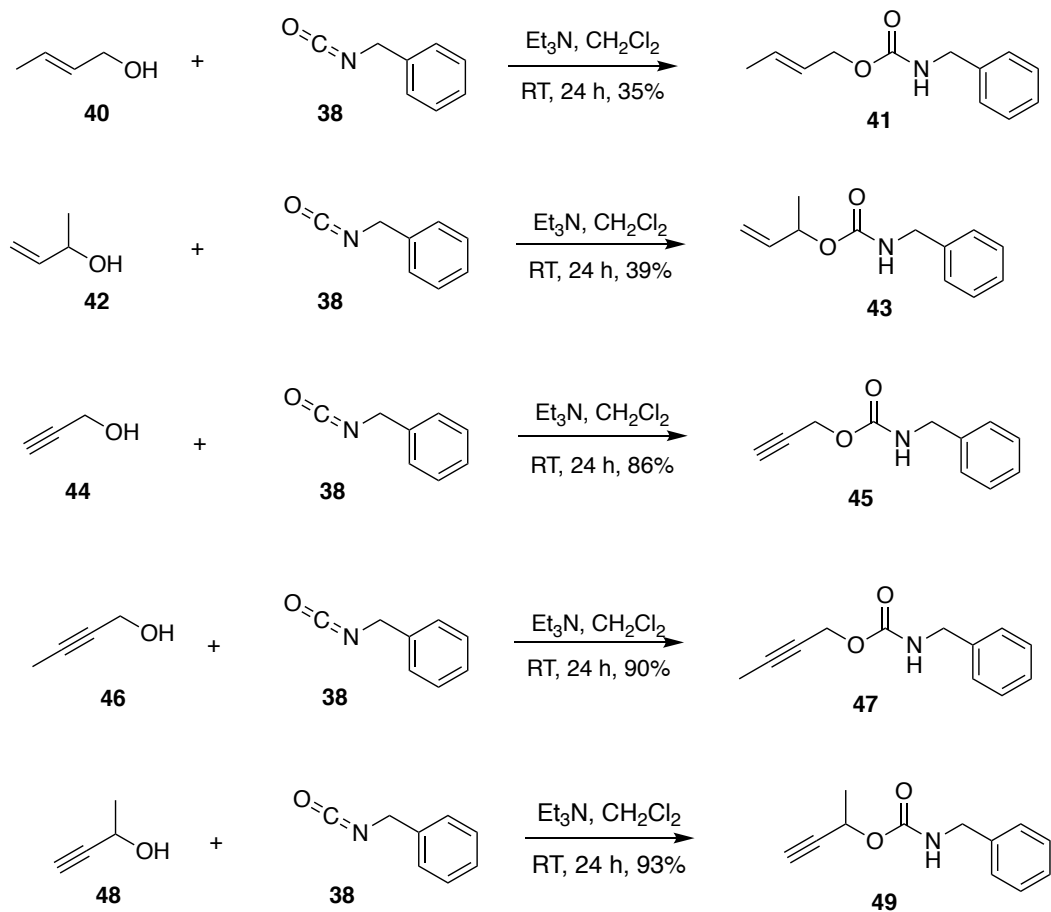
Scheme 29: Synthesis of the allyl and propargyl carbamate as model linkers that undergoes

cleavage reactions catalysed by Pd.
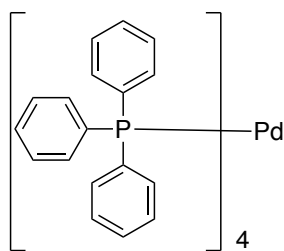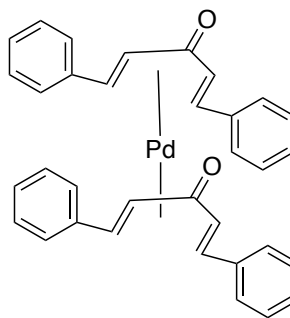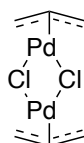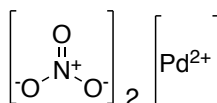
Figure 49: Pd species structures and formula.

The Pd tetrakis complex (Pd(PPh$_3$)$_4$) was the most efficient catalyst for the deallylation reactions. In contrast, none of the four simple Pd species catalysed the allyl carbamate cleavage (table 12). This result is broadly in line with the previous reports, where Pd catalysed deallyation reactions requires strong reducing agents or phosphine ligands to reduce the Pd to Pd(0)-active species (although in our case we add Pd(0) directly).[207]
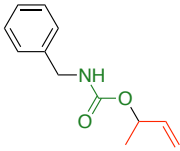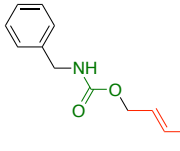
K$_2$CO$_3$, CD$_3$OD	Stable	Stable
5 mol% Pd(PPh$_3$)$_4$, K$_2$CO$_3$, CD$_3$OD	Complete conversion at 24 hours	Complete conversion at 24 hours
50 mol% Pd(PPh$_3$)$_4$, CD$_3$OD	Complete conversion at 24 hours	Complete conversion at 24 hours
5 mol% [PdCl(allyl)]$_2$, K$_2$CO$_3$, CD$_3$OD	No Reaction	No Reaction
5 mol% Pd (dba)$_2$, K$_2$CO$_3$, CD$_3$OD	No Reaction	No Reaction
5 mol% Pd (NO$_3$)$_2$, K$_2$CO$_3$, CD$_3$OD	No Reaction	No Reaction
5 mol% PdCl$_2$, K$_2$CO$_3$, CD$_3$OD	No Reaction	No Reaction

Table 12: The cleavage of the allyl carbamate derivatives by different Pd(0) and Pd(II) in the presence of base.

However the poor activity of Pd(dba)$_2$ suggests a more complex role for the phosphine ligands in activating the Pd species.[217,218,219,220] The use of the Pd(dba)$_2$ in the presence of the phosphine ligand is based on the dba being a poor ligand for the reaction, that therefore needs to be replaced by phosphine ligands to produce the active complex Pd(0)(PPh$_3$)$_2$ before the oxidative addition step (figure 50).[221,218,222] Adding 2 equiv. of PPh$_3$ affords a major complex Pd(0)(dba)(PPh$_3$)$_2$ which is unreactive and a minor complex Pd(0)(PPh$_3$)$_2$ which is the reactive complex that catalyses the oxidative addition.[221,223] The catalytic activity is dependent on the concentration of the Pd(0)(PPh$_3$)$_2$ in the solution, and therefore the dba and PPh$_3$ concentrations.[223,218,217]

$$Pd(0)(dba)_2 \longrightarrow Pd(0)(dba) + (dba)$$

$$Pd(0)(dba) \xrightarrow{2PPh_3} Pd(0)(dba)(PPh_3)_2 \underset{dba}{\overset{2PPh_3}{\rightleftharpoons}} Pd(0)(PPh_3)_4$$
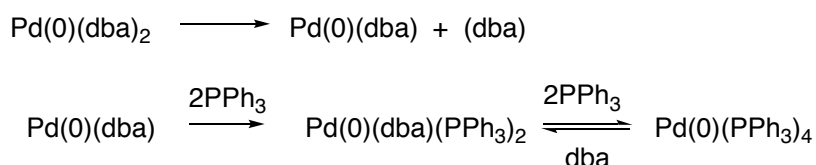
Figure 50: The ligands exchange between Pd(dba)$_2$ and triphenylphosphine.[223,221,217]

As the allyl carbamate compounds **41** and **43** have β-hydrogens, we suspected the Pd recovery from the η^3 π-allyl complex could proceed through a β-hydride elimination pathway to provide diene derivatives, as this process is suspected to be faster than the nucleophile pathway (figure 41, path B).[197,198] The external allyl carbamate **43** was successfully cleaved when the reaction was carried out in CD$_3$OD in the presence of Pd(PPh$_3$)$_4$ catalyst (5 mol%) under basic conditions, as well as the presence of 50 mol% Pd(PPh$_3$)$_4$ under neutral conditions, but not with lower Pd loadings.

From the poor reactivity of these systems under neutral conditions and the presence of alkene and methyl peaks corresponding to the methoxy allyl produced under basic conditions, we concluded that the β-hydride elimination didn't occur; therefore, the Pd catalyst cycle needed a nucleophile to recover the Pd from the η^3 π-allyl complex and release the allylated nucleophile (figure 51). The addition of the nucleophile can occur at two different sites to produce compound **51** or compound **52** (figure 52). The ^{1}H NMR showed the appearance of compound **52** and compound **51** in a 1:3 ratio (figure 51, third spectrum). More compound **51** formed in comparison to compound **52**, which we expect is a result of the secondary alkane cation being more stable than the primary alkane, therefore it is attacked more by nucleophile (figure 52).
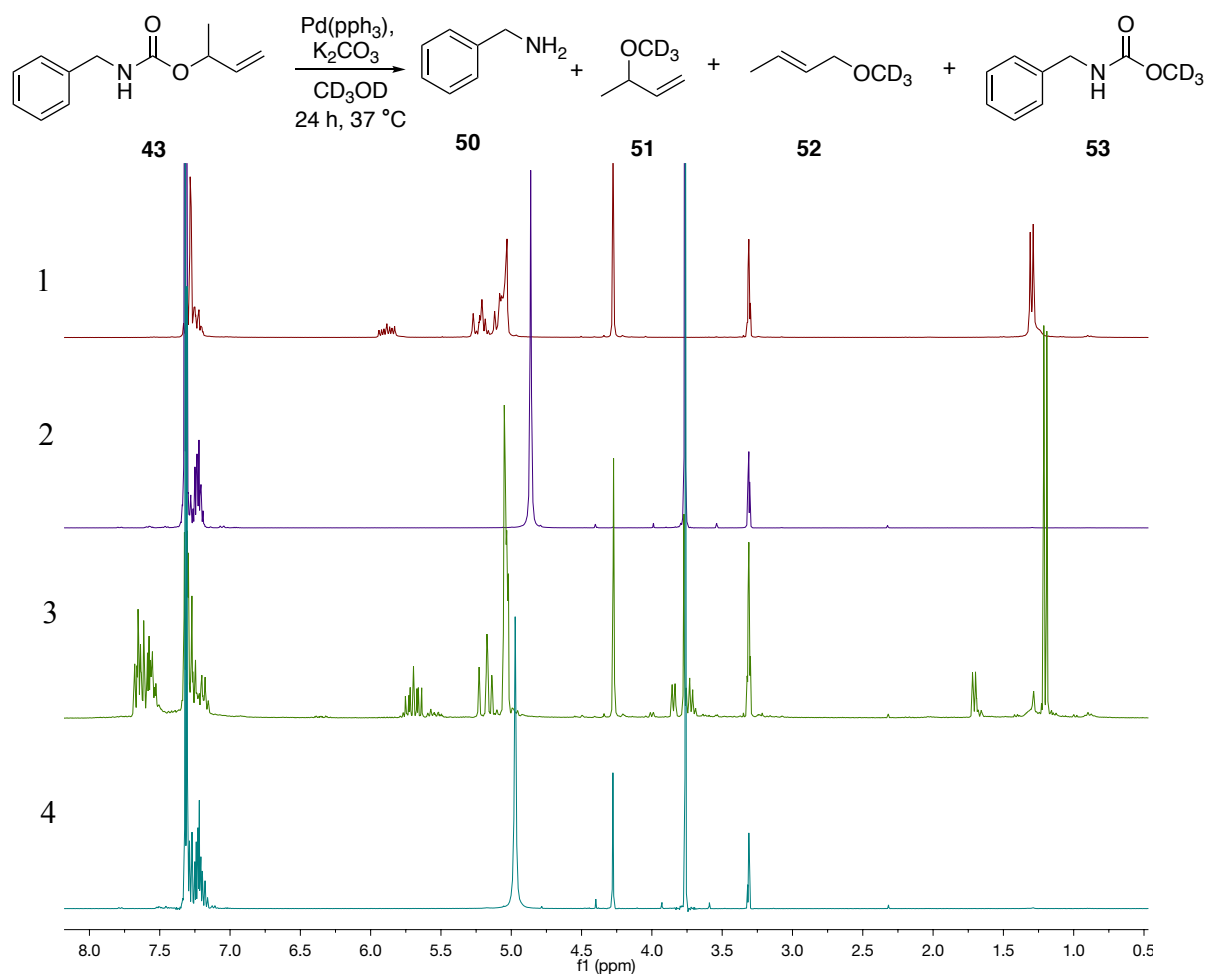
Figure 51: Comparison of ^{1}H NMR spectra for; 1- external allyl carbamate **43** in CD$_3$OD, 2- benzyl amine **50** suspected cleavage product in CD$_3$OD, 3- Pd catalysed cleavage of external allyl carbamate **43** in presence of potassium carbonate in CD$_3$OD and 4- direct reaction between potassium carbonate and benzyl amine **50** in CD$_3$OD.
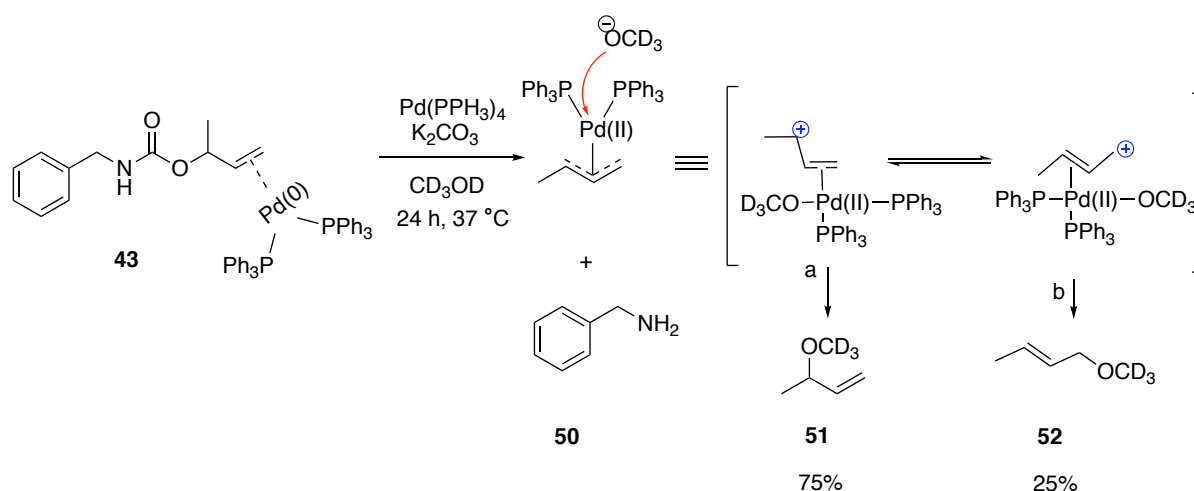
Figure 52: Pd catalysed cleavage of external allyl carbamate **43** provides mixture of the

compound **51** and compound **52**.

However, the ^{1}H NMR showed appearance of a peak at 4.25 ppm which is similar to the

protons between benzyl and carbamate in the starting material **43**, the absence of the C**H**-

CH-CH$_2$ allyl proton at 5.25 ppm confirms the starting material **43** is no longer present in the

reaction (figure 51). While the EI+ MS showed appearance of molecular weight 168, which

corresponds to methyl-D$_3$ benzylcarbamate **53** (figure 53). To better understand how this

compound forms in the reaction mixture, benzyl amine **50** was mixed with K$_2$CO$_3$ in CD$_3$OD

for 24 hours, the ^{1}H NMR showed appearance of protons at 4.25 ppm (figure 51, fourth

spectrum), which is consistent with formation of methyl-D$_3$ benzylcarbamate **53**.
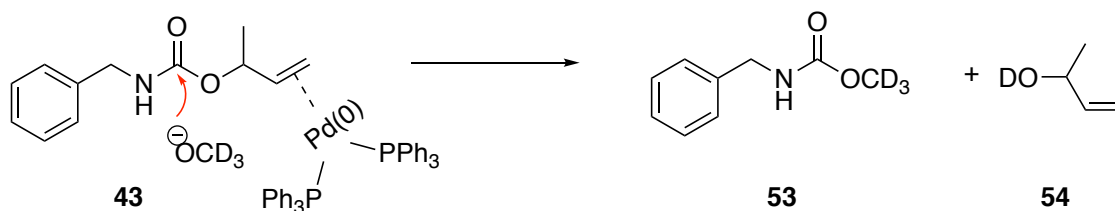
Figure 53: The possible formation of the methyl-d$_3$ benzylcarbamate **53** by direct methoxide

attack to the allyl carbamate.

The internal allyl carbamate **41** also was successfully cleaved when the reaction was carried out in CD$_3$OD in the presence of Pd(PPh$_3$)$_4$ catalyst (5 mol%) under basic conditions, as well as under neutral conditions in the presence of 50 mol% Pd(PPh$_3$)$_4$. This was confirmed by ^{1}H NMR, which showed the same benzyl amine **50** and mixture of internal **52** and external allyl **51** products in a 1:1.5 ratio (figure 54). This result was interesting as it suggests that while the Pd-allyl species retains the same reactivity, there is some contribution from a more direct reaction pathway where the regioselectivity remains controlled by the starting material.[224] Also, the ^{1}H NMR and EI+ MS again showed the appearance of the methyl-D$_3$ benzylcarbamate **53** (figure 55).
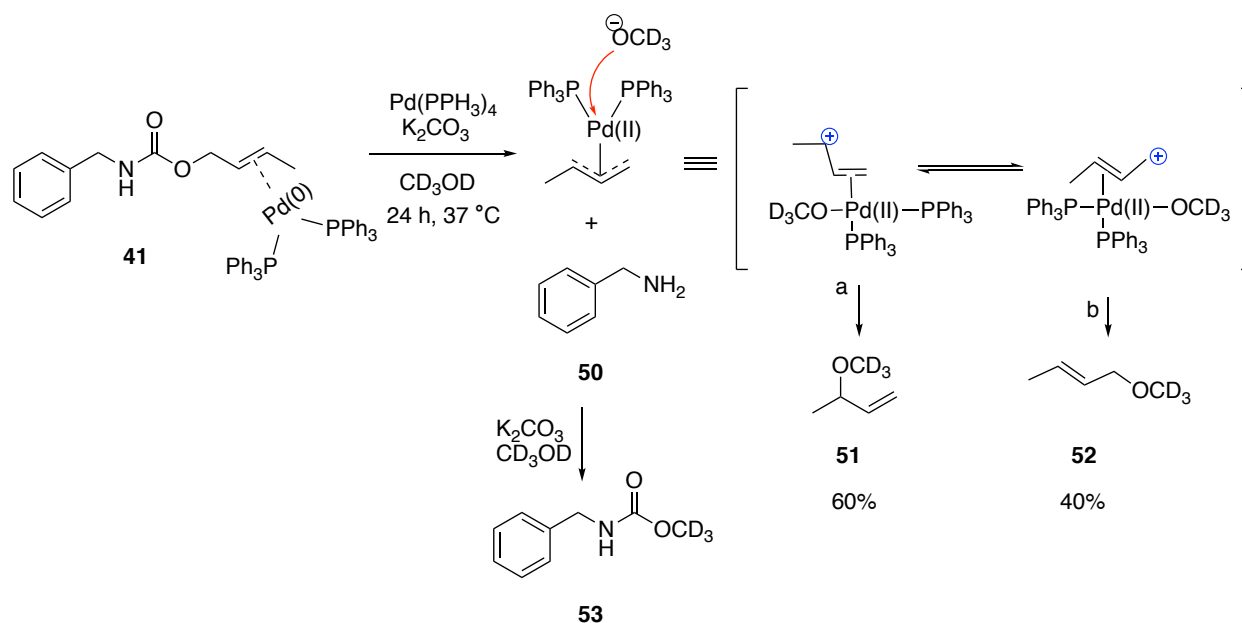
Figure 54: Mechanism of Pd catalysed internal allyl carbamate **41** cleavage, providing a mixture of compound **51**, **52** and **53**.
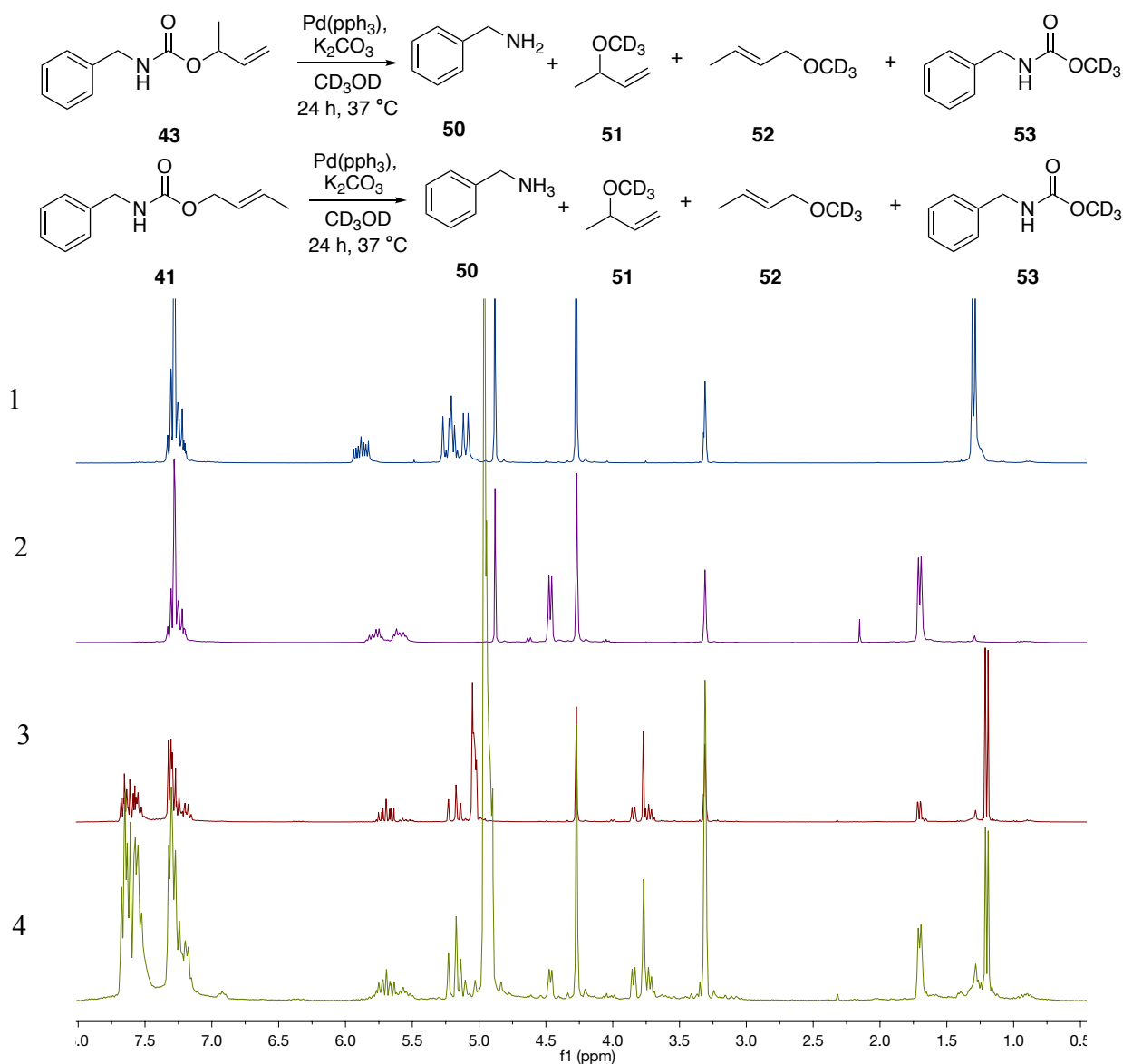
Figure 55: Comparison of ^{1}H NMR spectra for; 1- external allyl carbamate **43** in CD$_3$OD, 2-internal allyl carbamate **41** in CD$_3$OD, 3- Pd catalysed cleavage of the external allyl carbamate **43** in presence of potassium carbonate in CD$_3$OD, 4- Pd catalysed cleavage of the internal allyl carbamate **41** in presence of potassium carbonate in CD$_3$OD.

External propargyl carbamates **45** and **49** were stable in basic conditions, however in contrast to the allyl system these compounds are stable to Pd(PPh$_3$)$_4$, which didn't catalyse the depropargyltion reaction when the reaction was carried out with 5 mol% Pd(PPh$_3$)$_4$ in the

presence of base or 50 mol% Pd(PPh$_3$)$_4$ in neutral conditions (table 13). Interestingly these compounds are also stable (or poorly reactive) to the simple Pd reagents under neutral conditions, however under basic conditions these molecules are efficiently cleaved by the four simple Pd species. We found that the most efficient catalyst for the depropargylation reaction was [PdCl(allyl)]$_2$, which provided 100% cleavage within 24 hours followed by the Pd dba)$_2$, which provided 50% cleavage within 24 hours. That is in line with the previous report which found the most efficient depropargylation reaction of the Proc-caged rhodamine was obtained when [PdCl(allyl)]$_2$ and Pd (dba)$_2$ were used in the absence of any additional reagents.[160]
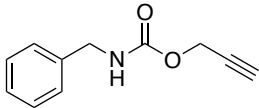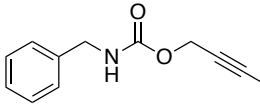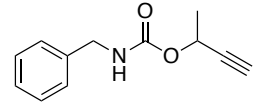
Pd source			
5 mol% Pd(PPh$_3$)$_4$, K$_2$CO$_3$, CD$_3$OD	No reaction	No reaction	No reaction
5 mol% [PdCl(allyl)]$_2$, K$_2$CO$_3$, CD$_3$OD	Complete conversion at 24 hours, 37 °C	Complete exchange of alcohols at 48 hours, 60 °C	Complete conversion at 2 hours, 37 °C
5 mol% Pd (dba)$_2$, K$_2$CO$_3$, CD$_3$OD	Starting Material + Products at 24 hours, 37 °C	Starting Material + exchange product at 48 hours, 60 °C	Complete conversion at 24 hours, 37 °C
5 mol% Pd (NO$_3$)$_2$, K$_2$CO$_3$, CD$_3$OD	Starting Material + Products at 24 hours, 37 °C	Starting Material + exchange product at 2 hours, 60 °C	Complete conversion at 24 hours, 37 °C
5 mol% PdCl$_2$, K$_2$CO$_3$, CD$_3$OD	Starting Material + Products at 24 hours, 37 °C	Starting Material + exchange product at 2 hours, 60 °C	Complete conversion at 24 hours, 37 °C

Table 13: The cleavage of the propargyl carbamate derivatives by different Pd(0) and Pd(II) catalysts in the presence of base.

External alkyne carbamate **45** was successfully cleaved when the reaction was carried out in CD$_3$OD in the presence of 5 mol% [PdCl(allyl)]$_2$ catalyst under basic conditions. The success of the cleavage reaction was confirmed by ^{1}H NMR and EI+ MS. However, the peak at 4.35 ppm, corresponding to the environment next to the alkyne **55** is smaller than expected, which may be due to the exchange with deuterium in the presence of Pd. Once again, the ^{1}H NMR and the EI+ MS confirmed that the methyl-d$_3$ benzylcarbamate **53** was formed under the reaction conditions (figure 56). To confirm that the peaks at 3.75 ppm and 4.25 correspond to product formation additional benzylamine was added to the reaction mixture after cleavage completion, resulting in an increase in the C**H**2 of the benzylamine **50** protons, with no new signals observed (figure 56, third spectrum).
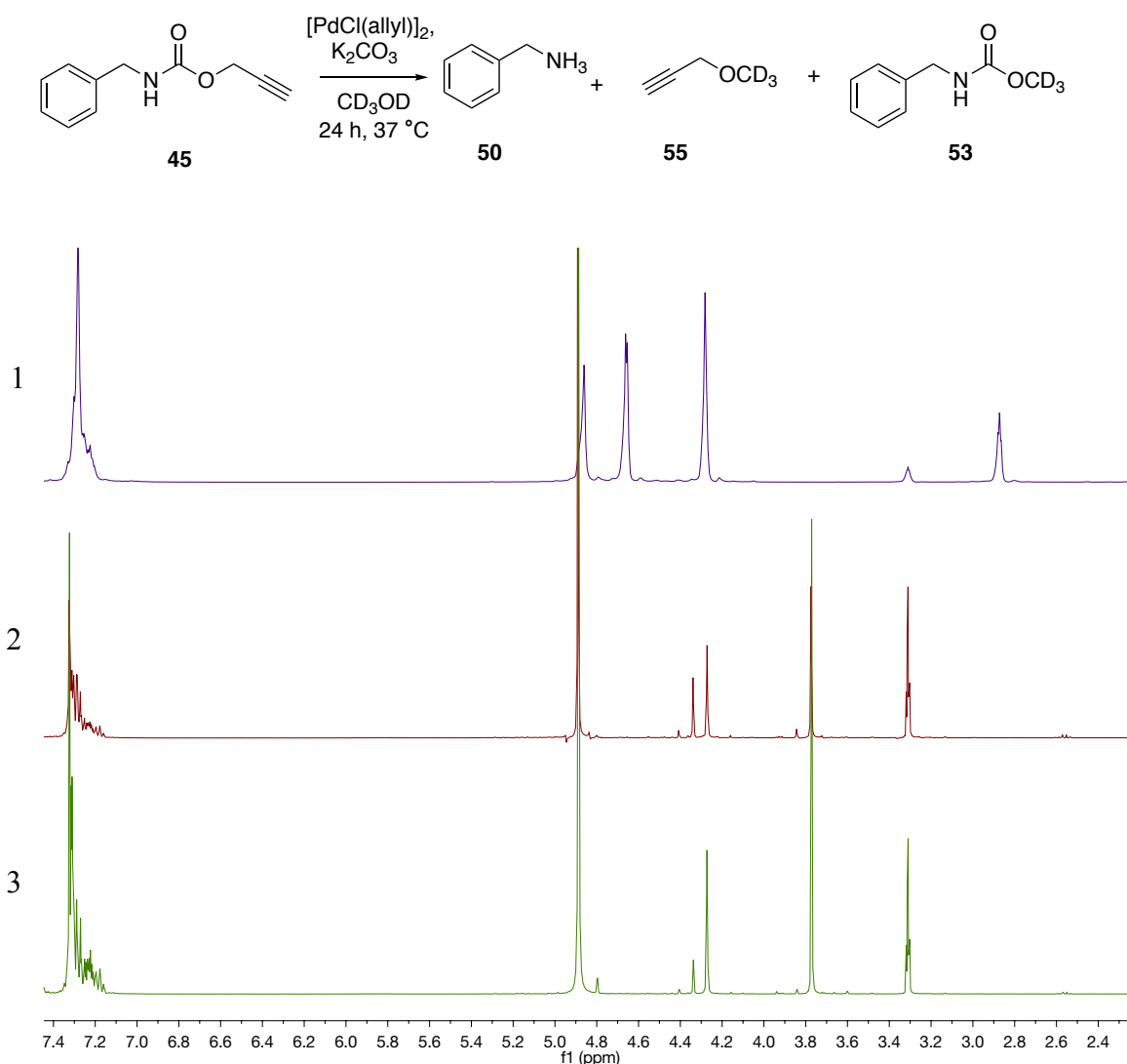
Figure 56: Comparisons of ^{1}H NMR spectra for; 1- external propargyl carbamate **45** in CD$_3$OD, 2- Pd catalysed cleavage of the external propargyl carbamate **45** in presence of potassium carbonate in CD$_3$OD, 3- Pd catalysed cleavage of the external propargyl carbamate **45** in presence of potassium carbonate in CD$_3$OD (3) followed by addition of benzylamine.

External propargyl carbamates **49** were successfully cleaved when the reaction was carried out in CD$_3$OD in the presence of 5 mol% [PdCl(allyl)]$_2$ catalyst under basic conditions. This was confirmed by ^{1}H NMR and the EI+ MS (figure 57). Surprisingly, the methyl protons of compound **56** are almost absent in the reaction mixture. This cannot be due to formation of

a stable Pd complex because it is present at catalytic levels (compared to using 100 mol% Pd on allyl ester above), and is not likely to be deuterium exchange. One alternative is that the results from a change in the reaction pathway, as some studies have demonstrated the formation of different molecules resulting from allenylated products.[225,226]

The internal propargyl carbamate **47** was stable under the basic conditions at 37 °C, however in contrast to **45** and **49** neither of the Pd species catalysed the depropargylation reaction when the reaction was carried out in presence or absence of base in CD_3OD at 37 °C for 24 hours. To optimise the depropargylation reaction of the internal propargyl carbamate **47**, the reaction temperature was increased to 60 °C, which resulted in a reaction that exclusively formed the methyl-d_3 benzylcarbamate **53**. While it is possible that the benzylamine **50** forms in this reaction and then is more fully converted to the carbamate at the higher temperature, it is more likely that direct nucleophilic attack by methoxide results in this change in product profile (scheme 30).

Based on these findings we decided to progress assessing all these systems under the more mild aqueous conditions that would be required should this chemistry be conducted on the immobilised protein systems.
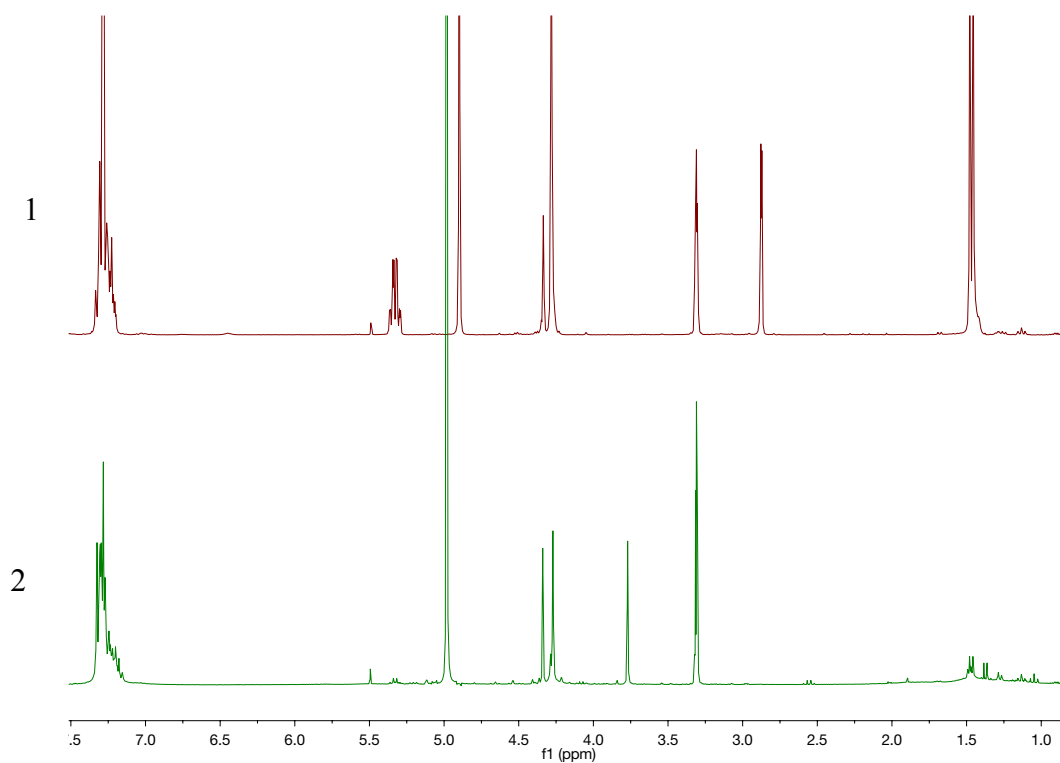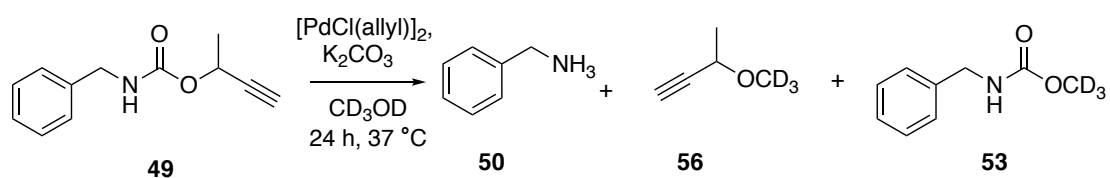
Figure 57: Comparison of ^{1}H NMR spectra for; 1- external propargyl carbamate **49** in CD$_3$OD, 2- Pd catalysed cleavage of the external propargyl carbamate **49** in presence of potassium carbonate in CD$_3$OD.
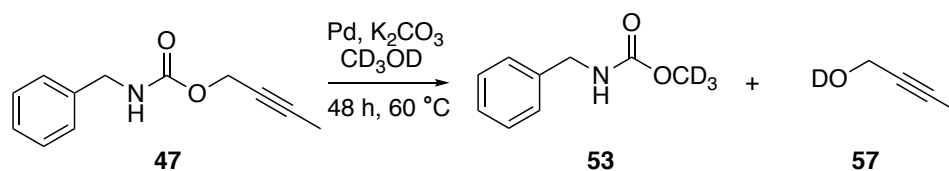
Scheme 30: Direct methoxide attack to provide methyl-d$_3$ benzylcarbamate **53**.

In order to address this, we prepared water soluble molecules **63**, **67**, **71** and **75** in three steps (scheme 31). The commercially available allyl and propargyl molecules **58**, **64**, **68** and **72** were treated with carbonyldiimidazole (CDI) **59** to offer the amine-reactive imidazolide derivatives **60**, **65**, **69** and **73**.[227] The commercially available N-Boc-ethylenediamine **61** was added to the imidazolide to offer the carbamate derivatives **62**, **66**, **70** and **74** in good yields.[228] This was followed by Boc deprotection under acidic conditions to offer the final water soluble model linker molecules **63**, **67**, **71** and **75**.[229] These water-soluble carbamate derivatives were mixed with K_2CO_3 in D_2O for 24 hours to test their stability. Unfortunately, the propargyl carbamates **71** and **75** were not stable and given we already had concerns about the aqueous solubility of allyl Pd (II) chloride dimer we conducted no further work on this linker system.

In contrast, the allyl carbamates **63** and **67** were stable in the basic conditions, however they did not cleave when the reaction was carried out in D_2O in the presence of $Pd(PPh_3)_4$ catalyst. That was unsurprising as the $Pd(PPh_3)_4$ has poor aqueous solubility and previous reports mention the importance of the nucleophile in the deallylation reaction, which is likely to be more important under these less basic conditions.[208]
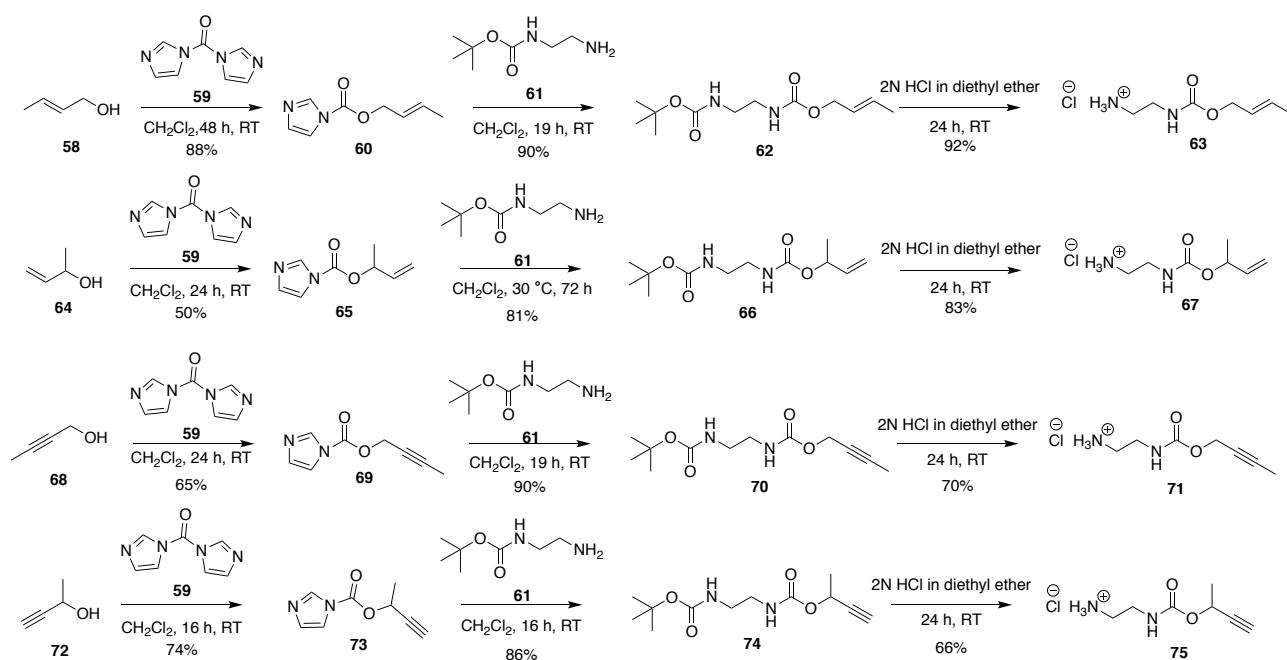
Scheme 31: The synthesis of water-soluble allyl and propargyl carbamates **63**, **67**, **71** and **75** as water soluble model linkers.

To optimise the deallylation reaction in the aqueous conditions, we carried out the reaction with a water soluble Pd species in the presence of an external nucleophile (scheme 32). We were encouraged by literature demonstrating that combining the electron-deficient water-soluble phosphine o-DANPHOS with the barbituric acid anion **76** (pK$_a$ 4) as a water-soluble soft nucleophile resulted in efficient uncaging of allyl species in aqueous conditions, where it was found that the carbon based nucleophilic dimethylbarbituric acid with PBS provided 90% cleavage of the allyl carbamate when used with the o-DANPHOS-derived Pd catalyst.[209] The electron-deficient ligand is thought to provide the catalytically active coordinatively unsaturated Pd species Pd⁰L4-n, whereas more electron-rich ligands stabilise the coordinatively saturated Pd species Pd⁰L4 which is catalytically inactive.[207,209]
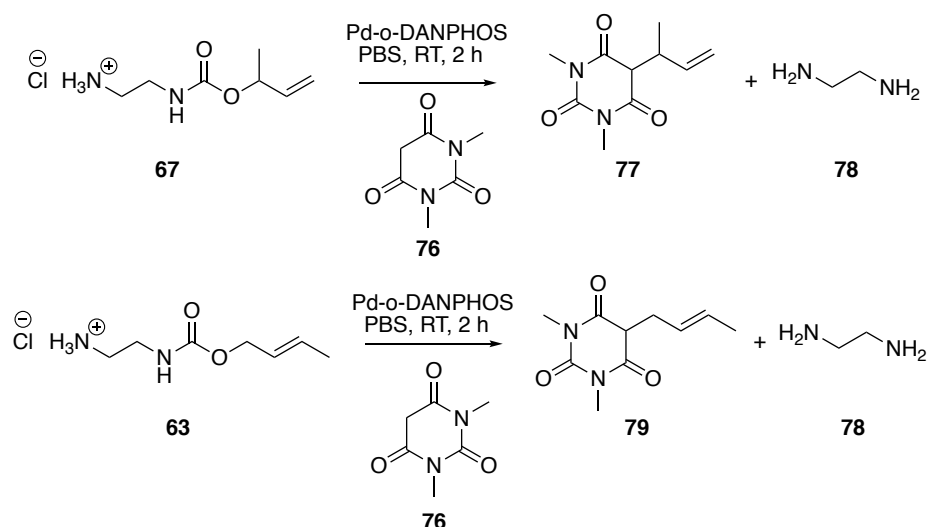
Scheme 32: Pd-o-DANPHOS complex catalysed cleavage of the allyl carbamates **63** and **67** in the presence of the external nucleophile (barbituric acid anion) **76**.

This system proved to offer superior reactivity to our previous efforts in non-aqueous conditions, with allyl carbamates **63** and **67** successfully cleaved within 2 hours. The allyl carbamates **63** successfully cleaved to form a clearly defined mixture of reaction products **78** and **79**. This was confirmed by ^{1}H NMR, which showed shift of the C**H**$_2$-CH=CH-CH$_3$ allylic protons from 4.50 ppm to 2.90 ppm and the NH$_2$-CH$_2$-C**H**$_2$-NHCO$_2$ protons next to carbamate from 3.1 ppm to 3.3 ppm (figure 58). Mass spectrometry showed the presence of the 1,3-dimethylbarbituric allyl molecule **79** when its acidic C**H** proton is exchanged with deuterium. This demonstrates the complexity of using aqueous NMR to monitor these reactions, as the chemical shifts of the NH$_2$-C**H**$_2$ environments in both starting material and product are influenced by ionisation of the amine. In the case of the ethylene diamine product we anticipate these peaks will be especially as the second pKa of this molecule is 7.5, meaning small pH changes around the initial pH of 7.4 are likely to significantly impact on ionisation. To confirm the desired product had formed we added more ethylenediamine **78** to the reaction after cleavage completion, this presumably raises the pH/reduces ionisation

resulting in the ethylenediamine 4 protons at 3.3 ppm shifting into 2.75 ppm, however no new signals were observed (figure 58).
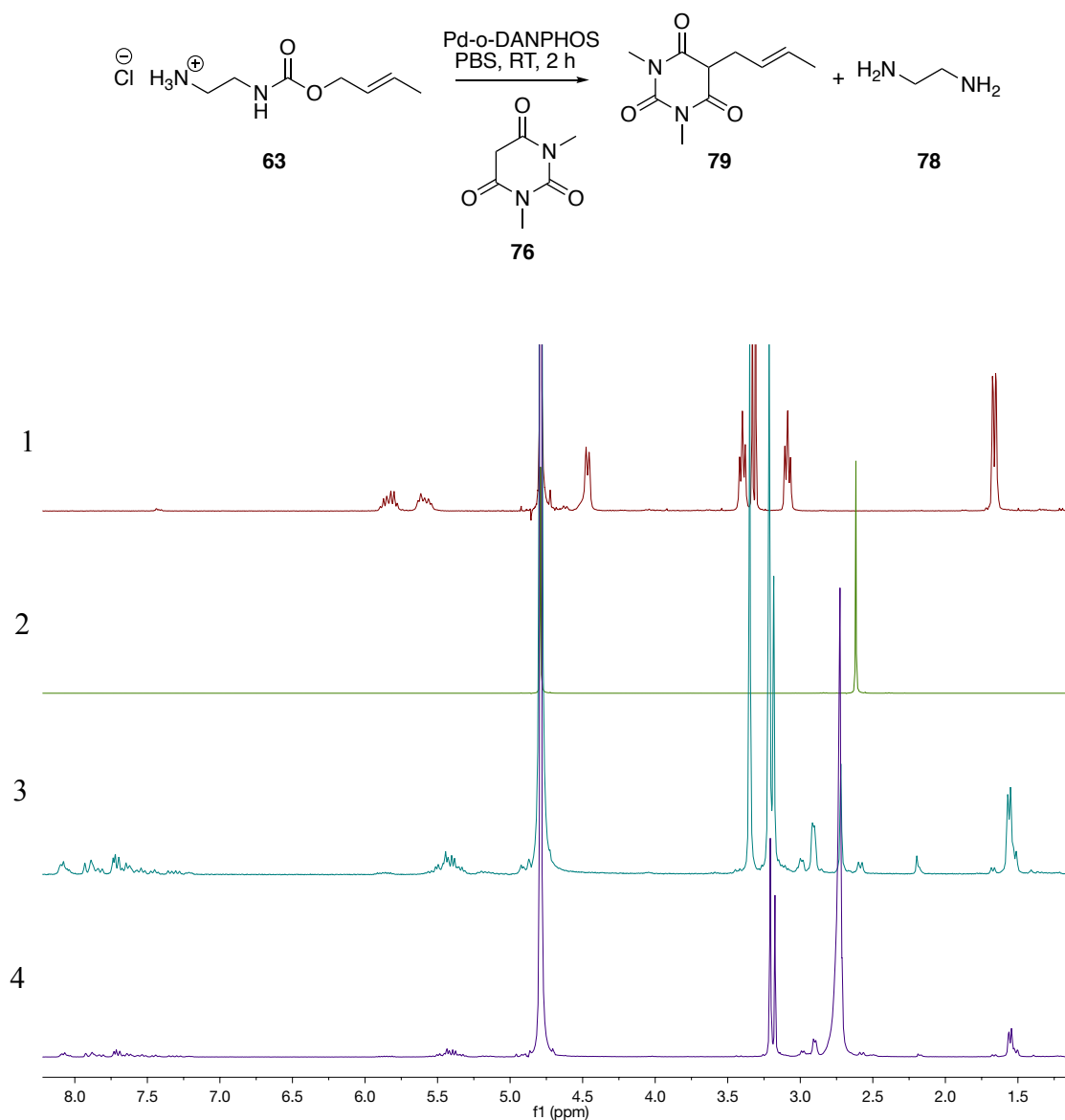
Figure 58: Comparison of ^{1}H NMR spectra for; 1- allyl carbamate **63** in PBS, 2- ethylenediamine **78** cleavage product in PBS, 3- Pd-o-DANPHOS catalysed cleavage of the allyl carbamate **63** In presence of barbituric acid anion **76** in PBS, 4- Pd-o-DANPHOS catalysed cleavage of the allyl carbamate **63** In presence of barbituric acid anion **76** in PBS (3) followed by addition of ethylenediamine **78**.

To confirm that allyl cleavage was due to the Pd catalyst control reactions were performed (table 14). The o-DANPHOS-derived Pd catalyst provided 45% cleavage of the allyl carbamate **63** in the absence of the dimethylbarbituric acid **76**, however in the absence of the Pd-o-DANPHOS no cleavage was observed. We are therefore satisfied that these cleavage conditions should be suitable for use in the solid phase system.

	O-DANPHOS (0.4 equiv.)	Dimethylbarbituric acid 76 (1 equiv.)	Time	Cleavage %
A	X	X	2 H	100%
B	X		2 H	45%
C		X	2 H	0
D			2 H	0

Table 14: Different reaction condition for deallylation of **63**.

2.3 Second generation solid phase alkylation agent system with allyl carbamate as a cleavable linker

With the allyl carbamate linker in hand, we turned our attention to immobilisation onto the solid support. To avoid the issues with agarose stability under the CuAAC chemistry conditions which we faced during the immobilisation of the allyl ester linker onto the aldehyde-modified agarose gel, the NHS-activated agarose was selected to provide the activated solid support for the alkylation linker. The NHS-activated agarose provides a long spacer arm that could help in simplifying the synthesis of the alkylation linker, as the long chain linker is hard to purify and this long spacer arm is expected to be necessary to allow sufficient reactivity between the protein and agarose.

The NHS-activated agarose is an amine-reactive solid support that can be used for a rapid immobilisation of species containing a primary or secondary amines in a simple one-step reaction to form a chemically stable amide linkage. Given the unreacted primary amine can be detected by several primary amine detection assays, we anticipated that we should be able to detect the concentration of the unreacted linker without needing to the fluorophore model system previously used. The alkylation linker was redesigned to include a primary amine to immobilise onto the NHS-activated agarose, retaining the allyl carbamate as a cleavable group. The chloroacetamide was included as the thiol alkylation agent, with no secondary functionality in the model system (figure 59).

80
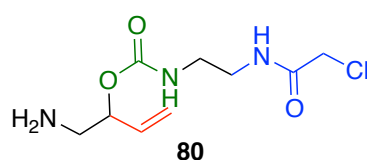
Figure 59: Thiol alkylation linker with cleavable group and primary amine to immobilise onto solid support.

Several assays can be used to detect the free primary amine in order to estimate the coupling efficiency. The fluorescamine assay can be used for quantitative and qualitative primary amine detection as fluorescamine is a powerful fluorogenic reagent that generates a fluorescent product when reacted with primary amino compounds.[230] At basic pH, fluorescamine reacts stoichiometrically with primary amines at room temperature within a fraction of a second to give fluorophores which are stable for several hours,[231] The excess of the reagents is hydrolysed in few seconds to give non-fluorescent products, therefore concentration of primary amine is proportional to the resulting fluorescence.[231] This negates the need for a separate markers as the unreacted primary amine in the coupling solution

following incubation with the NHS-activated agarose can be treated with fluorescamine, with the emission at 479 nm proportional to the amount of the unreacted amine based on a standard curve generated with the amine sample used in the reaction (scheme 33).
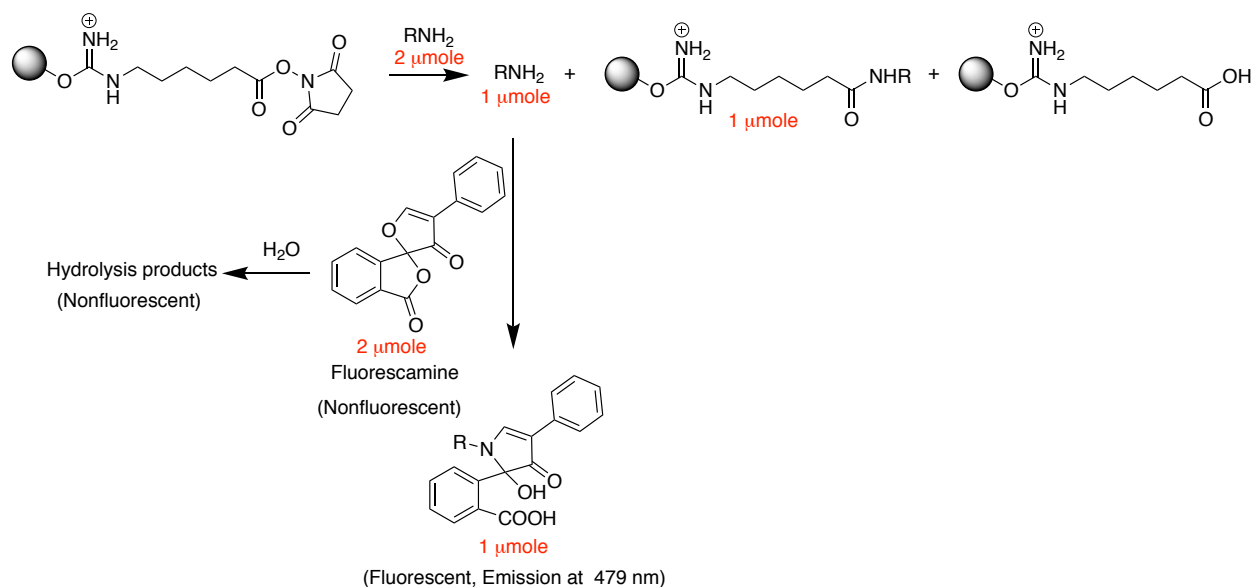
Scheme 33: Analysis of the immobilised alkylation linker onto agarose by fluorescamine detection of unreacted amine.

2.3.1 Synthesis of the alkylation linker with allyl carbamate

The alkylation linker **80** was prepared in 5 steps by using compound **6** that was prepared before in the alkylation linker **1** (scheme 34). Compound **6** was treated with carbonyldiimidazole (CDI) **59** in dichloromethane at room temperature to offer 67% of the amine-reactive imidazolide **81** as confirmed by mass spectrometry, ^{13}C NMR and ^{1}H NMR.[227]

Then, the commercially available N-Boc-ethylenediamine **61** was added to the imidazole **81** in dichloromethane at room temperature to offer compound **82** in 86% yield.[228] This was followed by Boc deprotection under acidic conditions to offer compound **83** in 93% yields.[229]
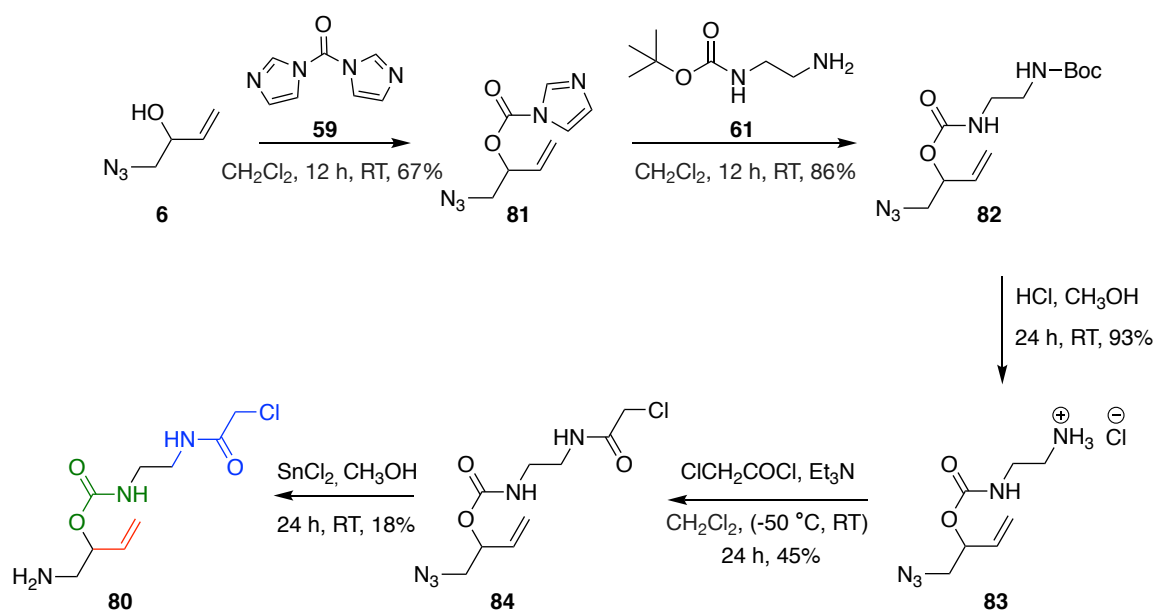
Scheme 34: Synthesis of the alkylation linker with allyl carbamate **80**.

The next step was the preparation of the chloroacetamide, which was achieved by treatment of compound **83** with the commercially available chloroacetyl chloride (ClCH$_2$COCl) in dichloromethane in the presence of triethylamine for 24 hours to provide compound **84** in 45% yield.[232] The final step in the synthesis of the alkylation linker **80** was the azide reduction to primary amine. This could not be achieved by hydrogenation due to the high reactivity of the alkene and chloride under these conditions, and we were also concerned about potential reactivity of the chloride using typical Staudinger-type azide reduction conditions. Therefore, compound **84** was treated with tin chloride (SnCl$_2$) in methanol at room temperature for 24 hours to offer the final alkylation linker **80**, IR confirmed the disappearance of azide group at 2100 cm^{-1}.[233] However, after purification very low yield (18%) was obtained and it was not complete pure.

In order to facilitate the purification of the alkylation linker **80** by silica chromatography, the primary amine was protected with Boc group **85**, followed by Boc deprotection to offer the

alkylation linker **80** again (scheme 35).[234,235] However, ^{1}H NMR showed similar impurities in

the alkylation linker **80** in compound **85**. Therefore, we tried to reduce the azide by using iron

instead of tin chloride using a model azide compound **39** to preserve our supply of compound

84 (scheme 36). However, when compound **39** was treated with iron in the presence of

hydrogen chloride in ethanol for 24 hours at room temperature, no primary amine was

observed.[236]
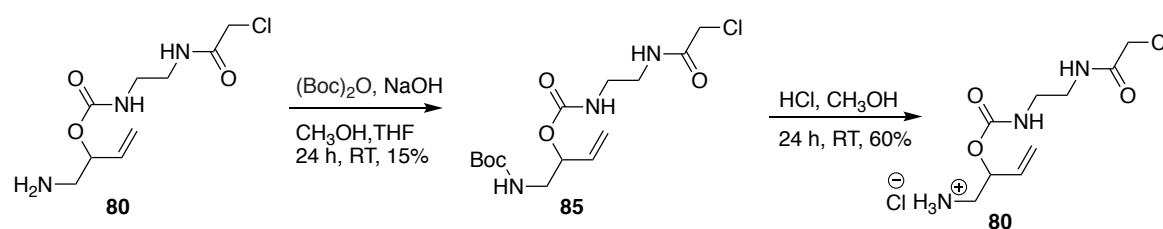
Scheme 35: Protection of primary amine to facilitate purification process followed by

deprotection. [234,235]
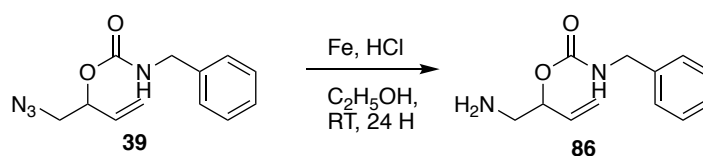
Scheme 36: Investigation of the efficiency of the iron to reduce azide **39**.[236]

In order to optimise the synthesis of the alkylation linker **80**, we decided to change the

sequence of the synthesis pathway, conducting the azide reduction in the first step to offer

the primary amine followed by amine protection reaction, which will add two more steps but

allow to investigate more reduction conditions such as triphenylphosphine that we can not

use to reduce compound **84** (scheme 37). However, when compound **6** was treated with

triphenylphosphine in THF and H_2O at room temperature, after 48 hours we obtained the primary amine in very low yield.[237,238]
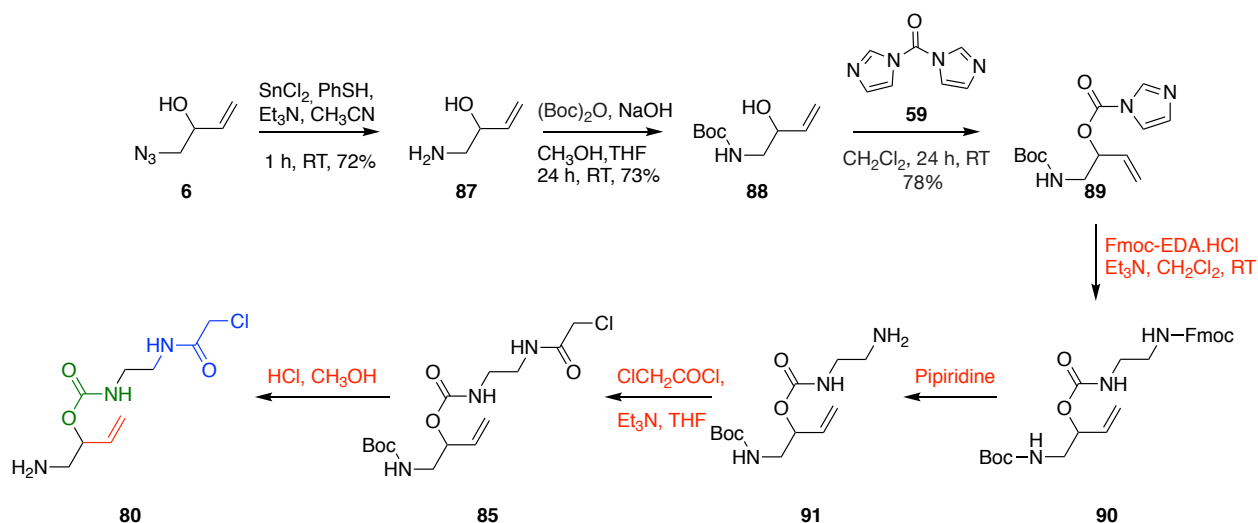
Scheme 37: Second pathway for the synthesis of the alkylation linker with allyl carbamate **80**.

To optimise the azide reduction, a model compound **82** was used to investigate to preserve our supply of starting material (scheme 38). Therefore, azide compound **82** was treated with different reducing agents in different conditions (table 15). The mixture of tin chloride ($SnCl_2$) with thiophenol (PhSH) was the most efficient azide reduction condition trialled, yielding 82% of primary amine **92** in 1 hour at room temperature.[239,240,241] IR confirmed the disappearance of azide group at 2100 cm^{-1}. In contrast, the using tin chloride ($SnCl_2$) alone without thiophenol and base provided low yield (22%) of primary amine **92** in 24 hours. Moreover, triphenylphosphine provided very low yield of primary amine in longer reaction time (table 15).[242]
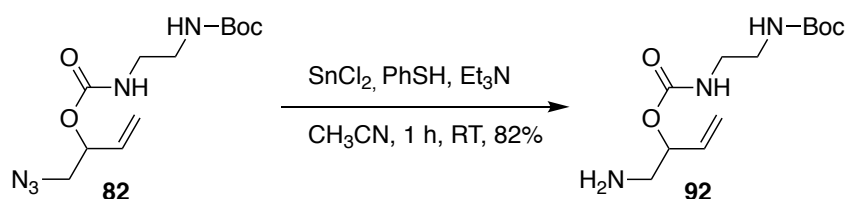
Scheme 38: Model azide compound to investigate the azide reduction reaction.

Reducing agent	Additive	Time	Yield
PPh$_3$, THF, H$_2$O		24 hours	20%
PPh$_3$, CH$_2$Cl$_2$, H$_2$O		24 hours	28%
PPh$_3$, CH$_2$Cl$_2$, H$_2$O	Na$_2$CO$_3$	24 hours	16%
SnCl$_2$, CH$_3$OH		24 hours	22%
SnCl$_2$, CH$_3$CN	PhSH, Et$_3$N	1 hour	82%

Table 15: different reaction condition for azide reduction into primary amine.

After finding an efficient conditions for the azide reduction reaction, compound **6** was mixed with tin chloride and thiophenol in acetonitrile (CH$_3$CN) at room temperature for 1 hour to yield 72% of primary amine **87**.[240] The second step in the alkylation linker **80** synthesis was the protection of the primary amine by Boc group, followed by addition of CDI **59** to give amine-reactive imidazolide **89** (scheme 37).[234,227]

The following steps in the planned synthesis of the alkylation linker **80** were the formation of the carbamate by replacing the imidazole of compound **89** by the primary amine of the mono-Fmoc ethylene diamine hydrochloride (Fmoc-EDA.HCl) followed by Fmoc deprotection under basic conditions. Therefore, the amine-reactive imidazolide **89** was treated with the commercially available Fmoc-EDA.HCl in dichloromethane in the presence of 5 equiv. of triethylamine at room temperature.[228] Unfortunately, imidazole **89** was apparently unstable in the basic conditions and the Fmoc group in Fmoc-EDA.HCl was also deprotected to some extent, with ^{1}H NMR showing a mixture of products including a range of fluorenyl compounds

and imidazole. Therefore, we decided to decrease the amount of triethylamine to 1 equiv. instead of 5 equiv., however no reaction occurred after 24 hours, therefore we added more 2 equiv. triethylamine, however once again the Fmoc group was not stable and ^{1}H NMR showed mixtures of products. In a final attempt to optimise the reaction, 2.8 equiv. of *N,N*-diisopropylethylamine (DIPEA) was used instead of triethylamine. Unfortunately, the Fmoc group was deprotected and ^{1}H NMR showed mixtures of products after 1 hour. Our conclusion was that both imidazole **89** and Fmoc-EDA.HCl are unstable under these basic conditions, therefore, we tried to avoid adding base by neutralizing the primary amine before mixing with imidazole **89**. Therefore, Fmoc-EDA.HCl in methanol was passed through the strong cation exchange (SCX) chromatography column, eluting with methanolic ammonia to offer neutral Fmoc-EDA. Following concentration this was added to imidazole **89** in dichloromethane at room temperature. Unfortunately, there was still evidence of Fmoc deprotection even in the absence of the additional base, although it is possible this occurred during neutralisation.

We therefore decided to add ethylenediamine directly followed by reaction with chloroacetyl chloride without purification, which saved 2 steps in the synthesis of the alkylation linker **80** (scheme 39).[228] Therefore, the imidazole **89** was treated with excess of the commercially available ethylenediamine (10 equiv.) in dichloromethane at room temperature for 2 hours. To avoid issues with purification of the primary amine this intermediate was taken into the next step without any purification, therefore it is treated with chloroacetyl chloride in THF in presence of triethylamine for 24 hours to offer compound **85**.[232] The final step in the alkylation linker **80** synthesis was Boc deprotection under acidic conditions (scheme 39).
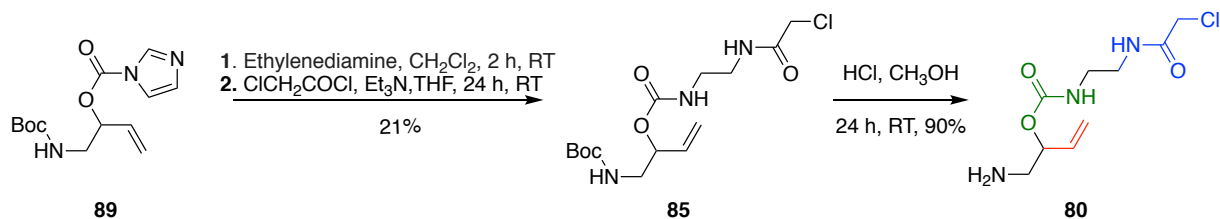
Scheme 39: Optimised synthesis of the alkylation linker **80**.

2.3.2 A model system to investigate the immobilisation and release

Ethanolamine (ETA) was used as a simple water-soluble primary amine in order to investigate the best conditions for the immobilisation of the primary amine onto the NHS-activated agarose **93** (scheme 40). The detection conditions were validated by incubating different concentrations of the ethanolamine in PBS with 1 mM fluorescamine in acetonitrile (1:1). Fluorescence was directly proportional to the ethanolamine concentration across a concentration range from 1 μM to 125 μM (figure 60). To make sure the fluorescence produced is due to the reaction of the unreacted primary amine with fluorescamine some additional controls were undertaken. No fluorescence was observed when *N*-hydroxysuccinimide and triethylamine were treated with fluorescamine (figure 61, A) or when the NHS-activated agarose was incubated with PBS and then the washed solvents treated with fluorescamine (figure 61, B).
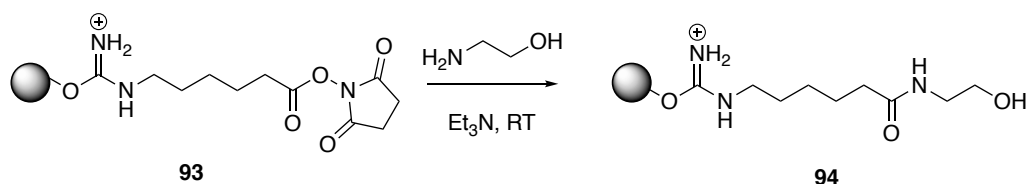
Scheme 40: Immobilisation of ethanolamine onto NHS-agarose.
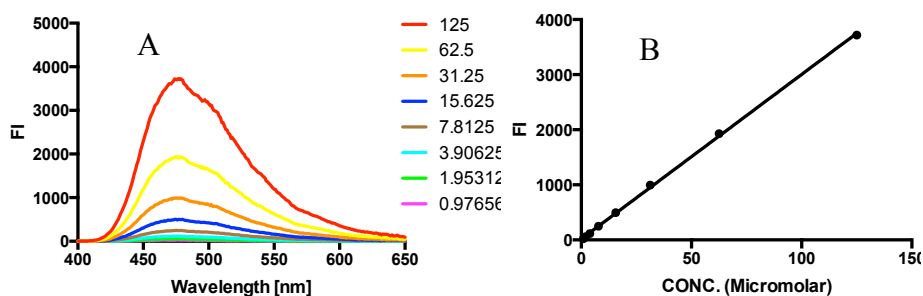
Figure 60: A- The florescence of the Ethanolamine treated with fluorescamine; B- The standard curve of ethanolamine fluorescence in PBS.
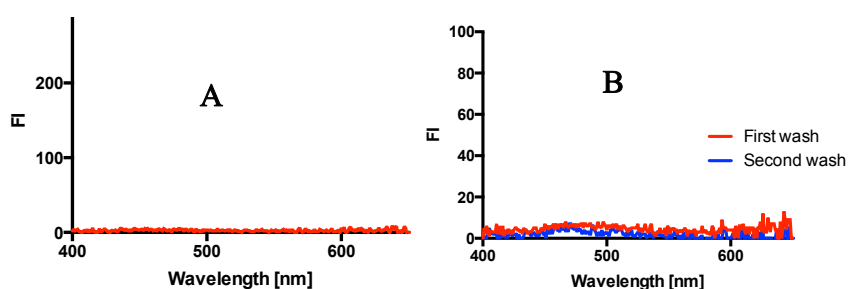
Figure 61: A- Emission spectra of *N*-Hydroxysuccinimide and triethylamine treated with fluorescamine; B- Emission spectra of the washed solvents of NHS-agarose treated with fluorescamine.

To investigate the coupling time to NHS-agarose, 0.25 equiv. of ethanolamine (relative to the reported NHS loading) in PBS was mixed with the NHS-activated agarose for 2 hours and 24 hours at room temperature. Unreacted amine was isolated by repeated washing until fractions showed no amine content on analysis. The fluorescence of the unreacted ethanolamine confirmed that most of the amine (82%) was immobilised onto agarose after just 2 hours reaction, while increasing the reaction time improved the coupling yield to 91% (table 16).

NHS-agarose (μmole)	ETA (μmole)	Coupling time (H)	Coupling solution	Washed ETA (μmole)	Reacted ETA (μmole)	Coupling %
4.2	1.1	2	PBS	0.2	0.9	82%
4.2	1.1	24	PBS	0.1	1.0	91%

Table 16: Investigation of coupling time in the reaction between NHS-agarose **93** and ethanolamine.

With the loading and detection methods established, amine allyl carbamate *N*-Boc ethylenediamine **92** was used to investigate the loading efficiency of the NHS-activated agarose **93** with the primary amine and the release from the solid support by Pd catalysis in aqueous conditions (scheme 41). The NHS-activated agarose **93** was mixed with 0.25 equiv. of the amine allyl carbamate *N*-Boc **92** in PBS for 24 hours at room temperature. The fluorescence of the washed unreacted amine confirmed that 69% of the amine allyl carbamate *N*-Boc was immobilised onto agarose **95** (table 17, entry 1).
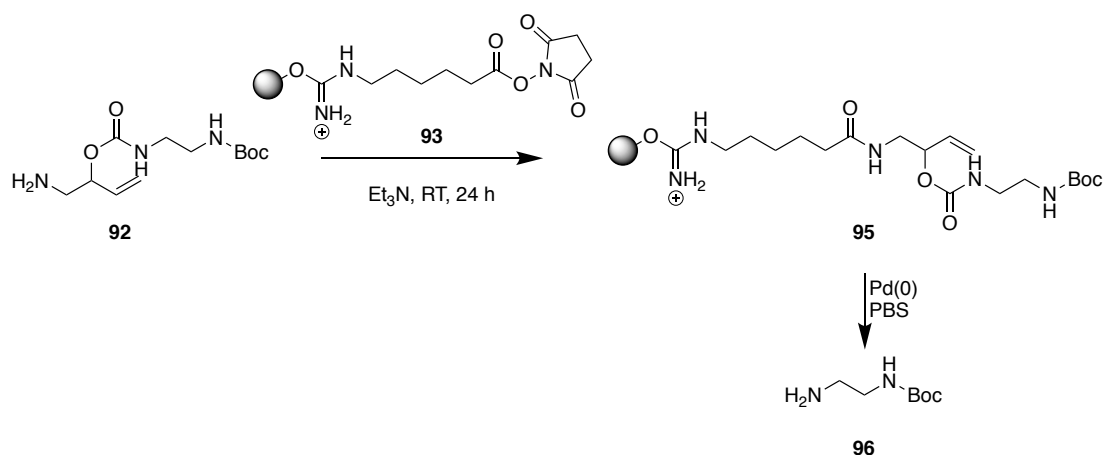
Scheme 41: The loading of the NHS-activated agarose with the model primary amine molecule and the release from the solid support by Pd catalysis.

Given the increased lipophilicity of the Boc containing compound **92** relative to ethanolamine it is possible the loading is limited by poor aqueous solubility. Therefore, to optimise the coupling efficiency, acetonitrile was used as the coupling solvent. The reaction of the NHS-activated agarose **93** with 0.25 equiv. of the amine allyl carbamate *N*-Boc **92** in acetonitrile for 24 hours at room temperature resulted in 100% of amine immobilisation onto the agarose **95** (table 17, entry 2). In addition to increased solubility, the improvement when the reaction is carried out in acetonitrile is also likely to be due to the increased stability of the NHS ester in non-aqueous media, whereas in PBS the amide formation reaction is competing with the hydrolysis of the NHS ester.

	NHS-agarose (µmole)	amine (µmole)	Coupling time (H)	Coupling solution	Washed amine (µmole)	Reacted amine (µmole)	Coupling %
1	20.0	5.0	24 H	PBS	1.6	3.4	69%
2	20.0	5.0	24 H	CH$_3$CN	0	5.0	100%

Table 17: The loading of the NHS-activated agarose with the model primary amine **92** in different coupling solvent.

To investigate the stability of the NHS ester, the NHS-activated agarose **93** was mixed with ethanolamine at room temperature for 24 hours. The unreacted ethanolamine was washed with the coupling solvent and detected, followed by the addition of further ethanolamine to the agarose to evaluate the capacity for further loading (i.e. the presence of residual NHS-ester).

In the first coupling reaction between 0.5 equiv. of ethanolamine and the NHS-activated agarose **93** in PBS, 47% of the NHS ester was converted to the amide **94** (97% of the ethanolamine reacted). Following the second addition of 1.0 equiv. ethanolamine to the agarose, just 12% of the ethanolamine was coupled with the agarose, suggesting the remaining 41% of the NHS ester **93** had been hydrolyzed during the initial incubation (table 18, entry 2). In keeping with this result, when the NHS-activated agarose **93** was kept in PBS at room temperature for 24 hours before ethanolamine addition, the fluorescence of the washed ethanolamine was proportional to the amount of the added ethanolamine (8.0 μmole), confirming the hydrolysis of the NHS ester in PBS (table 18, entry 1).

	NHS-agarose (μmole)	ETA (μmole)	Coupling time (H)	Coupling solution	Washed ETA (μmole)	Reacted ETA (μmole)	Coupling %	Added more ETA	Washed ETA (μmole)	Reacted ETA (μmole)
1	4.2	0	24	PBS	0	0	0	8	8.8	0
2	4.4	2.1	24	PBS	0.1	2.0	97%	4.2	3.7	0.5
3	4.2	4.2	24	PBS	2.5	1.7	41%	NA		
4	4.4	8.4	24	PBS	5.3	3.1	71%	4.2	5.9	
5	4.2	1.1	24	CH$_3$CN	0	1.1	100%	4.2	0.1	4.1
6	4.4	2.1	24	CH$_3$CN	0	2.1	100%	4.2	0.3	3.9
7	4.4	4.2	24	CH$_3$CN	0	4.2	100%	4.2	0.2	4.0
8	4.2	4.2	24	CH$_3$CN	0	4.2	100%	4.2	0.4	3.8
9	4.4	8.4	24	CH$_3$CN	0.5	7.9		4.2	0.4	3.8
10	4.2	1.1	24	DMF	0.1	1.0	91%	4.2	0.4	3.8
11	4.4	2.1	24	DMF	0	2.1	100%	4.2	1.0	3.2
12	4.4	4.2	24	DMF	0.2	4.0	95%	4.2	1.7	2.5
13	4.4	8.4	24	DMF	1.0	7.4		4.2	1.4	2.8

Table 18: Investigation of the stability of the NHS ester in different coupling solvents.

To optimise the coupling efficiency in PBS, the ratio between the NHS-activated agarose **93** and the primary amine was further investigated. Therefore, the NHS-activated agarose **93** was mixed with 0.25 equiv., 0.5 equiv., 1.0 equiv. and 2.0 equiv. of the ethanolamine in PBS at room temperature for 24 hours. As expected the best coupling yield with respect to the NHS ester was obtained when the ethanolamine was used in excess, however the reaction was more efficient at lower equiv. (table 19).

The use of acetonitrile or DMF as the coupling solvent optimised the coupling efficiency, resulting in better coupling yield in the first addition and more coupling after the second addition (table 18, entry 5-13). 100% of the ethanolamine was reacted when the NHS-activated agarose **93** mixed with 0.25 equiv., 0.5 equiv. and 1.0 equiv. of the ethanolamine in acetonitrile (table 18, entry 5-8), confirming the stability of the NHS ester in the acetonitrile. The reaction of the NHS-activated agarose **93** with 0.25 equiv., 0.5 equiv. and 1.0 equiv. of ethanolamine in DMF for 24 hours at room temperature produced 91%, 100% and 95% respectively of the immobilisation onto agarose (table 18, entry 10-12).

NHS-agarose 93 (µmole)	ETA (µmole)	Coupling time (H)	Coupling solution	Washed ETA (µmole)	Reacted ETA (µmole)	Coupling %
4.2	1.1	24	PBS	0.1	1.0	91%
4.4	2.1	24	PBS	0.1	2.0	95%
4.2	4.2	24	PBS	2.5	1.7	40%
4.4	8.4	24	PBS	5.3	3.1	70%

Table 19: Investigation of the ratio between the NHS-activated agarose **93** and the primary amine to optimise the coupling reaction.

However, the fluorescence of the unreacted ethanolamine after the second addition in acetonitrile and DMF was less than expected based on the initial agarose loading; e.g. 1.1 μmole ethanolamine mixed with 4.2 μmole NHS-activated agarose resulted in all 1.1 μmole ethanolamine coupling with 26% of the agarose-NHS sites *via* amide linkage, to leave 3.1 μmole of the NHS ester free. When another 4.2 μmole ethanolamine was added to this 3.1 μmole NHS ester, surprisingly just 0.1 μmole ethanolamine was washed following the second addition (table 18, entry 5-13). Moreover, when the NHS-activated agarose was mixed with excess of ethanolamine in acetonitrile or DMF in the first addition, the recovery of the unreacted ethanolamine is less than the expected (table 18, entry 9 and 13).

We were concerned that the difference between solvents may be partly driven by differences in their ability to 'swell' the agarose particles, resulting in ineffective washing of the amine when using organic solvents. To examine this unactivated agarose was used to investigate the reactivity/affinity of ethanolamine toward the agarose itself in these solvents, to explain the apparent overloading of the NHS-activated agarose. The unactivated agarose was mixed with different concentrations of the ethanolamine in the different coupling solutions at room temperature for 24 hours, then the unreacted ethanolamine washed with the coupling solvent and treated with fluorescamine. The fluorescence of the washed ethanolamine was proportional to the amount of the added ethanolamine when the reaction was occurred in PBS (table 20, entry 1-3). While 4% of the ethanolamine was lost at higher concentration, this is probably due to measurement and dilution errors (table 20, entry 1). However, the concentration of the washed ethanolamine in the acetonitrile and DMF is significantly less than expected, with more than 20% of the ethanolamine lost. While this may be explained by the lower solubility of the ethanolamine in these aprotic solvents, it is most likely due to changes in the structure of the agarose beads (which swell less in non-aqueous solvents)

and/or the inability of the solvents to out-compete the hydrogen bonding of ethanolamine to the agarose (table 20, entry 4-9).

	ETA (μmole)	Coupling solution	Washed ETA (μmole)	lost ETA (μmole)
1	8.4	PBS	8.1	0.3
2	4.2	PBS	4.6	
3	2.1	PBS	2.1	0
4	8.4	CH₃CN	6.8	1.6
5	4.2	CH₃CN	2.9	1.3
6	2.1	CH₃CN	1.2	0.9
7	8.4	DMF	6.1	2.3
8	4.2	DMF	2.6	1.6
9	2.1	DMF	1.2	0.9

Table 20: Reactivity of ethanolamine toward inactivated agarose in different coupling solvents.

Given the best coupling was obtained when the reaction was carried in acetonitrile due to stability of the NHS ester under more anhydrous conditions, the issue of poor elution of unreacted amine could be solved by conducting the immobilisation in acetonitrile then washing the unreacted amine using PBS. The NHS-activated agarose **93** was mixed with the amine allyl carbamate *N*-Boc **92** in acetonitrile or DMF at room temperature for 24 hours then the unreacted amine **92** was washed with the coupling solvents followed by PBS. The using amine in excess resulted in 100% immobilisation **95** (based on NHS) when the reaction is carried in acetonitrile and 88% immobilisation in DMF (table 18, entry 2 and 3), while using 1

equiv. of the amine allyl carbamate *N*-Boc **92** in acetonitrile produced 64% immobilisation

onto the agarose **95** (table 21, entry 1).

	NHS-agarose 93 (μmole)	amine 92 (μmole)	Coupling time (H)	Coupling solution	Washed amine (μmole)	Reacted amine (μmole)	Coupling %
1	4.0	3.9	24	CH$_3$CN	1.4	2.5	64%
2	4.0	8.0	24	CH$_3$CN	3.9	4.1	100%
3	4.0	5.6	24	DMF	2.1	3.5	88%

Table 21: Investigation of acetonitrile and dimethylformamide in the coupling of primary

amine **92** with NHS-agarose **93**, with unreacted amine washed with PBS.

After Optimisation of the loading of the agarose with primary amines, we turned our

attention to the release from agarose. A simple water-soluble molecule (amine allyl

carbamate ethanolamine **98**) was prepared (scheme 42) and used as a model system to

investigate the immobilisation onto the NHS-activated agarose **93** and the release from the

solid support by Pd catalysed de-allylation in aqueous conditions (scheme 43).

Scheme 42: Synthesis of the simple water-soluble molecule (amine allyl carbamate ethanolamine **98**).

Scheme 43: A model system to investigate the immobilisation onto the NHS-activated agarose **93** and the release from the solid support by Pd catalysis.

The NHS-activated agarose **93** was mixed with 0.25 equiv. of the amine **98** in PBS at room temperature for 24 hours. The unreacted amine **98** was washed away, and any unreacted ester of the NHS-activated agarose **93** was blocked with 1 M ethanolamine. Pd-o-DANPHOS

complex in PBS was added to the allyl carbamate agarose **99** in the presence of the dimethylbarbaturic acid **76** to release the primary amine (ethanolamine), which was detected by fluorescamine. The fluorescence of the released ethanolamine after the treatment with 5 mol% of the Pd-o-DANPHOS complex shows that only 15% of the amine had been recovered. Adding more Pd-o-DANPHOS complex results in release more amine to improve the cleavage to 17% (based on amine recovery, table 22, entry 1). When 10 mol% Pd-o-DANPHOS complex was added directly to the amine allyl carbamate *N*-Boc ethylenediamine immobilised onto the agarose **95**, 23% of the *N*-Boc ethylenediamine **96** was released (table 22, entry 2). Increasing the Pd(0) to 100 mol% resulted in improvement, leading to recovery of 30% of the *N*-Boc ethylenediamine **96** (table 22, entry 3).

	NHS-agarose 93 (µmole)	amine (µmole)	Coupling time (H)	Coupling solution	Washed amine (µmole)	Reacted amine (µmole)	Coupling %	Pd-o-DANPHOS	Released amine (µmole)	Cleavage %
1	23	5.8	24	PBS	22	3.5	61%	10 mol%	0.6	17%
2	4.0	5.6	24	DMF	2.1	3.5	63%	10 mol%	0.8	23%
3	20.0	15.0	24	PBS	3.6	11.4	76%	100 mol%	3.5	30%

Table 22:Pd catalysed de-allylation in aqueous conditions.

To ensure the resulting cleavage is due to Pd catalysed deallylation rather than hydrolysis, the amine allyl carbamate *N*-Boc ethylenediamine immobilised onto the agarose **95** was treated with all cleavage reagents without Pd. After 24 hours, washed with PBS and treated with fluoreascamine, no fluorescence was observed at 479 nm (figure 62).
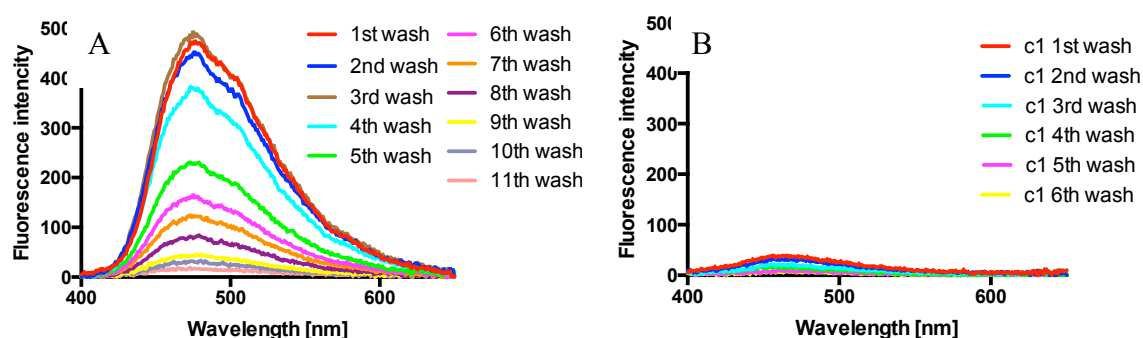
Figure 62: A-Fluorescence spectrum of the released amine by Pd catalysis; B- Fluorescence spectrum of the control cleavage reaction without Pd.

The low cleavage yield could be due to the detection method, for example it is possible the Pd complex quenches the fluorescence. To investigate the effect of the Pd complex on the fluorescence of the primary amine, ethanolamine was treated with fluorescamine in the presence and absence of the Pd complex, each one repeated three times to minimise error (figure 63). 100 µM ethanolamine was treated with 1 mM fluorescamine then the emission @ 479 was measured to give a fluorescence reading of 1244 (100%) (table 23, entry 1). The presence of the Pd-o-DANPHOS complex and dimethylbarbituric acid **76** reduced the fluorescence to 70% of the expected level (table 23, entry 3), while the presence of the Pd without the phosphine ligand and dimethylbarbituric acid **76** caused greater reduction in the fluorescence to 44% (table 23, entry 4). The phosphine ligand and dimethylbarbituric acid **76** did not affect the fluorescence (table 23, entry 5 and 6). It is clear that the Pd species used to cleave the linker can quench the reactivity and/or fluorescence in the fluorescamine assay, therefore, the cleavage in the previous model system is likely to be higher than suggested by the fluorescamine reading alone.

Ethanolamine (ETA) + Fluorescamine (Fluram) (Nonfluorescent) → (Fluorescent, Emission at 479 nm)
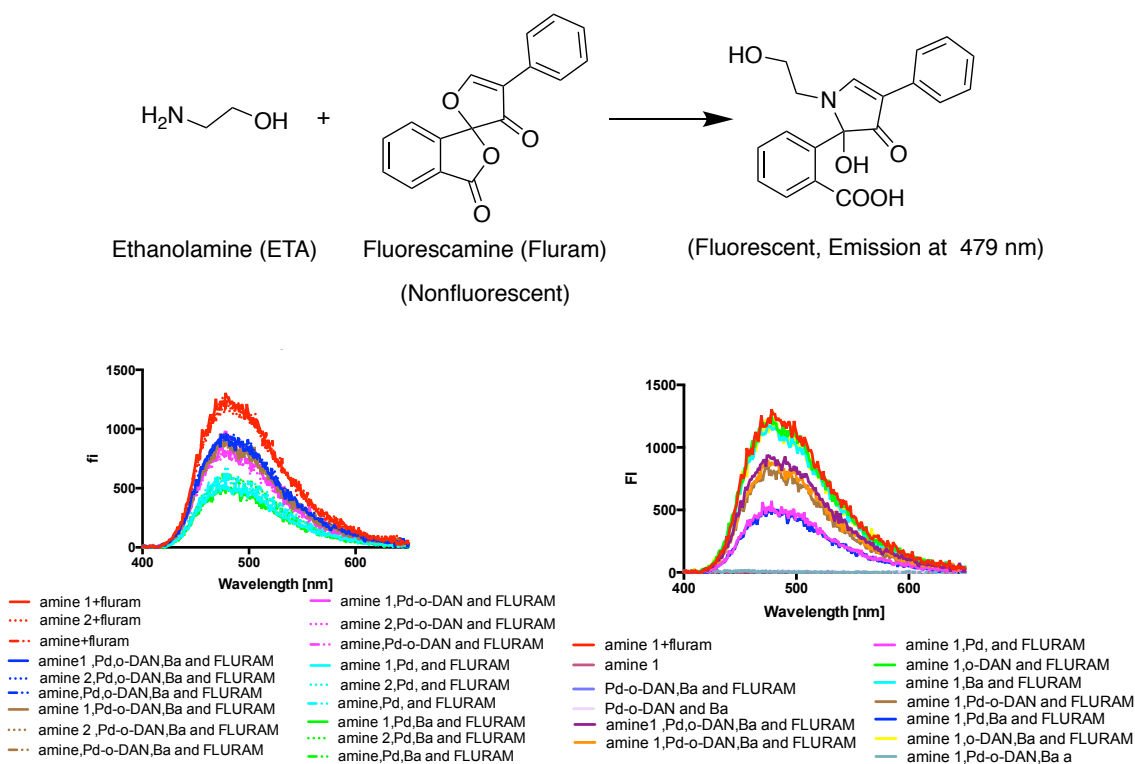
Figure 63: Investigation of the effect of the Pd complex on the fluorescence of the primary amine, (amine 1, amine 2 and amine 3 are ETA ,repeated three times).

	ETA	Pd(0)	o-DANPHOSE	DMBA	Pd-o-DAN	FLURAM	Flourescence	Flourescence	Flourescence	Average
1	x					x	1275	1226	1230	1243.66667
2	x	x	x	x		x	905	864	926	898.333333
3	x			x	x	x	866	840	903	869.666667
4	x	x				x	487	595	563	548.333333
5	x		x			x	1179	1267	1347	1264.33333
6	x			x		x	1139	1222	1278	1213
7	x				x	x	800	770	988	852.666667
8	x	x		x		x	513	499	583	531.666667
9	x		x	x		x	1158	1239	1287	1228
10				x	x	x	6	10	12	9.33333333
11	x						-1	-1	-2	-1.3333333
12			x	x			5	3	3	3.66666667
13	x			x	x		2	1	3	2

Table 23: Investigation of the effect of the Pd complex on the fluorescence of the primary amine.

To solve this quenching issue, any Pd would ideally be removed from the system before treating with fluorescamine, or otherwise an alternative detection method used that is not affected by Pd. Both of these improvements should be readily achieved during protein

alkylation which will allow; 1) separation of protein products from the cleavage reagents by size exclusion chromatography and/or dialysis and 2) detection by e.g. direct UV analysis, HPLC, and protein quantification methods such as BCA.

2.3.3 The solid-phase thiol alkylation linker

After finding the best immobilisation and release conditions, we turned our efforts to immobilisation of the thiol alkylation linker **80** onto the solid support and evaluate the use of catch-release methodology to selectively alkylate cysteine. The alkylation linker **80** was synthesised as a salt, which is insoluble in acetonitrile even after addition of the triethylamine, therefore PBS was used as the coupling solution. The NHS-activated agarose **93** was mixed with the thiol alkylation linker **80** in PBS for 24 hours at room temperature (scheme 44). The fluorescence of the unreacted alkylation linker **80** confirmed that 84% of agarose was loaded with alkylation linker when 1.0 equiv. had been added, while the loading was 77% (based on amine) when 0.4 equiv. was added (table 24). While the aqueous conditions are likely to have hydrolysed any 'unreacted' NHS ester **93** was blocked with 1M ethanolamine, to avoid the risk of side reactions this was still blocked by reaction with ethanolamine before the next alkylation step.
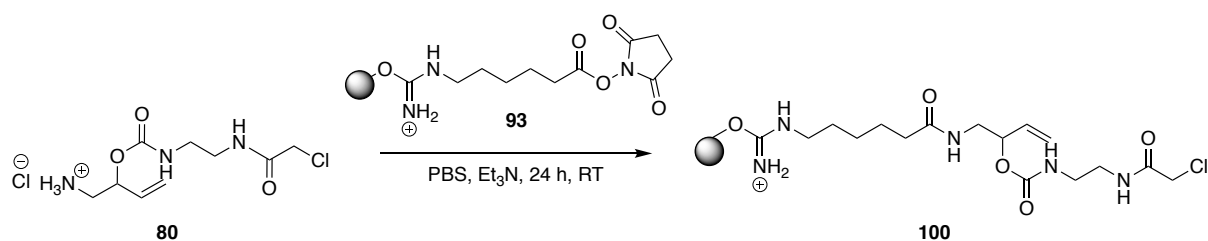
Scheme 44: Immobilisation of the thiol alkylation linker **80** onto the NHS-Agarose **93**.

	NHS-agarose 93 (μmole)	amine 80 (μmole)	Ratio (agarose: amine)	Washed amine (μmole)	Reacted amine (μmole)	Coupling %
1	17.6	35.2	(1:2)	22.8	12.4	72%
2	42	42	(1:1)	6.7	35.3	84%
3	21	8.5	(1:0.4)	1.9	6.6	77%

Table 24: Immobilisation of the thiol alkylation linker **80** onto the NHS-Agarose **93**.

2.3.4 Cysteine thiol alkylation

After successfully preparing the novel solid phase thiol alkylation system **100**, we turned our attention to investigating the thiol alkylation agents and comparing between the selectivity of the alkylation agents (chloroacetamide and iodoacetamide) toward thiols. Therefore, the solid phase iodoacetamide linker **101** was prepared by incubating the solid phase chloroacetamide linker **100** with excess of sodium iodide in PBS for 24 hours at room temperature (scheme 45). The standard protein (BSA) was used to investigate these novel solid phase thiol alkylation systems **100** and **101** in combination with a second solid phase reducing agent (the solid phase TCEP) to allow the direct reduction and alkylation of the protein, then the release of the alkylated protein investigated using catalytic Pd (scheme 45). BSA is an ideal model system as it contains a single reactive surface cysteine, and there is a wealth of literature using this protein as a model for novel cysteine alkylation reactions. The methods selected to detect the unreacted protein were the established fluorescamine assay, as well as the bicinchoninic acid (BCA) assay and HPLC.[243,244]

Scheme 45: Catch-release methodology to selectively alkylate cysteine.

The fluorescamine assay was initially used to detect the primary amine of the BSA based on the standard curve generated with BSA sample used in the reaction, while the bicinchoninic acid (BCA) assay was used to detect total protein in the solution.[245] [245] The BCA solution is an alkaline solution consisting of bicinchoninic acid, sodium carbonate, sodium bicarbonate, sodium tartrate and copper (II) sulfate pentahydrate.[245] The BCA assay is based on the formation of a strong complex between Cu^+ and BCA to forms a species with a strong chromophore.[246] The reduction of the Cu^{2+} ions to Cu^+ can occur by oxidation of cysteine, tyrosine or tryptophan amino acids which is a temperature independent reaction.[246] The

Cu^{2+} ions can also be reduced to Cu$^+$ by binding of the Cu^{2+} ions with the nitrogen atoms present in the peptide bonds in the protein, resulting in reduction of the Cu^{2+} ions to Cu$^+$ (Biuret test) which is temperature dependent reaction.[246] The Cu$^+$ ions formed by these processes are chelated by two molecules of bicinchoninic acid to provide a purple coloured complex that strongly absorbs light at 562 nm (figure 64).[245] The concentration of protein is proportional to the absorbance at 562 nm based on a standard curve generated with the protein sample used in the reaction. The reversed phase high performance liquid chromatography (RP-HPLC) with UV detector was used to analyse the total amount of protein in the solution based on a standard curve generated with the protein sample used in the reaction using absorbance at 280 nm to directly detect the protein concentration.[247,248,249]

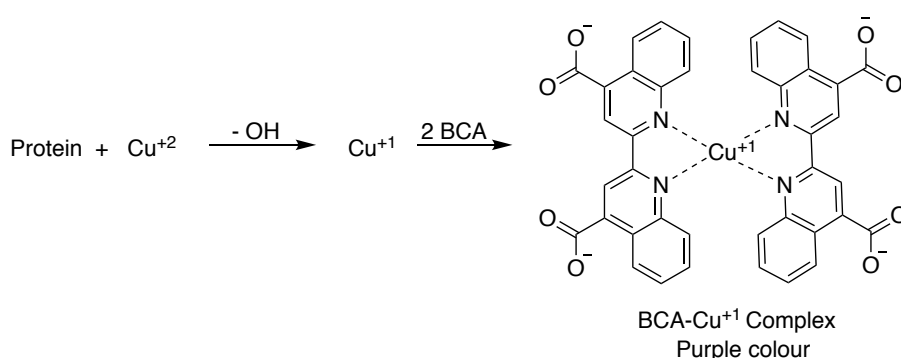

Figure 64: The bicinchoninic acid (BCA) assay to detect total protein in the solution.[245]
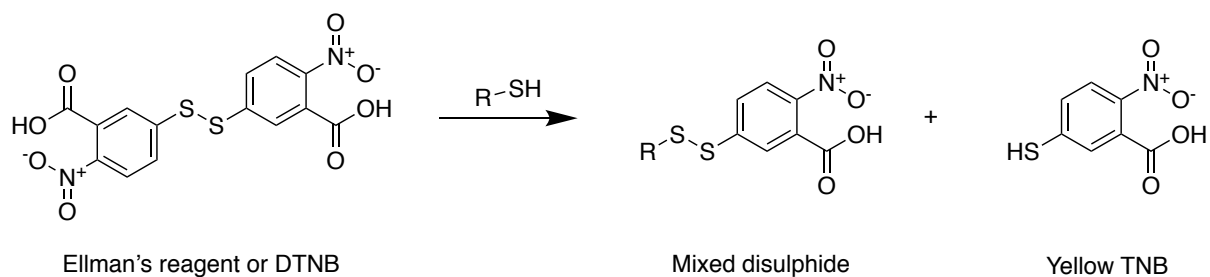
2.3.4.1 BSA alkylation in the solution phase

In order to investigate the ability of the iodoacetamide to alkylate BSA in the solution phase a simple thiol alkylation agent **105** was prepared (scheme 46) and incubated with BSA for 24 hours at room temperature in the presence of the solid phase TCEP (scheme 46). Ellman's reagent (5,5'-dithio-bis-[2-nitrobenzoic acid] or DTNB) was used to analyse the alkylation reaction.[250,251] Ellman's reagent reacts with sulfhydryl groups to provide a coloured product

that absorbs light at 412 nm (scheme 47).[252,253] Ellman's reaction confirmed about 50% of the protein has been alkylated **106** by comparing with concentration of control BSA (figure 65). HPLC appeared to show a mixture of BSA and alkylated BSA **106** (figure 66), suggesting that the alkylated products may be directly distinguished from unreacted BSA using this technique, however further mass spectrometry studies would be required to confirm the site(s) of reaction.
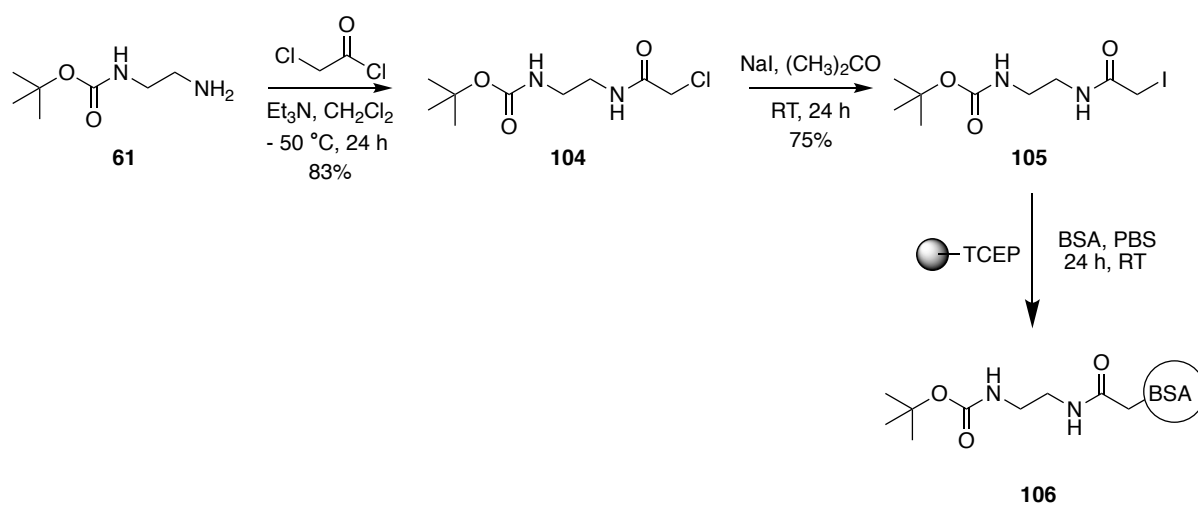
Scheme 46: Synthesis of the N-Boc ethylenediamine iodoacetamide **105** and BSA alkylation in the solution phase.

Scheme 47: Ellman's reagent to analyse the concentration of sulfhydryl groups in the
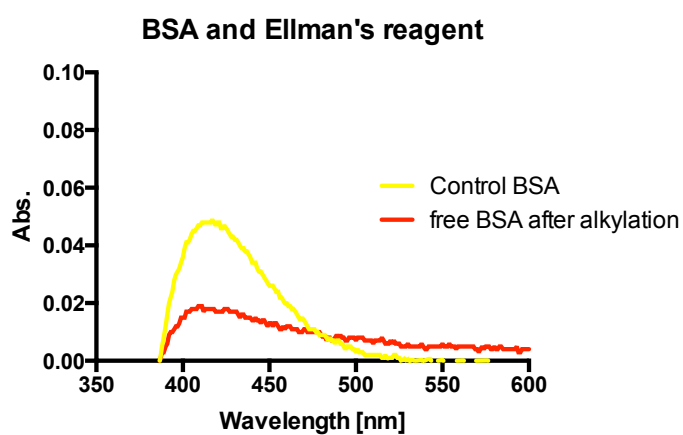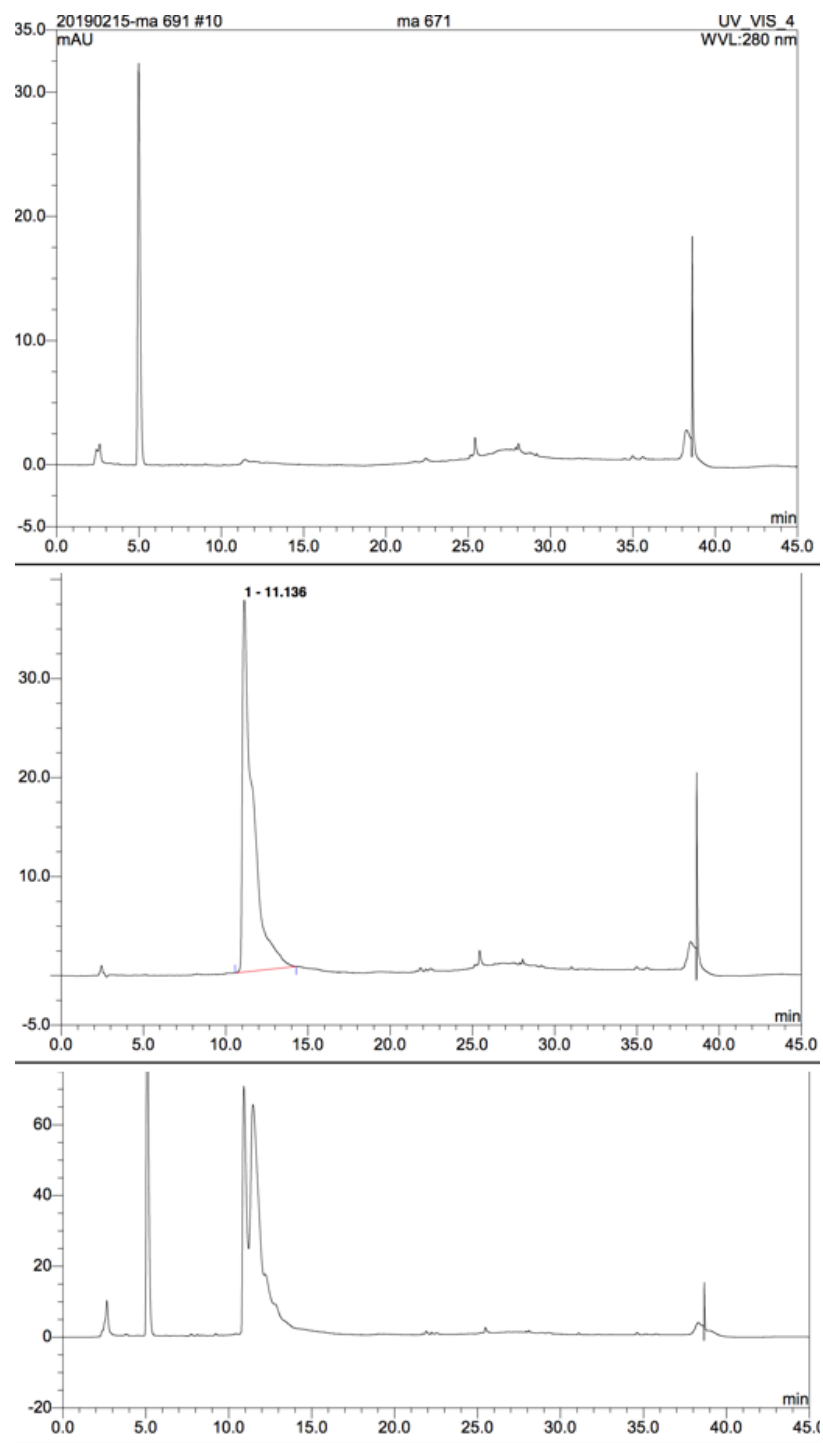
sample.

Figure 65: Thiol detection by Ellman's reagent.

Figure 66: HPLC of the BSA alkylation in the solution phase (Top: control with no BSA.

Middle: BSA alone. Bottom: alkylated mixture).

2.3.4.2 BSA alkylation in the solid phase

Before investigating the alkylation of BSA with the solid phase alkylation system, we were interested to investigate if there is any reactivity or affinity between BSA and agarose. Therefore, the unactivated agarose was mixed with different concentrations of the BSA in PBS at room temperature for 24 hours, then the unreacted BSA washed with PBS and detected. The fluorescamine assay, BCA assay and RP-HPLC confirmed that the washed protein was effectively equiv. to the amount of added protein (table 25). To investigate if there was any reactivity between BSA and the solid phase TCEP, BSA was mixed with the solid phase TCEP in PBS at room temperature for 24 hours. The fluorescamine assay, BCA assay and RP-HPLC confirmed that the washed protein was again effectively equiv. to the amount of the added protein (table 25).

	0.40 µmole BSA + control agarose	0.20 µmole BSA + control agarose	0.10 µmole BSA + control agarose	0.05 µmole BSA + control agarose	0.02 µmole BSA + control agarose	0.01 BSA + control agarose µmole	0.10 µmole BSA + solid phase TCEP
Fluorescamine	0.43 µmole	0.21 µmole	0.07 µmole	0.03 µmole	0.02 µmole	0.01 µmole	0.12 µmole
BCA	0.37 µmole	0.20 µmole	0.11 µmole	0.05 µmole	0.02 µmole	0.01 µmole	0.11 µmole
RH-HPLC	0.42 µmole	0.21 µmole	0.10 µmole	0.05 µmole	0.02 µmole	0.01 µmole	0.08 µmole

Table 25: BSA affinity toward Agarose and TCEP immobilised onto agarose analysed by fluorescamine, BCA and HPLC.

In order to investigate the utility of our catch-release system, BSA was incubated with the solid phase alkylation linker (**100** or **101**) for 24 hours at room temperature, then the unreacted protein washed with PBS and detected. The fluorescamine detection of the

unreacted protein showed that 65% of protein was immobilised when the solid phase chloroacetamide **100** was used in combination with TCEP immobilised onto agarose (figure 67) with the RP-HPLC confirming that 66% of the protein had been lost (figure 67). The replacement of chloroacetamide **100** by iodoacetamide **101** improved the alkylation yield to 93% according to fluorescence of the unreacted protein and 92% according to the BCA assay. However, the RP-HPLC suggested a lower loading, with 80% of the BSA reacted (figure 67).
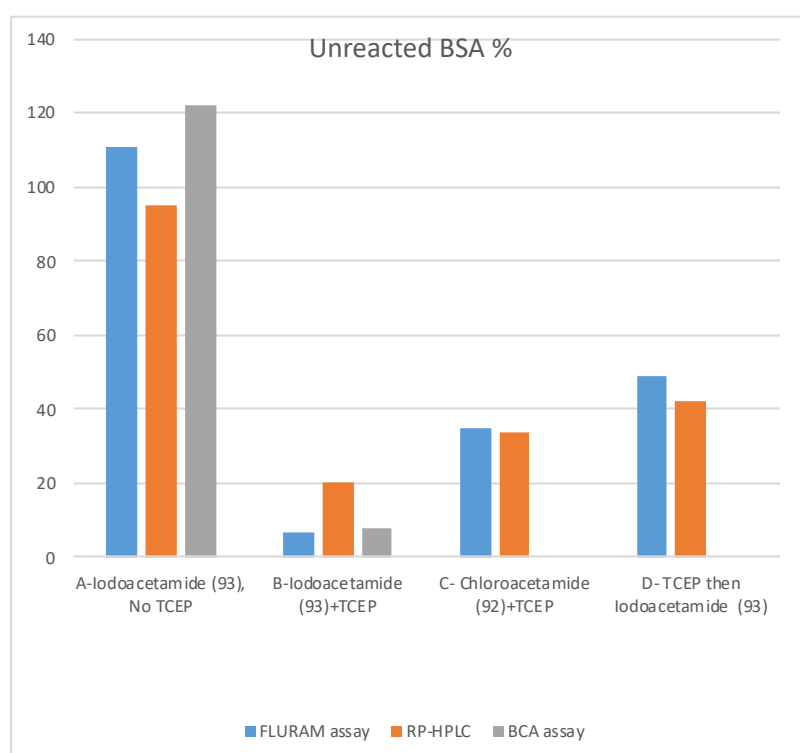

Figure 67: Percentage of unreacted BSA after the solid phase alkylation analyzed by fluorescamine, BCA and RP-HPLC. **A**: solid phase alkylation **101** without reducing agent, **B**: solid phase alkylation **101** in the presence of TCEP-agarose, **C**: solid phase alkylation **100** in the presence of TCEP-agarose and **D**: TCEP-agarose used to reduce the disulfide bond of the BSA then removed from the system immediately before the alkylation step.

To investigate the importance of keeping the reducing agent in the system, BSA was incubated with the solid phase iodoacetamide linker **101** for 24 hours at room temperature with and without TCEP immobilised onto agarose. The fluorescamine detection of the washed protein suggested no reaction occurred in the absence of the reducing agent (figure 67), with the BCA assay and RP-HPLC confirming the lack of reaction, presumably as a result of the BSA thiol being oxidised (figure 67). This strongly suggests that the alkylation is specific for the cysteine as any non-specific immobilisation through, for example, amine alkylation would not be dependent on TCEP.

When the TCEP was used to reduce the disulfide bond of the BSA then removed from the system immediately before the alkylation step, about half of the BSA thiol was loaded, suggesting that re-oxidation of the BSA thiol competes with the alkylation reaction. This was confirmed by the fluorescamine detection of the washed protein which showed 51% of BSA has been alkylated, and the RP-HPLC showing 58% alkylation (figure 67).

2.3.5 Pd catalysed release of the alkylated protein from the solid phase

Following the successful BSA alkylation and purification, we were interested to investigate the release of the alkylated protein from the solid phase by catalytic Pd. Given the Pd-o-DANPHOS complex quenched the formation/fluorescence of the fluorescamine primary amine products with the model system, the effect of the Pd on the BSA analysis methods was investigated. A known concentration of BSA in PBS was mixed with fluorescamine in the presence of the Pd-o-DANPHOS complex then the fluorescence of the mixture measured at 479 nm and compared to the fluorescence of BSA in the absence of the Pd-o-DANPHOS complex. As suspected, the Pd-o-DANPHOS complex quenched the fluorescence of BSA adducts, in this case resulting in effectively complete loss of signal (figure 68).
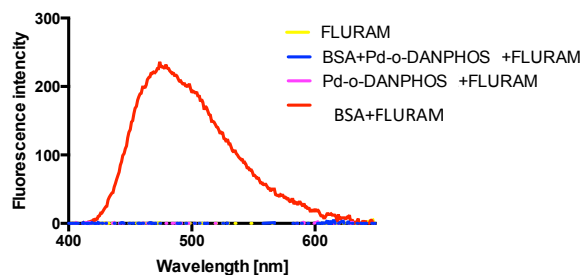
Figure 68: The effect of the Pd-o-DANPHOS on BSA fluorescence.

To investigate the effect of the Pd-o-DANPHOS complex on the BCA assay, a known concentration of BSA in PBS mixed with BCA solution in the presence and absence of the Pd-o-DANPHOS complex then the absorbance of the mixture measured at 562 nm. The Pd-o-DANPHOS complex increased the absorbance of the BCA-BSA mixture absorbance similar to the absorbance of the mixture of BCA solution with Pd-o-DANPHOS complex without BSA (figure 69). To use BCA or fluorescamine assays to analyse the total amount of the released protein, the protein should first be separated from the cleavage reagents before analysis methods, however the use of HPLC to analyse the released alkylated protein proved to be more straightforward, as the Pd-o-DANPHOS complex can be separated from the alkylated protein and the concentration of released protein directly determined based on the standard curve generated with the protein sample used in the reaction (figure 70).
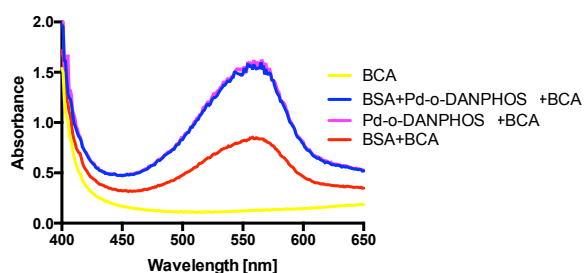

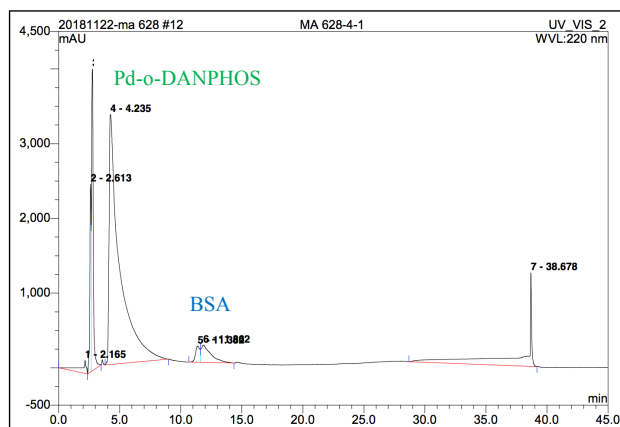Figure 69: The effect of the Pd-o-DANPHOS on the BCA assay.

Figure 70: HPLC of released BSA from the solid support with Pd complex.

Following immobilisation of BSA under optimised conditions, any remaining iodoacetamide **101** was quenched with excess of glutathione to prevent either reaction between this species and the phosphine ligand, or perhaps more importantly the alkylated BSA reacting again after cleavage (scheme 48). The solid phase alkylated BSA was then treated with 5 mol% Pd-o-DANPHOS complex and barbituric acid **76** in PBS at room temperature for 24 hours. After cleavage process the released protein was separated from the cleavage reagents by using a PD-10 size exclusion column, then treated with fluorescamine, however no fluorescence was observed. Unfortunately, the HPLC confirmed that the release of alkylated BSA from the solid support by using catalytic Pd had not proceeded as expected.
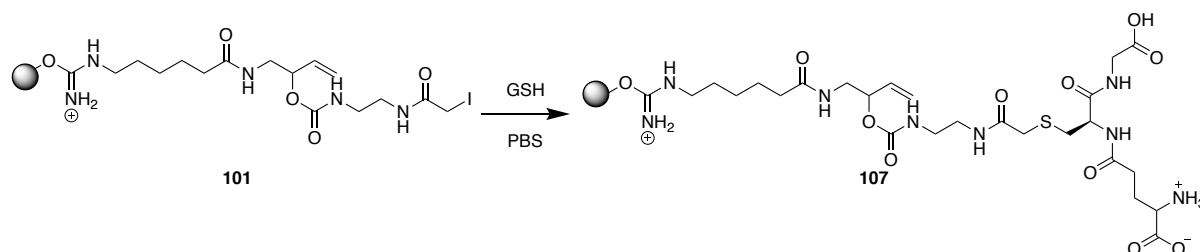

Scheme 48: Quenching of unreacted solid phase iodoacetamide **101** with excess glutathione before linker cleavage.

We were concerned that the presence of protein in the solid phase alkylated BSA had an effect on the cleavage reaction, resulting ineffective release of alkylated BSA, as Pd-o-DANPHOS was able to successfully catalyse the deallylation reaction in solution phase and in the model solid phase systems **95** and **99**. To examine this the allyl carbamate **67** was used to investigate the Pd catalysed deallylation reaction in the solution phase (scheme 49). The allyl carbamate **67** was treated with 5 mol% Pd-o-DANPHOS in PBS for 24 hours in the presence of agarose, solid phase TCEP or BSA. The efficiency of the cleavage catalysed by each Pd species was evaluated by ^{1}H NMR and mass spectrometry. In the reactions the BSA was attached to the solid support in order to avoid its signal in ^{1}H NMR (scheme 50) using a linker that was designed not to have any reactive sites that could be cleaved by Pd (scheme 50). In all control reactions the allyl carbamate **67** was successfully cleaved, this was confirmed by mass spectrometry showed the presence of the 1,3-dimethylbarbituric allyl molecule **77** (where its acidic **CH** proton is exchanged with deuterium). ^{1}H NMR showed the presence of ethylenediamine **78** protons at 3.4 ppm, to confirm the desired product had formed we added more ethylenediamine **78** to the reaction after cleavage completion, resulting in the ethylenediamine 4 protons at 3.4 ppm shifting into 2.9 ppm, however no new signals were observed.
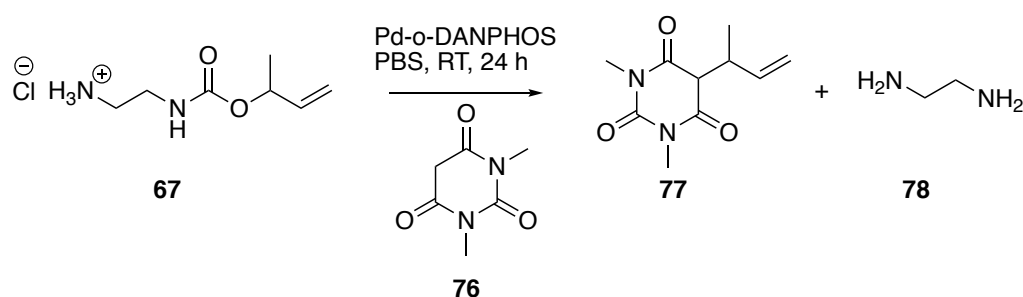
Scheme 49: The deallylation reaction of allyl carbamate **67** by Pd-o-DANOHOS catalyst.
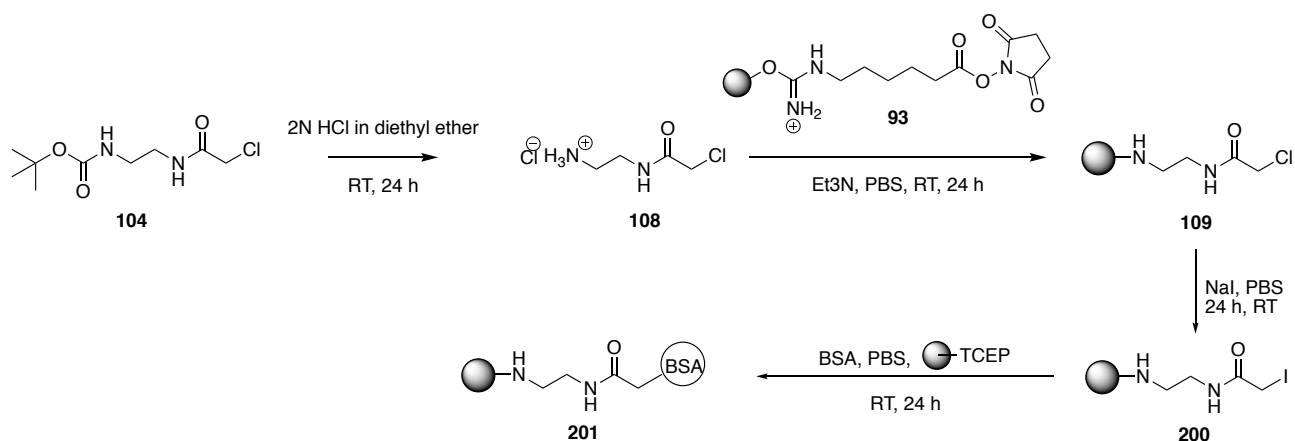
Scheme 50: Preparation of the solid phase BSA.

The control reactions strongly support the conclusion that the BSA has been immobilised via the expected linker-cysteine alkylation. Coupled with the apparently successful (if not absolutely quantified) cleavage of the model amine this result suggests the protein is interfering with the cleavage reaction, possibly due to steric hindrance as the agarose and BSA are large molecules that may prevent the large and highly charged Pd species from reaching the reactive site.

Chapter 3: Conclusion

The aim of this project was to develop a solid phase catch-release alkylation system to reliably provide clean products of nucleophilic cysteine thiol alkylation.

In the first attempt towards the project target, the alkylation linker was designed to include an azide group to attach to the solid phase by using a copper (I)-catalysed alkyne-azide cycloaddition (CuAAC) reaction and designed to include allyl ester group that can be cleaved by using catalytic Pd. The cleavage of the allyl ester by catalytic Pd under basic conditions and the thiol alkylation were investigated in the solution phase, however the instability of the allyl ester system under basic conditions meant that it could not to be used longer-term in the project.

To address this issue, several different allyl carbamate and propargyl carbamate derivatives have been synthesised in order to investigate their cleavage efficiency by catalytic Pd under mild conditions. Different simple and complex Pd(0) and Pd(II) catalysts were evaluated to study their efficiency to catalyse the cleavage of the allyl carbamate and propargyl carbamate derivatives. The cleavage reactions were monitored by using ^{1}H NMR and MS.

The Pd tetrakis complex (Pd(PPh$_3$)$_4$) was the most efficiency catalyst for the deallylation reactions, in contrast, none of the four simple Pd species catalyse the allyl carbamate cleavage. The allyl Pd (II) chloride dimer (allyl$_2$Pd$_2$Cl$_2$) and the bis(dibenzylideneacetone) Pd (0) (Pd(dba)$_2$) were the most efficiency catalysts for the depropargyltion reactions, in contrast, the Pd(PPh$_3$)$_4$ didn't catalyse the depropargyltion reaction.

The water-soluble propargyl carbamate derivatives were not stable under basic conditions and as we already had concerns about the aqueous solubility of allyl Pd (II) chloride, no further work was conducted on this linker system. Although the water-soluble allyl carbamate

derivatives were stable under basic conditions, they were not cleaved by Pd(PPh$_3$)$_4$ under basic conditions in the absence of the external nucleophile. However, the combination of the Pd species with the electron-deficient water-soluble phosphine o-DANPHOS and the barbituric acid anion as a water-soluble soft nucleophile resulted in efficient cleavage of the allyl carbamate derivatives in aqueous conditions within 2 hours.

In the second attempt toward the solid phase alkylation linker we tried to optimise several properties; 1- the linker stability was improved by using allyl carbamate instead of allyl ester, 2- the CuAAC reaction side effect on the agarose was removed by using N-hydroxysuccinimide ester functionalised agarose to immobilise an amine-containing linker onto agarose by amide formation, 3- the estimation method for the immobilisation onto the solid support was improved by using fluorescamine to detect the concentration of the unreacted amine directly.

The alkylation linker was redesigned to include the primary amine for immobilisation onto the NHS-activated agarose, retaining the allyl carbamate as a cleavable group. The immobilisation of the primary amine model molecule onto NHS-activated agarose and the cleavage of the allyl carbamate on the solid support were then investigated, demonstrating that most of the amine was immobilised onto agarose after 24 hours of incubation at room temperature in PBS. However, the best coupling of the model molecules with NHS-activated agarose was obtained when the reaction was carried in acetonitrile due to the stability of NHS-activated agarose under more anhydrous conditions.

The selectivity of the solid phase iodoacetamide linker and the solid phase chloroacetamide linker toward a protein cysteine thiols was investigated by using BSA in the presence of the solid phase TCEP. Fluorescamine, BCA and HPLC assays were used to estimate the efficiency of the alkylation process, with the best alkylation yield of BSA obtained when the solid phase

iodoacetamide linker was used in the presence of the solid phase TCEP. However, the release of the alkylated protein using the Pd-o-DANPHOS/barbituric acid conditions did not proceed as expected. Further control reactions demonstrated there is no apparent incompatibility between the components of this system, therefore we hypothesise the failure of the cleavage was due to the steric hindrance affect of the large molecules (BSA and agarose) preventing the Pd species from reaching the reactive site.

3.1 Future Work

The majority of the project aims have been achieved; 1) the solid phase thiol alkylation linker has been optimised, prepared and shown to selectively alkylate cysteine thiols in the model protein BSA to capture the alkylated protein on the solid phase, 2) the cleavage of the alkylation linker in the solution phase has been confirmed by ^{1}H NMR and MS. However, the release of the alkylated protein did not proceed as expected meaning the system is not yet ready for application to the synthesis of CCL2-conjugates.

To progress this project, we propose to synthesise a longer linker that will provide more space for the Pd species to access the cleavage site. The longer linker could be synthesised in 10 steps starting with commercially available 2-[2-(2-chloroethoxy)ethoxy]ethanol (Figure 71). We would propose to investigate the cleavage of the linker allyl carbamate in both solution and solid phases by using the Pd-o-DANPHOS complex.

Once the cleavage reaction is confirmed, we would propose to investigate the thiol alkylation in solution phase by using a simple thiol compound such as cystamine or mercaptoethanol. The success of the alkylation process in solution phase would be determined by NMR and MS. Moreover, we would propose to investigate the alkylation to simple protein (such as BSA) in combination with a second solid phase reducing agent and more fully quantify the effect of this on the final protein yield and purity. The success of the alkylation process could be determined by amount of the unreacted protein that can be determined by several technique such as fluorescamine assay, BCA or HPLC.

In addition, in order to more fully understand the cleavage efficiency we would propose to directly quantify the amount of protein level onto the solid phase. This may be possible BCA, however as we have we used agarose as solid support there may be side reactions with

copper in the BCA assay. Once the protein alkylation level is confirmed, we would propose to

investigate the release of protein from the solid support by using catalytic Pd (5 mol%). The

success of the cleavage process would initially be investigated by HPLC.
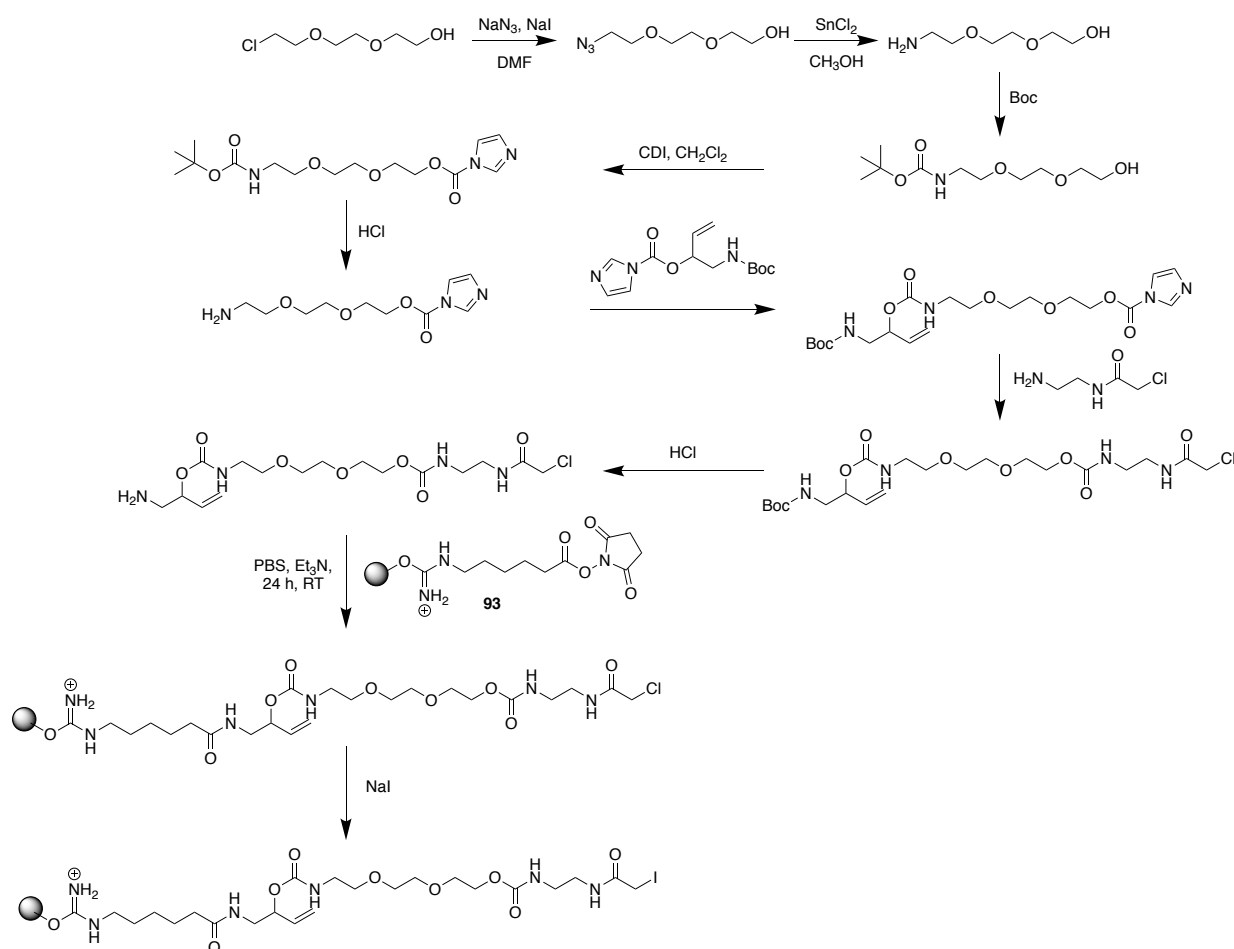

Figure 71: Plan to synthesise longer alkylation linker to have enough space to the Pd in the reactive site.

In addition to this work, we would propose to synthesise a longer linker with a maleimide

thiol alkylation agent to compare with haloacetamide thiol alkylation agents (figure 72).

Moreover, we would propose to investigate the alkylation reactions of the simple thiol

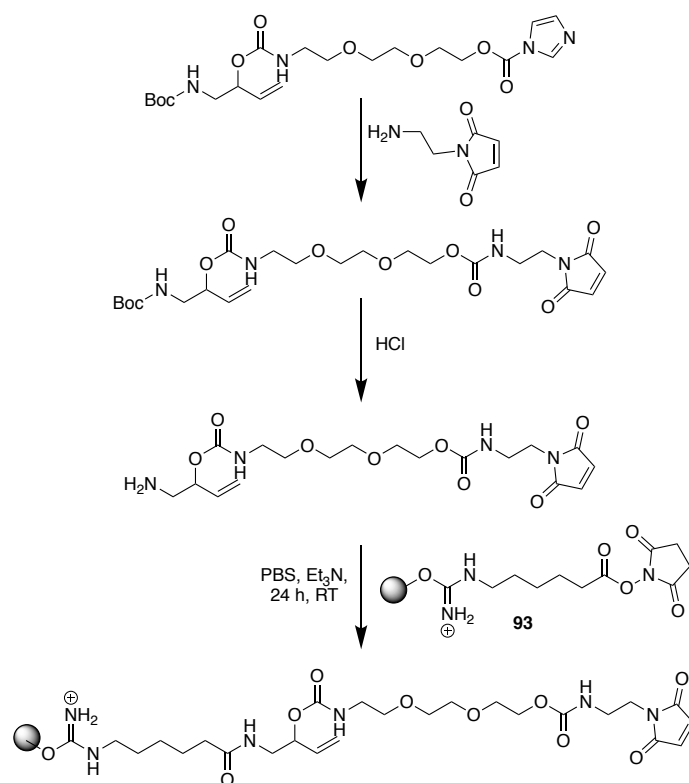compounds and protein by solid maleimide linker.

Figure 72: Plan to synthesise longer maleimide linker.

Following this work, we would propose to investigate the alkylation of a CCL2-Cys protein using either the current or optimised system, since this molecule contains a more exposed cysteine residue. Once the alkylation of the CCL2-Cys protein is confirmed we would redesign the alkylation linkers to include an orthogonal functional group, such as an azide, that would allow for the subsequent modification of the alkylated protein with a range of species (for example fluorophores) using CuAAC or SPAC chemistry.

Finally, redesign of the alkylation linker could allow direct alkylation with an FK866 drug derivative, ahead of preparation of the CCL2-FK866 conjugate (figure 73).
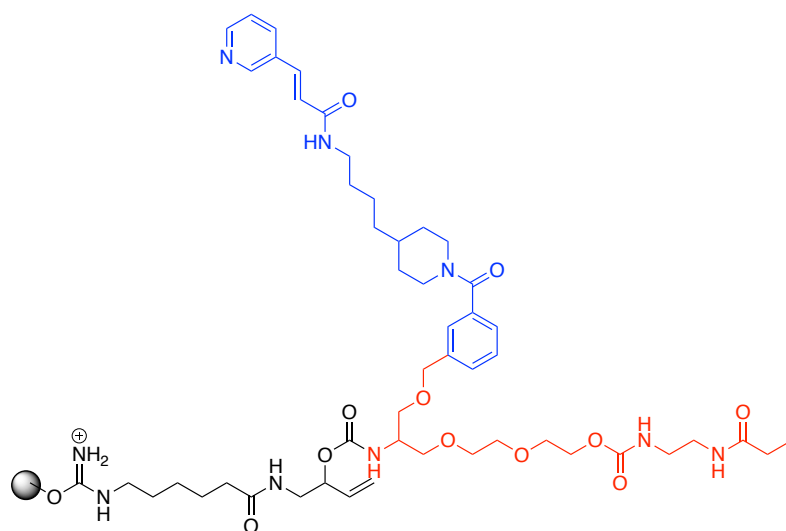
Figure 73: The solid iodoacetamide thiol alkylation linker containing an FK866 derivative.

Chapter 4: Experimental

4.1 General Experimental Procedures.

Reagents and solvents that are available commercially are used without further purification and purchased from Sigma-Aldrich, Acros, Alfa Aesar, Fisher Chemicals, Fluorochem or Strem chemical. Anhydrous solvents are supplied via a solvent purification system (SPS) and maintained under inert (N_2) atmosphere. The reactions were monitored by the thin layer chromatography (TLC) was carried out on Merck aluminium backed TLC plates silica gel 60 F254 (0.25 mm thickness) and stained with standard TLC stains (potassium permanganate solution, $KMnO_4$) followed by heating with a hot-air gun (~300 °C, 10 seconds) then visualised using a short wavelength UV lamp. The silica gel (particle size 40-63 µm mesh) was used in Flash column chromatography. ^1H NMR spectra were recorded at 300 MHz on a Bruker AVIII300 NMR Spectrometer and at 400 MHz on a Bruker AV400 Bruker Spectrometer. ^{13}C NMR spectra were recorded using the standard and Pendant techniques at 100 MHz on Bruker AVIII400 and AV400 Spectrometers, and were proton decoupled. Chemical shifts (δ) are reported in parts per million (ppm) relative to TMS (δ 0.00) for ^1H NMR and ^{13}C NMR measurements. Coupling constants (J) are expressed in Hertz (Hz). Infrared spectra were collected using a Perkin Elmer Spectrometer and signals are expressed in cm^{-1}. Mass spectra were recorded with an electrospray MS Waters LCT Time of Flight Mass Spectrometer using electrospray ionisation (ESI). High-resolution mass spectrometry (HRMS) were recorded on an LCT spectrometer utilising a lock-mass incorporated into the mobile phase. Reverse phase (RP) HPLC analysis was run through a Kinetex® C18-EVO column (Phenomenex®): 5 µm, 100 Å, 250 x 4.60 mm, eluting with (A) H_2O/0.1% TFA and (B) CH_3CN/0.1% TFA. The following gradient was used: 70% (A) to 50% (B) over 15 min at 1 mL/min, and compounds were detected using UV-Vis detector and absorbance at 220 nm, 280 nm and 350 nm. All solvents used were HPLC grade and the column was maintained at 40 °C. UV-Vis spectra were recorded

on a Shimadzu UV-1800 spectrometer or CLARIOstar BMG labtech microplate reader sampling a wavelength range from 250 - 800 nm at 1.0 nm intervals. Fluorescence spectra were recorded on 96-well plate CLARIOstar BMG labtech microplate reader.

4.2 General procedure for fluorescamine assay, adapted from a known procedure.[231]

A stock solution of primary amine ligand in PBS was prepared, and the same stock used in the experimental work (e.g. coupling with NHS-agarose) and to make the standard curve. From the primary amine ligand stock solution, the standards solutions were prepared by serial dilution. In 96 well black-walled microplate, 100 µL of each standard or unknown sample were added in replicate. Then 100 µL of 1M fluorescamine (Alfa Aesar) in CH_3CN were added to each well and the fluorescence measured at 37 °C, exciting at 390 nm and reading the emission at 479 nm. The standard curve was prepared by plotting the average measurement at 479 nm for each primary amine ligand standard vs. its concentration in µM.

4.3 General procedure for BCA assay (adapted from the Thermo ScientificTM PierceTM BCA Protein Assay protocol).

The BCA Protein Assay kit was purchased from the Thermo Science. The working reagent (WR) was prepared by mixing BCA Reagent A (50 parts) with BCA Reagent B (1 part). Bovine serum albumin (BSA) (99 mg) was dissolved in PBS (2 mL) and this stock solution used in the thiol alkylation reaction and to make the BSA standard curve. From the BSA stock solution, the standards solutions in PBS were prepared by serial dilution in range from 20 µM to 1 µM. In 96 well microplate, 25 µL of each standard or unknown sample were pipetted in duplicate alongside protein-free controls (blanks). Then 200 µL of the WR was added to each well and

mixed for 30 seconds using a plate shaker. The microplate was covered and incubated at 37

°C for 30 minutes, then cooled to room temperature and the absorbance was measured at

562 nm on a microplate reader. The average of the blank standard replicates absorbance at

562 nm was subtracted from each absorbance of the individual standard and unknown

sample replicates at 562 nm. The standard curve was prepared by plotting the average blank-

corrected 562 nm measurement for each BSA standard vs. its concentration in µM.

4.4 Abbreviations.

| Abbreviation	Full meaning	Abbreviation	Full meaning
s	Singlet	EtOAc	Ethyl acetate
d	Doublet	Et$_2$O	Diethyl ether
dd	Doublet of Doublets	Na$_2$SO$_4$	Sodium sulfate
ddd	Doublet of Doublets of Doublet	MgSO$_4$	Magnesium sulfate
dddd	Doublet of Doublets of Doublet of Doublets	NaOH	Sodium hydroxide
t	Triplet	NaHCO$_3$	Sodium bicarbonate
dt	Doublet of Triplet	t-BuOH	tert-*Butanol*
m	Multiplet	PBS	Phosphate buffer solution
CH$_2$Cl$_2$	Dichloromethane	HCl	*Hydrochloric acid*
THF	Tetrahydrofuran	TFA	Trifluoroacetic acid
CH$_3$CN	Acetonitrile	Abs.	Absorbance
DMF	Dimethylformamide	FI	Fluorescence intensity
DMSO	Dimethyl sulfoxide	Conc.	concentration

4.5 Synthesis and characterisation of the compounds.

4.5.1 Preparation of 1-azidobut-3-en-2-yl (2-chloroacetyl)glycinate **1**, adapted from a known procedure.[171]
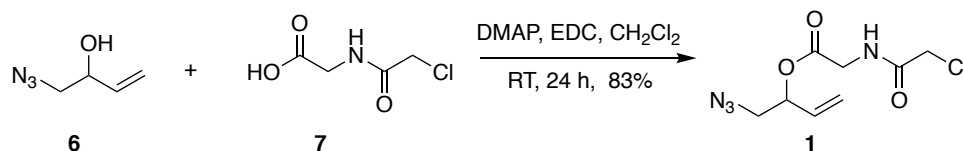

1-Ethyl-3-(3-dimethylaminopropyl)carbodiimide (EDC) (253 mg, 1.32 mmol) was added to a solution of alcohol **6** (50.0 mg, 0.44 mmol), acid **7** (433 mg, 1.77 mmol), and dimethylaminopyridine (DMAP) (54.0 mg, 0.44 mmol) in anhydrous CH_2Cl_2 (3.5 mL) under argon at ambient temperature. The reaction mixture was stirred until TLC indicated complete consumption of the alcohol starting material. After 24 hours the reaction was cooled to 0 °C. The urea by-product was removed *via* vacuum filtration. The filtrate was washed with saturated aqueous $NaHCO_3$ and brine, then the organic layer dried over Na_2SO_4 and concentrated *in vacuo.* The residue was purified by silica gel column chromatography (1% - 10% CH_3OH / CH_2Cl_2) to afford the 1-azidobut-3-en-2-yl (2-chloroacetyl)glycinate **1** as a viscous oil (89.9 mg, 83% yield); Rf = 0.6, CH_3OH / CH_2Cl_2, 1:9; IR (thin film)/cm^{-1} υ_{max} ; 3309, 2935, 2099, 1748, 1662, 1534, 1187, 938, 661; ^{1}H NMR (300 MHz, CDCl$_3$) δ 7.07 (s, 1H), 5.81 (ddd, J = 17.1, 10.5, 6.4 Hz, 1H), 5.52 – 5.32 (m, 3H), 4.16 (dd, J = 5.4, 1.5 Hz, 2H), 4.10 (s, 2H), 3.47 – 3.40 (m, 2H); ^{13}C NMR (100 MHz, CDCl$_3$) δ: 168.3, 166.2, 132.0, 120.0, 74.9, 53.5, 42.3, 41.6; MS *m/z* (ES+) 269.0 (M + Na$^+$); HRMS $C_8H_{11}N_4O_3$ Cl Na requires M, 269.0417, Found (M) 269.0421.

4.5.2 Preparation of 1-azidobut-3-en-2-ol **6** from ((1-azidobut-3-en-2-yl)oxy)(*tert*-butyl)dimethylsilane **11**, adapted from a known procedure.[164]
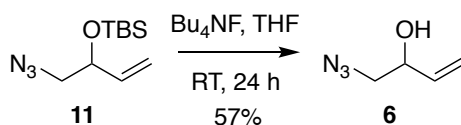
A THF solution of tetra- butylammonium fluoride (Bu$_4$NF) (0.68 mL, 0.68 mmol) was added to a 0 °C, THF solution (4 mL) of ((1-azidobut-3-en-2-yl)oxy)(*tert*-butyl)dimethylsilane **11** (70.0 mg, 0.31 mmol). The resulting mixture was allowed to warm ambient temperature and after 24 hours saturated, aqueous NH$_4$Cl (5 mL) and brine (10 mL) were added. The phases were separated, and the aqueous phase was then extracted with EtOAc (3 x 20 mL). The combined organic phase was washed with brine (2 x 20 mL), dried over MgSO$_4$, filtered and concentrated *in vacuo*. The crude material was purified by silica gel column chromatography (10% - 50% EtOAc / hexane) to afford 1-azidobut-3-en-2-ol **6** (20 mg, 57%) as a light yellow oil; IR (thin film)/cm^{-1}υ$_{max}$; 2918, 2096, 1650, 1437, 1278, 1278, 1073, 991, 928; ^{1}H NMR (400 MHz, CDCl$_3$) δ 5.84 (ddd, *J* = 17.2, 10.5, 5.7 Hz, 1H), 5.35 (dt, *J* = 17.2, 1.4 Hz, 1H), 5.21 (dt, *J* = 10.5, 1.4 Hz, 1H), 4.33 – 4.27 (m, 1H), 3.35 – 3.24 (m, 2H); ^{13}C NMR (100 MHz, CDCl$_3$) δ: 137.1, 116.9, 71.9, 56.4; Data agrees with literature values.[164]

4.5.3 Preparation of 1-azidobut-3-en-2-ol **6**, that was adapted from a known procedure.[2]
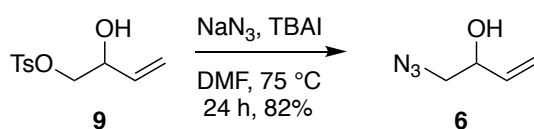
A DMF solution (20 mL) of 2-hydroxybut-3-en-1-yl 4-methylbenzenesulfonate **9** (3.0 g, 12.0 mmol), tetrabutylammonium iodide (TBAI) (0.6 g, 0.6 mmol), and sodium azide (NaN$_3$) (2.7 g, 37.0 mmol) was maintained at 75 °C. After 24 hours brine (20 mL) was added, the phases were separated, and the aqueous phase was extracted with diethyl ether (8 X 50 mL). The

combined organic phase was washed with brine (50 mL), dried over Na_2SO_4, filtered and concentrated *in vacuo* to afford 1-azidobut-3-en-2-ol **6** (1.2 g, 82%) as brown oil.[164] IR (thin film)/cm^{-1} υ_{max}; 2918, 2096, 1650, 1437, 1278, 1278, 1073, 991, 928; ^{1}H NMR (400 MHz, CDCl$_3$) δ 5.84 (ddd, *J* = 17.2, 10.5, 5.7 Hz, 1H), 5.35 (dt, *J* = 17.2, 1.4 Hz, 1H), 5.21 (dt, *J* = 10.5, 1.4 Hz, 1H), 4.33 – 4.27 (m, 1H), 3.35 – 3.24 (m, 2H); ^{13}C NMR (100 MHz, CDCl$_3$) δ: 137.1, 116.9, 71.9, 56.4; Data agrees with literature values.[164]

4.5.4 Preparation of (2-chloroacetyl)glycine **7**, adapted from a known procedure.[170]
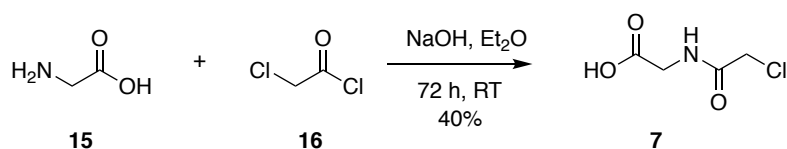
Glycine **15** (1 g, 13.3 mmol) was dissolved in 2.5 N NaOH (400 mL), and diethyl ether (7 mL) was added. The mixture was cooled (0 °C), and the solution of chloroacetyl chloride **16** (1.5 mL, 13.3 mmol) in 5 mL of ether was added dropwise over 30 min. The mixture was stirred for 45 min at 0 °C, then allowed to gradually warm up to ambient temperature while stirring for further 72 hours. The organic layer was separated, and the aqueous layer was extracted with diethyl ether (10 mL). The aqueous layer was acidified (pH 2) and extracted with EtOAc (4 × 15 mL). The combined EtOAc extracts were washed with 100 mL of brine, dried over Na_2SO_4, filtered and concentrated *in vacuo* to afford a colourless oil. Hexane (10 mL) were added to the obtained oil, and the solvent was removed to give a white solid. The crude product was recrystallised from diethyl ether to afford (2-chloroacetyl)glycine **7** (800 mg, 40%); ^{1}H NMR (300MHz, CD$_3$OD) δ: 4.10 (s, 2H), 4.00 (s, 2H); ^{13}C NMR (100MHz, CD$_3$OD) δ: 171.1, 168.3, 41.5, 40.7; MS *m/z* (EI+) 151.0 (M).

4.5.5 Preparation of 2-hydroxybut-3-en-1-yl 4-methylbenzenesulfonate **9**, adapted from a known procedure.[162]
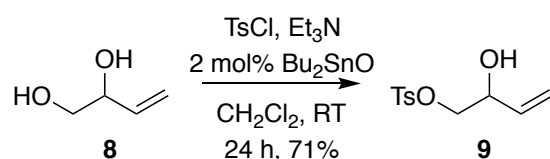
To a solution of the 3-buten-1,2-diol **8** (10.0 g, 114 mmol) in anhydrous CH_2Cl_2 (100 mL) were added dibutyl tin oxide (0.56 g, 2.30 mmol), *p*-Toluenesulfonyl chloride (TsCl) (21.7 g, 114 mmol), and triethylamine (15.8 mL, 114 mmol). The reaction mixture was stirred until TLC indicated complete consumption of the starting material. The reaction was quenched with water (100 mL), and the layers were separated. The aqueous layer was extracted with CH_2Cl_2 (2 x 100 mL), the combined organic layers were washed sequentially with water (100 mL) and brine (100 mL), dried over Na_2SO_4, and filtered, and the filtrate was concentrated *in vacuo*. The residue was purified by silica gel column chromatography (10% EtOAc / hexane) to afford the desired 2-hydroxybut-3-en-1-yl 4-methylbenzenesulfonate **9** (19.6 g, 71%) as colourless oil; Rf = 0.7, EtOAc / petroleum ether, 1:1; ^{1}H NMR (300 MHz, CDCl₃) δ 7.78 (d, *J* = 8.0 Hz, 2H), 7.38 (d, *J* = 8.0 Hz, 2H), 5.78 (ddd, *J* = 17.3, 10.5, 5.5 Hz, 1H), 5.40 (dt, *J* = 17.3, 1.4 Hz, 1H), 5.27 (dt, *J* = 10.5, 1.4 Hz, 1H), 4.42 (dddd, *J* = 7.0, 5.5, 3.3, 1.6 Hz, 1H), 4.09 (dd, *J* = 10.2, 3.3 Hz, 1H), 3.93 (dd, *J* = 10.2, 7.0 Hz, 1H), 2.48 (s, 3H); ^{13}C NMR (100 MHz, CDCl₃) δ 145.5, 135.1, 133.1, 130.4, 128.4, 118.5, 73.4, 70.8, 22.1; MS *m/z* (ES+) 265.1 (M + Na⁺); Data agrees with literature values.[164,254]

4.5.6 Preparation of 2-((*tert*-butyldimethylsilyl)oxy)but-3-en-1-yl 4-methylbenzenesulfonate **10**, adapted from a known procedure.[164]
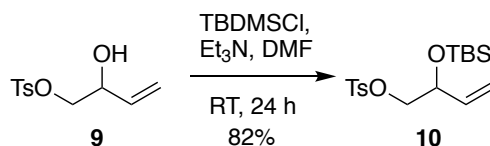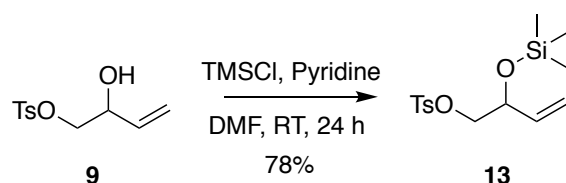

tert-Butyldimethylsilyl chloride (TBDMSCl) (12.4 g, 82.4 mmol) and triethylamine (11.5 mL, 82.4 mmol) were added to a 0 °C, DMF solution (80 mL) of 2-hydroxybut-3-en-1-yl 4-methylbenzenesulfonate **9** (5 g, 20.6 mmol). The reaction mixture was allowed to warm to ambient temperature. After 24 hours brine (80 mL) was added and the aqueous phase was then extracted with diethyl ether (2 x 100 mL). The combined organic layers were dried over MgSO$_4$, filtered and concentrated *in vacuo*. The residue was purified by silica gel column chromatography (10% EtOAc / hexane) to afford 2-((*tert*-butyldimethylsilyl)oxy)but-3-en-1-yl 4-methylbenzenesulfonate **10** (6.0 g, 82%); R$_f$ = 0.9, EtOAc / hexane, 1:1; ^{1}H NMR (300MHz, CDCl$_3$) δ: 7.77 (d, J = 8.1 Hz, 2H), 7. 34 (d, J = 8.1 Hz, 2H), 5.76 - 5.63 (m, 1H), 5.30 (d, J = 17.2 Hz, 1H),5.18 - 5.12 (m, 1H),4.33 (m, 1H), 3.92 - 3.77 (m, 2H), 2.45 (s, 3H), 0.85 (s, 9H), 0.02 (s, 6H); ^{13}C NMR (100MHz, CDCl$_3$) δ: 144.8, 136.1, 133.0, 129.8, 117.2, 73.0, 71.3, 30.90, 25.7, 21.6, 18.2, - 4.8; MS *m/z* (ES+) 379.1 (M + Na). Data agrees with literature values.[164]

4.5.7 Preparation of ((1-azidobut-3-en-2-yl)oxy)(*tert*-butyl)dimethylsilane **11**, adapted from a known procedure.[164]
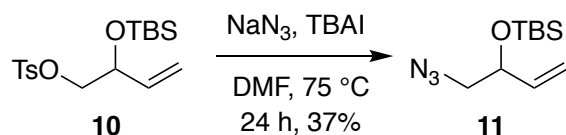
A DMF solution (4 mL) of 2-((*tert*-butyldimethylsilyl)oxy)but-3-en-1-yl 4-methylbenzenesulfonate **10** (297 mg, 0.834 mmol), tetrabutylammonium iodide (TBAI) (30.8 mg, 0.08 mmol), and sodium azide (NaN$_3$) (162 mg, 2.50 mmol) was maintained at 75 °C. After 24 hours brine (5 mL) was added, the phases were separated, and the aqueous phase was extracted with diethyl ether (5 x 10 mL). The combined organic phase was washed with brine (50 mL), dried over Na$_2$SO$_4$, filtered and concentrated *in vacuo* to afford ((1-azidobut-3-en-2-yl)oxy)(*tert*-butyl)dimethylsilane **11** (70.0 mg, 37%) as brown oil; ^{1}H NMR (300MHz, CDCl$_3$) δ: 5.88 - 5.73 (m, 1H), 5.35 - 5.27 (dt, J = 17.2, 1.3 Hz, 1H), 5.21 - 5.15 (dt, J = 10.7, 1.3 Hz, 1H), 4.32 - 4.25 (m, 1H), 3.17 (d, J = 5.4, 2H), 0.92 (S, 9H), 0.09 (s, 6H); ^{13}C NMR (100MHz, CDCl$_3$) δ: 138.0, 116.3, 73.5, 57.1, 25.8, 18.1, - 4.6; MS *m/z* (AP+) 228.2 (M + H). Data agrees with literature values.[164]

4.5.8 Preparation of 2-((trimethylsilyl)oxy)but-3-en-1-yl 4-methylbenzenesulfonate **13**.[164]

Trimethylsilyl chloride (TMSCl) (0.21 mL, 1.65 mmol) and pyridine (5 mL) were added to a 0 °C, DMF solution (5 mL) of 2-hydroxybut-3-en-1-yl 4-methylbenzenesulfonate **9** (100 mg, 0.413 mmol). The reaction mixture was allowed to warm to ambient temperature. After 24 hours brine (10 mL) was added and the aqueous phase was then extracted with diethyl ether

(2 x 8 mL). The combined organic layers were dried over MgSO$_4$, filtered and concentrated *in vacuo* to afford 2-((trimethylsilyl)oxy)but-3-en-1-yl 4-methylbenzenesulfonate **13** (100 mg, 78%); ^{1}H NMR (300MHz, CDCl$_3$) δ: 7.70 (d, J = 8.0 Hz, 2H), 7. 25 (d, J = 8.0 Hz, 2H), 5.68 - 5.55 (m, 1H), 5.24 (dt, J = 17.2, 1.2 Hz, 1H), 5.11 - 5.05 (dt, J = 10.4, 1.2 Hz, 1H), 4.28 - 4.20 (m, 1H), 3.86 - 3.71 (m, 2H), 2.36 (s, 3H), 0.00 (s, 9H); ^{13}C NMR (100MHz, CDCl$_3$) δ: 144.8, 135.9, 133.1, 129.9, 128.0, 117.3, 72.9, 71.2, 21.6, 0.0; MS *m/z* (ES+) 337.1 (M + Na).

4.5.9 Preparation of 2-((*tert*-butyldiphenylsilyl)oxy)but-3-en-1-yl 4-methylbenzenesulfonate **14**.[164]
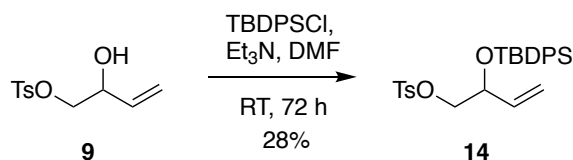
To a solution of 2-hydroxybut-3-en-1-yl 4-methylbenzenesulfonate **9** (200 mg, 0.826 mmol) in DMF (6.6 mL) at 0 °C were added *tert*-Butyldiphenylsilyl chloride (TBDPSCl) (0.86 mL, 3.30 mmol) and triethylamine (0.46 mL, 3.30 mmol). The reaction mixture was allowed to warm to ambient temperature. After 72 hours brine (7 mL) was added and the aqueous phase was then extracted with diethyl ether (2 x 20 mL). The combined organic layers were dried over MgSO$_4$, filtered and concentrated *in vacuo*. The residue was purified by silica gel column chromatography (10% EtOAc / hexane) to afford 2-((*tert*-butyldiphenylsilyl)oxy)but-3-en-1-yl 4-methylbenzenesulfonate **14** (110 mg, 28%); R$_f$ = 0.97, EtOAc / hexanes, 1:1; ^{1}H NMR (300MHz, CDCl$_3$) δ: 7.70 - 7.60 (m, 7H), 7.40 - 7.25 (m, 7H), 5.76-5.63 (m, 1H), 5.15 - 5.00 (m, 2H), 4.33 (m, 1H), 3.92-3.77 (m, 2H), 2.15 (s, 3H), 0.95 (s, 9H); ^{13}C NMR (100MHz, CDCl$_3$) δ:137.3, 135.9, 134.8, 133.4, 129.9, 127.7, 117.1, 74.1, 48.4, 30.9, 29.7, 26.9, 19.4; MS *m/z* (ES+) 503.2 (M + Na). Data agrees with literature values.[255]

4.5.10 Preparation of 1-azidobut-3-en-2-yl acetylglycinate **18**, adapted from a known procedure.[171]
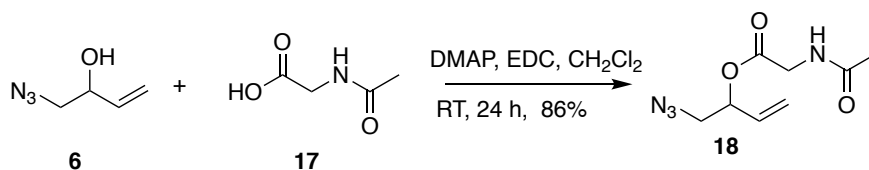
Prepared using an identical method to 4.5.1; Rf = 0.6, CH$_3$OH / CH$_2$Cl$_2$, 1:9; IR (thin film)/cm^{-1}

υ_{max}; 3309, 2096, 1742, 1655, 1545, 1437, 1375, 1209, 996, 688; ^{1}H NMR (400 MHz, CDCl$_3$) δ

6.16 (s, 1H), 5.84 – 5.74 (m, 1H), 5.48 – 5.29 (m, 3H), 4.17 – 4.01 (m, 2H), 3.47 – 3.36 (m, 2H),

2.03 (d, J = 3.0 Hz, 3H); ^{13}C NMR (100MHz, CDCl$_3$) δ: 170.1, 168.9, 131.9, 119.5, 74.4, 53.3,

41.2, 22.7; MS m/z (ES+) 235.1 (M + Na$^+$), HRMS C$_8$H$_{12}$N$_4$O$_3$Na requires M, 235.0807, Found

(M) 235.0810.

4.5.11 Preparation of 1-(4-((1,3-dioxoisoindolin-2-yl)methyl)-1H-1,2,3-triazol-1-yl)but-3-en-2-yl acetylglycinate **22**, that was adapted from a known procedure.[173]
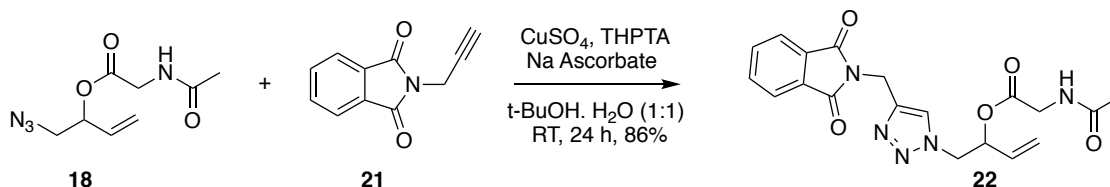
1-azidobut-3-en-2-yl acetylglycinate **18** (114 mg, 0.54 mmol), 2-(prop-2-yn-1-yl)isoindoline-1,3-dione

21 (100 mg, 0.54 mmol), Copper (II) sulfate (1.87 mg, 0.01 mmol), and tris(3-hydroxypropyltriazolylmethyl)amine (THBTA) (5.00 mg, 0.01 mmol) were stirred in t-BuOH.H$_2$O

solution (1:1, 1 mL), followed by addition of sodium ascorbate (46.6 mg, 0.24 mmol). The

reaction mixture was stirred until TLC indicated complete consumption of the starting

material. After 24 hours of the reaction, brine (7 mL) was added and the aqueous phase was

then extracted with EtOAc (2 x 20 mL). The combined organic layers were dried over MgSO$_4$,

filtered and concentrated *in vacuo* to afford the 1-(4-((1,3-dioxoisoindolin-2-yl)methyl)-1H-

1,2,3-triazol-1-yl)but-3-en-2-yl acetylglycinate **22** (180 mg, 86% yield); Rf = 0.5, CH$_3$OH / CH$_2$Cl$_2$, 5%; IR (thin film)/cm^{-1} υ_{max}; 1714, 1547, 1396, 1187, 938, 715; ^{1}H NMR (400 MHz, CDCl$_3$) δ 7.84 (dd, J = 5.5, 3.0 Hz, 2H), 7.72 (dd, J = 5.5, 3.0 Hz, 2H), 7.67 (s, 1H), 6.17 (s, 1H), 5.77 (ddd, J = 17.0, 10.6, 6.3 Hz, 1H), 5.65 – 5.59 (m, 1H), 5.43 – 5.30 (m, 2H), 5.05 – 4.92 (m, 2H), 4.60 (dd, J = 14.4, 3.8 Hz, 1H), 4.51 – 4.43 (m, 1H), 4.13 – 4.06 (m, 1H), 3.92 (dd, J = 18.3, 5.0 Hz, 1H), 2.04 (s, 3H); ^{13}C NMR (100MHz, CDCl$_3$) δ: 170.3, 168.7, 167.7, 134.2, 132.0, 131.2, 123.6, 123.5, 120.5, 73.4, 52.7, 41.3, 33.1, 22.9; MS *m/z* (ES+) 420.1 (M + Na$^+$); HRMS C$_{19}$H$_{19}$N$_5$O$_5$23Na requires M, 420.1284, Found (M) 420.1283.

4.5.12 Preparation of 1-azidobut-3-en-2-yl (2-iodoacetyl)glycinate **24**, that was adapted from a known procedure.[256]
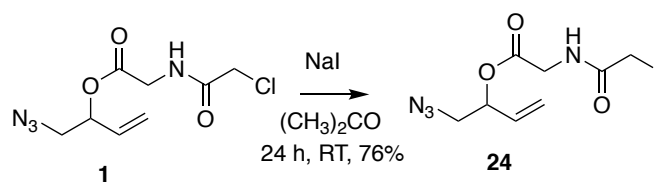
To the solution of 1-azidobut-3-en-2-yl (2-chloroacetyl)glycinate **1** (80.0 mg, 0.33 mmol) in acetone, sodium iodide (197.85 mg, 1.32 mmol) was added. The reaction mixture was stirred until TLC indicated complete consumption of the starting material. The sodium chloride salt was removed by filtration and the filtrate was washed with brine, then the organic layer dried over Na$_2$SO$_4$ and concentrated *in vacuo* to afford 1-azidobut-3-en-2-yl (2-iodoacetyl)glycinate **24** (83.5 mg, 76% yield); IR (thin film)/cm^{-1} υ_{max}; 3330, 2945, 2832, 1651, 1411, 1019; ^{1}H NMR (400 MHz, CDCl$_3$) δ 6.56 (s, 1H), 5.81 (ddd, J = 17.1, 10.6, 6.4 Hz, 1H), 5.48 (tdt, J = 6.4, 4.6, 1.2 Hz, 1H), 5.44 – 5.33 (m, 2H), 4.13 (dd, J = 5.3, 1.2 Hz, 2H), 3.75 (s, 2H), 3.49 – 3.38 (m, 2H); ^{13}C NMR (100 MHz, CDCl$_3$) δ 168.6, 167.3, 132.1, 120.1, 75.0, 53.6, 42.3, 29.8; MS *m/z* (ES+) 361.0 (M + Na$^+$), HRMS C$_8$H$_{11}$N$_4$O$_3$NaI requires M, 360.9774, Found (M) 360.9770.

4.5.13 Preparation of 1-(4-(((*tert*-butoxycarbonyl)amino)methyl)-1H-1,2,3-triazol-1-yl)but-3-en-2-yl (2-chloroacetyl)glycinate **26**, that was adapted from a known procedure.[173]
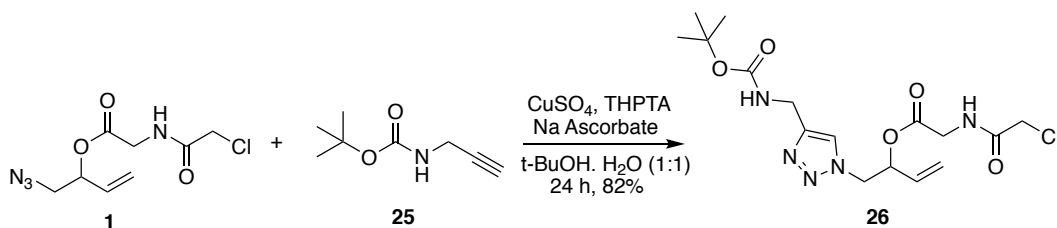
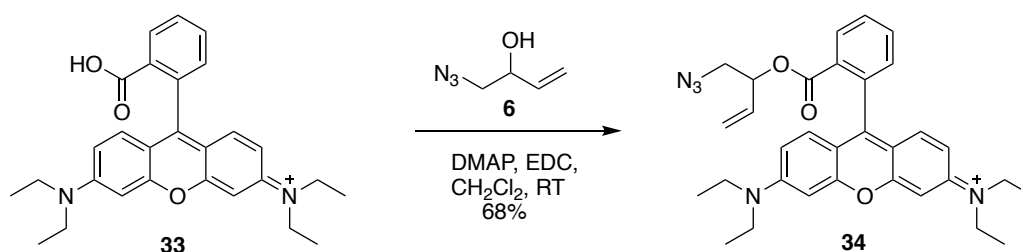Prepared using an identical method to 4.5.11; IR (thin film)/cm^{-1} υ_{max}; 3350, 2850, 1650, 1500, 1130; ^{1}H NMR (400 MHz, CDCl$_3$) δ 7.57 (s, 1H), 7.16 (d, *J* = 6.7 Hz, 1H), 5.78 (ddd, *J* = 17.0, 10.5, 6.3 Hz, 1H), 5.71 – 5.62 (m, 1H), 5.46 – 5.24 (m, 3H), 4.62 (dd, *J* = 14.4, 3.9 Hz, 1H), 4.50 (dd, *J* = 14.4, 7.5 Hz, 1H), 4.37 (d, *J* = 5.9 Hz, 2H), 4.09 (s, 2H), 4.05 (dd, *J* = 5.6, 3.0 Hz, 2H), 1.43 (s, 9H) ; ^{13}C NMR (100 MHz, CDCl$_3$) δ 167.7, 166.4, 155.8, 145.6, 131.0, 122.8, 120.4, 79.5, 73.6, 52.4, 42.2, 41.3, 36.0, 28.2; MS *m/z* (ES+) 424.1 (M + Na$^+$); HRMS C$_{16}$H$_{24}$N$_5$O$_5$NaCl requires M, 424.1364, Found (M) 424.1358.

4.5.14 Preparation of 1-(4-(aminomethyl)-1H-1,2,3-triazol-1-yl)but-3-en-2-yl (2-chloroacetyl)glycinate **27**, that was adapted from a known procedure.[257]
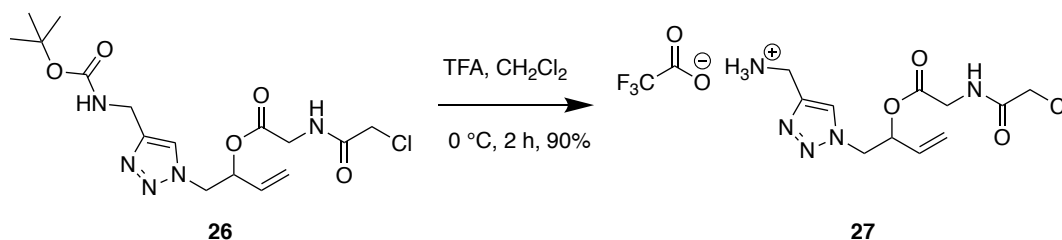
To a solution of molecule **26** (0.17 g, 0.42 mmol) in CH$_2$Cl$_2$ (10 mL) at 0 °C was added TFA (10 mL). The reaction mixture was stirred for 2 hours, until TLC indicated complete consumption of the starting material, then diluted with diethyl ether and concentrated under *vacuo* and evaporated 7 times after adding diethyl ether to remove the residual TFA to afford 1-(4-

(aminomethyl)-1H-1,2,3-triazol-1-yl)but-3-en-2-yl (2-chloroacetyl)glycinate **27** (0.12 g, 90 %);

^{1}H NMR (300 MHz, D$_2$O) δ 8.17 (s, 1H), 5.98 – 5.82 (m, 1H), 5.74 (dddd, J = 7.0, 5.2, 4.3, 1.2 Hz, 1H), 5.43 – 5.32 (m, 2H), 4.89 – 4.80 (m, 1H), 4.79 – 4.66 (m, 1H), 4.34 (s, 2H), 4.18 (s, 2H), 4.10 – 4.03 (m, 2H); ^{13}C NMR (100 MHz, CD$_3$OD) δ 169.5, 168.9, 140.6, 132.4, 126.2, 119.3, 74.0, 53.2, 42.3, 41.8, 34.9.

4.5.15 Preparation of *N*-(9-(2-(((1-azidobut-3-en-2-yl)oxy)carbonyl)phenyl)-6-(diethylamino)-3H-xanthen-3-ylidene)-N-ethylethanaminium **34**.

Prepared using an identical method to 4.5.1; Rf = 0.6, CH$_3$OH / CH$_2$Cl$_2$, 1%; IR (thin film)/cm^{-1} υ$_{max}$; 3392, 2100, 1587, 1467, 1413, 1338, 1180, 1132, 1074, 682; ^{1}H NMR (400 MHz, CDCl$_3$) δ 8.31 (dd, J = 7.6, 1.3 Hz, 1H), 7.80 (dtd, J = 33.2, 7.6, 1.4 Hz, 2H), 7.34 (dd, J = 7.6, 1.3 Hz, 1H), 7.08 (t, J = 9.7 Hz, 2H), 6.92 (ddd, J = 14.9, 9.7, 2.5 Hz, 2H), 6.83 (d, J = 2.5 Hz, 2H), 5.54 (ddd, J = 17.1, 10.5, 6.4 Hz, 1H), 5.32 – 5.26 (m, 1H), 5.20 – 5.11 (m, 2H), 3.70 – 3.60 (m, 8H), 3.33 – 3.19 (m, 2H), 1.32 (t, J = 7.1 Hz, 12H); ^{13}C NMR (100 MHz, CDCl$_3$) δ 164.1, 158.2, 157.9, 157.7, 155.5, 133.5, 133.4, 131.8, 131.4, 131.2, 130.5, 129.7, 119.7, 114.4, 113.6, 96.4, 74.2, 53.4, 46.2, 12.7; MS *m/z* (ES+) 538.3 (M), HRMS C$_{32}$H$_{36}$N$_5$O$_3$ requires M, 538.2818, Found (M) 538.2813.

4.5.16 Preparation of 1-azidobut-3-en-2-yl (4-bromophenyl)carbamate **37,** that was adapted

from a known procedure.[258]
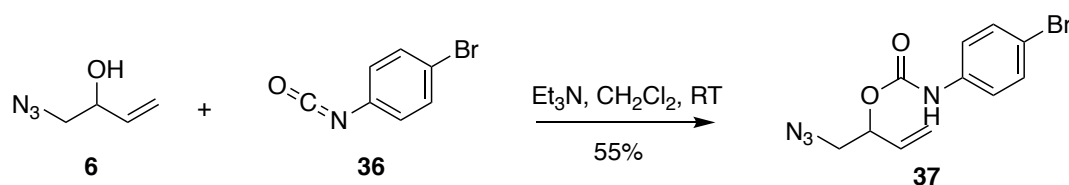
A flame-dried round- bottomed flask was degassed, flushed with argon, and charged with 4-

bromophenyl isocyanate **36** (0.2 mL, 2.1 mmol), anhydrous CH_2Cl_2 (4 mL), triethylamine (0.3 mL,

2.1 mmol) and 1-azidobut-3-en-2-ol **6** (80 mg, 0.7 mmol). The reaction mixture was stirred at

room temperature until TLC indicated complete consumption of the starting material. The

reaction mixture was then diluted with CH_2Cl_2 (5 mL), washed with 1M HCl (3 x 5 mL), water

(5 mL), and brine (5 mL), and then concentrated *in vacuo*. The crude product was purified by

silica gel column chromatography (5%-10%-20% EtOAc / hexane) to afford the 1-azidobut-3-

en-2-yl (4-bromophenyl)carbamate **37** (50 mg, 55%); Rf = 0.8, EtOAc / petroleum ether, 1:1;

^{1}H NMR (400 MHz, CD$_3$OD) δ 7.75 – 7.68 (m, 1H), 7.60 (dd, *J* = 8.0, 1.5 Hz, 1H), 7.38 – 7.31 (m,

1H), 7.08 (td, *J* = 7.8, 1.6 Hz, 1H), 5.93 (ddd, *J* = 17.3, 10.7, 5.8 Hz, 1H), 5.50 – 5.28 (m, 3H),

3.50 (dd, *J* = 5.5, 3.4 Hz, 2H); ^{13}C NMR (100 MHz, CD$_3$OD) δ 137.1, 134.6, 133.7, 129.0, 127.3,

126.0, 118.6, 75.5, 54.6.

### 4.5.17 Preparation of 1-azidobut-3-en-2-yl benzylcarbamate **39**.
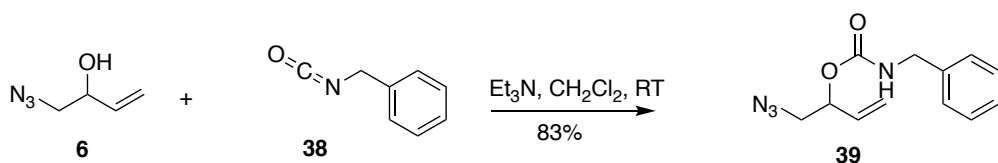
Prepared using an identical method to 4.5.16; Rf = 0.8, EtOAc / petroleum ether, 1:1; IR (thin film)/cm^{-1} υ_{max}; 3327, 2098, 1703, 1522, 1453, 1245, 1135, 1028, 934, 698; ^{1}H NMR (300 MHz, CDCl$_3$) δ 7.39 – 7.27 (m, 5H), 5.84 (ddd, *J* = 16.9, 10.6, 5.9 Hz, 1H), 5.47 – 5.28 (m, 3H), 5.12 (s, 1H), 4.40 (d, *J* = 6.0 Hz, 2H), 3.49 – 3.32 (m, 2H); ^{13}C NMR (100 MHz, CDCl$_3$) δ 138.6, 133.9, 129.2, 129.1, 128.1, 128.0, 119.0, 74.5, 54.4, 45.6; MS *m/z* (ES+) 269.1 (M +Na$^+$), HRMS C$_{12}$H$_{14}$N$_4$O$_2$Na requires M, 269.1014, Found (M) 269.1016.

4.5.18 Preparation of (*E*)-but-2-en-1-yl benzylcarbamate **41.**
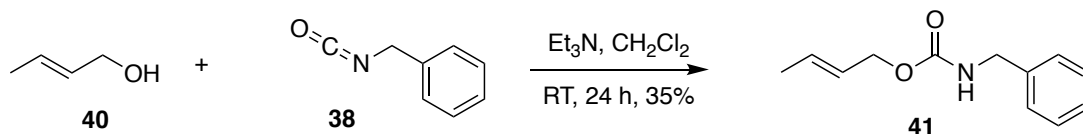
Prepared using an identical method to 4.5.16; ^{1}H NMR (300 MHz, CD$_3$OD) δ 7.36 – 7.12 (m, 5H), 5.77 (dp, *J* = 14.8, 8.4, 7.4 Hz, 1H), 5.67 – 5.44 (m, 1H), 4.47 (dt, *J* = 6.2, 1.3 Hz, 2H), 4.27 (s, 2H), 1.75 – 1.62 (m, 3H); ^{13}C NMR (100 MHz, CD$_3$OD) δ 140.7, 131.2, 129.4, 128.2, 128.1, 127.2, 66.5, 45.4, 17.9; MS *m/z* (EI+) 205.1 (M), HRMS-EI+ (M) calc. mass for C$_{12}$H$_{15}$NO$_2$ 205.1103, found 205.1110.

4.5.19 Preparation of But-3-en-2-yl benzylcarbamate **43**.
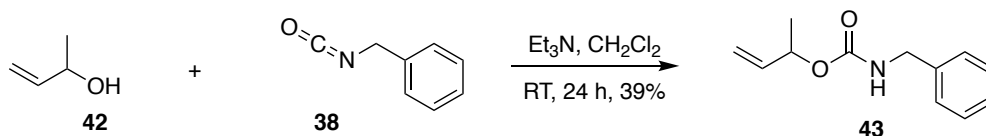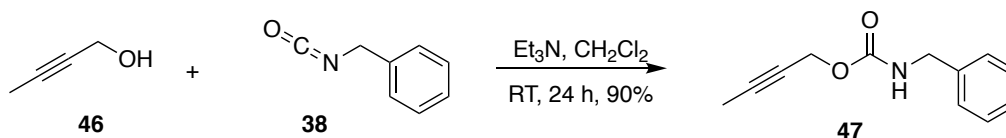

Prepared using an identical method to 4.5.16; ^{1}H NMR (300 MHz, CD$_3$OD) δ 7.37 – 7.17 (m, 5H), 5.88 (ddd, J = 16.6, 10.6, 5.6 Hz, 1H), 5.30 – 5.15 (m, 3H), 4.27 (s, 2H), 1.30 (d, J = 6.5 Hz, 3H); ^{13}C NMR (100 MHz, CD$_3$OD) δ 164.8, 140.0, 129.7, 128.4, 128.3, 115.6, 72.8, 45.6, 20.9; MS m/z (EI+) 205.1 (M), HRMS-EI+ (M) calc. mass for C$_{12}$H$_{15}$NO$_2$ 205.1103, found 205.1108.

4.5.20 Preparation of Prop-2-yn-1-yl benzylcarbamate **45**.
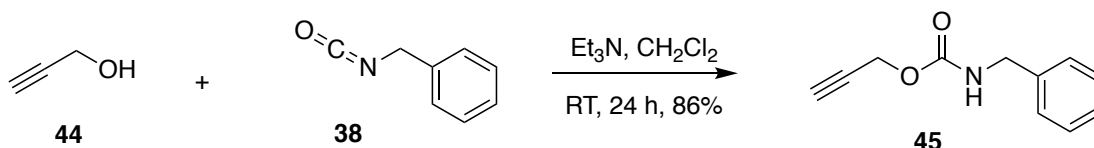
Prepared using an identical method to 4.5.16; ^{1}H NMR (400 MHz, CDCl$_3$) δ 7.36 – 7.22 (m, 5H), 5.10 (s, 1H), 4.68 (d, J = 2.3 Hz, 2H), 4.35 (d, J = 5.9 Hz, 2H), 2.44 (t, J = 2.3 Hz, 1H); ^{13}C NMR (100 MHz, CDCl$_3$) δ 155.6, 138.2, 128.8, 127.7, 127.7, 78.4, 74.8, 52.8, 45.4; MS m/z (EI+) 189.1 (M). Data agrees with literature values.[259]

### 4.5.21 Preparation of But-2-yn-1-yl benzylcarbamate **47**.

Prepared using an identical method to 4.5.16; IR (thin film)/cm^{-1} υ_{max}; 3337, 2483, 1695, 1525, 1442, 1352, 1248, 1153, 1040, 975; ^{1}H NMR (300 MHz, CD$_3$OD) δ 7.37 – 7.15 (m, 5H), 4.62 (q, J = 2.4 Hz, 2H), 4.29 (s, 2H), 1.82 (t, J = 2.4 Hz, 3H); ^{13}C NMR (100 MHz, CD$_3$OD) δ 158.4, 140.5, 129.5, 128.3, 128.1, 83.2, 74.9, 53.9, 45.5, 3.1; MS m/z (EI+) 203.1 (M), HRMS-EI+ (M) calc. mass for C$_{12}$H$_{13}$NO$_2$ 203.0946, found 203.0953.

4.5.22 Preparation of But-3-yn-2-yl benzylcarbamate **49**.
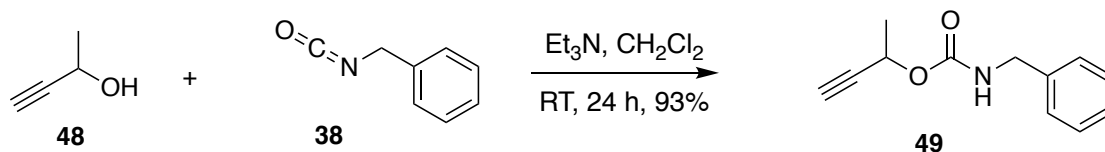
Prepared using an identical method to 4.5.16; ^{1}H NMR (300 MHz, CDCl$_3$) δ 7.36 – 7.16 (m, 5H), 5.40 (qd, J = 6.7, 2.1 Hz, 1H), 4.99 (s, 1H), 4.34 (s, 2H), 2.43 (d, J = 2.1 Hz, 1H), 1.47 (d, J = 6.7 Hz, 3H); ^{13}C NMR (100 MHz, CDCl$_3$) δ 155.3, 138.3, 128.8, 127.7, 82.7, 72.9, 60.9, 45.1, 21.7; MS m/z (EI+) 203.1 (M), HRMS-EI+ (M) calc. mass for C$_{12}$H$_{13}$NO$_2$ 203.0946, found 203.0950. Data agrees with literature values.[260]

4.5.23 Preparation of (*E*)-but-2-en-1-yl 1H-imidazole-1-carboxylate **60**, that was adapted from a known procedure.[227]
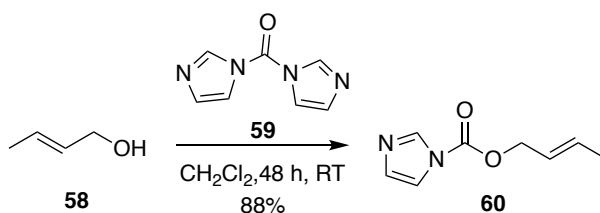
To a solution of 1,1'-carbonyldiimidazole (CDI) **59** (337 mg, 2.08 mmol) in CH$_2$Cl$_2$ at 0 °C was added (*E*)-but-2-en-1-ol **58** (0.27 ml, 3.12 mmol) dropwise under argon. The reaction mixture was stirred at 0 °C for 1 h, and then allowed to warm to room temperature and stirred until TLC indicated complete consumption of the starting material. The reaction mixture was diluted CH$_2$Cl$_2$, washed with water (2 times), dried over Na$_2$SO$_4$, and concentrated *in vacuo* to afford the (*E*)-but-2-en-1-yl 1H-imidazole-1-carboxylate **60** (303 mg, 88%); ^{1}H NMR (400 MHz, CDCl$_3$) δ 8.13 (t, J = 1.0 Hz, 1H), 7.42 (t, J = 1.5 Hz, 1H), 7.05 (dd, J = 1.5, 1.0 Hz, 1H), 5.94 (dqt, J = 15.3, 6.5, 1.1 Hz, 1H), 5.68 (dtq, J = 15.3, 6.8, 1.7 Hz, 1H), 4.81 (dq, J = 6.8, 1.1 Hz, 2H), 1.80

– 1.73 (m, 3H); ^{13}C NMR (100 MHz, CDCl$_3$) δ 148.7, 137.3, 134.3, 130.7, 123.6, 117.3, 69.0, 18.0; MS *m/z* (EI+) 166.1 (M). Data agrees with literature values.[261]

4.5.24 Preparation of (*E*)-but-2-en-1-yl *tert*-butyl ethane-1,2-diyldicarbamate **62**, that was adapted from a known procedure.[228]
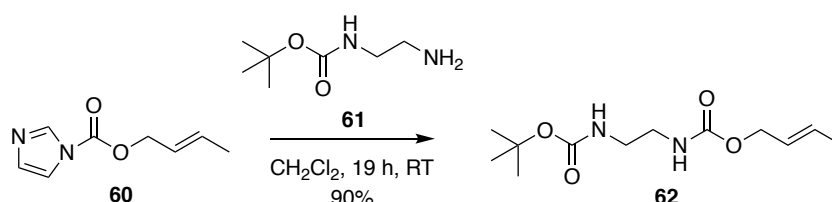

To a solution of the (*E*)-but-2-en-1-yl 1H-imidazole-1-carboxylate **60** (291 mg, 1.75 mmol) in CH$_2$Cl$_2$ at room temperature was added a solution of *N*-Boc-ethylenediamine **61** (0.28 ml, 1.75 mmol) dissolved in CH$_2$Cl$_2$, dropwise under argon. The reaction mixture was stirred at 30 °C until TLC indicated complete consumption of the starting material. Then the reaction mixture was diluted CH$_2$Cl$_2$, washed with water (3 times), dried over Na$_2$SO$_4$, and concentrated *in vacuo* to afford the (*E*)-but-2-en-1-yl *tert*-butyl ethane-1,2-diyldicarbamate **62** (371 mg, 90%); IR (thin film)/cm^{-1} υ$_{max}$; 3325, 2934, 1680, 1540, 1264, 1150, 964, 640; ^{1}H NMR (300 MHz, CD$_3$OD) δ 5.84 – 5.70 (m, 1H), 5.58 (dtd, *J* = 14.9, 6.2, 1.6 Hz, 1H), 4.52 – 4.36 (m, 2H), 3.19 – 3.05 (m, 4H), 1.70 (dq, *J* = 6.2, 1.3 Hz, 3H), 1.43 (s, 9H); ^{13}C NMR (100 MHz, CDCl$_3$) δ 157.0, 156.5, 131.0, 125.8, 79.6, 65.8, 41.5, 40.8, 28.5, 17.9; MS *m/z* (ES+) 281.15 (M + Na$^+$); HRMS-ES+ (M + Na$^+$) Calc. for C$_{12}$H$_{22}$N$_2$O$_4$Na 281.1477, Found 281.1480.

4.5.25 Preparation of (*E*)-2-(((but-2-en-1-yloxy)carbonyl)amino)ethan-1-aminium **63**, that was adapted from a known procedure.[229]
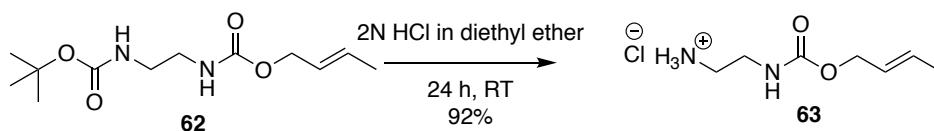
A solution of concentrated HCl in diethyl ether (2N) (3 ml) was added to the (*E*)-but-2-en-1-yl *tert*-butyl ethane-1,2-diyldicarbamate **62** (87.0 mg, 0.34 mmol) at ambient temperature. The reaction mixture was stirred at ambient temperature until TLC indicated complete consumption of the starting material and a salt product precipitated in diethyl ether. The precipitated product was isolated by filtration, then transferred to a round bottom flask by washing with diethyl ether and concentrated from diethyl ether *in vacuo* at ambient temperature (8 times) to afford the (*E*)-2-(((but-2-en-1-yloxy)carbonyl)amino)ethan-1-aminium **63** as an HCl salt (60.2 mg, 92%); IR (thin film)/cm^{-1} υ_{max}; 3450, 2357, 2158,1652, 1506, 1264, 1025, 668; ^{1}H NMR (400 MHz, CD$_3$OD) δ 5.80 (dq, *J* = 13.2, 6.4 Hz, 1H), 5.65 – 5.54 (m, 1H), 4.48 (d, *J* = 6.4 Hz, 2H), 3.38 (t, *J* = 5.9 Hz, 2H), 3.04 (t, *J* = 5.9 Hz, 2H), 1.71 (dq, *J* = 6.4, 1.3 Hz, 3H); ^{13}C NMR (100 MHz, CD$_3$OD) δ 131.6, 127.2, 67.1, 41.4, 39.7, 18.1; MS *m/z* (ES+) 159.11 (M + H$^+$), HRMS-ES+ (M + H$^+$) Calc. for C$_7$H$_{15}$N$_2$O$_2$ 159.1134, Found 159.1133.

4.5.26 Preparation of But-3-en-2-yl 1*H*-imidazole-1-carboxylate **65**.
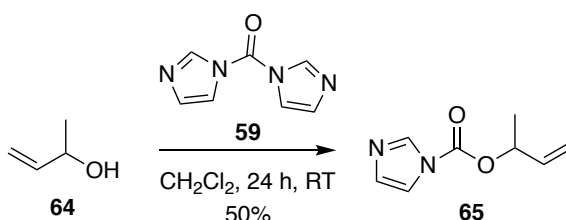
Prepared using an identical method to 4.5.23; ^{1}H NMR (400 MHz, CDCl$_3$) δ 8.13 (t, *J* = 1.1 Hz, 1H), 7.42 (t, *J* = 1.5 Hz, 1H), 7.06 (dd, *J* = 1.5, 1.1 Hz, 1H), 5.93 (ddd, *J* = 17.0, 10.5, 6.5 Hz, 1H),

5.53 (pt, *J* = 6.5, 1.1 Hz, 1H), 5.38 (dt, *J* = 17.0, 1.1 Hz, 1H), 5.27 (dt, *J* = 10.5, 1.1 Hz, 1H), 1.50

(d, *J* = 6.5 Hz, 3H); ^{13}C NMR (100 MHz, CDCl$_3$) δ 148.1, 137.2, 136.1, 130.7, 118.0, 117.2, 76.14,

20.0; MS *m/z* (EI+) 166.1 (M).

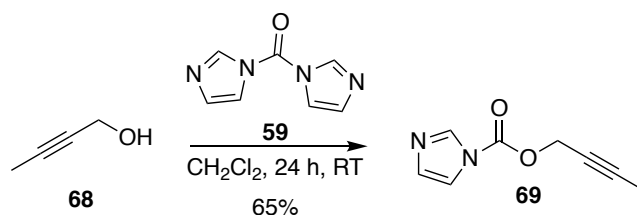### 4.5.27 Preparation of But-3-en-2-yl *tert*-butyl ethane-1,2-diyldicarbamate **66**.
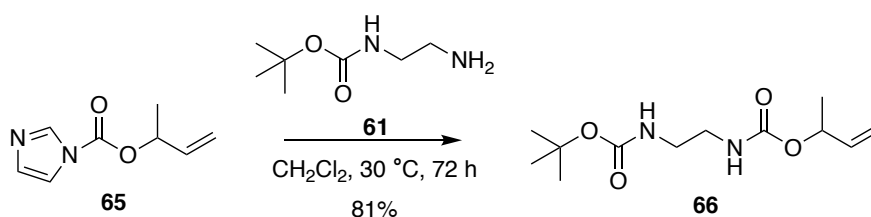
Prepared using an identical method to 4.5.24; IR (thin film)/cm^{-1} υ$_{max}$; 3331, 2938, 2831, 1680,

1532, 1265, 1158, 1021, 639; ^{1}H NMR (400 MHz, CD$_3$OD) δ 5.87 (ddd, *J* = 17.3, 10.6, 5.6 Hz,

1H), 5.28 – 5.06 (m, 3H), 3.14 (ddt, *J* = 9.0, 7.0, 5.0 Hz, 4H), 1.43 (s, 9H), 1.28 (d, *J* = 6.5 Hz,

3H); ^{13}C NMR (100 MHz, CD$_3$OD) δ 140.0, 115.5, 72.7, 41.9, 41.5, 29.0, 20.9; MS *m/z* (ES+)

281.15 (M + Na$^+$); HRMS-ES+ (M + Na$^+$) Calc. for C$_{12}$H$_{22}$N$_2$O$_4$Na 281.1477, Found 281.1478.

4.5.28 Preparation of 2-(((but-3-en-2-yloxy)carbonyl)amino)ethan-1-aminium **67**.
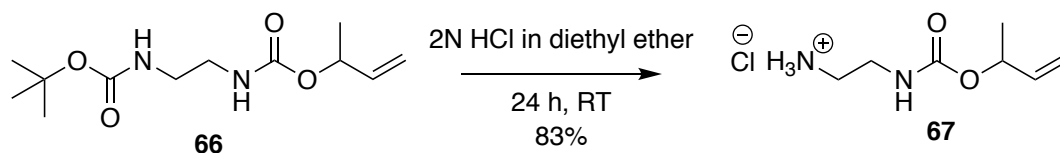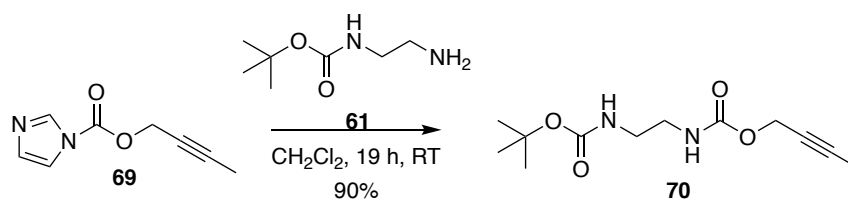

Prepared using an identical method to 4.5.25; IR (thin film)/cm^{-1} υ$_{max}$; 3019, 2933, 1692, 1526,

1258, 1140, 1050, 993, 929, 777; ^{1}H NMR (400 MHz, CD$_3$OD) δ 5.95 – 5.82 (m, 1H), 5.30 – 5.06

(m, 3H), 3.39 (t, *J* = 6.0 Hz, 2H), 3.05 (t, *J* = 6.0 Hz, 2H), 1.30 (d, *J* = 6.5 Hz, 3H); ^{13}C NMR (100

MHz, CD$_3$OD) δ 158.8, 139.5, 115.6, 73.0, 41.0, 39.4, 20.6; MS *m/z* (ES+) 159.11 (M + H$^+$);

HRMS-ES+ (M + H$^+$) Calc. for C$_7$H$_{15}$N$_2$O$_2$ 159.1134, Found 159.1132.

4.5.29 Preparation of But-2-yn-1-yl 1*H*-imidazole-1-carboxylate **69**.
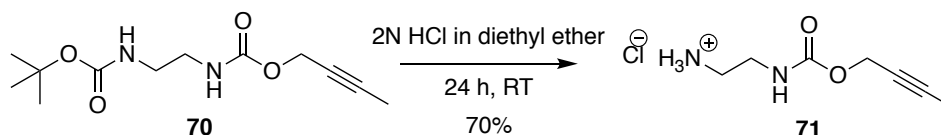

Prepared using an identical method to 4.5.23; ^{1}H NMR (400 MHz, CDCl$_3$) δ 8.09 (t, *J* = 1.0 Hz, 1H), 7.38 (t, *J* = 1.4 Hz, 1H), 7.01 (dd, *J* = 1.7, 0.8 Hz, 1H), 4.89 (q, *J* = 2.4 Hz, 2H), 1.82 (t, *J* = 2.4 Hz, 3H); ^{13}C NMR (100 MHz, CDCl$_3$) δ 148.3, 137.2, 130.7, 117.2, 85.4, 71.6, 56.4, 3.7; MS *m/z* (EI+) 164.1 (M).

4.5.30 Preparation of But-2-yn-1-yl *tert*-butyl ethane-1,2-diyldicarbamate **70**.

Prepared using an identical method to 4.5.24; IR (thin film)/cm^{-1} υ$_{max}$; 3326, 1684, 1524, 1366, 1249, 1162, 995, 780; ^{1}H NMR (300 MHz, CD$_3$OD) δ 4.58 (q, *J* = 2.4 Hz, 2H), 3.21 − 3.07 (m, 4H), 1.81 (t, *J* = 2.4 Hz, 3H), 1.43 (s, 9H); ^{13}C NMR (100 MHz, CD$_3$OD) δ 158.4, 83.1, 80.1, 74.9, 53.8, 41.9, 41.2, 28.7, 3.1; MS *m/z* (ES+) 279.13 (M + Na$^+$); HRMS-ES+ (M + Na$^+$) Calc. for C$_{12}$H$_{20}$N$_2$O$_4$Na 279.1321, Found 279.1322.
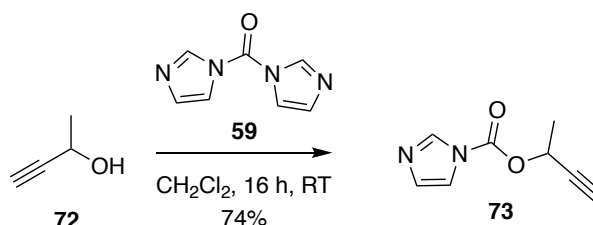
4.5.31 Preparation of 2-(((but-2-yn-1-yloxy)carbonyl)amino)ethan-1-aminium **71**.

Prepared using an identical method to 4.5.25; IR (thin film)/cm^{-1} υ$_{max}$; 2471, 1673, 1203, 1120, 971, 822; ^{1}H NMR (300 MHz, D$_2$O) δ 4.60 (q, *J* = 2.4 Hz, 2H), 3.41 (t, *J* = 5.8 Hz, 2H), 3.09 (t, *J* =

5.8 Hz, 2H), 1.79 (t, J = 2.4 Hz, 3H); MS m/z (ES+) 157.1 (M + H$^+$); HRMS-ES+ (M + H$^+$) Calc. for

$C_7H_{13}N_2O_2$ 157.0977, Found 157.0977.

4.5.32 Preparation of But-3-yn-2-yl 1H-imidazole-1-carboxylate 73.
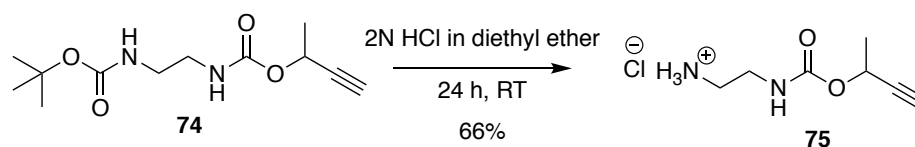

Prepared using an identical method to 4.5.23; IR (thin film)/cm^{-1} υ_{max}; 1746, 1252, 1088, 1062, 1020, 894, 825, 747, 669; ^{1}H NMR (400 MHz, CDCl$_3$) δ 8.15 (t, J = 1.0 Hz, 1H), 7.44 (t, J = 1.4 Hz, 1H), 7.07 (dd, J = 1.4, 1.0 Hz, 1H), 5.63 (qd, J = 6.7, 2.1 Hz, 1H), 2.60 (d, J = 2.1 Hz, 1H), 1.68 (dd, J = 6.7, 0.7 Hz, 3H); ^{13}C NMR (100 MHz, CDCl$_3$) δ 147.8, 137.3, 130.9, 117.3, 80.3, 75.2, 64.8, 21.3; MS m/z (EI+) 164.1 (M), HRMS-EI+ (M) calc. mass for $C_8H_8N_2O_2$ 164.0586, found 164.0587.

## 4.5.33 Preparation of But-3-yn-2-yl $tert$-butyl ethane-1,2-diyldicarbamate 74.
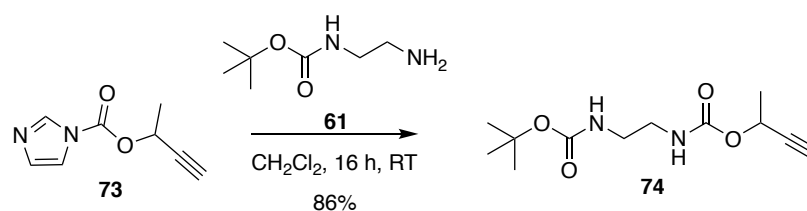
Prepared using an identical method to 4.5.24; IR (thin film)/cm^{-1} υ_{max}; 3327, 2359, 1683, 1542, 1267, 1171, 988, 668; ^{1}H NMR (400 MHz, CD$_3$OD) δ 5.30 (qd, J = 6.7, 2.1 Hz, 1H), 3.25 − 3.06 (m, 4H), 2.86 (d, J = 2.1 Hz, 1H), 1.46 (d, J = 6.7 Hz, 3H), 1.43 (s, 9H); ^{13}C NMR (100 MHz, CD$_3$OD) δ 157.9, 83.6, 80.1, 74.1, 61.6, 41.8, 41.2, 28.7, 22.0; MS m/z (ES+) 279.14 (M + Na$^+$); HRMS-ES+ (M + Na$^+$) Calc. for $C_{12}H_{20}N_2O_4Na$ 279.1321, Found 279.1330.

4.5.34 Preparation of 22-(((but-3-yn-2-yloxy)carbonyl)amino)ethan-1-aminium **75**.

Prepared using an identical method to 4.5.25; IR (thin film)/cm^{-1} υ_{max}; 2923, 1698, 1523, 1253, 1089, 1027, 955, 755; ^{1}H NMR (300 MHz, D$_2$O) δ 5.23 (qd, J = 6.8, 2.0 Hz, 1H), 3.40 (t, J = 5.8 Hz, 2H), 3.08 (t, J = 5.8 Hz, 2H), 2.88 (d, J = 2.0 Hz, 1H), 1.45 (d, J = 6.8 Hz, 3H); ^{13}C NMR (100 MHz, CD$_3$OD) δ 158.0, 83.3, 74.4, 62.0, 41.0, 39.4, 22.0; MS m/z (ES+) 157.1 (M + H$^+$); HRMS-ES+ (M + H$^+$) Calc. for C$_7$H$_{13}$N$_2$O$_2$ 157.0977, Found 157.0978.

4.5.35 Preparation of 1-aminobut-3-en-2-yl (2-(2-chloroacetamido)ethyl)carbamate **80**.
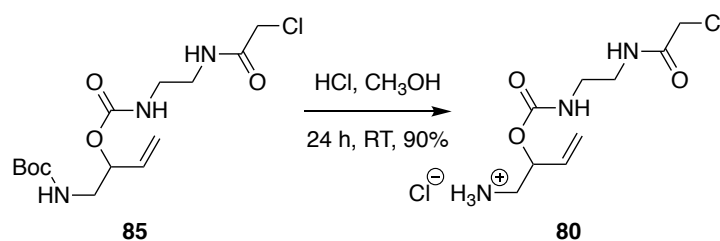
Prepared using an identical method to 4.5.25; IR (thin film)/cm^{-1} υ_{max}; 3396, 2944, 2389, 1651, 1426, 1251, 1163, 994, 771; ^{1}H NMR (300 MHz, CD$_3$OD) δ 5.86 (s, 1H), 5.51 − 5.31 (m, 3H), 4.08 (s, 2H), 3.58 − 3.40 (m, 2H), 3.29 − 3.03 (m, 4H); ^{13}C NMR (100 MHz, CD$_3$OD) δ 170.1, 157.7, 134.1, 119.6, 72.6, 43.8, 43.5, 41.7, 40.6; MS m/z (ES+) 250.31 (M + H$^+$); HRMS-ES+ (M + H$^+$) Calc. for C$_9$H$_{17}$N$_3$O$_3$ 35Cl 250.0958, Found 250.0956.

4.5.36 Preparation 1-aminobut-3-en-2-yl (2-(2-chloroacetamido)ethyl)carbamate **80** by azide reduction by using tin chloride in CH$_3$OH, that was adapted from a known procedure.[233]
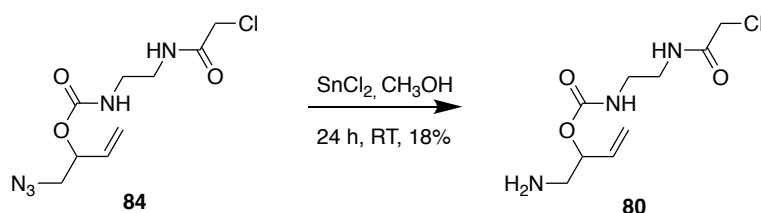
To a suspension of tin (II) chloride (375 mg, 1.98 mmol) in CH$_3$OH (5.0 mL) at room temperature were added 1-azidobut-3-en-2-yl (2-(2-chloroacetamido)ethyl)carbamate **84** (182 mg, 0.66 mmol) and stirred at room temperature until TLC indicated complete consumption of the starting material. After 24 hours, the reaction solvent was concentrated *in vacuo.* The residue was purified twice by silica gel column chromatography (10% CH$_3$OH / CH$_2$Cl$_2$) to offered 1-aminobut-3-en-2-yl (2-(2-chloroacetamido)ethyl)carbamate **80** (29.7 mg, 18%); IR (thin film)/cm^{-1} υ_{max}; 3396, 2944, 2389, 1651, 1426, 1251, 1163, 994, 771; ^{1}H NMR (300 MHz, CD$_3$OD) δ 5.86 (s, 1H), 5.51 – 5.31 (m, 3H), 4.08 (s, 2H), 3.58 – 3.40 (m, 2H), 3.29 – 3.03 (m, 4H); ^{13}C NMR (100 MHz, CD$_3$OD) δ 170.1, 157.7, 134.1, 119.6, 72.6, 43.8, 43.5, 41.7, 40.6; MS *m/z* (ES+) 250.31 (M + H$^+$); HRMS-ES+ (M + H$^+$) Calc. for C$_9$H$_{17}$N$_3$O$_3$ 35Cl 250.0958, Found 250.0956.

4.5.37 Preparation of 1-azidobut-3-en-2-yl 1*H*-imidazole-1-carboxylate **81**.
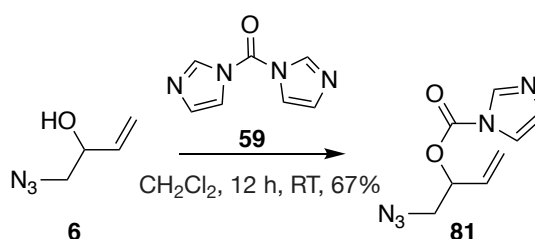
Prepared using an identical method to 4.5.23; IR (thin film)/cm^{-1} υ_{max}; 2098, 1757, 1473, 1389, 1280, 1238, 1172, 1095, 997, 832; ^{1}H NMR (300 MHz, CDCl$_3$) δ 8.16 (t, *J* = 1.1 Hz, 1H), 7.44 (t,

J = 1.5 Hz, 1H), 7.08 (dd, *J* = 1.7, 0.9 Hz, 1H), 5.91 (ddd, *J* = 17.2, 10.5, 6.6 Hz, 1H), 5.61 − 5.42

(m, 3H), 3.65 − 3.50 (m, 2H); ^{13}C NMR (100 MHz, CDCl$_3$) δ 147.5, 136.9, 131.0, 130.7, 120.9,

116.9, 77.4, 53.3; MS *m/z* (EI+) 207.1 (M); HRMS-EI+ (M) calc. mass for C$_8$H$_9$N$_5$O$_2$ 207.0756,

found 207.0757.

4.5.38 Preparation of 1-azidobut-3-en-2-yl *tert*-butyl ethane-1,2-diyldicarbamate **82**.
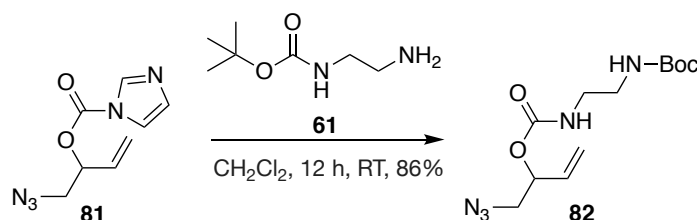

Prepared using an identical method to 4.5.24; IR (thin film)/cm^{-1} υ$_{max}$; 3340, 2098, 1690, 1517,

1365, 1250, 1165, 987; ^{1}H NMR (400 MHz, CDCl$_3$) δ 5.92-5.73 (m, 1H), 5.45 − 5.24 (m, 4H),

4.93 (s, 1H), 3.37 (t, *J* = 4.8 Hz, 2H), 3.27 (ddd, *J* = 13.3, 8.1, 3.7 Hz, 4H), 1.42 (s, 9H); ^{13}C NMR

(100 MHz, CDCl$_3$) δ 156.9, 155.4, 133.2, 118.3, 79.4, 73.6, 53.7, 41.4, 40.3, 28.2; MS *m/z* (ES+)

322.15 (M + Na$^+$); HRMS-ES+ (M + Na$^+$) Calc. for C$_{12}$H$_{21}$N$_5$O$_4$Na 322.1491, Found 322.1489.

4.5.39 Preparation of 2-((((1-azidobut-3-en-2-yl)oxy)carbonyl)amino)ethan-1-aminium **83**.
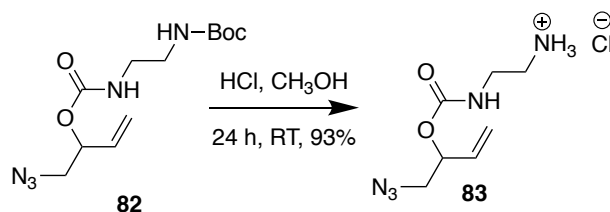

Prepared using an identical method to 4.5.25; IR (thin film)/cm^{-1} υ$_{max}$; 3015, 2942, 2328, 2108,

1710, 1534, 1442,1260, 1155; ^{1}H NMR (300 MHz, CD$_3$OD) δ 5.98 − 5.79 (m, 1H), 5.38 (dt, *J* =

17.2, 1.4 Hz, 1H), 5.34 − 5.21 (m, 2H), 3.60 − 3.35 (m, 4H), 3.07 (t, *J* = 6.1 Hz, 2H); ^{13}C NMR

(100 MHz, CD$_3$OD) δ 156.9, 133.6, 117.1, 74.0, 53.5, 39.5, 38.1; MS *m/z* (ES+) 200.1 (M + H$^+$);

HRMS-ES+ (M + H$^+$) Calc. for C$_7$H$_{14}$N$_5$O$_2$ 200.1147, Found 200.1146.

4.5.40 Preparation of 1-azidobut-3-en-2-yl (2-(2-chloroacetamido)ethyl)carbamate **84**, that was adapted from a known procedure.[262]
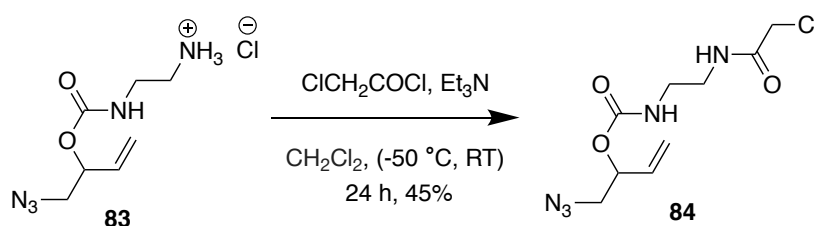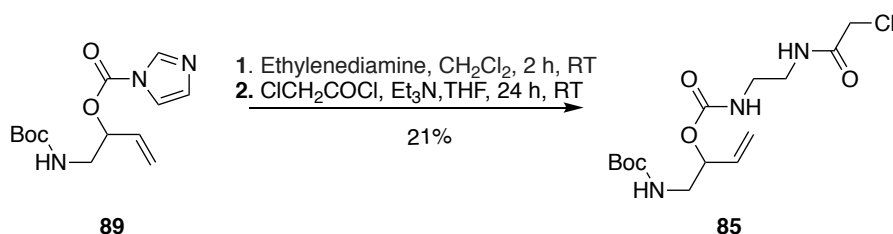

To a solution of a 2-(((((1-azidobut-3-en-2-yl)oxy)carbonyl)amino)ethan-1-aminium **83** (1.43 g, 6.08 mmol) in anhydrous CH_2Cl_2 at -50 °C under argon was added triethylamine (4.20 ml, 30.0 mmol) then chloroacetyl chloride (1.50 ml, 18.0 mmol) dropwise and the reaction mixture stirred under argon for 2 hours at -50 °C. The reaction mixture was then allowed to warm to ambient temperature and stirred until TLC indicated complete consumption of the starting material. Then the reaction mixture was diluted with brine and extracted with CH_2Cl_2. The combined organic layers were dried over Na_2SO_4, filtered and concentrated *in vacuo*, then the residue was purified by silica gel column chromatography (100% CH_2Cl_2) to afford the 1-azidobut-3-en-2-yl (2-(2-chloroacetamido)ethyl)carbamate **84** (757 mg, 45%); IR (thin film)/cm^{-1} υ_{max}; 3362, 2943, 2415, 2101, 1652, 1424, 1252, 1160, 972; ^{1}H NMR (300 MHz, CDCl$_3$) δ 7.19 (t, J = 5.8 Hz, 1H), 5.77 (ddd, J = 16.9, 10.6, 6.0 Hz, 1H), 5.63 (t, J = 5.8 Hz, 1H), 5.50 – 4.98 (m, 3H), 3.99 (s, 2H), 3.41 (dt, J = 6.0, 3.4 Hz, 2H), 3.34 (td, J = 4.9, 4.4, 2.0 Hz, 4H); ^{13}C NMR (100 MHz, CDCl$_3$) δ 167.1, 156.0, 133.3, 118.8, 74.3, 53.9, 42.6, 40.7, 40.5; MS *m/z* (ES+) 298.1 (M + Na$^+$), HRMS-ES+ (M + Na $^+$) Calc. for $C_9H_{14}N_5O_3$ NaCl 289.0683, Found 289.0685.

4.5.41   Preparation   of   1-((*tert*-butoxycarbonyl)amino)but-3-en-2-yl   (2-(2-chloroacetamido)ethyl)carbamate **85**, that was adapted from a known procedure.[234]
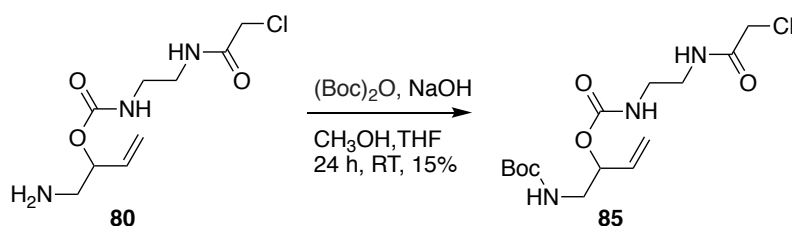
A suspension of NaOH (0.34 g, 8.50 mmol) in CH_3OH (20 mL) was heated to reflux to allow dissolution. This solution was cooled to room temperature and the 1-aminobut-3-en-2-yl (2-(2-chloroacetamido)ethyl)carbamate **80** (0.41 g, 4.71 mmol) was added under argon and stirred for 30 min. Then a solution of di-*tert*-butylcarbonate (2.1 g, 9.43 mmol) in anhydrous THF (20 mL) was added dropwise at room temperature. Stirred at room temperature until TLC indicated complete consumption of the starting material. After 24 hours, the reaction was concentrated *in vacuo* to offer a white solid residue. The residue was purified by silica gel column chromatography (50% ethyl acetate / hexane) to provide the 1-((*tert*-butoxycarbonyl)amino)but-3-en-2-yl (2-(2-chloroacetamido)ethyl)carbamate **85** (0.25 g, 15%); IR (thin film)/cm^{-1} υ_{max}; 3317, 2928, 2495, 1675, 1540, 1426, 1248, 1163, 954; ^{1}H NMR (300 MHz, CDCl$_3$) δ 7.17 (s, 1H), 6.11 – 5.89 (m, 1H), 5.77 (ddd, *J* = 16.9, 10.6, 5.9 Hz, 1H), 5.45 – 5.11 (m, 3H), 4.87 (s, 1H), 4.04 (d, *J* = 3.3 Hz, 2H), 3.55 – 3.09 (m, 6H), 1.42 (s, 9H); ^{13}C NMR (100 MHz, CDCl$_3$) δ 166.9, 156.2, 133.8, 117.7, 79.4, 74.2, 43.5, 42.3, 42.3, 40.4, 40.3, 28.2; MS *m/z* (ES+) 372.13 (M + Na$^+$); HRMS-ES+ (M + Na $^+$) Calc. for $C_{14}H_{24}N_3O_5$ NaCl 372.1302, Found 372.1308.

4.5.42 Preparation of 1-((*tert*-butoxycarbonyl)amino)but-3-en-2-yl (2-(2-chloroacetamido)ethyl)carbamate **85**.

To a solution of 1-((*tert*-butoxycarbonyl)amino)but-3-en-2-yl 1*H*-imidazole-1-carboxylate **89** (116 mg, 0.40 mmol) in anhydrous CH_2Cl_2 at 0 °C were added ethylenediamine (EDA) (0.54 mL, 8.10 mmol) dropwise under argon. The reaction mixture was stirred at 0 °C until TLC indicated complete consumption of the imidazole carboxylate after 2 hours. Then the reaction mixture was concentrated *in vacuo*. And characterised by ^{1}HNMR to confirm the complete consumption of the imidazole carboxylate. This crude product was dissolved with dry CH_2Cl_2 and cooled to −70 °C under argon. Triethylamine (0.29 mL, 2.80 mmol) was added followed by chloroacetyl chloride (0.75 mL, 9.40 mmol) dropwise and the reaction mixture stirred under argon for 2 hours at − 70 °C, then allowed to warm to room temperature and stirred until TLC indicated complete consumption of the starting material. The reaction mixture was diluted with brine and extracted with CH_2Cl_2. The combined organic layers were dried over Na_2SO_4, filtered and concentrated *in vacuo.* The residue was purified by silica gel column chromatography (50% EtOAc / hexane) to afford 1-((*tert*-butoxycarbonyl)amino)but-3-en-2-yl (2-(2-chloroacetamido)ethyl)carbamate **85** (47.6 mg, 21% yield); IR (thin film)/cm^{-1} υ_{max}; 3317, 2928, 2495, 1675, 1540, 1426, 1248, 1163, 954; ^{1}H NMR (300 MHz, CDCl$_3$) δ 7.17 (s, 1H), 6.11 − 5.89 (m, 1H), 5.77 (ddd, *J* = 16.9, 10.6, 5.9 Hz, 1H), 5.45 − 5.11 (m, 3H), 4.87 (s, 1H), 4.04 (d, *J* = 3.3 Hz, 2H), 3.55 − 3.09 (m, 6H), 1.42 (s, 9H); ^{13}C NMR (100 MHz, CDCl$_3$) δ 166.9, 156.2, 133.8, 117.7, 79.4, 74.2, 43.5, 42.3, 42.3, 40.4, 40.3, 28.2; MS *m/z* (ES+) 372.13

(M + Na⁺); HRMS-ES+ (M + Na⁺) Calc. for $C_{14}H_{24}N_3O_5$ NaCl 372.1302, Found 372.1308.

4.5.43 Preparation of 1-aminobut-3-en-2-ol 87, that was adapted from a known procedure.[240]
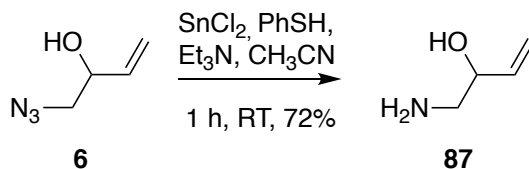
To a suspension of tin chloride (247 mg, 1.40 mmol) in acetonitrile at room temperature was added thiophenol (0.61 ml, 5.76 mmol) followed by triethylamine (0.60 ml, 4.32 mmol). A solution of 1-azidobut-3-en-2-ol **6** (109 mg, 0.96 mmol) in acetonitrile was added slowly at room temperature and the reaction mixture stirred at room temperature until TLC indicated complete consumption of the starting material (~1 h). The reaction solvent was concentrated *in vacuo*, then the residue was purified by silica gel column chromatography (90:10:1, CH_2Cl_2 / CH_3OH / NH_3 solution) to afford the 1-aminobut-3-en-2-ol **87** (60.2 mg, 72%) ; IR (thin film)/cm⁻¹ υ_{max}; 3383, 2930, 1650, 1388, 1254, 1099, 1009; ¹H NMR (400 MHz, CD₃OD) δ 5.89 (ddd, *J* = 17.2, 10.5, 5.4 Hz, 1H), 5.43 (dt, *J* = 17.2, 1.5 Hz, 1H), 5.26 (dt, *J* = 10.5, 1.5 Hz, 1H), 4.37 (dtd, *J* = 8.9, 3.7, 1.5 Hz, 1H), 3.07 (dd, *J* = 12.7, 3.7 Hz, 1H), 2.85 (dd, *J* = 12.7, 8.9 Hz, 1H); ¹³C NMR (100 MHz, CD₃OD) δ 138.3, 117.6, 69.5, 45.5.

4.5.44 Preparation of *tert*-butyl (2-hydroxybut-3-en-1-yl)carbamate 88.
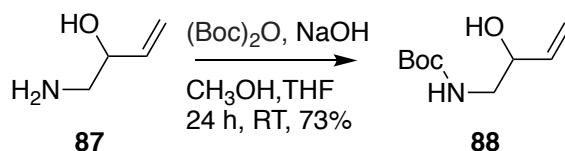
Prepared using an identical method to 4.5.41; IR (thin film)/cm⁻¹ υ_{max}; 3353, 2977, 1686, 1514, 1366, 1250, 1168, 991, 925; ¹H NMR (300 MHz, CD₃OD) δ 5.84 (ddd, *J* = 17.2, 10.5, 5.9 Hz, 1H), 5.28 (dt, *J* = 17.2, 1.6 Hz, 1H), 5.14 (dt, *J* = 10.5, 1.6 Hz, 1H), 4.10 (dtt, *J* = 6.9, 5.9, 1.6 Hz, 1H),

3.20 – 2.98 (m, 2H), 1.43 (s, 9H); ^{13}C NMR (100 MHz, CD$_3$OD) δ 157.2, 138.6, 114.7, 78.7, 71.4, 45.7, 27.3. Data agrees with literature values.[263]

## 4.5.45 Preparation of 1-((*tert*-butoxycarbonyl)amino)but-3-en-2-yl 1*H*-imidazole-1-carboxylate **89**.
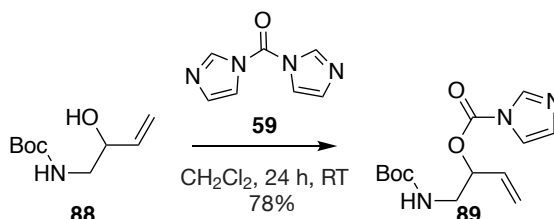
Prepared using an identical method to 4.5.23; IR (thin film)/cm^{-1} υ_{max}; 1762, 1691, 1529, 1477, 1389, 1281, 1240, 1166, 1061, 1001, 930, 824, 745, 661; ^{1}H NMR (300 MHz, CDCl$_3$) δ 8.15 (t, *J* = 1.1 Hz, 1H), 7.44 (t, *J* = 1.5 Hz, 1H), 7.06 (dd, *J* = 1.7, 0.9 Hz, 1H), 5.86 (ddd, *J* = 17.1, 10.6, 6.4 Hz, 1H), 5.52 – 5.35 (m, 3H), 5.13 (s, 1H), 3.62 – 3.35 (m, 2H), 1.40 (s, 9H); ^{13}C NMR (100 MHz, CDCl$_3$) δ 137.3, 135.2, 132.1, 130.6, 122.0, 120.4, 117.3, 80.2, 78.5, 43.5, 28.4; MS *m/z* (EI+) 281.15 (M); HRMS-EI+ (M) calc. mass for C$_{13}$H$_{19}$N$_3$O$_4$ 281.1376, found 281.1374.

## 4.5.46 Preparation of 1-aminobut-3-en-2-yl *tert*-butyl ethane-1,2-diyldicarbamate **92**.
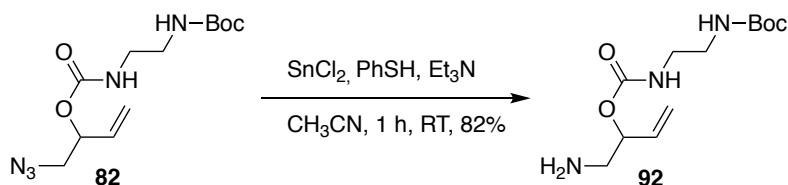
Prepared using an identical method to 4.5.43; IR (thin film)/cm^{-1} υ_{max}; 3000, 2700, 2350, 1500, 1450, 1050; ^{1}H NMR (300 MHz, CD$_3$OD) δ 5.87 (ddd, *J* = 17.2, 10.7, 5.4 Hz, 1H), 5.51 – 5.29 (m, 3H), 3.28 – 3.00 (m, 6H), 1.43 (s, 9H); ^{13}C NMR (100 MHz, CD$_3$OD) δ 158.5, 136.3, 117.5, 80.1, 77.3, 46.0, 41.8, 28.8; MS *m/z* (ES+) 374.18 (M + H$^+$); HRMS-ES+ (M + H$^+$) Calc. for C$_{12}$H$_{24}$N$_3$O$_4$ 374.1767, Found 374.1768.

4.5.47 Preparation of 1-azidobut-3-en-2-yl (2-hydroxyethyl)carbamate **97**.
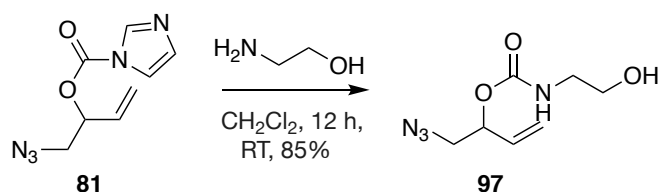
Prepared using an identical method to 4.5.24; IR (thin film)/cm^{-1} υ_{max}; 2101, 1703, 1529, 1256, 1145, 1069, 933; ^{1}H NMR (300 MHz, CDCl$_3$) δ 5.83 (ddd, J = 16.8, 10.6, 6.1 Hz, 1H), 5.44 – 5.15 (m, 4H), 3.74 (d, J = 4.9 Hz, 2H), 3.46 – 3.30 (m, 4H); ^{13}C NMR (100 MHz, CD$_3$OD) δ 156.1, 133.4, 118.8, 74.2, 62.2, 54.0, 43.6; MS *m/z* (ES+) 223.08 (M + Na$^+$); HRMS-ES+ (M + Na$^+$) Calc. for C$_7$H$_{12}$N$_4$O$_3$ 23Na 223.0807, Found 223.0808.

4.5.48 Preparation of 1-aminobut-3-en-2-yl (2-hydroxyethyl)carbamate **98**.
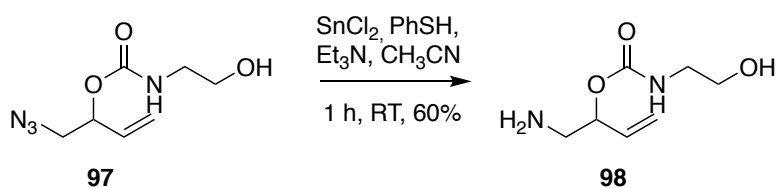
Prepared using an identical method to 4.5.43; IR (thin film)/cm^{-1} υ_{max}; 3338, 2943, 2831, 1646, 1549, 1409, 1254, 1020; ^{1}H NMR (400 MHz, CDCl$_3$) δ 5.79 (ddd, J = 16.9, 10.6, 5.8 Hz, 1H), 5.40 – 5.21 (m, 3H), 5.15 (d, J = 5.7 Hz, 1H), 3.72 (dt, J = 5.5, 3.6 Hz, 2H), 3.46 – 3.19 (m, 2H), 2.88 (qd, J = 13.6, 5.8 Hz, 2H); ^{13}C NMR (100 MHz, CDCl$_3$) δ 135.1, 118.1, 76.9, 62.5, 45.8, 44.0; MS *m/z* (ES+) 197.18 (M + Na$^+$); HRMS-ES+ (M + H $^+$) Calc. for C$_7$H$_{15}$N$_2$O$_3$ 175.1083, Found 175.1080.

4.5.49 Preparation of *tert*-butyl (2-(2-chloroacetamido)ethyl)carbamate **104**.
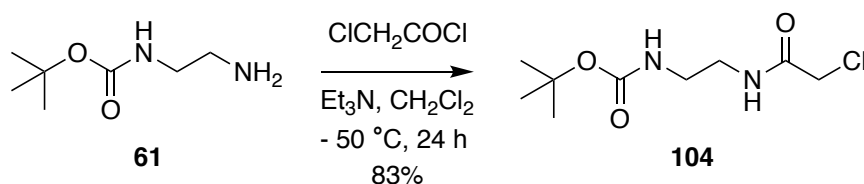
Prepared using an identical method to 4.5.40; ^{1}H NMR (400 MHz, CD$_3$OD) δ 4.07 (s, 2H), 3.34 (t, *J* = 6.1 Hz, 2H), 3.20 (t, *J* = 6.1 Hz, 2H), 1.46 (s, 9H); ^{13}C NMR (100 MHz, CD$_3$OD) δ 169.6, 158.6, 80.2, 43.1, 41.1, 40.5, 28.7; MS *m/z* (ES+) 259.0 (M + Na$^+$).

4.5.50 Preparation of *tert*-butyl (2-(2-iodoacetamido)ethyl)carbamate **105**.
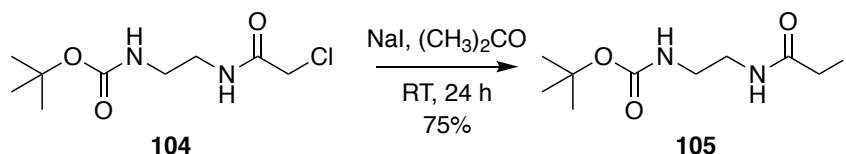
Prepared using an identical method to 4.5.12; IR (thin film)/cm^{-1} υ_{max}; 3347, 3308, 2933, 1678, 1650, 1528, 1283, 1164, 980, 867, 647; ^{1}H NMR (400 MHz, D$_2$O) δ 3.76 (s, 2H), 3.30 (t, *J* = 5.7 Hz, 2H), 3.22 (t, *J* = 5.7 Hz, 2H), 1.43 (s, 9H); ^{13}C NMR (100 MHz, CD$_3$OD) δ 171.6, 158.5, 80.2, 41.0, 40.5, 28.8, -2.2; MS *m/z* (ES+) 351.02 (M + Na$^+$), HRMS C$_9$H$_{17}$N$_2$O$_3$NaI requires M, 351.0182, Found (M) 351.0181.

## 4.6 Allyl carbamate cleavage using catalytic Pd in the solution phase

All stock solutions were prepared just before use. The Pd-o-DANPHOS complex (1:8 Pd:o-DANPHOS solution) was prepared by addition of a solution of Na$_2$PdCl$_4$ in D$_2$O to a solution of o-DANPHOS dihydrate (8.0 equiv.) in D$_2$O and mixed for 30 minutes. The stock solution of dimethyl barbituric acid in D$_2$O was prepared. To the allyl carbamates in D$_2$O in NMR tubes were added the solution of Pd-o-DANOHOSE complex in D$_2$O (0.1 − 1.0 equiv.) and the solution of the dimethyl barbituric acid in D$_2$O (1.0 equiv.). The reaction mixtures were stirred

at room temperature for 24 hours. The crude products were characterised by ^{1}H NMR and MS.

4.7 Immobilisation onto agarose and release

4.7.1- General procedure for immobilisation onto aldehyde- modified agarose

A. **Preparation of the solid alkyne 4 (reductive amination of the aldehyde modified agarose 2):**
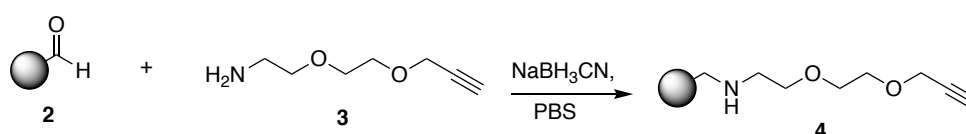
2-(2-(prop-2-yn-1-yloxy)ethoxy)ethan-1-amine **3** (0.90 mL, 6.30 mmol), aldehyde modified agarose **2** (15.0 mL, 0.60 mmol) and sodium cyanoborohydride (0.40 g, 6.30 mmol) were put in 5 mL of PBS (pH 7.4), then the mixture was rotated at room temperature for 24 hours. The reaction mixture was filtered and washed with 3 mL water then the filtrate was dried to afford the solid alkyne **4** as a white solid (4.90 g).

B. **General procedure of the copper catalysed azide-alkyne cycloaddition reaction (CuAAC) between rhodamine azide 34 and the solid-phase alkyne 4, that was adapted from a known procedure.**[173]
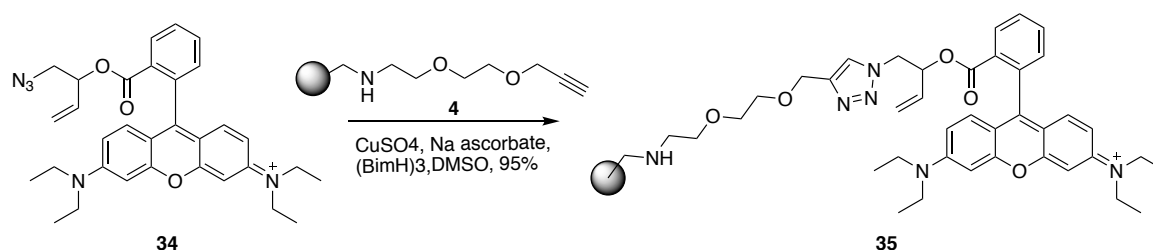
The stock solutions of the rhodamine azide **34** in DMSO were prepared just before use, this stock solution was used to make a calibration curve of the rhodamine azide **34** and to react

with the solid alkyne **4**. To the solution of the solid alkyne **4** (1 equiv.) in DMSO (1 mL) in the SPE Tube with a filter at the bottom, were added a solution of rhodamine azide **34** (0.25, 1 and 4 equiv.), copper sulfate (10 equiv.), tris(2-benzimidazolylmethyl)amine (5 equiv.) and sodium ascorbate (60 equiv.). Then the SPE tube was closed and reaction mixtures rotated at room temperature for 24 hours. The unreacted rhodamine azide **34** was washed by DMSO and analysed by UV-spectrometer to measure the rhodamine azide **34** absorption at 566 nm, and the washing step repeated until no more rhodamine azide **34** elution was observed.
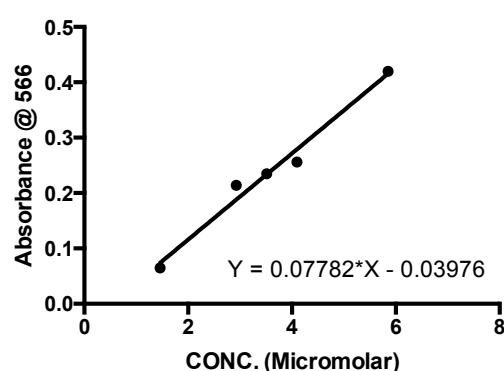

Figure 74: Calibration curve of Rhodamine Azide **34** at (λ_{max} = 566 nm).

	4.0 equiv.	1.0 equiv.	0.25 equiv.
Aldehyde modified agarose	1.2 µmole	1.2 µmole	4.8 µmole
Rhodamine azide 34	4.4 µmole	1.2 µmole	1.2 µmole
Abs. of the unreacted Rhodamine azide 34	0.501	0.617	0.271
Conc. of the unreacted Rhodamine azide 34	6.95 µM	8.44 µM	3.99 µM
Total wash volume	0.035 L	0.016 L	0.008 L
Dilution factor	10	2	2
Total unreacted Rhodamine azide 34	2.43 µmole	0.27 µmole	0.06 µmole
Total reacted Rhodamine azide 34	1.97 µmole	0.93 µmole	0.56 µmole
Observed loading yield	164 %	77 %	47 %

Table 26: The calculation of the loading efficiency and the CuAAC reaction efficiency after CuAAC reaction between Rhodamine azide **34** and solid-phase alkyne **4** based on the absorbance of the unreacted Rhodamine azide **34** at 566 using standard curve of Rhodamine azide **34** in the figure 74.
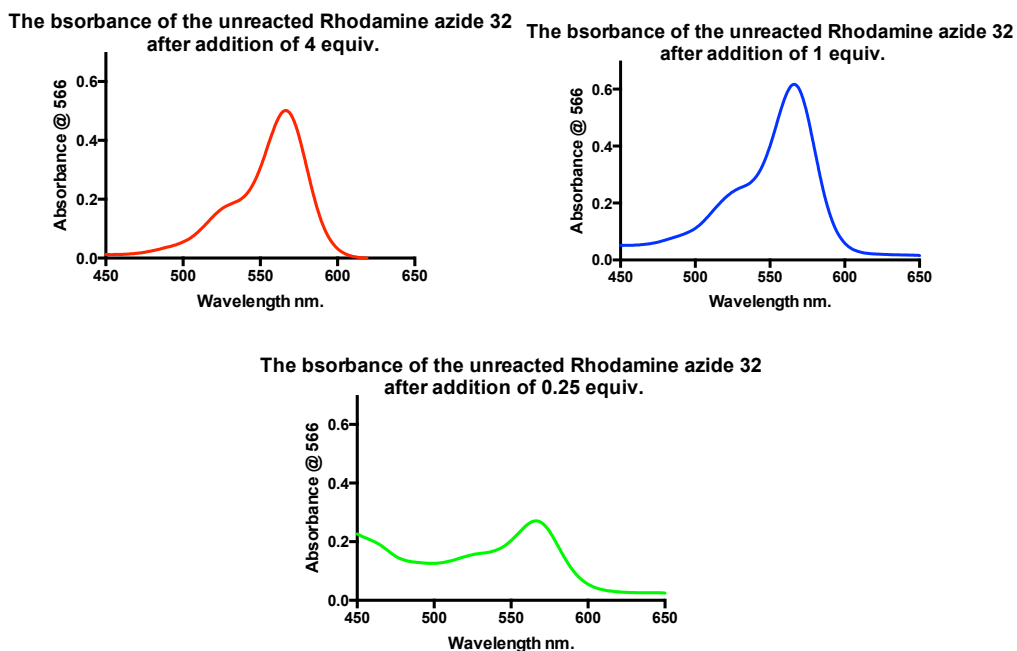
The bsorbance of the unreacted Rhodamine azide 32 after addition of 4 equiv.

The bsorbance of the unreacted Rhodamine azide 32 after addition of 1 equiv.

The bsorbance of the unreacted Rhodamine azide 32 after addition of 0.25 equiv.

Figure 75: Absorbance of the unreacted Rhodamine azide **34** at 566 after CuAAC reaction

between Rhodamine azide **34** and solid alkyne **4**.

C. Deprotection of allyl ester in the solid model system 35 by using one equiv. Pd to afford

rhodamine B.

Tetrakis(triphenylphosphine)Pd(0) (2.60 mg, 2.2 μmol) was added to the solid model system

35 (1.2 μmol) in CH_3OH (0.5 mL). After 24 h of rotation at room temperature, the reaction

mixture was filtered by washing with CH_3OH until the filter paper colour changed from purple

colour to white to make sure all rhodamine B has been recovered. The rhodamine B

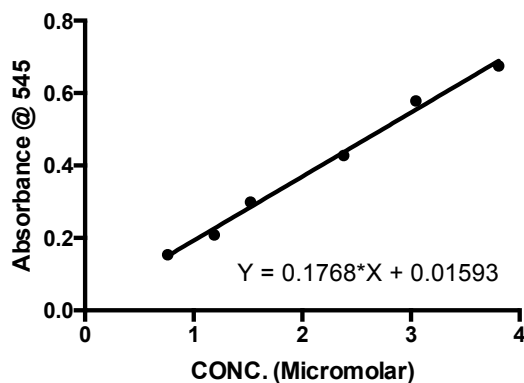absorbance was measured by UV-spectrometry to determine concentration (C).

Figure 76: Calibration curve of Rhodamine B at (λ_{max} = 545 nm).

Absorbance of the cleaved Rhodamine B	0.706
Concentration of the cleaved Rhodamine B	3.90 µM
Total wash volume	0.001 L
Total cleaved Rhodamine B	0.004 µmole
Loaded Rhodamine azide 34	0.930 µmole
Cleavage yield	0.4%

Table 27: The calculation of the cleavage efficiency of the allyl ester in the model system **35** based on the absorbance of the Rhodamine B at 545 using standard curve of Rhodamine B in the figure 76.
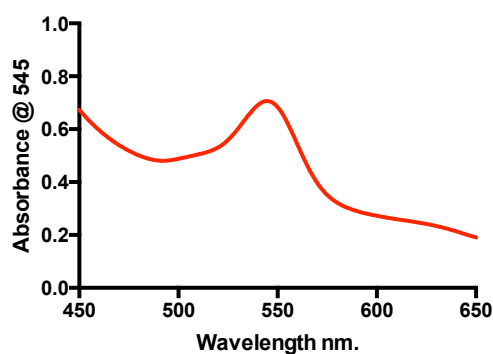

Figure 77: UV scan of rhodamine B recovered from cleavage of the model system **35** by 1 equiv. Pd.

4.7.2 Immobilisation into NHS-agarose

A- General procedure for immobilisation into NHS-agarose

The NHS-activated agarose gel supplied in 100% isopropanol was pipetted into an SPE tube with a filter at the bottom, then washed with cold 1 mM HCl (10 medium volumes) followed by washing with PBS immediate before use. The stock solution of the ligand (primary amine molecule) in PBS was prepared and added to the washed NHS-activated agarose (the ratio of the between the NHS-activated agarose gel and coupling solution is 1.0:0.5), then 5 equiv. TEA added to the reaction mixture. The SPE tube was closed and the reaction mixtures were rotated at room temperature for 24 hours. Then the unreacted ligands were washed by PBS and analysed by using fluorescamine assay, and the washing step repeated until no more amine eluted from the solid phase.

A.1 The coupling reaction between ethanolamine (ETA) and NHS-agarose
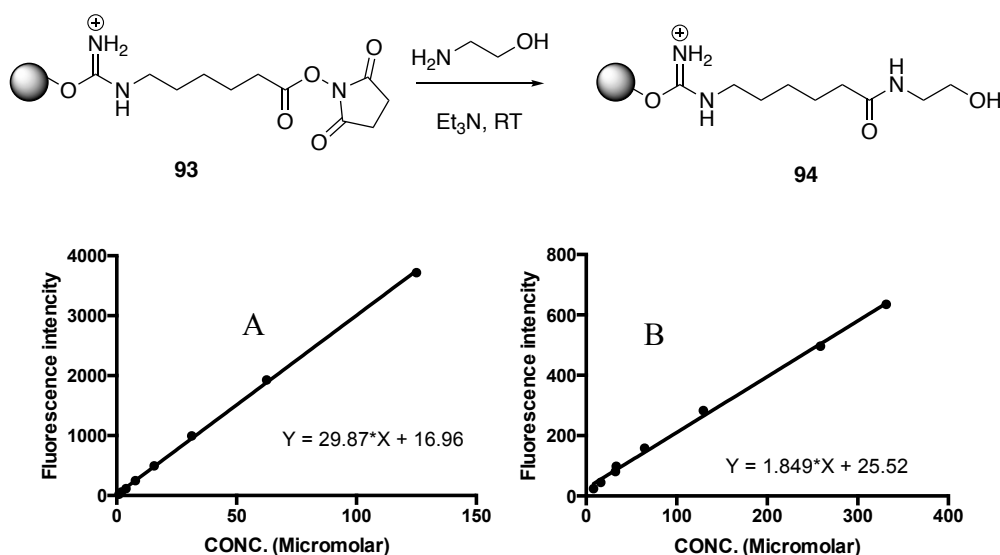

Figure 78: Calibration curve of ethanolamine using fluorescamine assay, for different ethanolamine stock solutions.

WASHES	FI	CONC. µM	Wash Volume L	Unreacted ETA µmole
1st washX100	1464	48.4	0.001	4.84
2nd wash X10	1212	40.0	0.001	0.40
3rd wash	901	29.6	0.001	0.03
4th wash	29	0.403	0.001	0.00
Washed ETA				5.27
Added ETA				8.4
Reacted ETA				3.13
NHS-agarose				4.4
Coupling %				71

Table 28: The calculation of the coupling % after reaction of 2 equiv. ethanolamine with NHS-agarose by using standard curve in figure 78A.
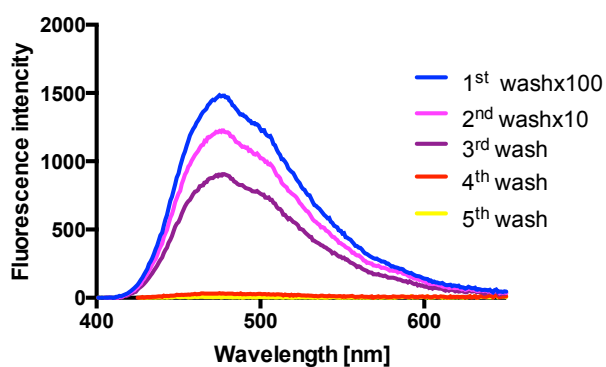

Figure 79: The fluorescence of the unreacted ethanolamine after reaction of 2 equiv.

ethanolamine with NHS-agarose.

WASHES	FI	CONC. μM	Wash Volume L	Unreacted ETA μmole
1st washX100	147	65.7	0.0001268	0.833
2nd wash X100	151	67.9	0.0001	0.679
3rd wash X10	624	324	0.0001	0.324
4th wash X2	481	246	0.001	0.493
5th wash	244	118	0.001	0.118
6th wash	59	18.1	0.001	0.018
7th wash	26	0.259	0.001	0.000
Washed ETA				2.47
Added ETA				4.2
Reacted ETA				1.74
NHS-agarose				4.2
Coupling %				41

Table 29: The calculation of the coupling % after reaction of 1 equiv. ethanolamine with
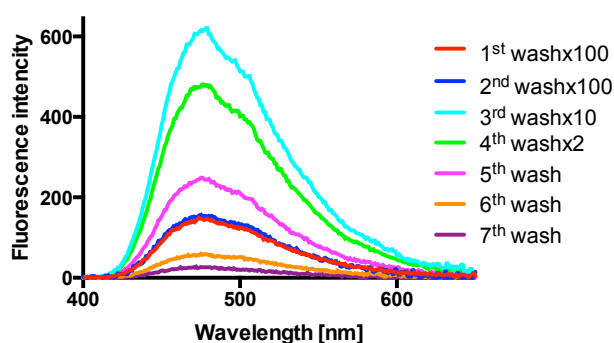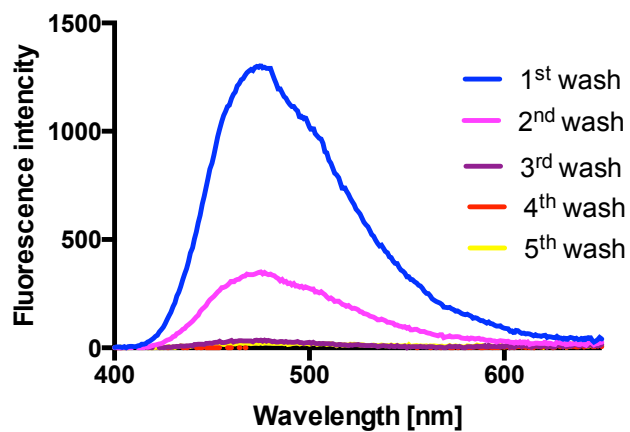
NHS-agarose by using standard curve in figure 78B.

Figure 80: The fluorescence of the unreacted ethanolamine after reaction of 1 equiv.

ethanolamine with NHS-agarose.

WASHES	FI	CONC. µM	Wash Volume L	Unreacted ETA µmole
1st wash	1291	42.7	0.001	0.043
2nd wash	338	10.7	0.001	0.011
3rd wash	34	0.571	0.001	0.001
Washed ETA				0.054
Added ETA				2.1
Reacted ETA				2.05
NHS-agarose				4.4
Coupling %				97

Table 30: The calculation of the coupling % after reaction of 0.5 equiv. ethanolamine with

NHS-agarose by using standard curve in figure 78A.

Figure 81: The fluorescence of the unreacted ethanolamine after reaction of 0.5 equiv.

ethanolamine with NHS-agarose.

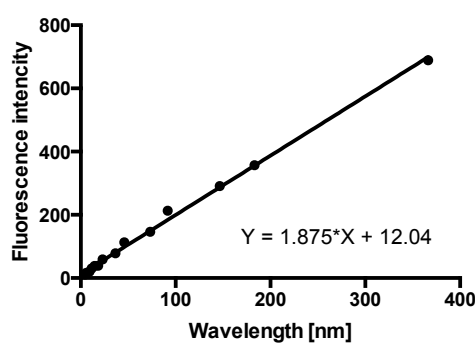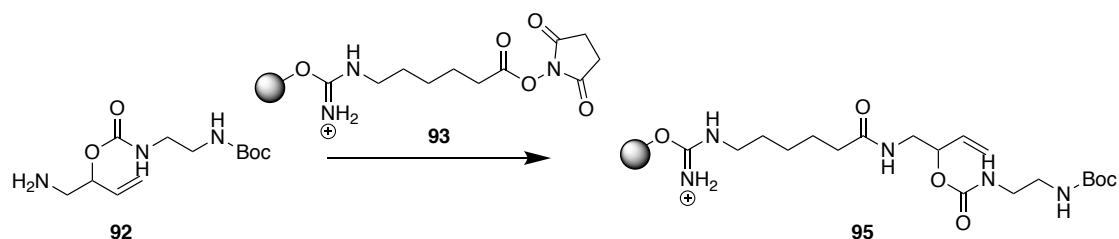**A.2 The coupling reaction between amine 92 and NHS-agarose 93:**

Figure 82: Calibration curve of the amine **92** using fluorescamine assay.

WASHES	FI	CONC. μM	Wash Volume L	Unreacted ETA μmole
1st washX4	570	298	0.0027306	3.25
2nd wash X2	447	232	0.001	0.464
3rd wash X2	130	62.9	0.001	0.126
4th wash X2	41	15.4	0.001	0.031
5th wash X2	26	7.45	0.001	0.015
6th wash X2	13	0.515	0.001	0.001
Washed amine				3.89
Added amine				8
Reacted amine				4.11
NHS-agarose				4
Coupling %				102

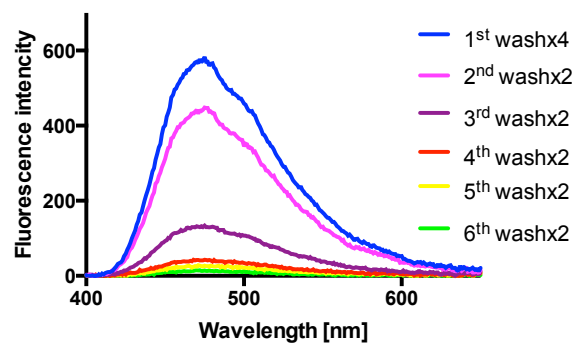Table 31: The calculation of the coupling of amine **92** with NHS-agarose by using standard curve in figure 82.

Figure 83: The fluorescence of the unreacted amine **92**.

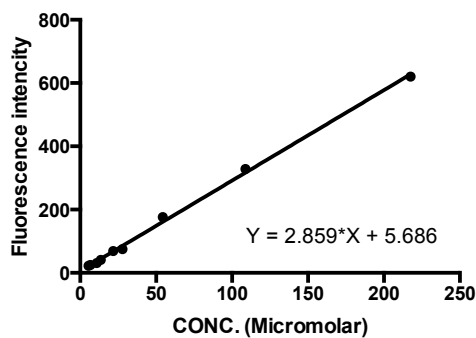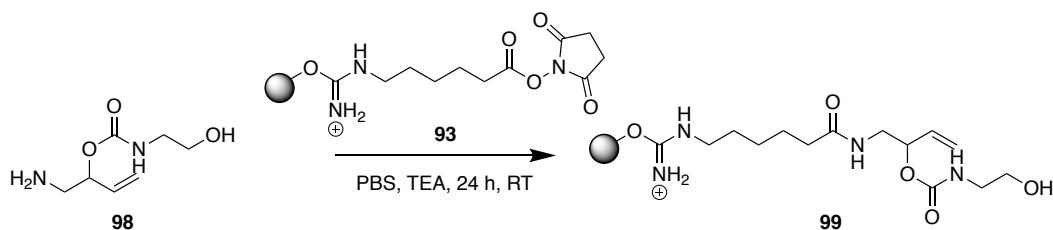## A.3 The coupling reaction between amine 98 and NHS-agarose 93:

Figure 84: Calibration curve of the amine **98** using fluorescamine assay.

WASHES	FI	CONC. μM	Wash Volume L	Unreacted amine μmole
1st washX2	549	190	0.0056	2.13
2nd wash	266	91.0	0.001	0.091
3rd wash	22	5.71	0.001	0.006
Washed amine **90**				2.23
added amine **90**				5.75
reacted amine **90**				3.53
NHS-agarose				23
Coupling %				61

Table 32: The calculation of the coupling of amine **98** with NHS-agarose by using standard
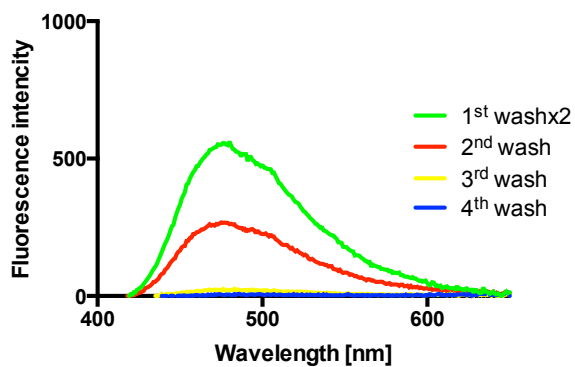
curve in figure 84.

Figure 85: The fluorescence of the unreacted amine **98**.

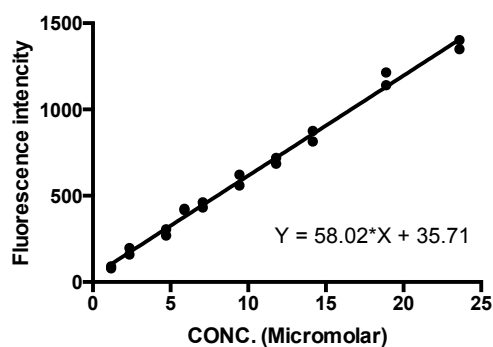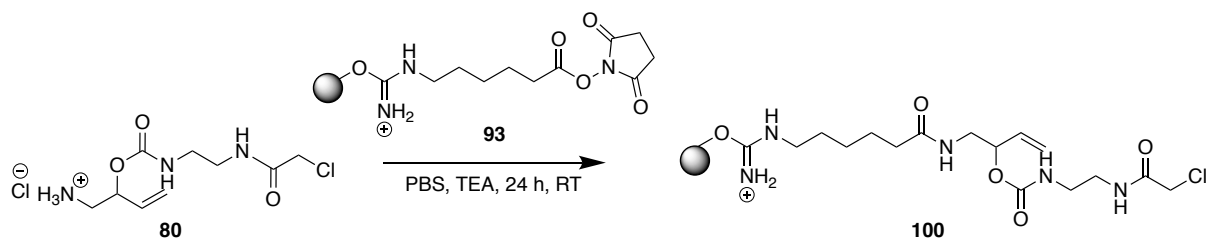**A.4 The coupling reaction between the alkylation linker 80 and NHS-agarose 93:**

Figure 86: Calibration curve of the alkylation linker **80** using fluorescamine assay.

WASHES	FI	CONC. µM	Wash Volume L	Unreacted amine µmole	Average unreacted amine µmole
1st washX100	376	5.87	0.003	1.76	1.84
1st washX100	407	6.40	0.003	1.92	
2nd wash	1188	19.9	0.003	0.06	0.058
2nd wash	1144	19.1	0.003	0.06	
3rd wash	426	6.73	0.003	0.02	0.020
3rd wash	434	6.87	0.003	0.02	
4th wash	184	2.56	0.003	0.008	0.007
4th wash	155	2.06	0.003	0.006	
Washed amine **73**					1.93
added amine **73**					8.5
reacted amine **73**					6.57
NHS-agarose					21
Coupling %					77

Table 33: The calculation of the coupling of amine **80** with NHS-agarose by using standard
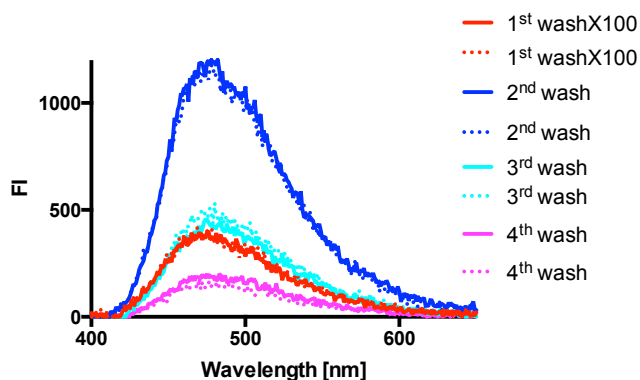
curve in figure 86.

Figure 87: The fluorescence of the unreacted amine **80**.

B- General procedure for NHS-agarose ester 93 quenching

After coupling completed and washing the unreacted ligand, 1M ethanolamine in PBS was added to the unreacted NHS-agarose ester. After 24 hours, the unreacted ethanolamine was washed with PBS,with the washing step repeated 10 times to ensure all ethanolamine has been removed.

C- General procedure for BSA alkylation
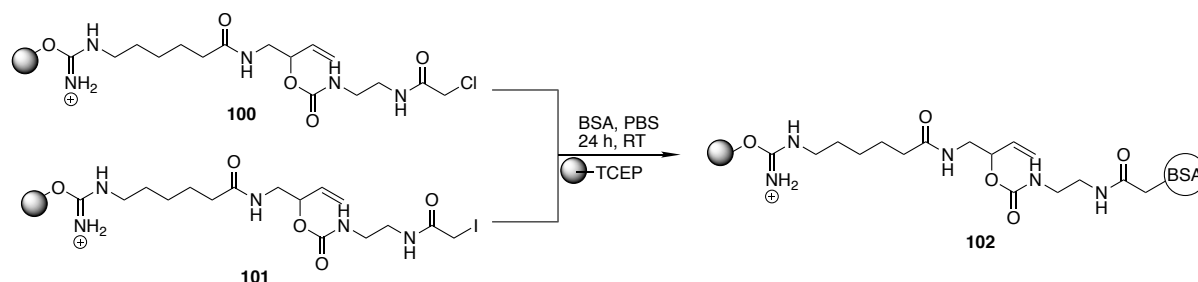
The stock solution of BSA in PBS (1 mM) was prepared just before use. To the solid phase thiol alkylation system in the SPE tube was added the solid phase TCEP (8 equiv.), followed by washing with PBS two times. Then BSA in PBS was added and the reaction mixture rotated at room temperature for 24 hours. Unreacted BSA was washed with PBS and analysed by using fluorescamine assay, BCA assay or RP-HPLC, and the washing step repeated until no more elution of BSA was observed.
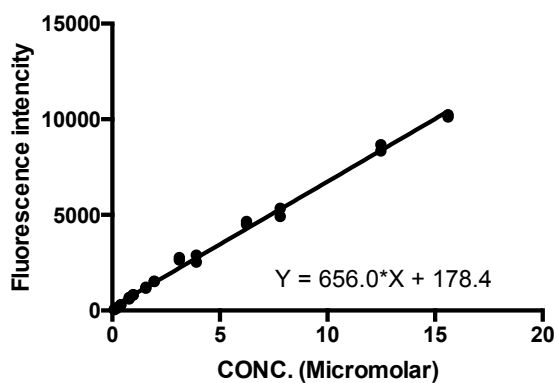
Figure 88: Calibration curve of BSA using fluorescamine assay, using the BSA stock solution

that used in the reaction of BSA with the solid phase alkylation linker **101**.

Washed	FI at 479 nm	Conc. μM	Wash Volume L	unreacted BSA μmole	Average unreacted BSA μmole
1st washX100	1315	1.73	0.003	0.052	0.046
1st washX100	1062	1.35	0.003	0.04	
2nd wash	847	1.02	0.003	0.003	0.003
2nd wash	935	1.15	0.003	0.003	
3rd wash	398	0.33	0.003	0.001	0.001
3rd wash	360	0.28	0.003	0.0008	
Washed BSA					0.050
Added BSA					0.7
Reacted BSA					0.650
Alkylation %					93

Table 34: The calculation of BSA alkylation by the solid phase alkylation linker **101** by using
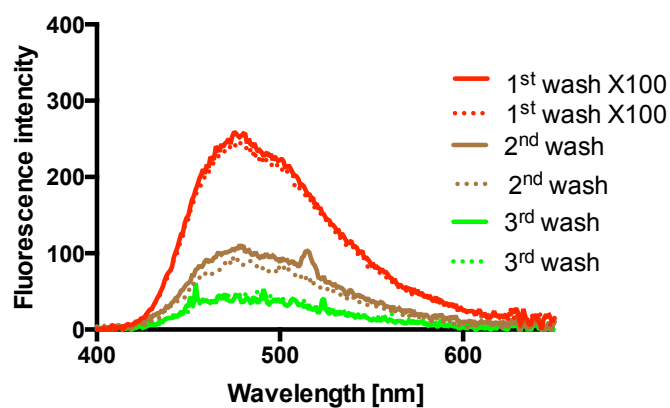
standard curve in figure 88.

Figure 89: The fluorescence of the unreacted BSA washed after reaction of BSA with the
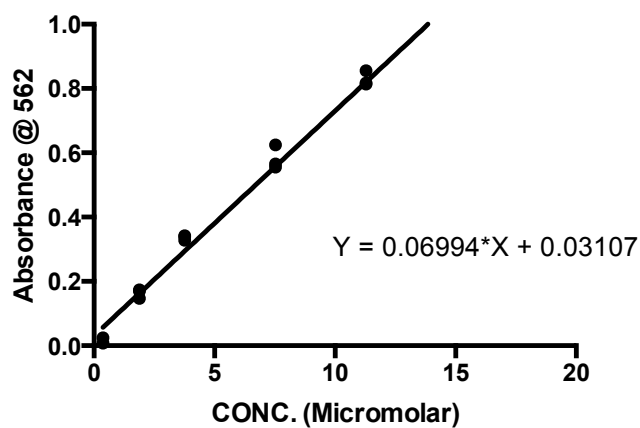
solid phase alkylation linker **101**.

Figure 90: Calibration curve of BSA using BCA protein assay (37°C/30-minutes incubation),

using the BSA stock solution that used in the reaction of BSA with the solid phase alkylation

linker **101**.

Washed	Abs. at 562 nm	Conc. µM	Wash Volume L	unreacted BSA µmole	Average unreacted BSA µmole
1st washX100	0.156	1.78	0.003	0.053	0.047
1st washX100	0.143	1.60	0.003	0.048	
1st washX100	0.123	1.31	0.003	0.039	
2nd wash	0.194	2.33	0.003	0.007	0.007
2nd wash	0.198	2.38	0.003	0.007	
2nd wash	0.206	2.50	0.003	0.007	
3rd wash	0.055	0.34	0.003	0.001	0.001
3rd wash	0.059	0.40	0.003	0.001	
3rd wash	0.071	0.57	0.003	0.002	
4th wash	0.133	1.45	0.003	0.004	0.004
4th wash	0.144	1.61	0.003	0.005	
4th wash	0.119	1.25	0.003	0.004	
Washed BSA					0.051
Added BSA					0.7
Reacted BSA					0.65
Alkylation %					93

Table 35: The calculation of BSA alkylation by the solid phase alkylation linker **101** by using
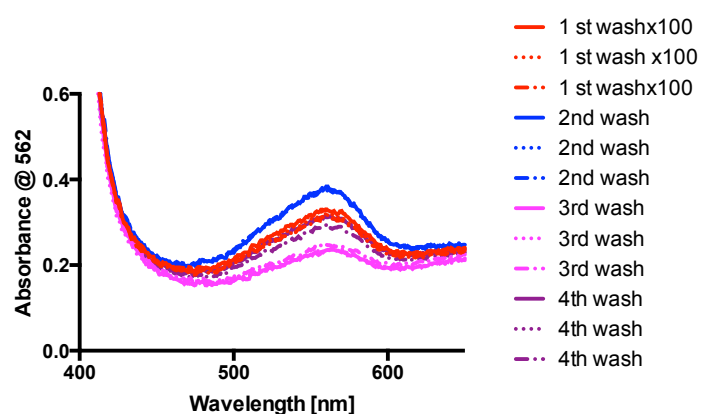
standard curve in figure 90.

Figure 91:Determination of the unreacted BSA concentration by using BCA assay (37°C/30-
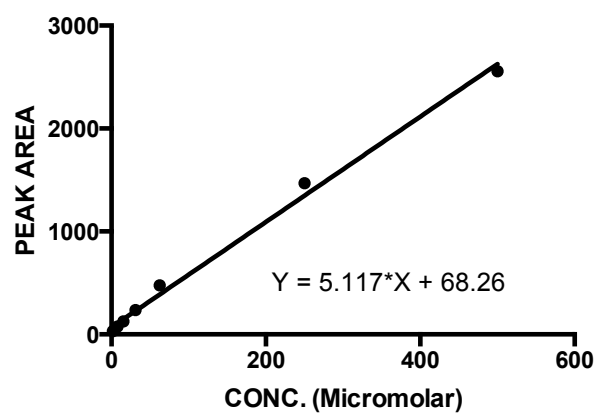
minutes incubation).

$$Y = 5.117 * X + 68.26$$

Figure 92: the calibration curve of BSA in HPLC.

Washes	Peak Area	Conc. μM	Wash Volume L	unreacted BSA μmole
1ˢᵗ washX10	49.8	4.79	0.003	0.144
Washed BSA				0.144
Added BSA				0.7
Reacted BSA				0.556
Alkylation %				79

Table 36: The calculation of BSA alkylation by the solid phase alkylation linker **101** by using
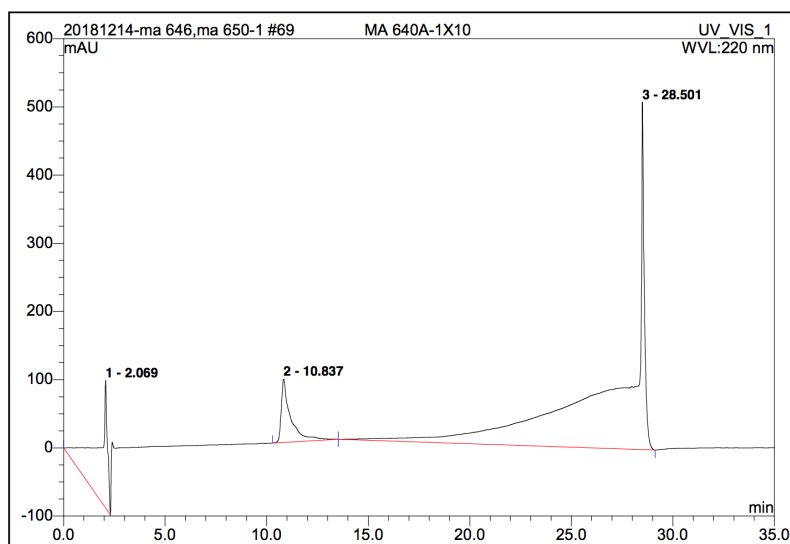
standard curve in figure 92.

Figure 93: HPLC of the unreacted BSA washed after treatment with the solid phase
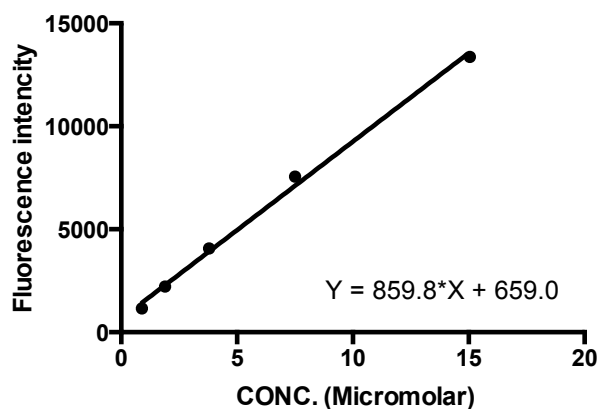
alkylation linker **101**.

Figure 94: The standard curve of BSA and fluorescamine in PBS, using the BSA stock solution

that was used in the reaction of BSA with the solid phase alkylation linker **100**.

Washed	FI at 479 nm	Conc. μM	Wash Volume L	unreacted BSA μmole	Average unreacted BSA μmole
1st washX100	3180	2.93	0.002	0.586	0.584
1st washX100	3160	2.91	0.002	0.582	
2nd wash X100	2218	1.81	0.002	0.363	0.369
2nd wash X100	2269	1.87	0.002	0.375	
3rd wash	2979	2.70	0.002	0.005	0.006
3rd wash	3194	2.95	0.002	0.006	
Washed BSA					0.958
Added BSA					2.72
Reacted BSA					1.77
Alkylation %					65

Table 37: The calculation of BSA alkylation by the solid phase alkylation linker **100** by using
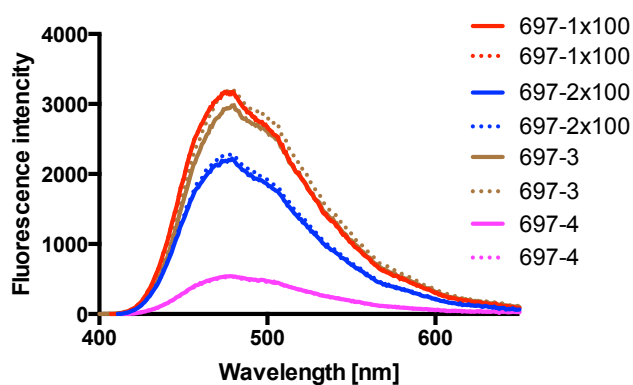
standard curve in figure 94.

Figure 95: The fluorescence of the unreacted BSA that washed after reaction of BSA with the

solid phase alkylation linker **100**.

Washes	Peak Area	Conc. µM	Wash Volume L	unreacted BSA µmole
1st wash X10	190	240	0.002	0.479
2nd wash X10	170	21.2	0.002	0.425
3rd wash	58.6	6.001	0.002	0.012
Washed BSA				0.916
Added BSA				2.72
Reacted BSA				1.81
Alkylation %				66

Table 38: The calculation of BSA alkylation by the solid phase alkylation linker **100** by using

Standard curve in figure 92.
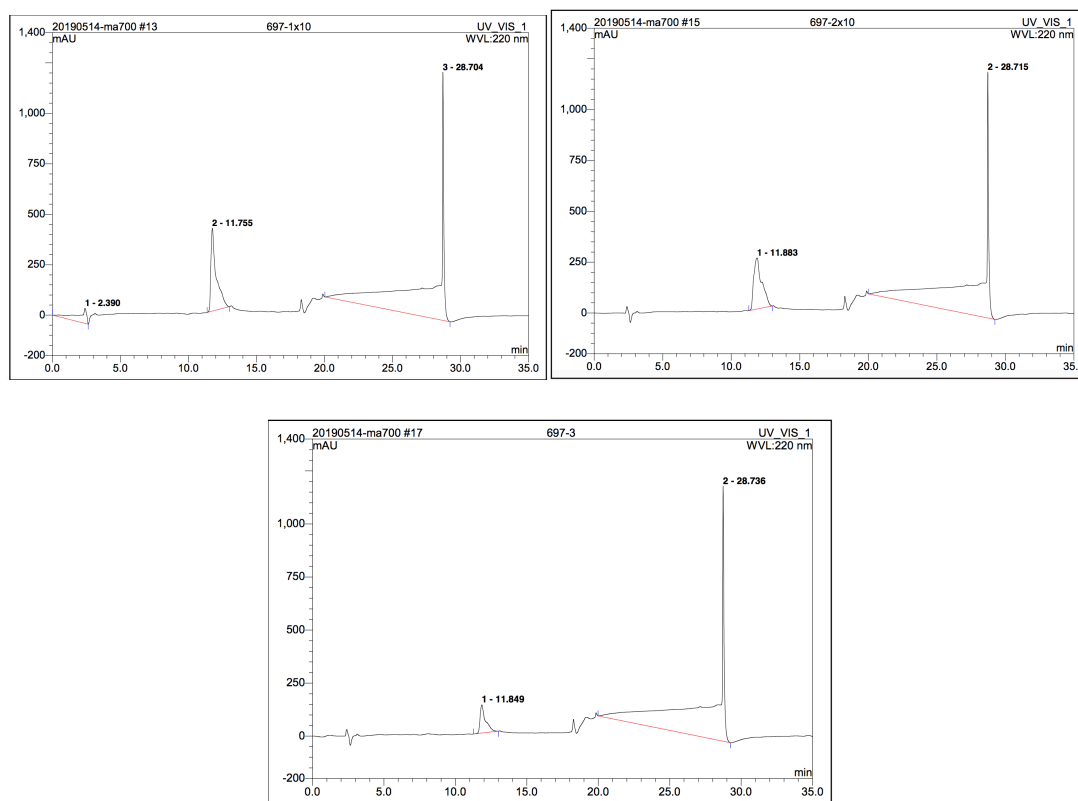

Figure 96: HPLC of the unreacted BSA after treatment with the solid phase alkylation linker

100, showing the three washes of the unreacted BSA.

D- The allyl carbamate cleavage by using catalytic Pd in the solid phase

All stock solutions were prepared just before use. The Pd-o-DANPHOS complex (1:8 Pd-o-DANPHOS solution) was prepared by addition of a solution of Na$_2$PdCl$_4$ in PBS to a solution of o-DANPHOS dihydrate (8.0 equiv.) in PBS and mixed for 30 minutes. The stock solution of dimethyl barbituric acid in PBS was prepared. The solid phase system in PBS was treated with a solution of Pd-o-DANOHOS complex in PBS (0.1 – 1.0 equiv.) and the solution of the dimethyl barbituric acid in PBS (1.0 equiv.). The reaction mixtures were rotated at room temperature for 24 hours then the cleaved substrates with cleavage reaction reagents were washed and analysed.

The deallylation reaction of the solid phase allyl carbamate 95 by using Pd-o-DANPHOS complex:
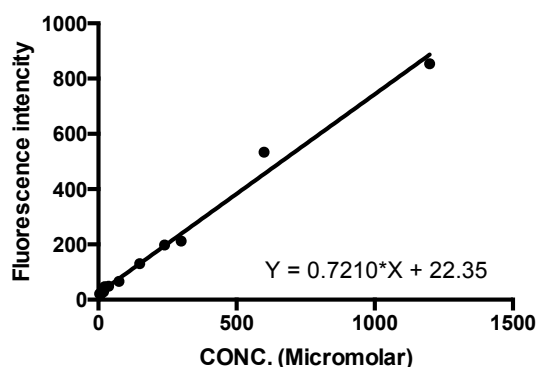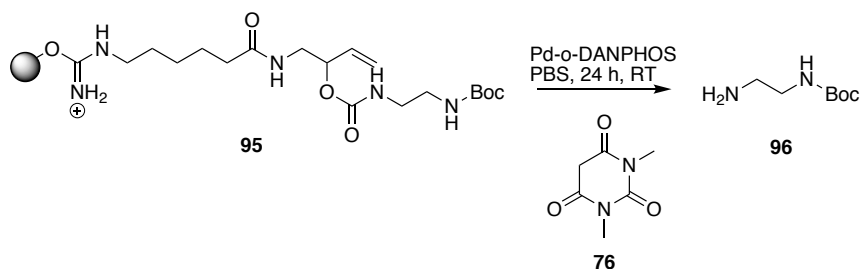

Figure 97: Calibration curve of the N-Boc ethylenediamine (the cleaved product) of the solid phase allyl carbamate **95** by using fluorescamine assay.
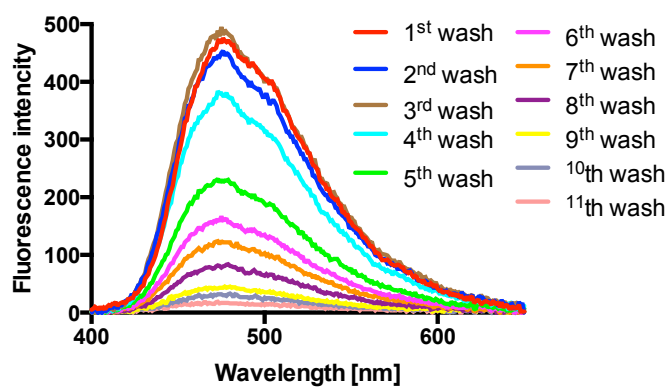
Figure 98: The fluorescence of the cleaved N-Boc ethylenediamine after deallylation

reaction of the solid phase allyl carbamate **95** by 1 equiv. Pd.

Washes	FI at 479 nm	Conc. µM	Wash Volume L	Cleaved amine µmole
1ˢᵗ wash	472	624	0.001621	1.011
2ⁿᵈ wash	448	590	0.001	0.590
3ʳᵈ wash	483	639	0.001	0.639
4ᵗʰ wash	374	488	0.001	0.488
5ᵗʰ wash	230	288	0.001	0.288
6ᵗʰ wash	157	187	0.001	0.187
7ᵗʰ wash	122	138	0.001	0.138
8ᵗʰ wash	84	85.5	0.001	0.086
9ᵗʰ wash	44	30.0	0.001	0.030
10ᵗʰ wash	32	13.4	0.001	0.013
Washed amine				3.47
Loaded amine				11.4
Cleavage %				30

Table 39: The calculation of the cleavage yield of the solid phase allyl carbamate **95** after

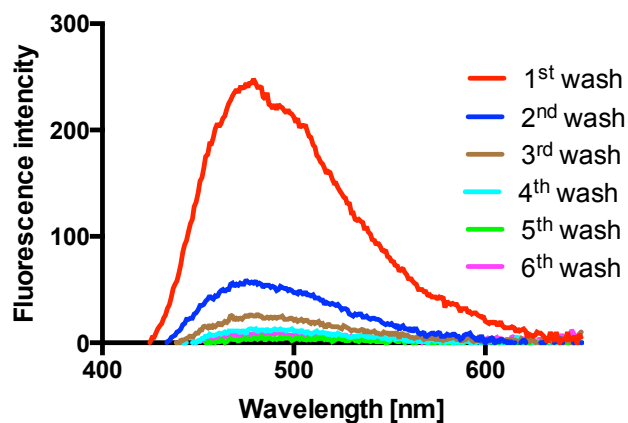using 1 equiv. Pd by using the standard curve in figure 97.

Figure 99: The fluorescence of the cleaved N-Boc ethylenediamine after deallylation

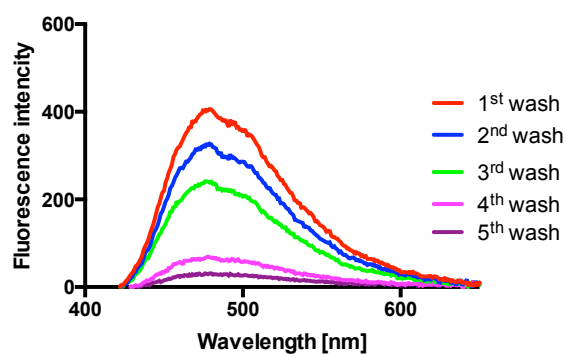reaction of the solid phase allyl carbamate **95** by 0.1 equiv. Pd.

Washes	FI at 479 nm	Conc. μM	Wash Volume L	Cleaved amine μmole
1st wash	248	313	0.002	0.692
2nd wash	56	46.7	0.002	0.093
3rd wash	25	3.67	0.001	0.004
Washed amine				0.789
Loaded amine				3.5
Cleavage %				23

Table 40: The calculation of the cleavage yield of the solid phase allyl carbamate **95** after

using 0.1 equiv. Pd by using the standard curve in figure 97.

The deallylation reaction of the solid phase allyl carbamate 99 by using Pd:
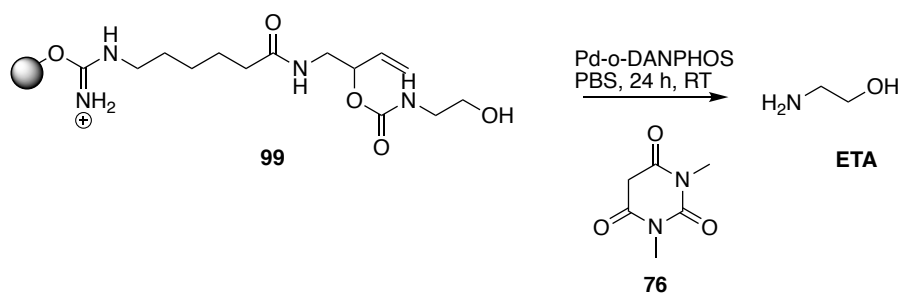
The first addition of the 0.05 eqiv. Palladium
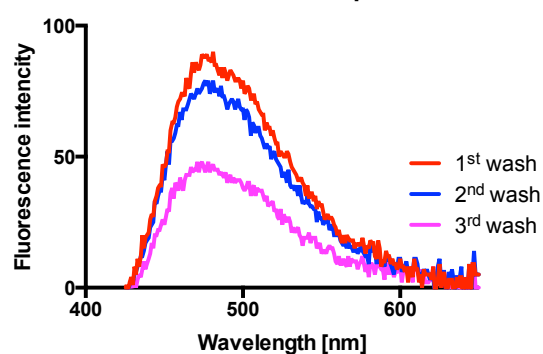
Second addition of 0.05 equiv. Palladium

Figure 100: The fluorescence of the cleaved ethanolamine after deallylation reaction of the

solid phase allyl carbamate **99** by using 0.05 equiv. Pd followed by addition more 0.05 equiv.

Pd.

Washes	FI at 479 nm	Conc. µM	Wash Volume L	Cleaved ETA µmole
1st wash	406	206	0.001	0.227
2nd wash	327	163	0.001	0.163
3rd wash	238	115	0.001	0.115
4th wash	68	23.0	0.001	0.023
5th wash	31	2.96	0.001	0.003
1st wash after second addition of 0.05 equiv. Pd	87	33.3	0.001	0.037
2nd wash after second addition of 0.05 equiv. Pd	74	26.2	0.001	0.026
3rd wash after second addition of 0.05 equiv. Pd	44	10.0	0.001	0.010
Total washed amine				0.604
Loaded amine				3.5
Cleavage %				17

Table 41: The calculation of the cleavage yield of the solid phase allyl carbamate **99** after

using 0.1 equiv. Pd by using the standard curve in figure 78B.

Chapter 5: References

1   J. W. Vardiman, J. Thiele, D. A. Arber, R. D. Brunning, M. J. Borowitz, A. Porwit, N. L. Harris, M. M. Le Beau, E. Hellström-Lindberg, A. Tefferi and C. D. Bloomfield, *Blood*, 2009, **114**, 937–951.

2   A. N. Stark, J. Thorogood, C. Head, B. E. Roberts and C. S. Scott, *Br. J. Cancer*, 1987, **56**, 59–63.

3   M. Meggendorfer, A. Roller, T. Haferlach, C. Eder, F. Dicker, V. Grossmann, A. Kohlmann, T. Alpermann, K. Yoshida, S. Ogawa, H. P. Koeffler, W. Kern, C. Haferlach and S. Schnittger, *Blood*, 2012, **120**, 3080–3089.

4   C. B. Benton, A. Nazha, N. Pemmaraju and G. Garcia-manero, *Crit. Rev. Oncol. Hematol.*, 2015, **95**, 222–242.

5   D. T. Bowen, *Hematol Oncol*, 2005, **23**, 26–33.

6   S. Benzarti, M. Daskalakis, A. Feller, V. Ulrike, A. Schnegg-kaufmann, A. Rüfer, A. Holbro, A. Schmidt and R. Benz, *Cancer Epidemiol.*, 2019, **59**, 51–57.

7   F. Matanes, B. M. A. Abdelazeem, G. Shah and V. Reddy, *Ther Adv Hematol*, 2019, **10**, 1–9.

8   J. M. BENNETT, D. CATOVSKY, M. T. DANIEL, G. FLANDRIN, G. GALTON, H. GRALNICK, *Br. J. Haematol.*, 1994, **87**, 746–754.

9   J. W. Vardiman, N. L. Harris and R. D. Brunning, *Blood*, 2002, **100**, 2292–2302.

10   L. Bencheikh, M. Morabito, E. Met, C. Debord, E. Benayoun, A. Nloga, P. Fenaux, T. Braun, C. Willekens, B. Quesnel, L. Ad, M. Fontenay, P. Rameau, N. Droin, S. Koscielny, E. Solary and G. Francophone, *Blood*, 2015, **125**, 3618–3627.

11   C. A. Hudson, W. R. Burack, P. C. Leary, M. T. Ascp and J. M. Bennett, *Am J Clin Pathol*, 2018, **150**, 293–302.

12   L. M. and R. I. M. Cazzola, *Am. Soc. Hematol.*, 2011, 264–272.

13   S. Knapper, M. Dennis, M. W. Drummond, R. K. Hills, R. J. Dillon, C. Pocock, D. J. Culligan, P. Vyas, D. Wiseman, J. Zabkiewicz, M. Hodges, C. Cargo, J. Taylor, L. Upton, M. Wright and D. Bowen, *Blood*, 2018, **132**, 1818 LP – 1818.

14   P. Fenaux, U. Platzbecker, O. Gagey, P. Rameau, G. Meurice, W. Vainchenker and N. Droin, *Blood*, 2013, **121**, 2186–2199.

15   M. Bhatia, *Am. Soc. Hematol.*, 2007, 11–16.

16   S. Takagaki, R. Yamashita, N. Hashimoto, K. Sugihara, K. Kanari, K. Tabata, T. Nishie, S. Oka, M. Miyanishi, C. Naruse and M. Asano, *Sci. Rep.*, 2019, **9**, 1–11.

17   L. J. Appleby, N. Nausch, N. Midzi, T. Mduluza, J. E. Allen and F. Mutapi, *Immunol. Lett.*, 2013, **152**, 32–41.

18   S. Gordon and P. R. Taylor, *Nat. Rev. Immunol.*, 2005, **5**, 953–964.

19   C. Shi and E. G. Pamer, *Nat Rev Immunol*, 2014, **11**, 762–774.

20   L. Ziegler-heitbrock, P. Ancuta, S. Crowe, M. Dalod, V. Grau, D. N. Hart, P. J. M. Leenen, Y. Liu, G. Macpherson, G. J. Randolph and J. Scherberich, *Blood*, 2010, **116**, e74–e80.

21   C. Auffray, M. H. Sieweke and F. Geissmann, *Annu. Rev. Immunol.*, 2009, **27**, 669–692.

22   J. Yang, L. Zhang, C. Yu, X. Yang and H. Wang, *Biomark. Res.*, 2014, **2**, 1–9.

23   J. L. Collison, L. M. Carlin, M. Eichmann, F. Geissmann and M. Peakman, *J. Immunol.*, 2015, **195**, 1162–1170.

24   B. A. Imhof and M. Aurrand-lions, *Nat. Rev. Immunol.*, 2004, **4**, 432-444.

25   J. Cros, N. Cagnard, K. Woollard, N. Patey, S. Y. Zhang, B. Senechal, A. Puel, S. K. Biswas, D. Moshous, C. Picard, J. P. Jais, D. D'Cruz, J. L. Casanova, C. Trouillet and F. Geissmann, *Immunity*, 2010, **33**, 375–386.

26   L. B. Boyette, C. MacEdo, K. Hadi, B. D. Elinoff, J. T. Walters, B. Ramaswami, G. Chalasani, J. M. Taboas, F. G. Lakkis and Di. M. Metes, *PLoS One*, 2017, **12**, 1–20.

27   T. M. Handel and P. J. Domaille, *Biochemistry*, 1996, **35**, 6569–6584.

28   S. L. Deshmane and S. Kremlev, S. Amini and B. E. Sawaya, *J. Interf. Cytokine Res.*, 2009, **29**, 313–326.

29   L. B. Ford, V. Cerovic, S. W. F. Milling, J. Gerard, C. A. H. Hansell, R. J. B. Nibbs and R. J. B. Nibbs, *J. Immunol.*, 2014, **193**, 400–411.

30   M. Baggiolini and P. Loetscher, *Immunol. Today*, 2000, **21**, 418–420.

31   G. M. Clore and A. M. Gronenborn, *FASEB J.*, 1995, **9**, 57–62.

32   M. Mellado, M. Rodr and C. Mart, *Annu. Rev. Immunol*, 2001, **19**, 397–421.

33   S. J. Allen, S. E. Crown and T. M. Handel, *Annu. Rev. Immunol*, 2007, **25**, 787–820.

34   E. Lubowicka, A. Przylipiak, M. Zajkowska, B. M. Piskór, P. B. Malinowski, W. Fiedorowicz and S. B. A, *Biomed Res. Int.*, 2018, 1–9.

35   Â. M. Rodrõ, M. Mellado, A. J. Vila-coro, S. Ferna, Â. De Ana, D. R. Jones, A. Martõ, Â. L. Tora and C. Martõ, *EMBO J.*, 2001, **20**, 2497–2507.

36   N. F. Neel, E. Schutyser, J. Sai, G. Fan and A. Richmond, *Cytokine Growth Factor Rev.*, 2005, **16**, 637–658.

37   Y. Si, K. Croft and I. F. Charo, *J. Clin. Invest.*, 2010, **120**, 1192–1203.

38   S. Volpe, E. Cameroni, B. Moepps, S. Thelen, T. Apuzzo and M. Thelen, *PLoS One*, 2012, **7**, 1–10.

39   L. M. Mcintosh and J. L. Barnes, *Clin. Exp. Immunol.*, 2008, **155**, 295–303.

40   T. M. Handel, Z. Johnson, D. H. Rodrigues, A. C. Dos Santos, R. Cirillo, V. Muzio, S. Riva, M. Mack, M. Déruaz, F. Borlat, P. A. Vitte, T. N. C. Wells, M. M. Teixeira and A. E. Proudfoot, *J. Leukoc. Biol.*, 2008, **84**, 1101–1108.

41   M. Hasmann and I. Schemainda, *Cancer Res.*, 2003, **63**, 7436–7442.

42   L. Ma, C. Wang, Z. He, B. Cheng, L. Zheng and K. Huang, *Curr. Med. Chem.*, 2017, **24**.

43 R. He, B. Finan, J. P. Mayer and R. D. DiMarchi, *Molecules*, 2019, **24**, 11–14.

44 Y. Takaoka, A. Ojida and I. Hamachi, *Angew. Chemie - Int. Ed.*, 2013, **52**, 4088–4106.

45 J. W. Harper, E. J. Bennett, S. Diego and L. Jolla, 2016, **537**, 328–338.

46 G. Walsh and R. Jefferis, *Nat. Biotechnol.*, 2006, **24**, 1241–1252.

47 C. T. Walsh, S. Garneau-Tsodikova and G. J. Gatto, *Angew. Chemie - Int. Ed.*, 2005, **44**, 7342–7372.

48 A. Beck, L. Goetsch, C. Dumontet and N. Corvaïa, *Nat. Rev. Drug Discov.*, 2017, **16**, 315.

49 N. Krall, F. P. da Cruz, O. Boutureira and G. J. L. Bernardes, *Nat. Chem.*, 2015, **8**, 103.

50 G. Zhang, S. Zheng, H. Liu and P. R. Chen, *Chem. Soc. Rev.*, 2015, **44**, 3405–3417.

51 O. Boutureira and G. J. L. Bernardes, *Chem. Rev.*, 2015, **115**, 2174–2195.

52 P. Wang, S. Zhang, Q. Meng, Y. Liu, L. Shang and Z. Yin, *Org. Lett.*, 2015, **17**, 1361–1364.

53 Y. Xu, W. Wu, Q. Han, Y. Wang, C. Li, P. Zhang and H. Xu, *Open Biol.*, 2019, **9**, 1–10.

54 J. M. Chalker, G. J. L. Bernardes, Y. A. Lin and B. G. Davis, *Chem. - An Asian J.*, 2009, **4**, 630–640.

55 G. Lauc, A. Essafi, J. E. Huffman, C. Hayward, A. Knežević, J. J. Kattla, O. Polašek, O. Gornik, V. Vitart, J. L. Abrahams, M. Pučić, M. Novokmet, I. Redžić, S. Campbell, S. H. Wild, F. Borovečki, W. Wang, I. Kolčić, L. Zgaga, U. Gyllensten, J. F. Wilson, A. F. Wright, N. D. Hastie, H. Campbell, P. M. Rudd and I. Rudan, *PLoS Genet.*, 2010, **6**, 1–14.

56 G. Walsh, *Drug Discov. Today*, 2010, **15**, 773–780.

57 E. Higgins, *Glycoconj. J.*, 2010, **27**, 211–225.

58 L. Tong, G. Baskaran, M. Jones, J. Rhee and K. Yarema, *Biotechnol. Genet. Eng. Rev.*, 2003, 199–244.

59 C. E. Warren, *Curr. Opin. Biotechnol.*, 1993, **4**, 596–602.

60 D. E. Webster and M. C. Thomas, *Biotechnol. Adv.*, 2012, **30**, 410–418.

61   W. Hart, *Curr. Opin. Cell Biol.*, 1992, **4**, 1017–1023.

62   B. Laukens, C. De Visscher and N. Callewaert, *Future Microbiol.*, 2015, **10**, 21–34.

63   H. Li and M. d'Anjou, *Curr. Opin. Biotechnol.*, 2009, **20**, 678–684.

64   J. F. Ernst and S. K. Prill, *Med. Mycol.*, 2001, **39**, 67–74.

65   T. Kinoshita, *J. Lipid Res.*, 2016, **57**, 4–5.

66   L. Ganesan and I. Levental, *J. Membr. Biol.*, 2015, **248**, 929–941.

67   H. C. Hang and M. E. Linder, *Chem. Rev.*, 2011, **111**, 6341–6358.

68   H. Abe, M. Goto and N. Kamiya, *Chem. - A Eur. J.*, 2011, **17**, 14004–14008.

69   B. Chen, Y. Sun, J. Niu, G. K. Jarugumilli and X. Wu, *Cell Chem. Biol.*, 2018, **25**, 817–831.

70   H. Jiang, X. Zhang, X. Chen, P. Aramsangtienchai, Z. Tong and H. Lin, *Chem. Rev.*, 2018, **118**, 919–988.

71   E. W. Tate, K. A. Kalesh, T. Lanyon-Hogg, E. M. Storck and E. Thinon, *Curr. Opin. Chem. Biol.*, 2015, **24**, 48–57.

72   M. J. Nadolski and M. E. Linder, *FEBS J.*, 2007, **274**, 5202–5210.

73   J. You, A. Fitzgerald, P. J. Cozzi, Z. Zhao, P. Graham, P. J. Russell, B. J. Walsh, M. Willcox, L. Zhong, V. Wasinger and Y. Li, *Electrophoresis*, 2010, **31**, 1853–1861.

74   A. E. Bond, P. E. Row and E. Dudley, *Phytochemistry*, 2011, **72**, 975–996.

75   Z. Chen and P. a Cole, *Curr. Opin. Chem. Biol.*, 2015, **28**, 115–122.

76   S. J. Humphrey, D. E. James and M. Mann, *Trends Endocrinol. Metab.*, 2015, **26**, 676–687.

77   C. Seibert, C. T. Veldkamp, F. C. Peterson, B. T. Chait, B. F. Volkman and T.P. Sakmar, *Biochemistry*, 2008, **47**, 11251–11262.

78   J. H. Ippel, C. J. C. de Haas, A. Bunschoten, J. A. G. van Strijp, J. A. W. Kruijtzer, R. M. J. Liskamp and J. Kemmink, *J. Biol. Chem.*, 2009, **284**, 12363–12372.

79   T. Teramoto, Y. Fujikawa, Y. Kawaguchi, K. Kurogi, M. Soejima, R. Adachi, Y. Nakanishi, E. Mishiro-Sato, M. C. Liu, Y. Sakakibara, M. Suiko, M. Kimura and Y. Kakuta, *Nat. Commun.*, 2013, **4**, 1572.

80   S. Tanaka, T. Nishiyori, H. Kojo, R. Otsubo, M. Tsuruta, K. Kurogi, M. C. Liu, M. Suiko, Y. Sakakibara and Y. Kakuta, *Sci. Rep.*, 2017, **7**, 4–13.

81   K. L. Moore, *Proc. Natl. Acad. Sci. U. S. A.*, 2009, **106**, 14741–14742.

82   F. Monigatti, E. Gasteiger, A. Bairoch and E. Jung, *Bioinformatics*, 2002, **18**, 769–770.

83   A. D. Westmuckett, K. M. Thacker and K. L. Moore, *PLoS One*, 2011, **6**, 1–6.

84   J. W. Kehoe and C. R. Bertozzi, *Chem. Biol.*, 2000, **7**, 57–61.

85   Y. Kanan, J. C. Siefert, M. Kinter and M. R. Al-Ubaidi, *PLoS One*, 2014, **9**, e0105409.

86   L. Ma, G. Fenalti, J. Li, W. Zhang, X. Xie and H. Yang, *Science*, 2013, **341**, 1387–1390.

87   B. Lee, S. Sun, E. Jiménez-Moreno, A. A. Neves and G. J. L. Bernardes, *Bioorganic Med. Chem.*, 2018, **26**, 3060–3064.

88   O. Boutureira and G. J. L. Bernardes, *Chem. Rev.*, 2015, **115**, 2174–2195.

89   N. Krall, F. P. Da Cruz, O. Boutureira and G. J. L. Bernardes, *Nat. Chem.*, 2016, **8**, 103–113.

90   C. D. Spicer and B. G. Davis, *Nat. Commun.*, 2014, **5**, 4740.

91   J. a Burns, J. C. Butler, J. Moran and G. M. Whitesides, *J. Org. Chem.*, 1991, **56**, 2648–2650.

92   E. M. S. and C. R. Bertozzi, *Angew Chem Int Ed Engl. 2009*, 2009, **48**, 6974–6998.

93   H. Ban, J. Gavrilyuk and C. F. Barbas, *J. Am. Chem. Soc.*, 2010, **132**, 1523–1525.

94   Y. Yu, L. K. Zhang, A. V. Buevich, G. Li, H. Tang, P. Vachal, S. L. Colletti and Z. C. Shi, *J. Am. Chem. Soc.*, 2018, **140**, 6797–6800.

95   J. M. Antos and M. B. Francis, *J. Am. Chem. Soc.*, 2004, **126**, 10256–10257.

96   M. J. Matos, B. L. Oliveira, N. Martínez-Sáez, A. Guerreiro, P. M. S. D. Cal, J. Bertoldo, M. Maneiro, E. Perkins, J. Howard, M. J. Deery, J. M. Chalker, F. Corzana, G. Jiménez-Osés and G. J. L. Bernardes, *J. Am. Chem. Soc.*, 2018, **140**, 4004–4017.

97   S. Lin, X. Yang, S. Jia, A. M. Weeks, M. Hornsby, S. Peter, R. V Nichiporuk, A. T. Iavarone, J. A. Wells, F. D. Toste and C. J. Chang, *Science*, 2017, **355**, 597–602.

98   E. Calce and S. De Luca, *Chemistry*, 2017, **23**, 224–233.

99   S. B. Gunnoo and A. Madder, *ChemBioChem*, 2016, **17**, 529–553.

100   O. Koniev and A. Wagner, *Chem. Soc. Rev.*, 2015, **44**, 5495–5551.

101   R. J. Carey, F. A., Sundberg, *Advanced organic chemistry: part A: structure and mechanisms*, Springer Science & Business Media, 2007.

102   G. Klopman, *Chemical Reactivity and Reaction Paths*, Wiley, New York, 1974.

103   J. M. Harris and S. P. McManus, eds., Nucleophilicity, Vol. 215, *Advances in Chemistry Series*, American Chemical Society, Washington, DC, 1987.

104   J. F. Bunnett*, Annu. Rev. Phys. Chem.*, 1963, **14**, 271-290.

105   M. E. Niyazymbetov and D. H. Evans, *J. Chem. Soc., Perkin Trans. 2*, 1996, 1957-1961.

106   R. L. Fuchs and L. L. Cole, *J. Am. Chem. Soc.*, 1973, **95**, 3194.

107   R. G. Pearson and J. Songstad, *J. Am. Chem. Soc.*,1967, **89**, 1827-1836.

108   E. S. Boja and H. M. Fales, *Anal. Chem.*, 2001, **73**, 3576–3582.

109   S. Sechi and B. T. Chait, *Anal. Chem.*, 1998, **70**, 5150–5158.

110   J. Paulech, N. Solis and S. J. Cordwell, *Biochim. Biophys. Acta - Proteins Proteomics*, 2013, **1834**, 372–379.

111   S. Suttapitugsakul, H. Xiao, J. Smeekens and R. Wu, *Mol. Biosyst.*, 2017, **13**, 2574–2582.

112   C. H. Marchand, S. Fermani, J. Rossi, L. Gurrieri, D. Tedesco, J. Henri, F. Sparla, P. Trost, S. D. Lemaire and M. Zaffagnini, *Antioxidants*, 2019, **8**, 1-20.

113 P. G. Hains and P. J. Robinson, *J. Proteome Res.*, 2017, **16**, 3443–3447.

114 J. Davis, *Tetrahedron Lett.*, 1991, **32**, 6793–6796.

115 R. S. Swanwick, A. M. Daines, L. H. Tey, S. L. Flitsch and R. K. Allemann, *ChemBioChem*, 2005, **6**, 1338–1340.

116 D. Macmillan, R. M. Bill, K. A. Sage, D. Fern and S. L. Flitsch, *Chem. Biol.*, 2001, **8**, 133–145.

117 M. Sunbul, L. Nacheva and A. Jäschke, *Bioconjug. Chem.*, 2015, **26**, 1466–1469.

118 I. A. Ahmed and F. Gai, *Protein Sci.*, 2017, **26**, 375–381.

119 P. D. Senter and E. L. Sievers, *Nat. Biotechnol.*, 2012, **30**, 631–637.

120 B. Bernardim, P. Cal, M. J. Matos, B. L. Oliveira, N. Martínez-Saéz, I. S. Albuquerque, E. Perkins, F. Corzana, B. Burtoloso, G. Jiménez-Osés and G. Bernardes, *Nat. Commun.*, 2016, **7**, 1–9.

121 J. Strojil and H. Ciferská, *Klin. Farmakol. a Farm.*, 2010, **24**, 155–160.

122 P. Cal, G. Bernardes and P. Gois, *Angew. Chemie - Int. Ed.*, 2014, **53**, 10585–10587.

123 M. E. Smith, F. F. Schumacher, C. P. Ryan, L. M. Tedaldi, D. Papaioannou, G. Waksman, S. Caddick and J. R. Baker, *J. Am. Chem. Soc.*, 2010, **132**, 1960–1965.

124 J. E. Moore and W. H. Ward, *J. Am. Chem. Soc.*, 1956, **78**, 2414–2418.

125 Y. Zhang, V. S. Bhatt, G. Sun, P. Wang, *Bioconjug. Chem.*, 2008, **19**, 2221–2230.

126 D. J. Betting, K. Kafi, A. Abdollahi-Fard, S. A. Hurvitz and J. M. Timmerman, *J. Immunol.*, 2008, **181**, 4131–4140.

127 I. Haralampiev, M. Mertens, R. Schwarzer, A. Herrmann, R. Volkmer, P. Wessig and P. Müller, *Angew. Chemie - Int. Ed.*, 2015, **54**, 323–326.

128 J. Collins, J. Tanaka, P. Wilson, K. Kempe, T. P. Davis, M. P. Mcintosh, M. R. Whittaker and D. M. Haddleton, *Bioconjug. Chem.*, 2015, **26**, 633–638.

129 A. H. K. Al Temimi, R. Van Der Wekken-De Bruijne, G. Proietti, H. Guo, P. Qian and J. Mecinović, *Bioconjug. Chem.*, 2019, **30**, 1798–1804.

130 B. J. G. E. Pieters, J. C. J. Hintzen, Y. Grobben, A. H. K. Al Temimi, J. J. A. G. Kamps and J. Mecinović, *Bioconjug. Chem.*, 2019, **30**, 952–958.

131 Y. Tang, K. Meeth, S. Curtet, R. N. Cole, M. A. Holbert, S. Khochbin, B. M. Dancy, D. R. Colquhoun, R. Huang, B. C. Dancy, R. Marmorstein, P. A. Cole, Y. Hwang and M. K. Tarrant, *J. Am. Chem. Soc.*, 2010, **132**, 9986–9987.

132 C. M. Bunney, P. E., Zink, A. N., Holm, A. A., Billington, C. J., & Kotz, *J Am Chem Soc.*, 2018, **140**, 9478–9485.

133 J. M. Chalker, J. L. Bernardes and B. G. Davis, *Acc. Chem. Res.*, 2011, **44**, 730–741.

134 B. G. Davis, M. A. T. Maughan, M. P. Green, A. Ullman and J. B. Jones, *Tetrahedron Asymmetry*, 2000, **11**, 245–262.

135 D. P. Gamblin, P. Garnier, S. J. Ward, N. J. Oldham, A. J. Fairbanks and B. G. Davis, *Org. Biomol. Chem.*, 2003, **1**, 3642–3644.

136 D. P. Gamblin, P. Garnier, S. Van Kasteren, N. J. Oldham, A. J. Fairbanks and B. G. Davis, *Angew. Chemie - Int. Ed.*, 2004, **43**, 828–833.

137 P. M. Rendle, A. Seger, J. Rodrigues, N. J. Oldham, R. R. Bott, J. B. Jones, M. M. Cowan and B. G. Davis, *J. Am. Chem. Soc.*, 2004, **126**, 4750–4751.

138 G. J. L. Bernardes, J. P. Marston, A. S. Batsanov, J. A. K. Howard and B. G. Davis, *Chem. Commun.*, 2007, 3145–3147.

139 G. J. L. Bernardes, J. M. Chalker, J. C. Errey and B. G. Davis, *J. Am. Chem. Soc.*, 2008, **130**, 5052–5053.

140 O. Boutureira, G. J. L. Bernardes, F. D'Hooge and B. G. Davis, *Chem. Commun.*, 2011, **47**, 10010–10012.

141 M. Kunstelj, K. Fidler, Š. Škrajnar, M. Kenig, V. Smilović, M. Kusterle, S. Caserman, I. Zore, V. G. Porekar and S. Jevševar, *Bioconjug. Chem.*, 2013, **24**, 889–896.

142 E. J. Grayson, G. J. L. Bernardes, J. M. Chalker, O. Boutureira, J. R. Koeppe and B. G. Davis, *Angew. Chemie - Int. Ed.*, 2011, **50**, 4127–4132.

143 J. M. Chalker, L. Lercher, N. R. Rose, C. J. Schofield and B. G. Davis, *Angew. Chemie - Int. Ed.*, 2012, **51**, 1835–1839.

144 J. Dadová, S. R. Galan and B. G. Davis, *Curr. Opin. Chem. Biol.*, 2018, **46**, 71–81.

145 A. Chan, J. Tsai, V. Lo, G. Li, M. Wong, C. Che, A. Chan, J. Tsai, V. Lo, G. Li, M. Wong and C. Che, *Chem. Commun.*, 2013, **49**, 1428–1430.

146 Q. Zhou, *Biomedicines*, 2017, **5**, 1-15.

147 J. R. Junutula, H. Raab, S. Clark, S. Bhakta, D. D. Leipold, S. Weir, Y. Chen, M. Simpson, S. P. Tsai, M. S. Dennis, Y. Lu, Y. G. Meng, C. Ng, J. Yang, C. C. Lee, E. Duenas, J. Gorrell, V. Katta, A. Kim, K. McDorman, K. Flagella, R. Venook, S. Ross, S. D. Spencer, W. Lee Wong, H. B. Lowman, R. Vandlen, M. X. Sliwkowski, R. H. Scheller, P. Polakis and W. Mallet, *Nat. Biotechnol.*, 2008, **26**, 925–932.

148 J. P. M. Nunes, M. Morais, V. Vassileva, E. Robinson, V. S. Rajkumar, M. E. B. Smith, R. B. Pedley, S. Caddick, J. R. Baker and V. Chudasama, *Chem. Commun.*, 2015, **51**, 10624–10627.

149 S. J. Walsh, S. Omarjee, W. R. J. D. Galloway, T. T. L. Kwan, H. F. Sore, J. S. Parker, M. Hyvönen, J. S. Carroll and D. R. Spring, *Chem. Sci.*, 2019, **10**, 694–700.

150 S. S. Gori, P. Lorkiewicz, D. S. Ehringer, A. C. Belshoff, R. M. Higashi, T. W. Fan and M. H. Nantz, *Anal. Bioanal. Chem.*, 2014, **406**, 4371–9.

151 J. C. Lukesh, M. J. Palte and R. T. Raines, 2012, 4057–4059.

152 S. S. Gori, P. Lorkiewicz, D. S. Ehringer, A. C. Belshoff, R. M. Higashi, T. W. M. Fan and

M. H. Nantz, *Anal. Bioanal. Chem.*, 2014, **406**, 4371–4379.

153   J. A. Burns, J. C. Butler, J. Moran and G. M. Whitesides, *J. Org. Chem.*, 1991, **56**, 2648–2650.

154   E. B. Getz, M. Xiao, T. Chakrabarty, R. Cooke and P. R. Selvin, *Anal. Biochem.*, 1999, **273**, 73–80.

155   C. David, S. Foley and M. Enescu, *Phys. Chem. Chem. Phys.*, 2009, **11**, 2532–2542.

156   A. Zwyssig, E. M. Schneider, M. Zeltner, B. Rebmann, V. Zlateski, R. N. Grass and W. J. Stark, *Chem. - A Eur. J.*, 2017, **23**, 8585–8589.

157   P. Liu, B. W. O'Mara, B. M. Warrack, W. Wu, Y. Huang, Y. Zhang, R. Zhao, M. Lin, M. S. Ackerman, P. K. Hocknell, G. Chen, L. Tao, S. Rieble, J. Wang, D. B. Wang-Iverson, A. A. Tymiak, M. J. Grace and R. J. Russell, *J. Am. Soc. Mass Spectrom.*, 2010, **21**, 837–844.

158   O. Koniev and A. Wagner, *Chem. Soc. Rev.*, 2015, **44**, 5495–551.

159   E. Calce, M. Leone, F. A. Mercurio, L. Monfregola and S. De Luca, *Org. Lett.*, 2015, **17**, 5646–5649.

160   J. Li, J. Yu, J. Zhao, J. Wang, S. Zheng, S. Lin, L. Chen, M. Yang, S. Jia, X. Zhang and P. R. Chen, *Nat. Chem.*, 2014, **6**, 352–361.

161   L. Mendoza, G. Mamo, N. Flores, A. Gimenez and R. Hatti-Kaul, *J. Mol. Catal. B Enzym.*, 2011, **68**, 270–274.

162   M. Guillaume and Y. Lang, *Tetrahedron Lett.*, 2010, **51**, 579-582.

163   J. Yang, J. Wu and C. Qiao, *Synth. Commun.*, 2014, **44**, 1240–1244.

164   Y. Güneş, M. F. Polat, E. Sahin, F. F. Fleming and R. Altundas, *J. Org. Chem.*, 2010, **75**, 7092–8.

165   N. Bindman, R. Merkx, R. Koehler, N. Herrman and W. A. van der Donk, *Chem commun.*, 2010, **46**, 8935-8937.

166   L. Mateo-Vivaracho, J. Cacho and V. Ferreira, *J. Chromatogr. A*, 2008, **1185**, 9–18.

167   J. J. Yang, J. Z. Wu and C. Qiao, *Synth. Commun.*, 2014, **44**, 1240–1244.

168   I. H. Krouse and P. G. Wenthold, *J Am Soc Mass Spectrom*, 2005, **16**, 697-707.

169   A. E. Fedorov, A. M. Shestopalov and P. A. Belyakov, *Russ. Chem. Bull., Int. Ed.*, 2003, **52**, 2197-2202.

170   F. Wojciechowski, M. Suchy, A. X. Li, H. A. Azab, R. Bartha and R. H. E. Hudson, *Bioconjug. Chem.*, 2007, **18**, 1625–1636.

171   Y. C. Qin, C. E. Stivala and A. Zakarian, *Angew chemie - Int Ed*, 2007, **46**, 7466-7469.

172   M. L. de Ferreira, M. V. N. de Souza, S. M. S. V. Wardell, J. L. Wardell, T. R. A. Vasconcelos, V. F. Ferreira and M. C. S. Lourenço, *J Carbohydr Chem.*, 2010, **29**, 265-274.

173   V. V. Rostovtsev, L. G. Green, V. V. Fokin and K. B. Sharpless, *Angew. Chem. Int. Ed.*, 2002, **41**, 2596–2599.

174   M. M. Haugland, S. Borsley, D. F. Cairns-Gibson, A. Elmi and S. L. Cockroft, *ACS Nano*, 2019, **13**, 4101–4110.

175   J. E. Hein and V. V Fokin, *Chem. Soc. Rev.*, 2010, **39**, 1302–15.

176   A. A. Husain and K. S. Bisht, *RSC Adv.*, 2019, **9**, 10109–10116.

177   V. O. Rodionov, S. I. Presolski, D. D. Díaz, V. V. Fokin and M. G. Finn, *J. Am. Chem. Soc.*, 2007, **129**, 12705–12712.

178   R. S. Gomes, G. A. M. Jardim, R. L. de Carvalho, M. H. Araujo and E. N. da Silva Júnior, *Tetrahedron*, 2019, **75**, 3697–3712.

179   H. Ben El Ayouchia, L. Bahsis, H. Anane, L. R. Domingo and S. E. Stiriba, *RSC Adv.*, 2018, **8**, 7670–7678.

180   S. Diez-Gonzalez, *Curr. Org. Chem.*, 2011, **15**, 2830–2845.

181 L. Li and Z. Zhang, *Molecules*, 2016, **21**, 1–22.

182 V. Castro, H. Rodríguez and F. Albericio, *ACS Comb. Sci.*, 2016, **18**, 1–14.

183 E. Haldón, M. C. Nicasio and P. J. Pérez, *Org. Biomol. Chem.*, 2015, **13**, 9528–9550.

184 S. B. Ötvös, Á. Georgiádes, M. Ádok-Sipiczki, R. Mészáros, I. Pálinkó, P. Sipos and F. Fülöp, *Appl. Catal. A Gen.*, 2015, **501**, 63–73.

185 D. R. Vutukuri, P. Bharathi, Z. Yu, K. Rajasekaran, M. Tran and S. Tayumansvan, *J. Org. Chem.*, 2003, **68**, 1146–1149.

186 J. Tsuji, J. Kiji, S. Imamura and M. Morikawa, *J. Am. Chem. Soc.*, 1964, **86**, 4350–4353.

187 B. M. Trost and T. J. Dietsche, *J. Am. Chem. Soc.*, 1973, **95**, 8200–8201.

188 B. M. Trost, T. Zhang and J. D. Sieber, *Chem. Sci.*, 2010, **1**, 427–440.

189 O. Kuhn and H. Mayr, *Angew. Chemie - Int. Ed.*, 1999, **38**, 343–346.

190 J. E. Báckvall, R. E. Nordberg, K. Zetterberg and B. Akermark, *Organometallics*, 1983, **2**, 1625–1629.

191 P. Aleksandrowic, H. Piotrowska and W. Sas, *Tetrahedron*, 1982, **38**, 1321-1327.

192 B. M. Trost and E. Keinan, *J. Am. Chem. Soc.*, 1978, **100**, 7779–7781.

193 B. M. Trost, T. R. Verhoeven and J. M. Fortunak, *Tetrahedron Letters*, 1972, **25**, 2304-2501.

194 I. G. Rios, A. Rosas-Hernandez and E. Martin, *Molecules*, 2011, **16**, 970–1010.

195 B. M. Trost and M. L. Crawley, *Chem. Rev.*, 2003, **103**, 2921–2944.

196 B. M. Trost, P. E. Strege, L. Weber, T. J. Fullerton and T. J. Dietsche, *J. Am. Chem. Soc.*, 1978, **100**, 3407–3415.

197 C. Sköld, J. Kleimark, A. Trejos, L. R. Odell, S. O. Nilsson Lill, P. O. Norrby and M. Larhed, *Chem. - A Eur. J.*, 2012, **18**, 4714–4722.

198 S. Azpeitia, U. Prieto, E. San Sebastián, A. Rodríguez-Diéguez, M. A. Garralda and M. A.

Huertos, *Dalt. Trans.*, 2018, **47**, 6808–6818.

199   S. J. Blanksby and G. B. Ellison, *Acc. Chem. Res.*, 2003, **36**, 255–263.

200   E. Lallana, E. Fernandez-Megia and R. Riguera, *J. Am. Chem. Soc.*, 2009, **131**, 5748–5750.

201   A. K. Ghosh and M. Brindisi, *J. Med. Chem.*, 2015, **58**, 2895–2940.

202   N. Agenet, C. Amatore, S. Gamez, H. Gérardin, A. Jutand, G. Meyer and C. Orthwein, *Arkivoc*, 2002, **2002**, 92.

203   J. T. Weiss, J. C. Dawson, C. Fraser, W. Rybski, C. Torres-Sánchez, M. Bradley, E. E. Patton, N. O. Carragher and A. Unciti-Broceta, *J. Med. Chem.*, 2014, **57**, 5395–5404.

204   D. C. Miller, G. J. Choi, H. S. Orbe and R. R. Knowles, *J. Am. Chem. Soc.*, 2015, **137**, 13492–13495.

205   J. T. Weiss, J. C. Dawson, K. G. Macleod, W. Rybski, C. Fraser, C. Torres-Sánchez, E. E. Patton, M. Bradley, N. O. Carragher and A. Unciti-Broceta, *Nat. Commun.*, 2014, **5**, 1–9.

206   B. Liu, H. Wang, T. Wang, Y. Bao, F. Du, J. Tian, Q. Li and R. Bai, *Chem. Commun.*, 2012, **48**, 2867–2869.

207   A. L. Garner, F. Song and K. Koide, *J. Am. Chem. Soc.*, 2009, **131**, 5163–5171.

208   M. A. Miller, B. Askevold, H. Mikula, R. H. Kohler, D. Pirovich and R. Weissleder, *Nat. Commun.*, 2017, **8**, 1–13.

209   R. Friedman Ohana, S. Levin, M. G. Wood, K. Zimmerman, M. L. Dart, M. K. Schwinn, T. A. Kirkland, R. Hurst, H. T. Uyeda, L. P. Encell and K. V. Wood, *ACS Chem. Biol.*, 2016, **11**, 2608–2617.

210   M. Jbara, *Org. Biomol. Chem.*, 2018, **16**, 8–11.

211   R. M. Yusop, A. Unciti-Broceta, E. M. V. Johansson, R. M. Sánchez-Martín and M.

Bradley, *Nat. Chem.*, 2011, **3**, 239–243.

212   J. Tsuji and T. Mandai, *Angew. Chemie Int. Ed. English*, 1995, **34**, 2589–2612.

213   L. N. Guo, X. H. Duan and Y. M. Liang, *Acc. Chem. Res.*, 2011, **44**, 111–122.

214   V. Franckevičius, *Tetrahedron Lett.*, 2016, **57**, 3586–3595.

215   C. C. Su, G. H. Lee, Y. Wang and J. T. Chen, *J. Am. Chem. Soc.*, 1994, **116**, 4999–5000.

216   S. Ma, *European J. Org. Chem.*, 2004, 1175–1183.

217   C. Amatore, G. Broeker, A. Jutand and F. Khalil, *J. Am. Chem. Soc.*, 1997, **119**, 5176–5185.

218   E. Janusson, H. S. Zijlstra, P. P. T. Nguyen, L. Macgillivray, J. Martelino and J. S. McIndoe, *Chem. Commun.*, 2017, **53**, 854–856.

219   X. Bei, H. W. Turner, W. H. Weinberg, A. S. Guram and J. L. Petersen, *J. Org. Chem.*, 1999, **64**, 6797–6803.

220   C. Colletto, J. Burés and I. Larrosa, *Chem. Commun.*, 2017, **53**, 12890–12893.

221   C. Amatore, A. Jutand, F. Khalil, M. A. M'Barki and L. Mottier, *Organometallics*, 1993, **12**, 3168–3178.

222   I. J. S. Fairlamb, A. R. Kapdi and A. F. Lee, *Org. Lett.*, 2004, **6**, 4435–4438.

223   C. Amatore, A. Jutand and A. Thuilliez, *J. Organometalic Chem.*, 2002, **643**, 416–423.

224   G. C. Lloyd-Jones, S. C. Stephen, I. J. S. Fairlamb, A. Martorell, B. Dominguez, P. M. Tomlin, M. Murray, J. M. Fernandez, J. C. Jeffery, T. Riis-Johannessen and T. Guerziz, *Pure Appl. Chem.*, 2007, **76**, 589–601.

225   M. Li, Z. Wu and S.-K. Tian, *Nanoscale*, 2014, **4**, 1–14.

226   Z. Wang, A. Ying, Z. Fan, C. Hervieu and L. Zhang, *ACS Catal.*, 2017, **7**, 3676–3680.

227   S. T. Heller and R. Sarpong, *Org. Lett.*, 2010, **12**, 4572–4575.

228   J. A. Baccile, M. A. Morrell, R. M. Falotico, B. T. Milliken, D. L. Drew and F. M. Rossi,

Tetrahedron Lett., 2012, **53**, 1933–1935.

229   M. Tamaki, V. J. Hruby and G. Han, *J. Pept. Researc*, 2001, **58**, 338–341.

230   A. M. Felix and M. H. Jirienez, *Anal. Biochem.*, 1973, **381**, 377–381.

231   W. Leimgruber, M. Weigele, S. Udenfriend, W. Dairman, P. Bohlen and S. Stein, *Science*, 1972, **178**, 871–872.

232   A. Inam, R. L. Van Zyl, N. J. Van Vuuren, C. T. Chen, F. Avecilla, S. M. Agarwal and A. Azam, *RSC Adv.*, 2015, **5**, 48368–48381.

233   B. Guilbert and S. L. Flitsch, *J. Chem. Soc. Perkin Trans. 1*, 1994, 1181–1186.

234   A. Dahan, T. Ashkenazi, V. Kuznetsov, S. Makievski, E. Drug, L. Fadeev, M. Bramson, S. Schokoroy, E. Rozenshine-Kemelmakher and M. Gozin, *J. Org. Chem.*, 2007, **72**, 2289–2296.

235   D. S. Coffey, M. K. N. Hawk, S. W. Pedersen, S. J. Ghera, P. G. Marler, P. N. Dodson and M. L. Lytle, *Org. Process Res. Dev.*, 2004, **8**, 945–947.

236   P. K. Pradhan, S. Dey, P. Jaisankar and V. S. Giri, *Synth. Commun.*, 2005, **35**, 913–922.

237   M. Z. Lu, C. Q. Wang and T. P. Loh, *Org. Lett.*, 2015, **17**, 6110–6113.

238   B. Biannic, J. J. Bozell and T. Elder, *Green Chem.*, 2014, **16**, 3635–3642.

239   K. A. Ahrendt, J. A. Olsen, M. Wakao, J. Trias and J. A. Ellman, *Bioorganic Med. Chem. Lett.*, 2003, **13**, 1683–1686.

240   Farhanullah, T. Kang, E. J. Yoon, E. C. Choi, S. Kim and J. Lee, *Eur. J. Med. Chem.*, 2009, **44**, 239–250.

241   J. W. Lee and P. L. Fuchs, *Org. Lett.*, 1999, **1**, 179–182.

242   D. C. Batesky, M. J. Goldfogel and D. J. Weix, *J. Org. Chem.*, 2017, **82**, 9931–9936.

243   T. Huang, K. Anselme, S. Sarrailh and A. Ponche, *Int. J. Pharm.*, 2016, **497**, 54–61.

244   M. Umrethia, V. L. Kett, G. P. Andrews, R. K. Malcolm and A. D. Woolfson, *J. Pharm.*

Biomed. Anal., 2010, **51**, 1175–1179.

245   P. K. Smith, R. I. Krohn, G. T. Hermanson, A. K. Mallia, F. H. Gartner, M. D. Provenzano, E. K. Fujimoto, N. M. Goeke, B. J. Olson and D. C. Klenk, *Anal. Biochem.*, 1985, **150**, 76–85.

246   K. J. Wiechelman, R. D. Braun and J. D. Fitzpatrick, *Anal. Biochem.*, 1988, **175**, 231–237.

247   F. Al-Rimawi, *Int. Res. J. Pure Appl. Chem.*, 2014, 4, 585–593.

248   M. De Frutos, A. Cifuentes, J. C. Díez-Masa, E. Camafeita and E. Méndez, *HRC J. High Resolut. Chromatogr.*, 1998, **21**, 18–24.

249   M. Hamidi and N. Zarei, *Drug Test. Anal.*, 2009, **1**, 214–218.

250   G. L. Ellman, *Am. J. Anal. Chem.*, 1959, **82**, 70–77.

251   R. H. L. JOZEF SEDLAK, *Anal. Biochem.*, 1968, **25**, 192–205.

252   R. L. Blakeley and B. Zerner, *Methods in Enzymology*, 1983, **91**, 49–60.

253   C. Kuttner, M. Tebbe, H. Schlaad, I. Burgert and A. Fery, *ACS Appl. Mater. Interfaces*, 2012, **4**, 3484–3492.

254   J. A. Neal, D. Mozhdehi and Z. Guan, *J Am Chem Soc.*, 2015, **137**, 4846-4850.

255   Y. Jhillu Singh, G. Rao Yarrapothu and R. Vemula, *RSC Adv.*, 2013, **3**, 55–58.

256   A. Larkem and H. Larkem, *Indian J. Chem. - Sect. B Org. Med. Chem.*, 2002, **41**, 175–180.

257   Z. Xu, J. C. DiCesare and P. W. Baures, *J. Comb. Chem.*, 2010, **12**, 248–254.

258   D. C. Miller, G. J. Choi, H. S. Orbe and R. R. Knowles, *J. Am. Chem. Soc.*, 2015, **137**, 13492–13495.

259   H. K. Kim and A. Lee, *Org. Biomol. Chem.*, 2016, **14**, 7345–7353.

260   R. Ramesh, Y. Chandrasekaran, R. Megha and S. Chandrasekaran, *Tetrahedron*, 2007, **63**, 9153–9162.

261 T. Tanaka, N. Okamura, K. Bannai, A. Hazato, S. Sugiura, K. Tomimori, K. Manabe and S. Kurozumi, *Tetrahedron*, 1986, **42**, 6747–6758.

262 M. Suchý, R. Bartha and R. H. E. Hudson, *RSC Adv.*, 2013, **3**, 3249–3259.

263 R. A. T. M. van Benthem, H. Hiemstra and W. N. Speckamp, *J. Org. Chem.*, 1992, **57**, 6083–6085.

Chapter 6: Appendix
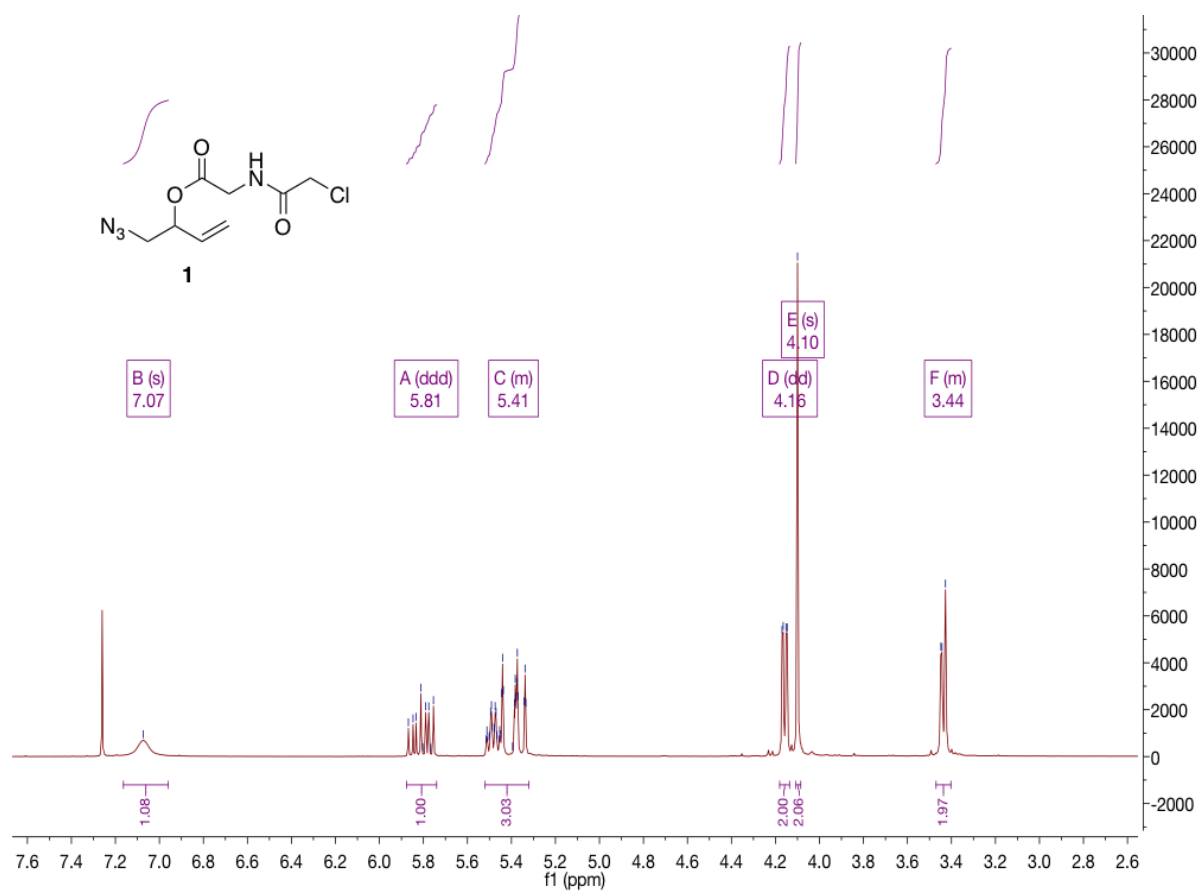
(A) ^{1}H NMR spectrum of 1-azidobut-3-en-2-yl (2-chloroacetyl)glycinate **1**.
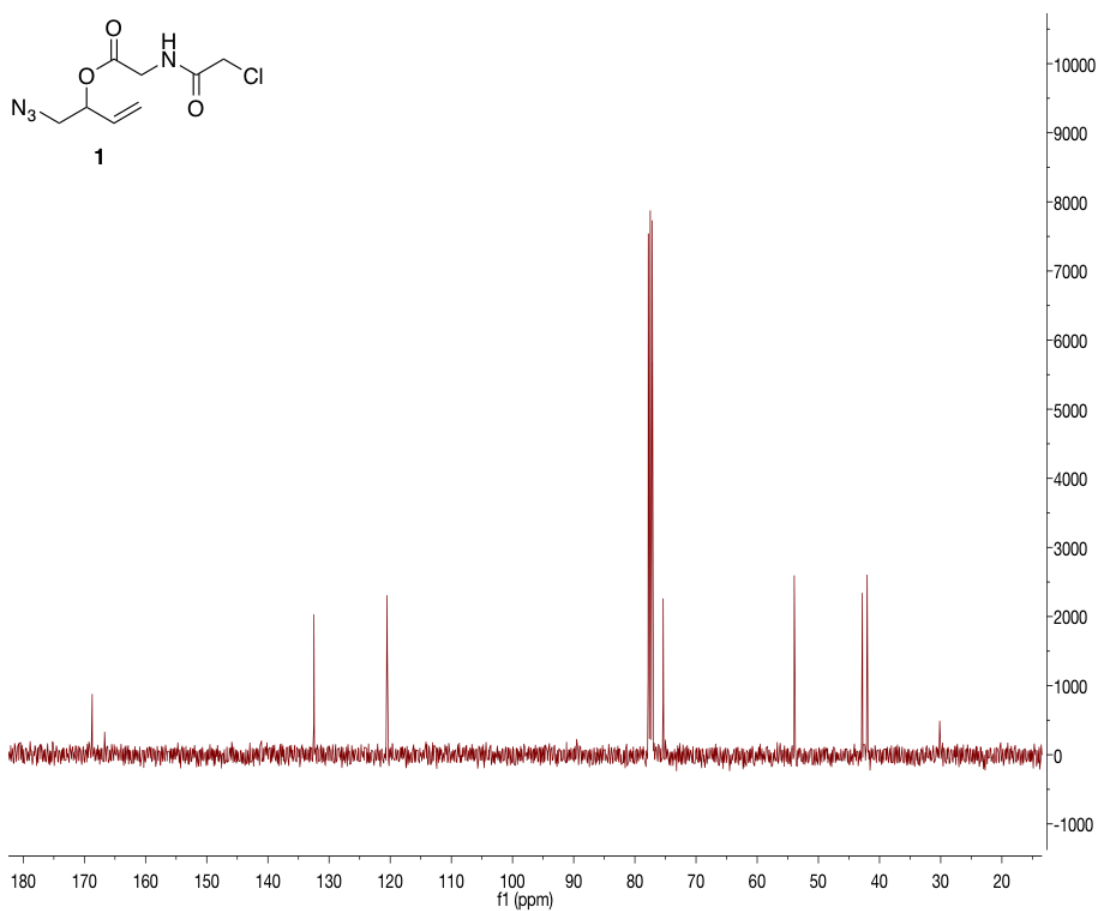
(B) ^{13}C NMR spectrum of 1-azidobut-3-en-2-yl (2-chloroacetyl)glycinate **1**.
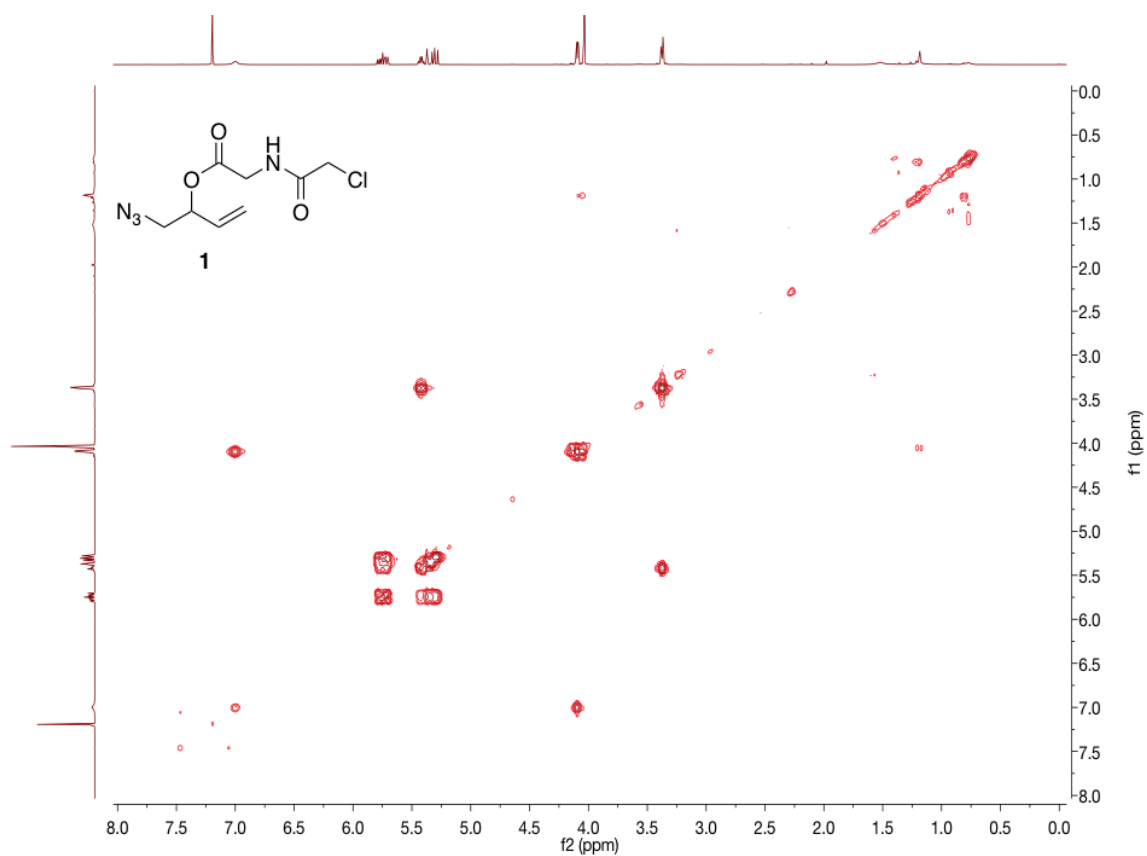
(C) COSY NMR spectrum of 1-azidobut-3-en-2-yl (2-chloroacetyl)glycinate **1**.

Figure 101: NMR spectra of 1-azidobut-3-en-2-yl (2-chloroacetyl)glycinate **1**.
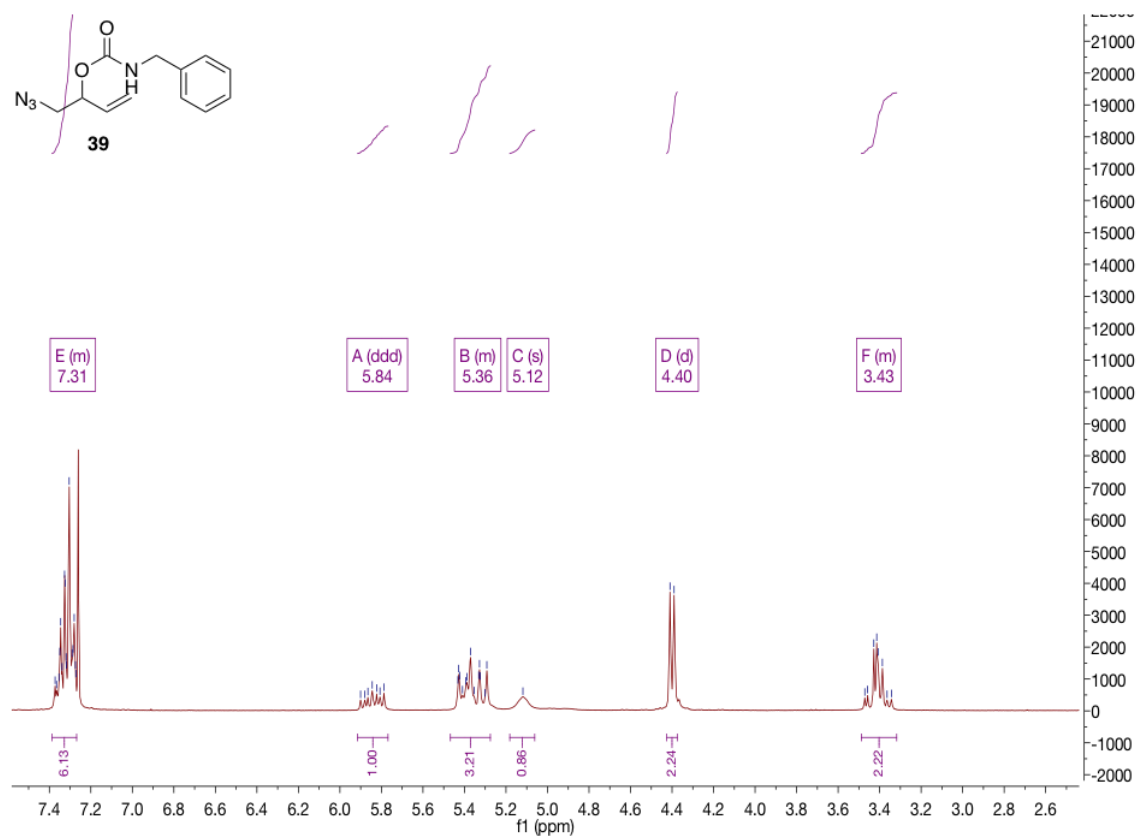
(A) ^{1}H NMR spectrum of 1-azidobut-3-en-2-yl benzylcarbamate **39**.
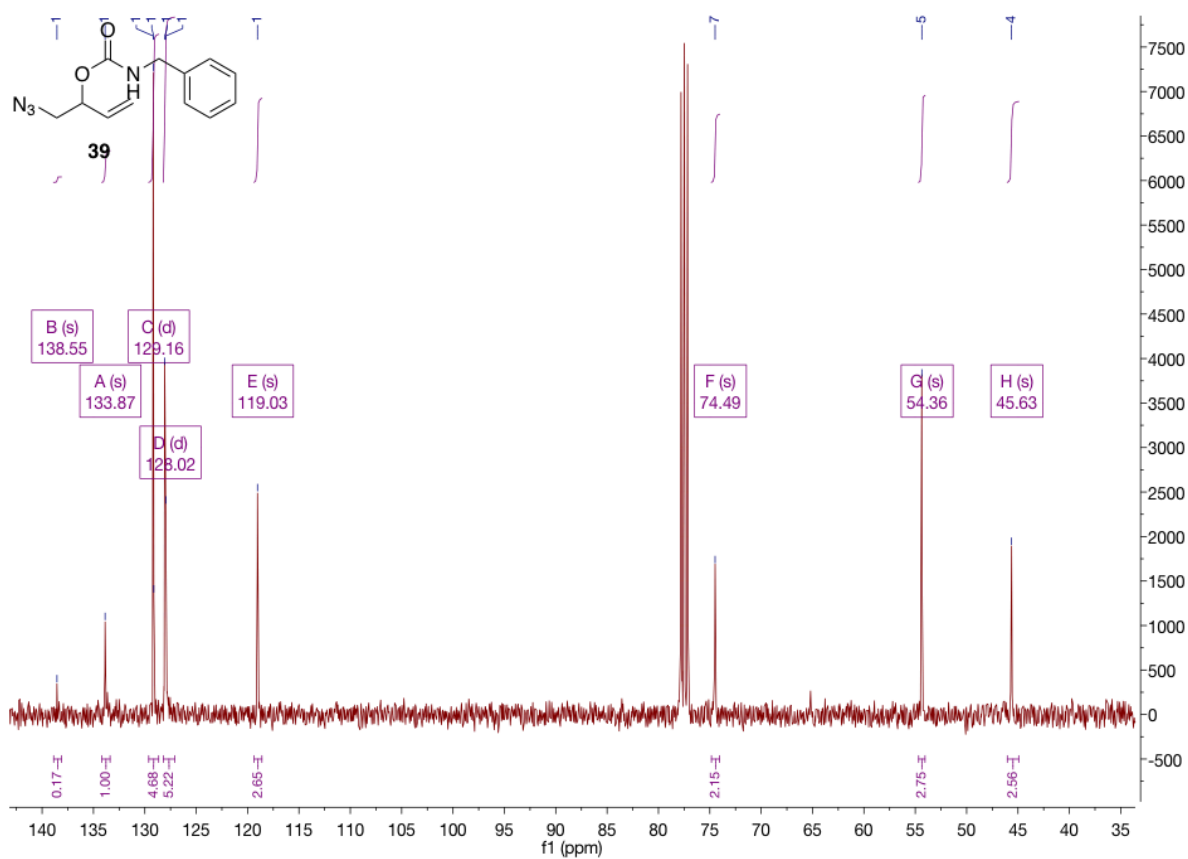
(B) ^{13}C NMR spectrum of 1-azidobut-3-en-2-yl benzylcarbamate **39**.

Figure 102: NMR spectra of 1-azidobut-3-en-2-yl benzylcarbamate **39**.
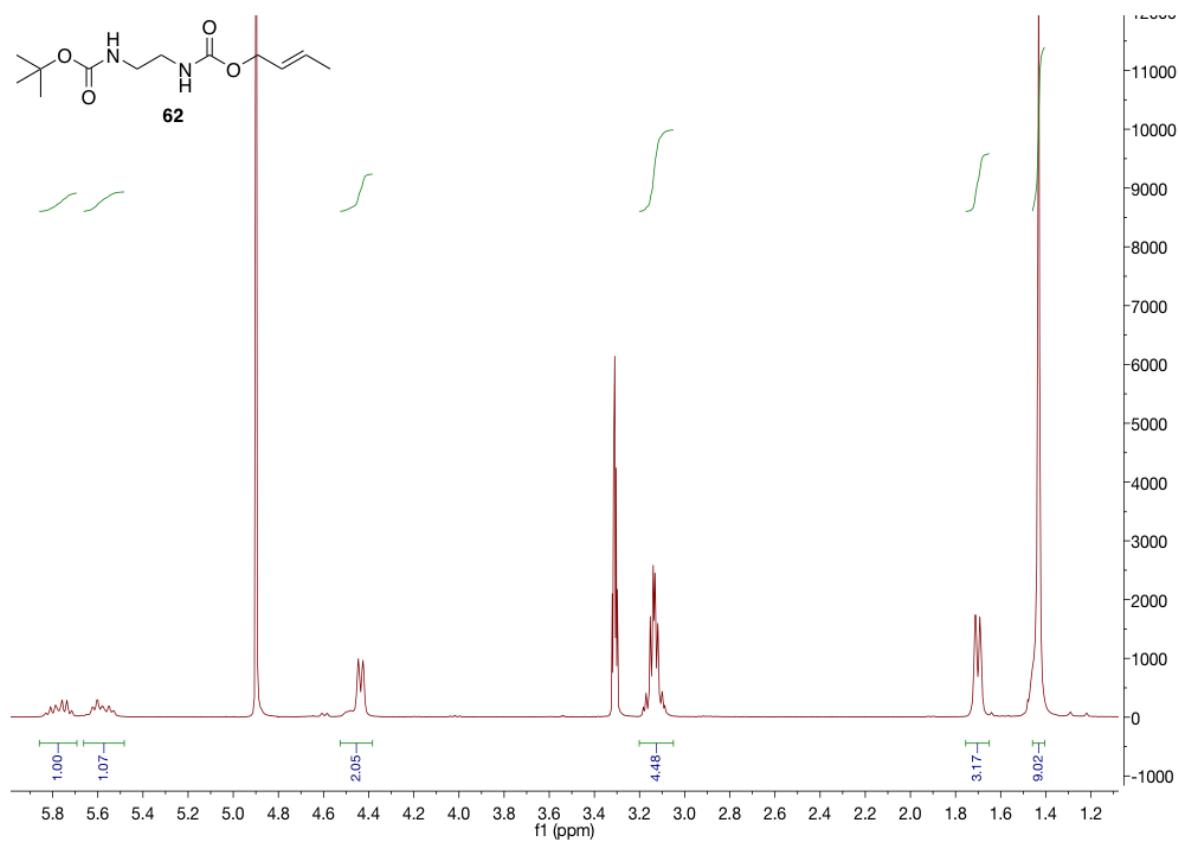
(A) ^{1}H NMR spectrum of (E)-but-2-en-1-yl *tert*-butyl ethane-1,2-diyldicarbamate **62**.
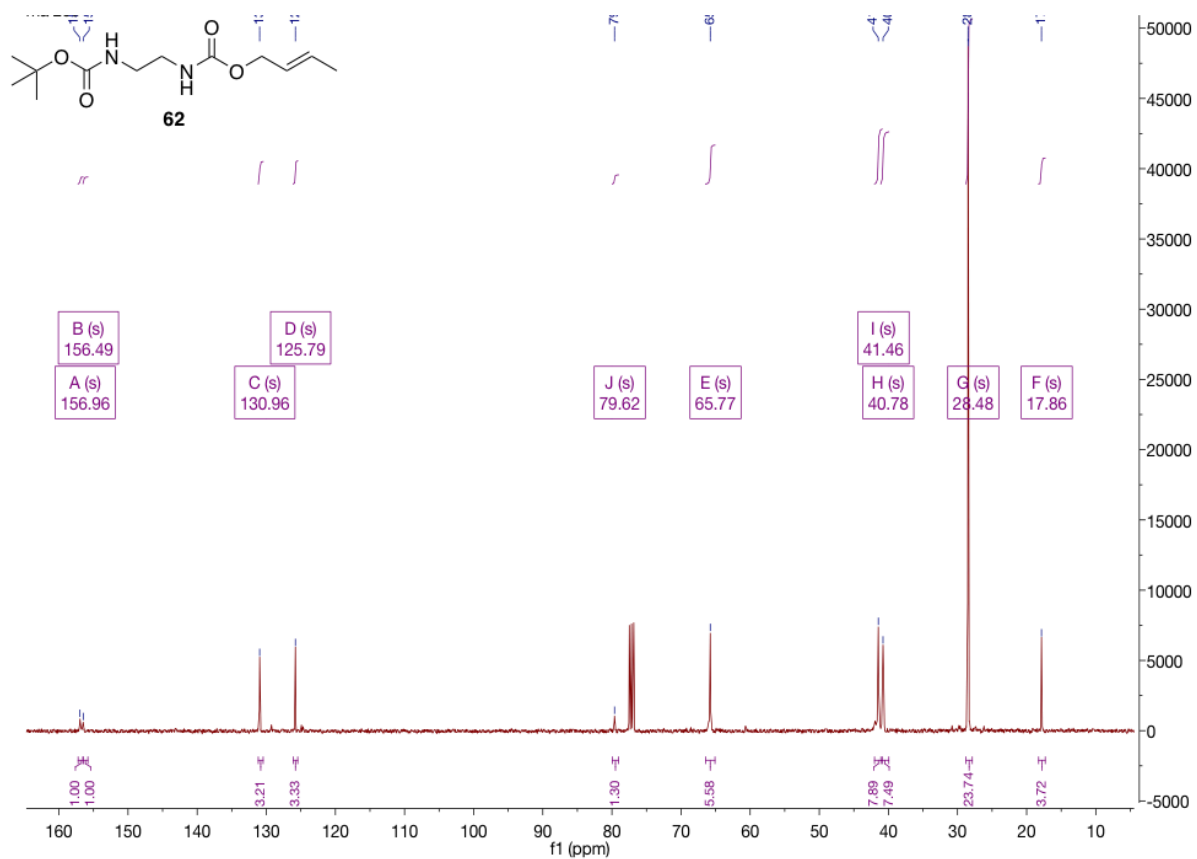
(B) ^{13}C NMR spectrum of (*E*)-but-2-en-1-yl *tert*-butyl ethane-1,2-diyldicarbamate **62**.
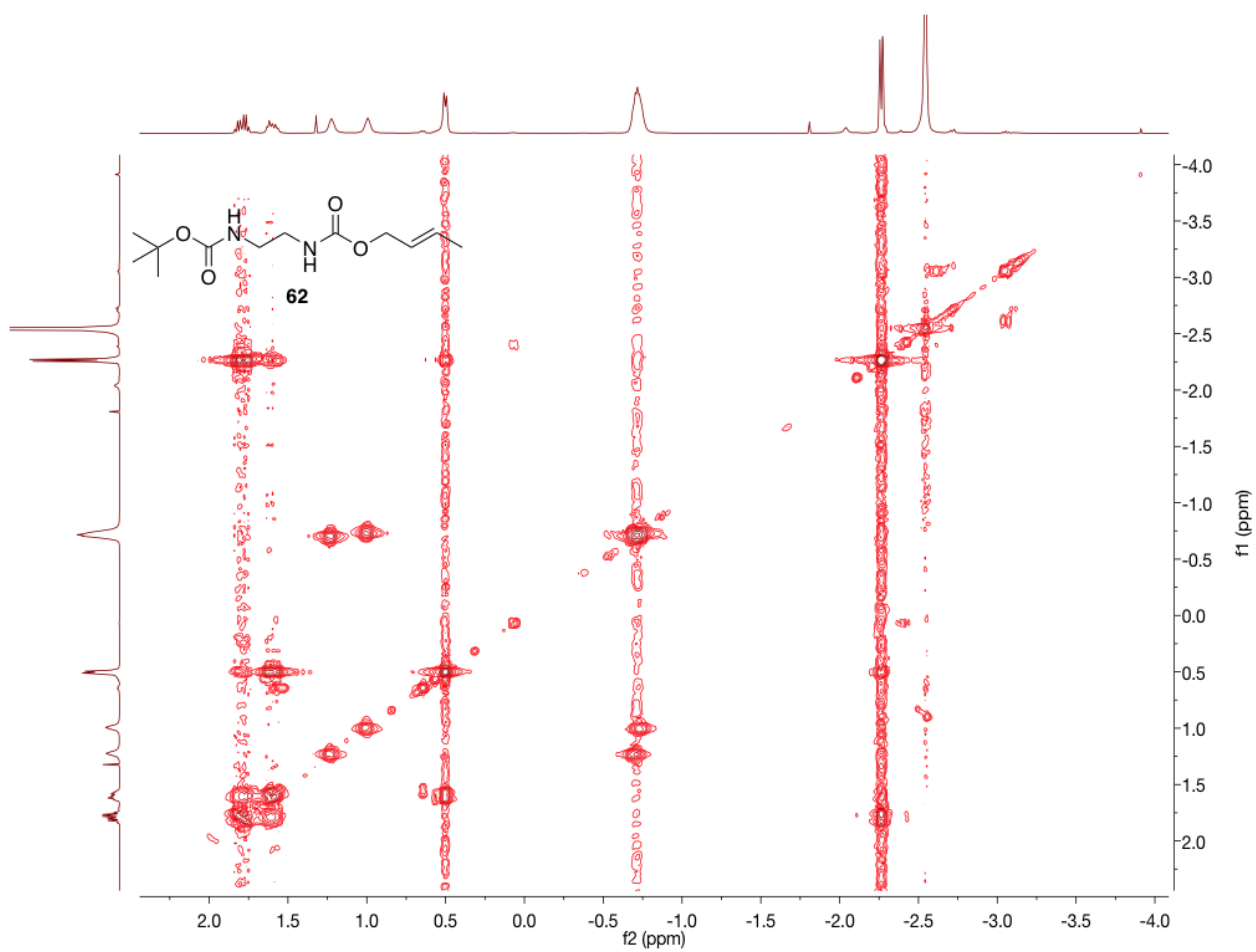
(C) COSY NMR spectrum of (*E*)-but-2-en-1-yl *tert*-butyl ethane-1,2-diyldicarbamate **62**.

Figure 103: NMR spectra of (*E*)-but-2-en-1-yl *tert*-butyl ethane-1,2-diyldicarbamate **62**.
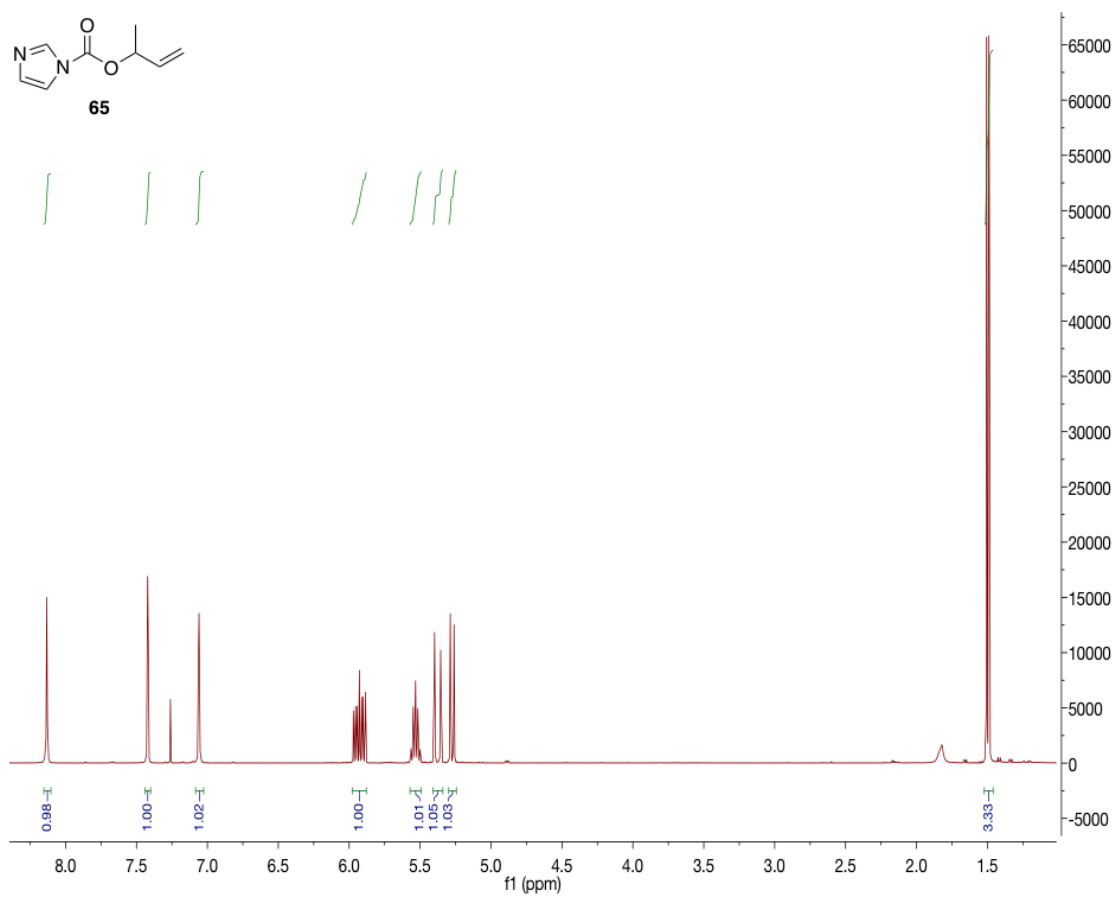
(A) ^{1}H NMR spectrum of But-3-en-2-yl 1*H*-imidazole-1-carboxylate **65**.
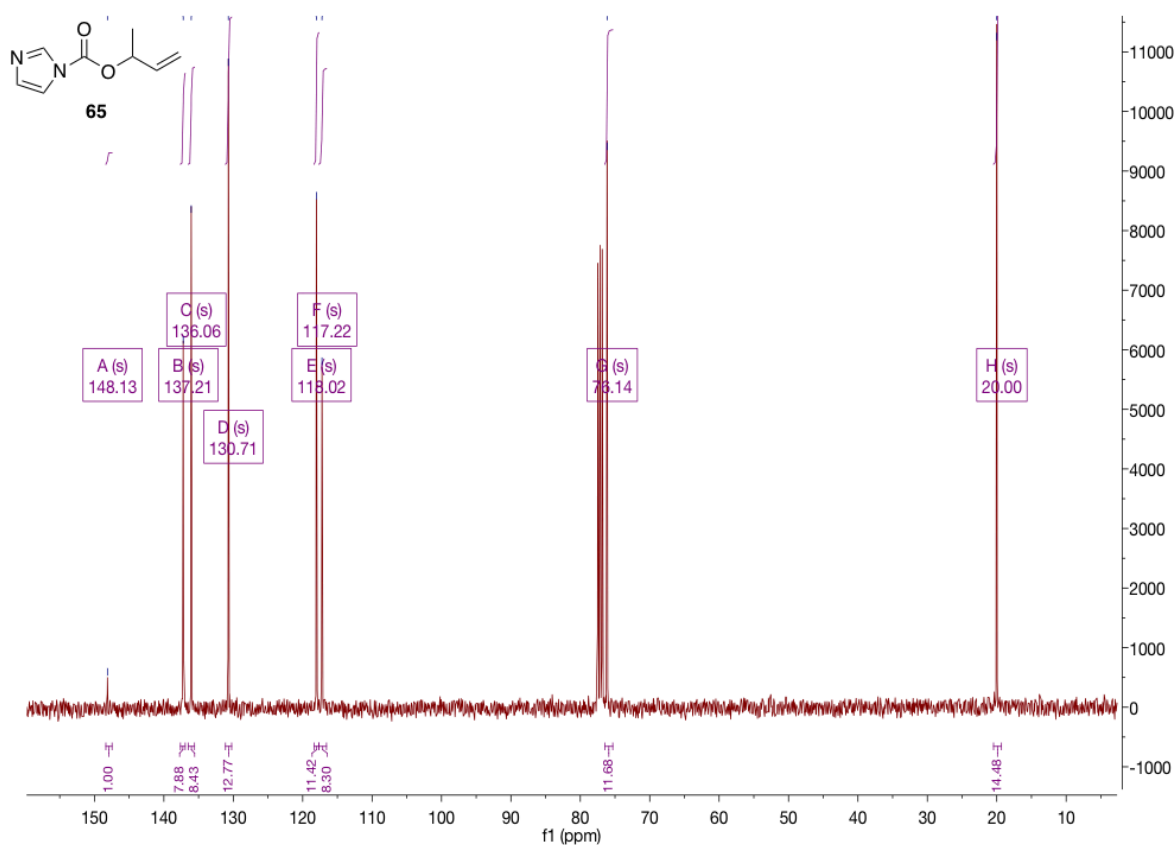
(B) ^{13}C NMR spectrum of But-3-en-2-yl 1*H*-imidazole-1-carboxylate **65**.
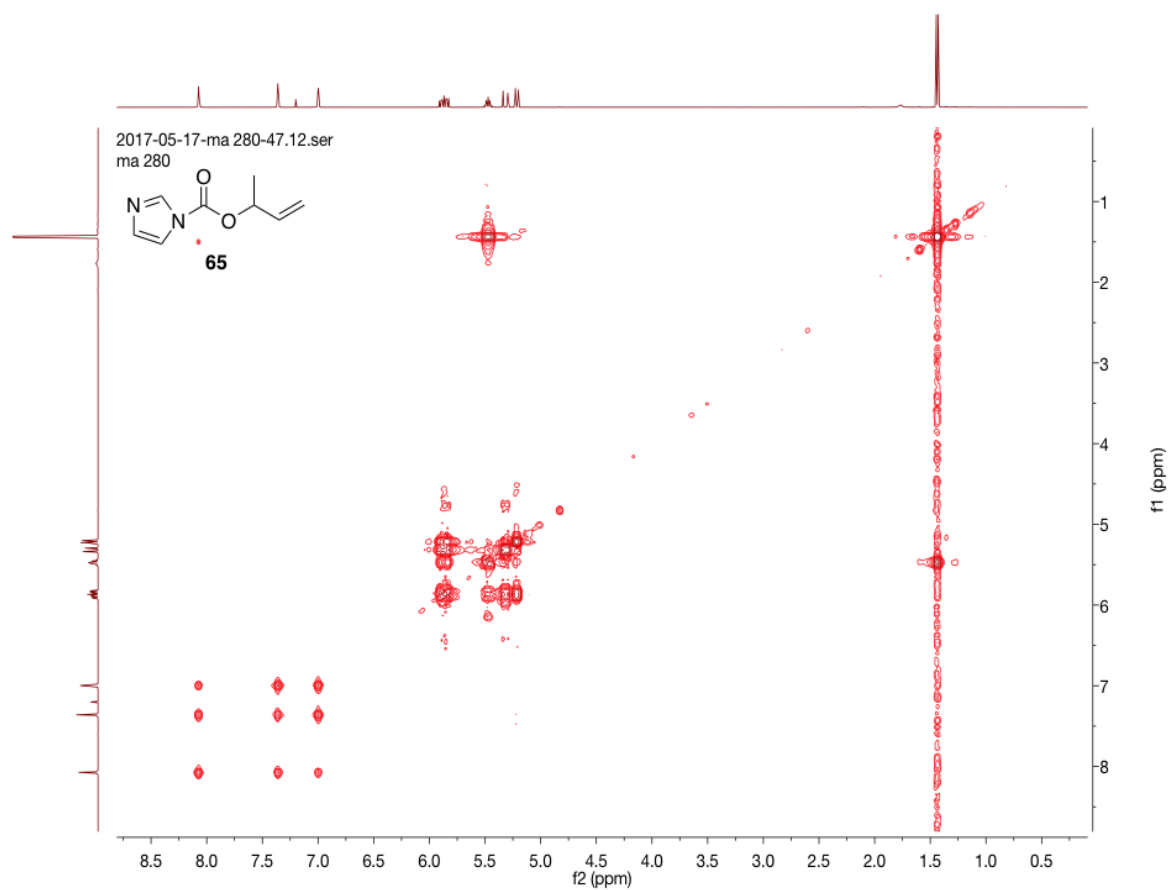
(A) COSY NMR spectrum of But-3-en-2-yl 1H-imidazole-1-carboxylate **65**.

Figure 104: NMR spectra of But-3-en-2-yl 1H-imidazole-1-carboxylate **65**.
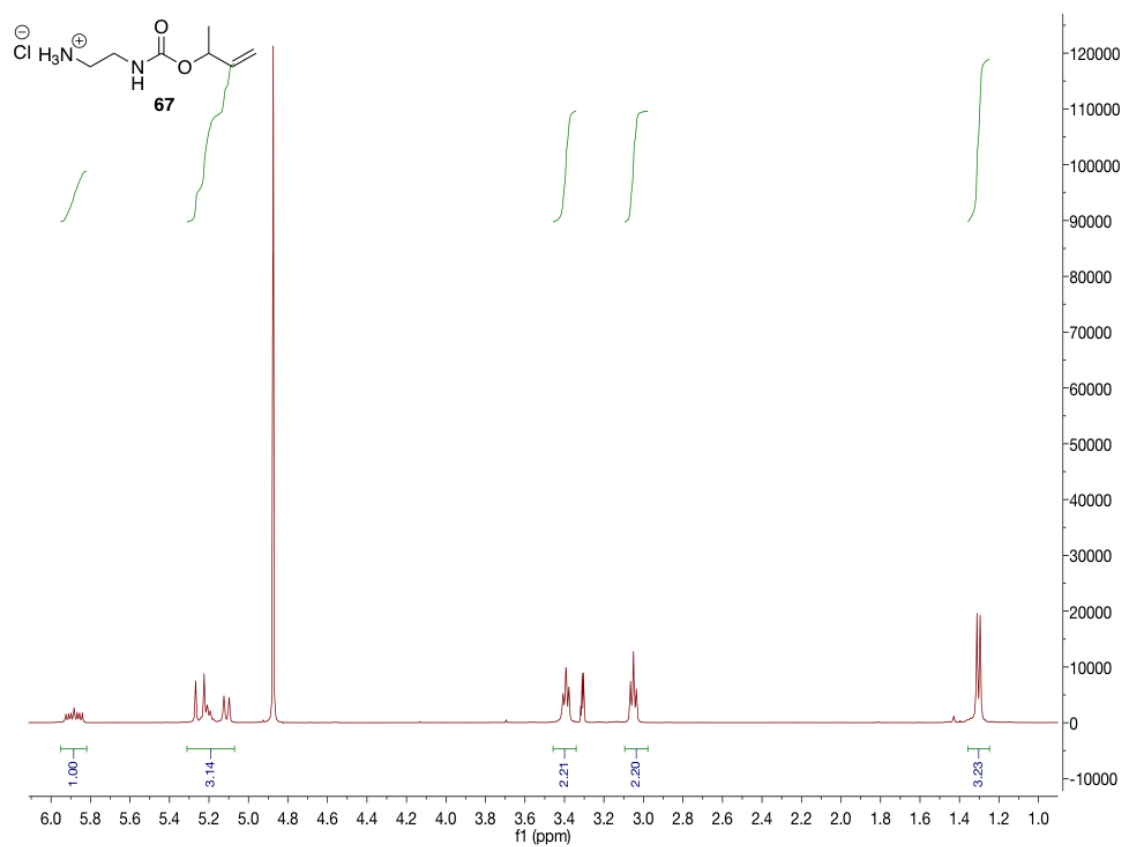
(A) ^{1}H NMR spectrum of 2-(((but-3-en-2-yloxy)carbonyl)amino)ethan-1-aminium **67**.
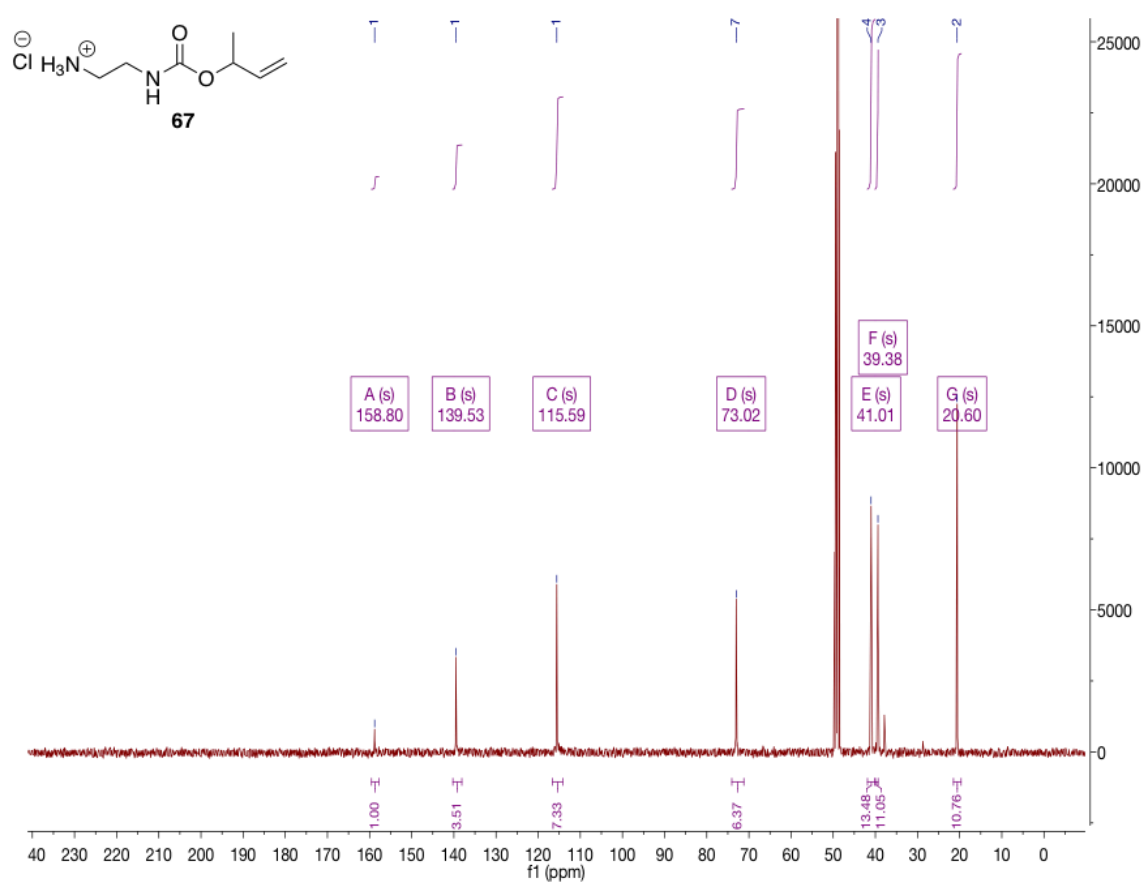
(B) ^{13}C NMR spectrum of 2-(((but-3-en-2-yloxy)carbonyl)amino)ethan-1-aminium **67**.
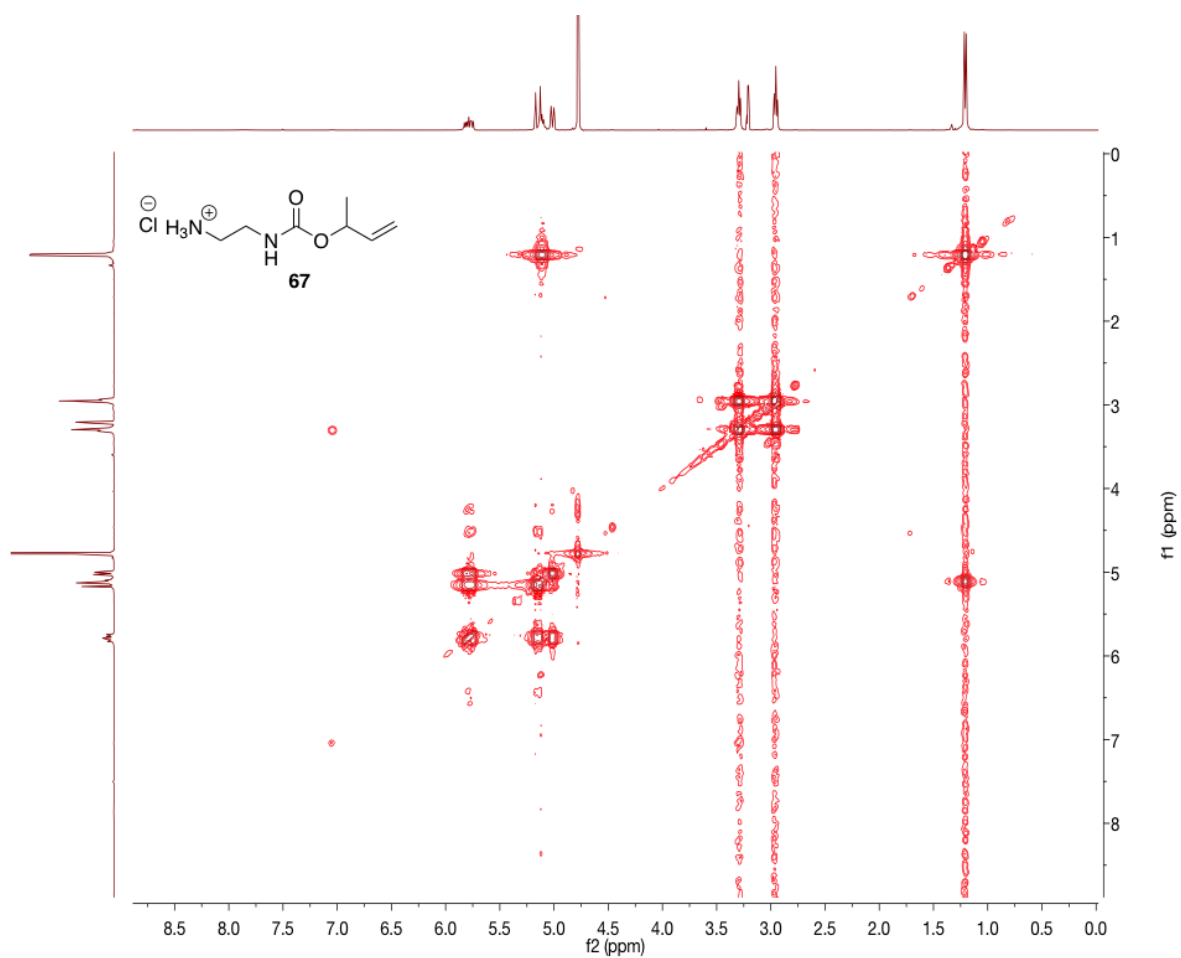
(C) COSY NMR spectrum of 2-(((but-3-en-2-yloxy)carbonyl)amino)ethan-1-aminium **67**.

Figure 105: NMR spectra of 2-(((but-3-en-2-yloxy)carbonyl)amino)ethan-1-aminium **67**.
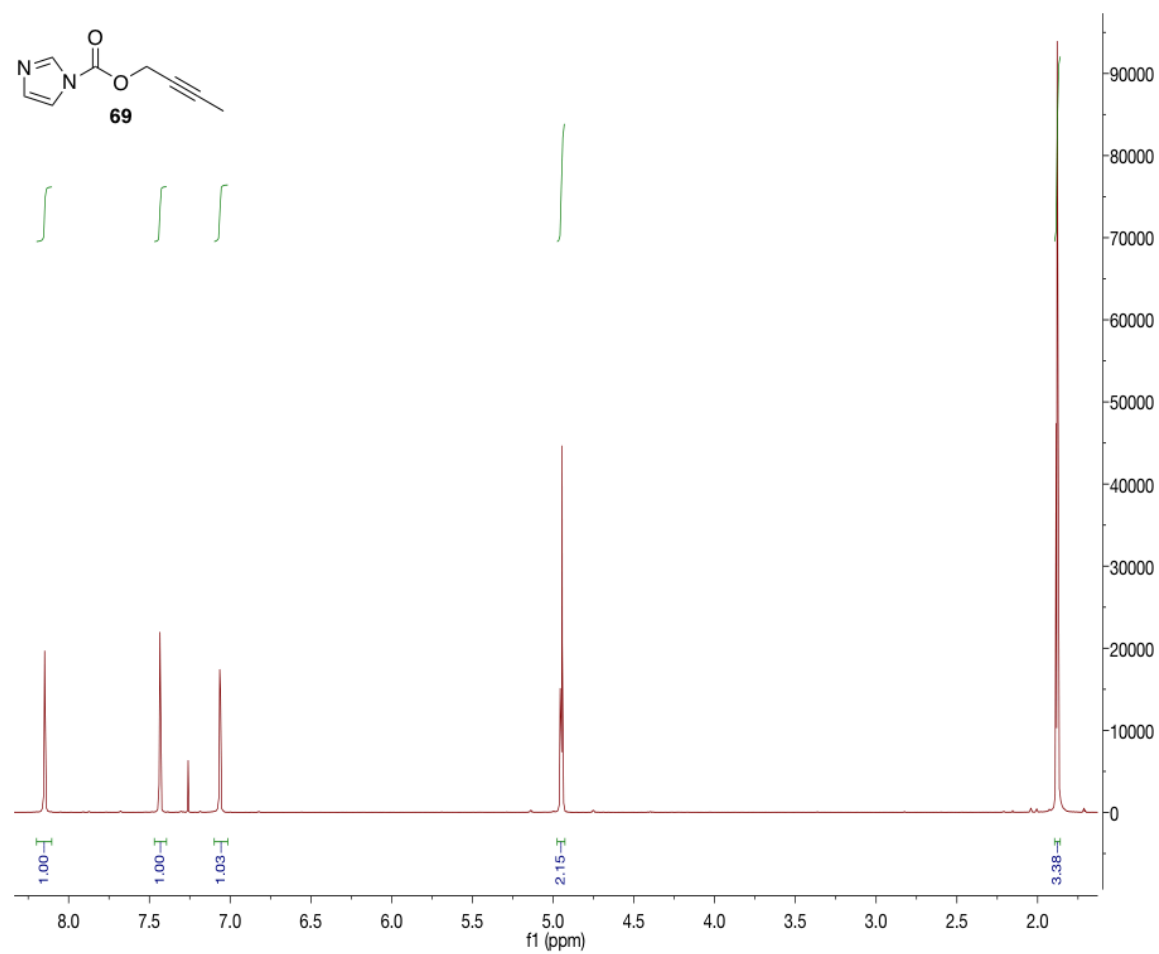
(B) ^{1}H NMR spectrum of But-2-yn-1-yl 1*H*-imidazole-1-carboxylate **69**.
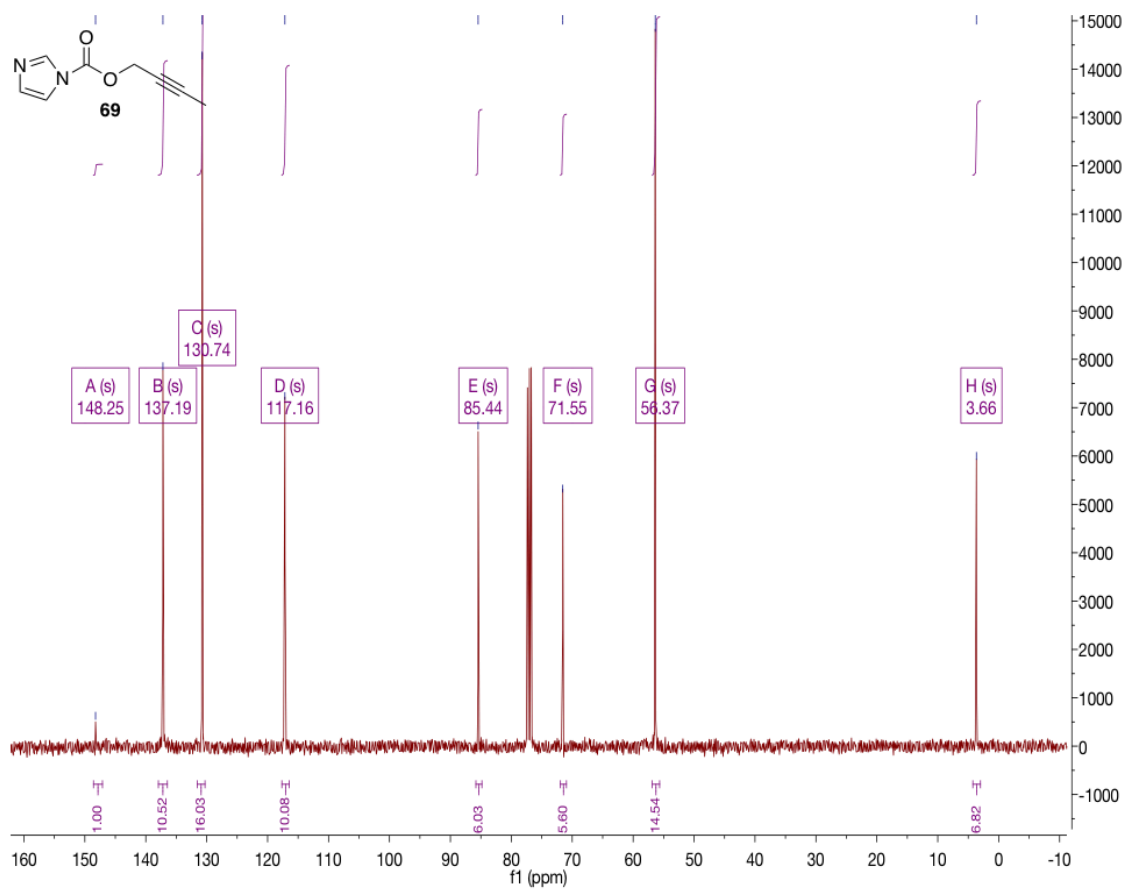
(C) ^{13}C NMR spectrum of But-2-yn-1-yl 1*H*-imidazole-1-carboxylate **69**.

Figure 106: NMR spectra of But-2-yn-1-yl 1*H*-imidazole-1-carboxylate **69**.
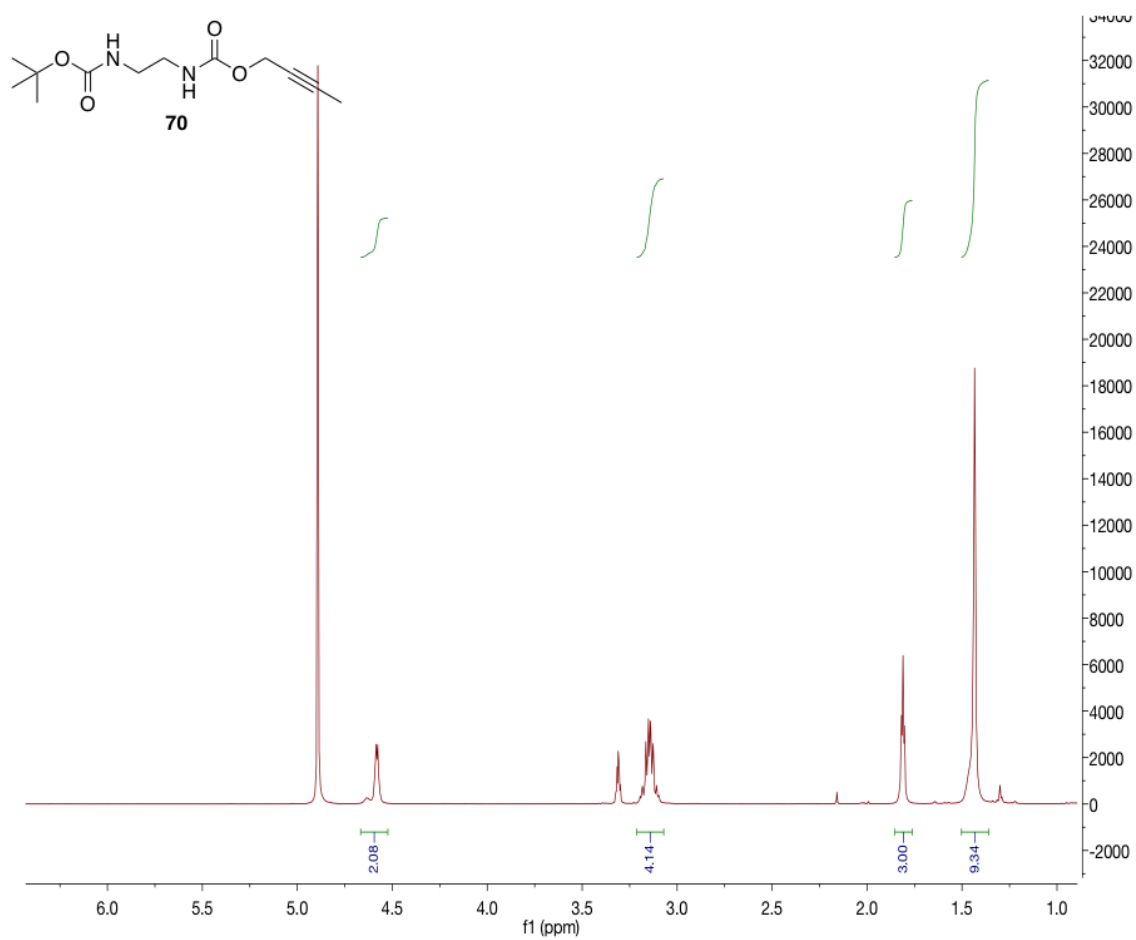
(A) ^{1}H NMR spectrum of But-2-yn-1-yl *tert*-butyl ethane-1,2-diyldicarbamate **70**.
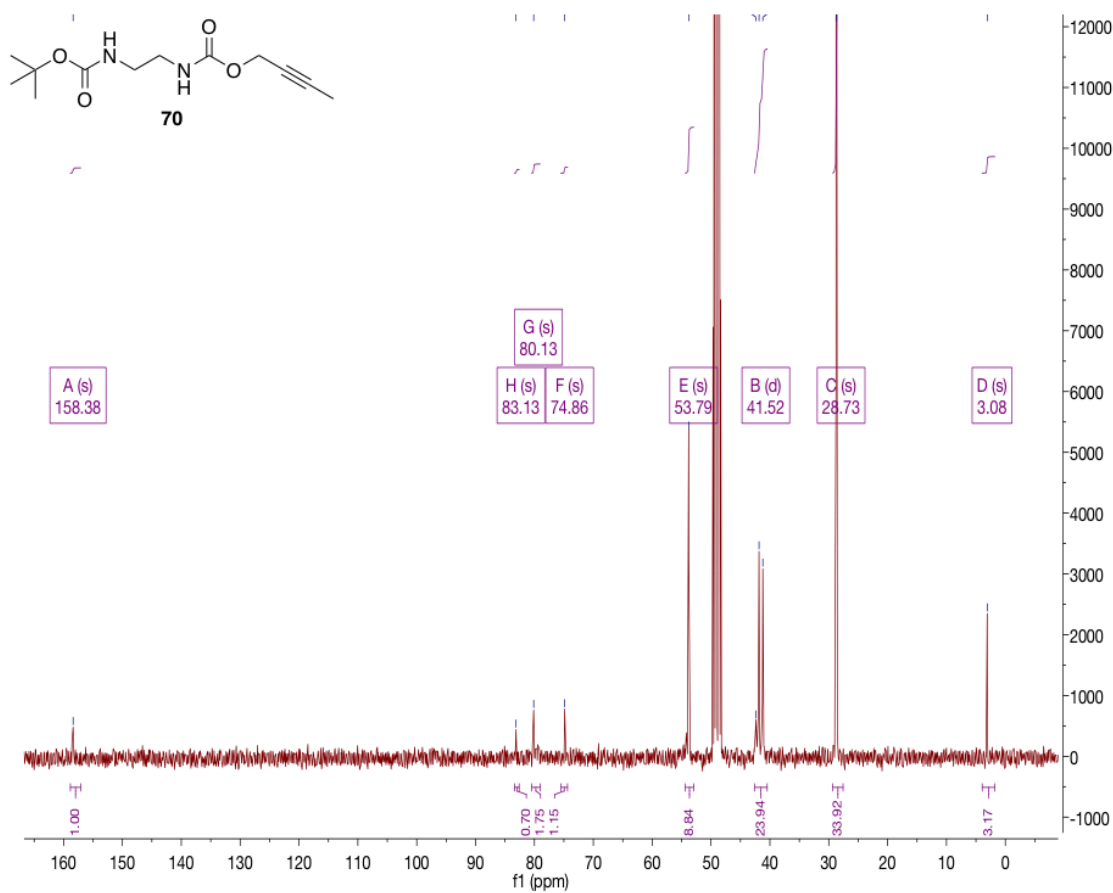
(B) ^{13}C NMR spectrum of But-2-yn-1-yl *tert*-butyl ethane-1,2-diyldicarbamate **70**.
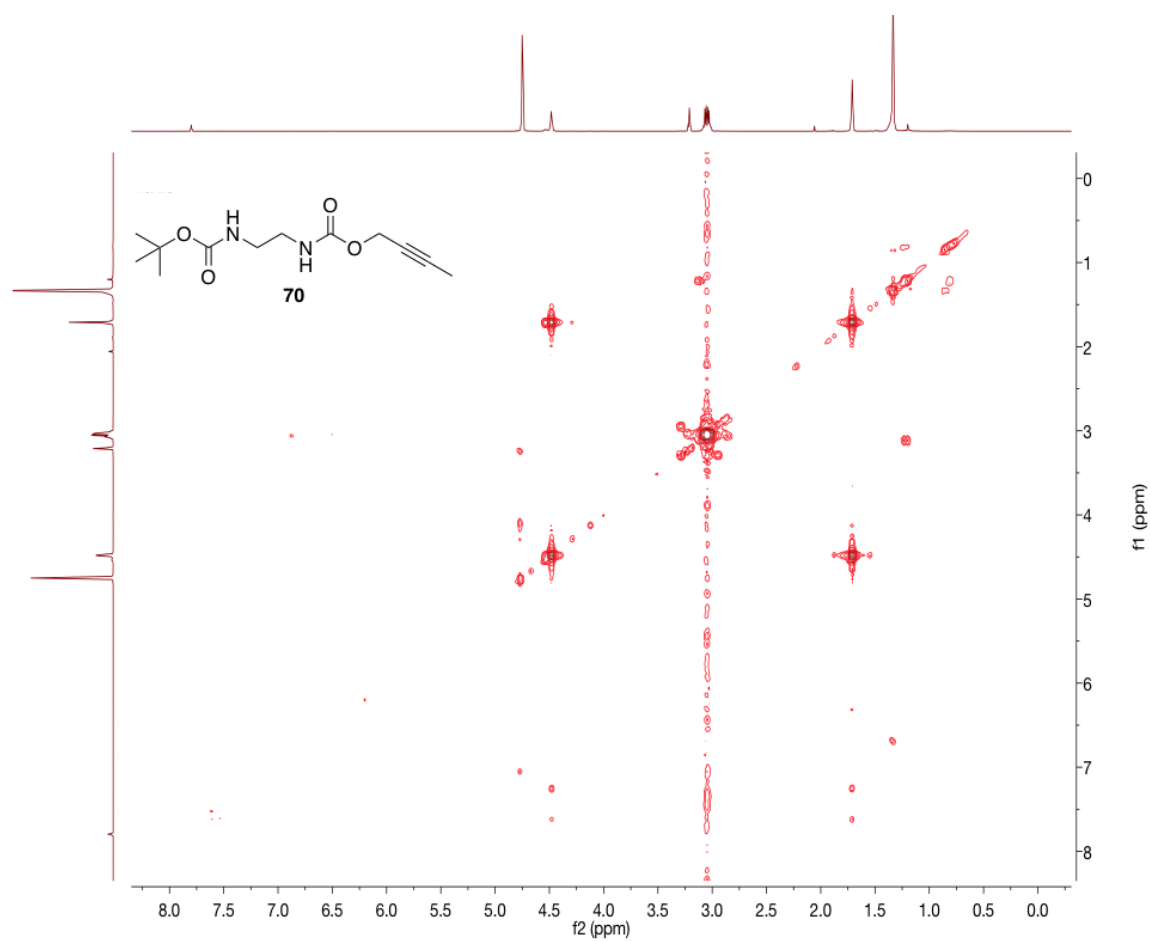
(C) COSY NMR spectrum of But-2-yn-1-yl *tert*-butyl ethane-1,2-diyldicarbamate **70**.

Figure 107: NMR spectra of But-2-yn-1-yl *tert*-butyl ethane-1,2-diyldicarbamate **70**.
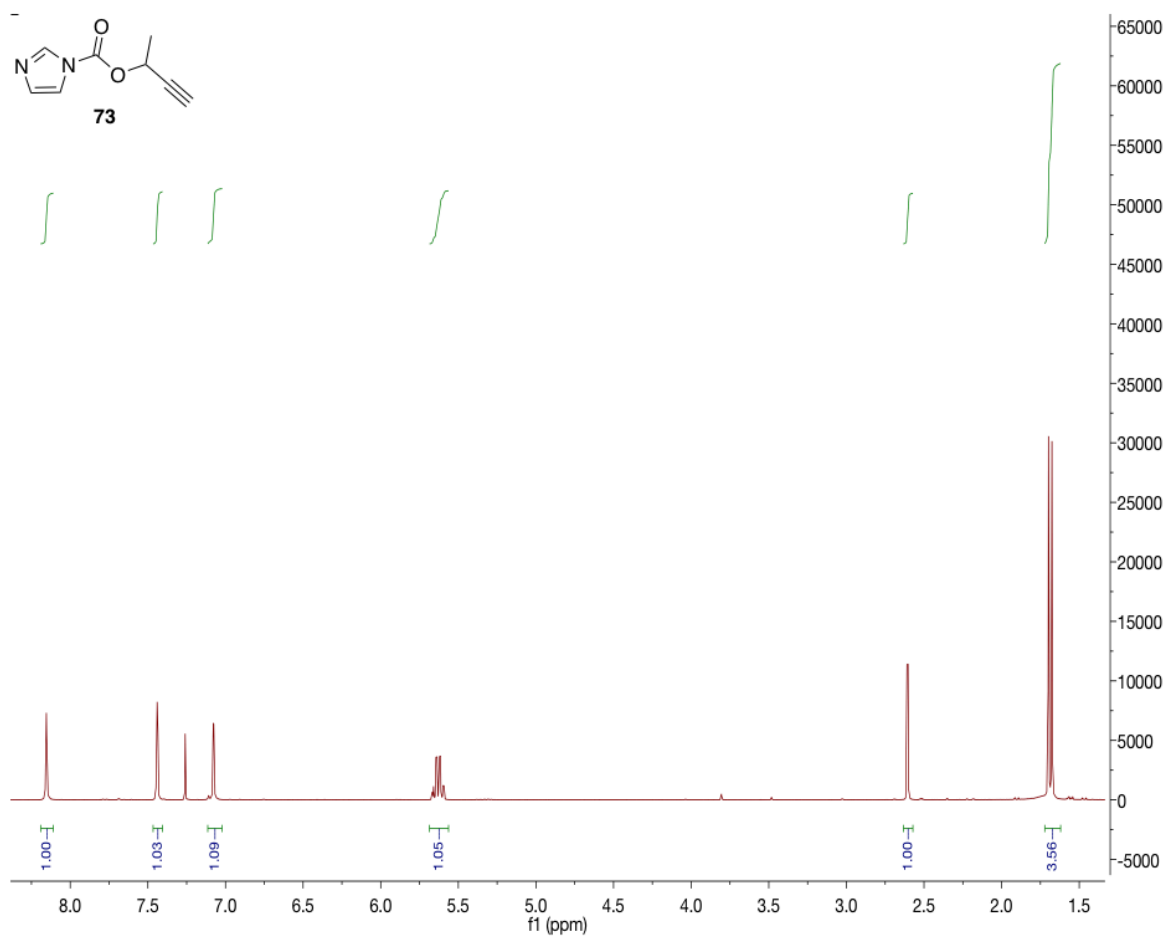
(A) ^{1}H NMR spectrum of But-3-yn-2-yl 1H-imidazole-1-carboxylate **73**.
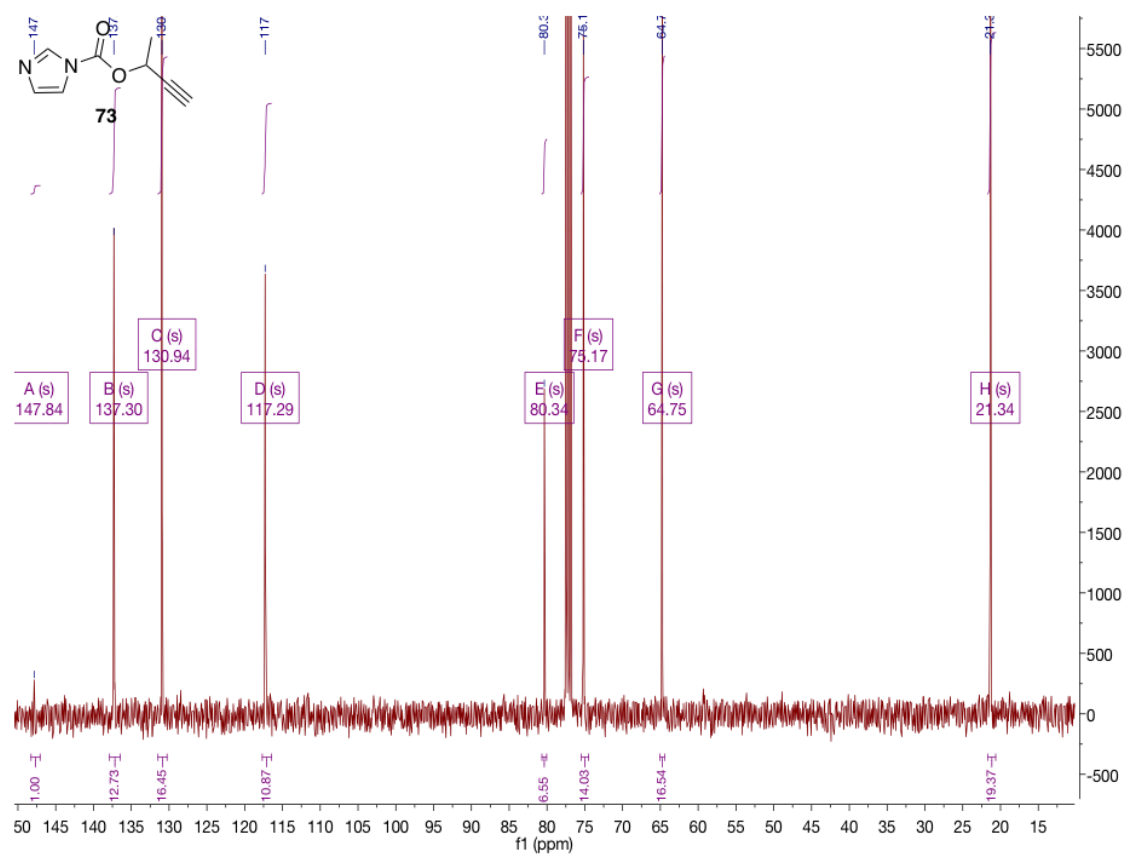
(B) ^{13}C NMR spectrum of But-3-yn-2-yl 1*H*-imidazole-1-carboxylate **73**.
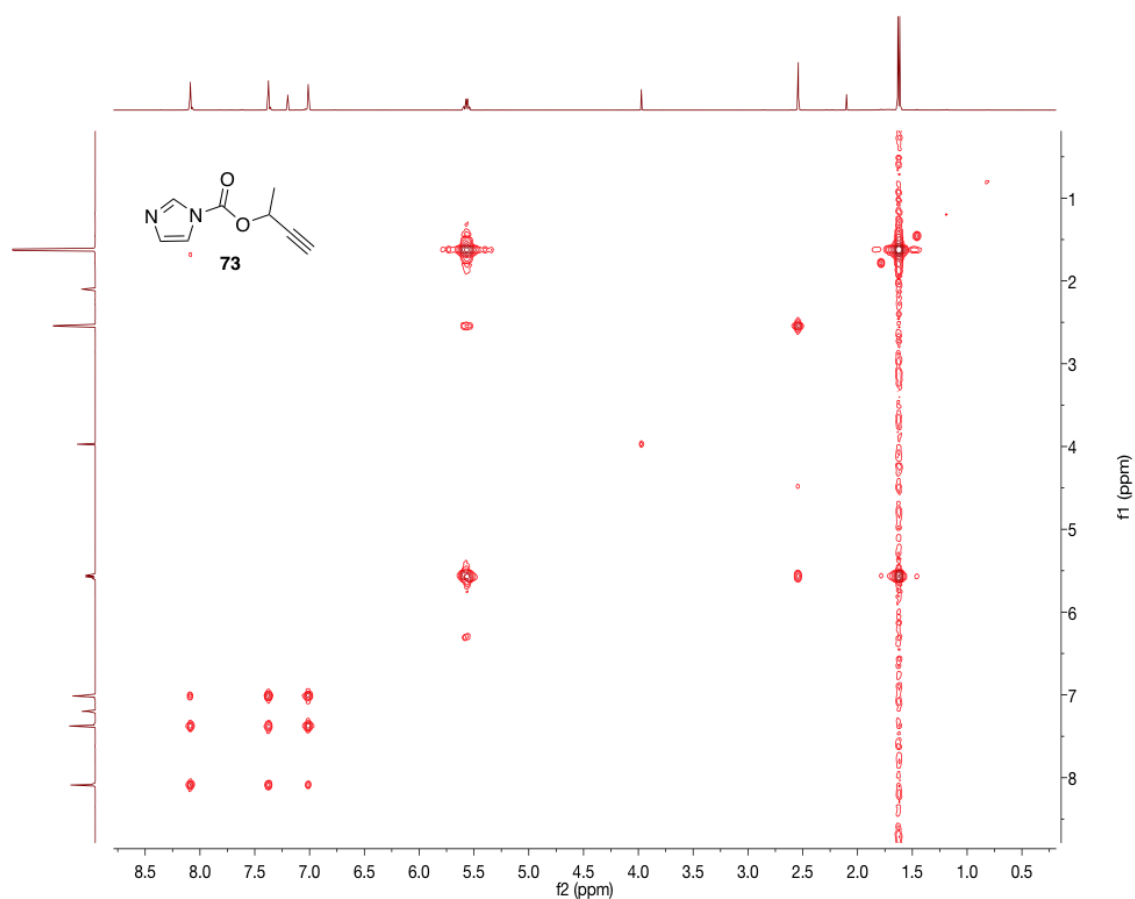
(C) COSY NMR spectrum of But-3-yn-2-yl 1*H*-imidazole-1-carboxylate **73**.

Figure 108: NMR spectra of But-3-yn-2-yl 1*H*-imidazole-1-carboxylate **73**.

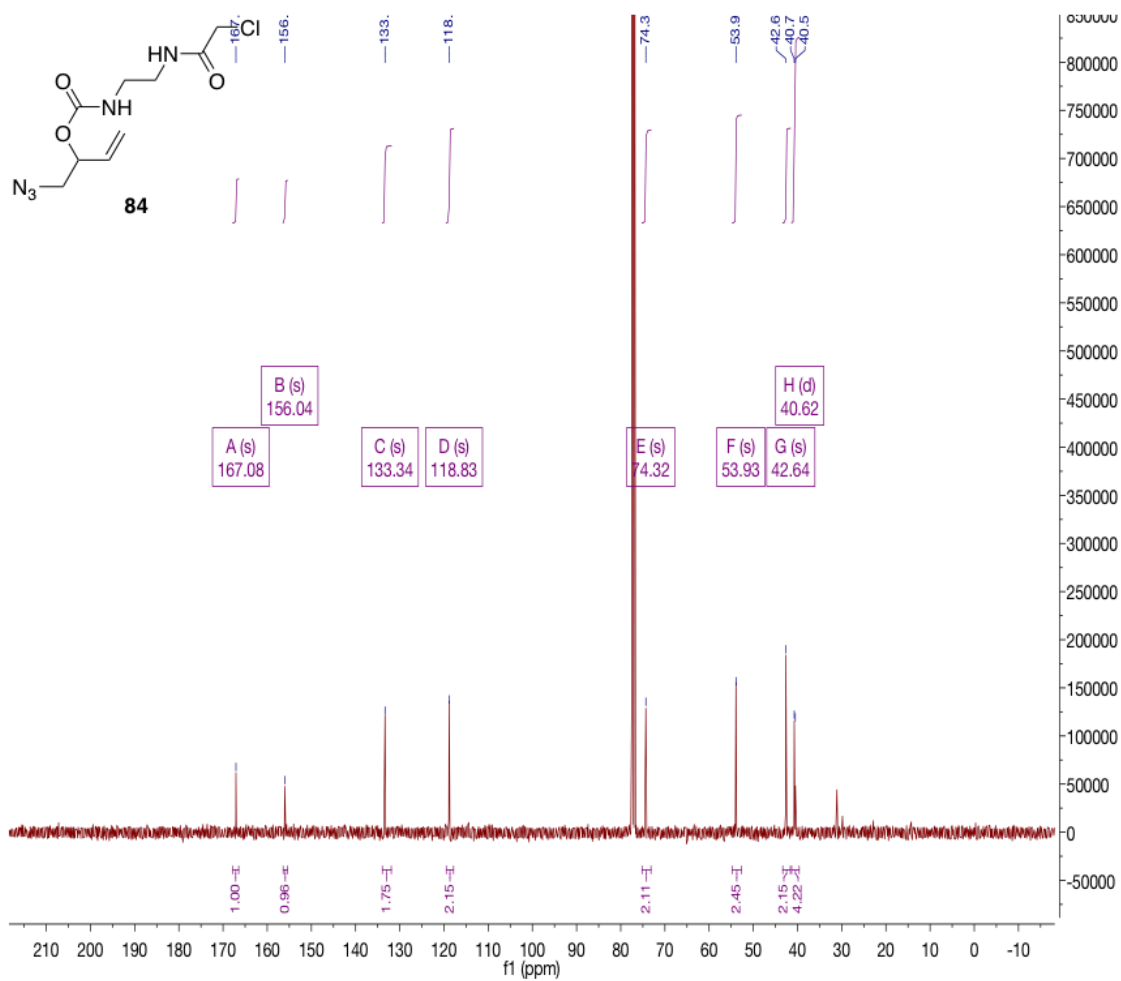(A) ^{1}H NMR spectrum of 1-aminobut-3-en-2-yl (2-(2-chloroacetamido)ethyl)carbamate **80**.
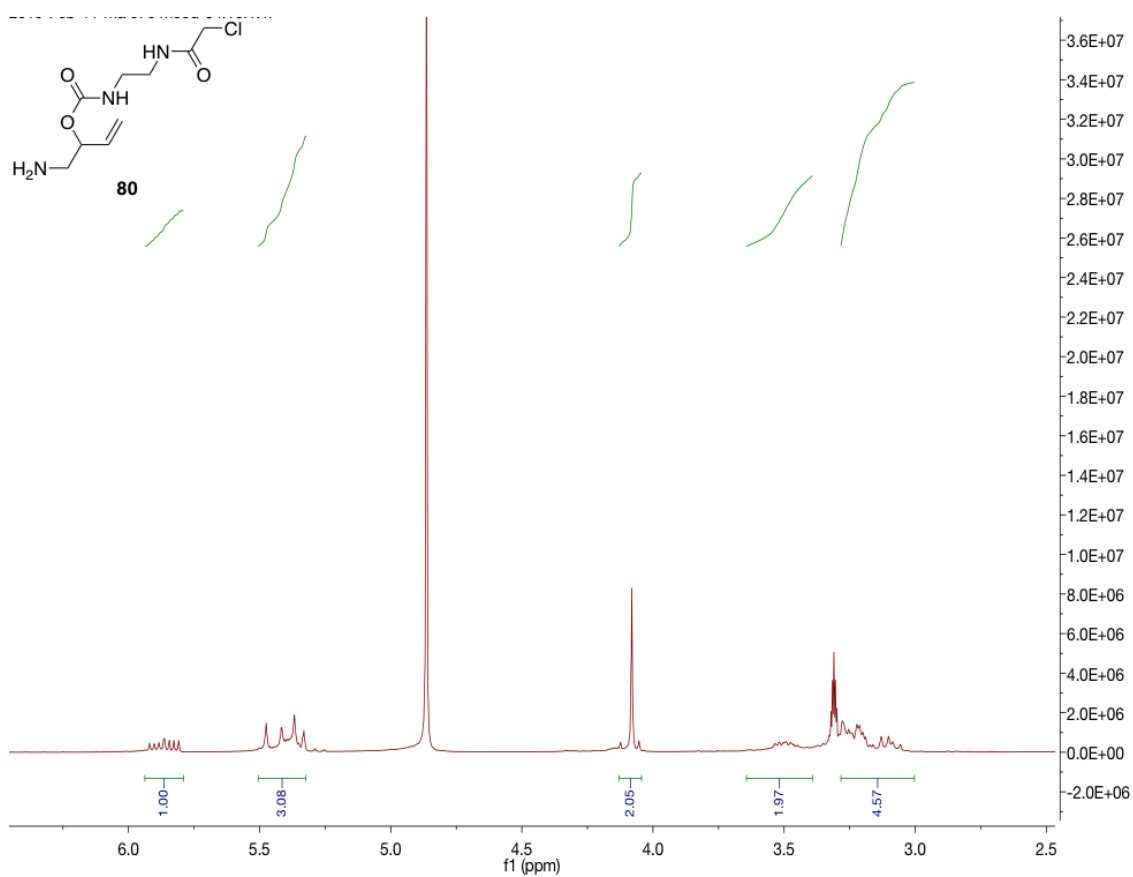
(B) ^{13}C NMR spectrum of 1-aminobut-3-en-2-yl (2-(2-chloroacetamido)ethyl)carbamate **80**.
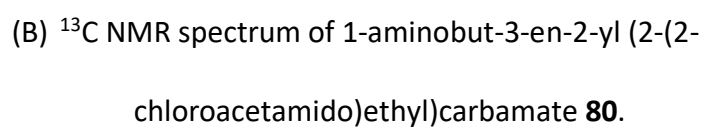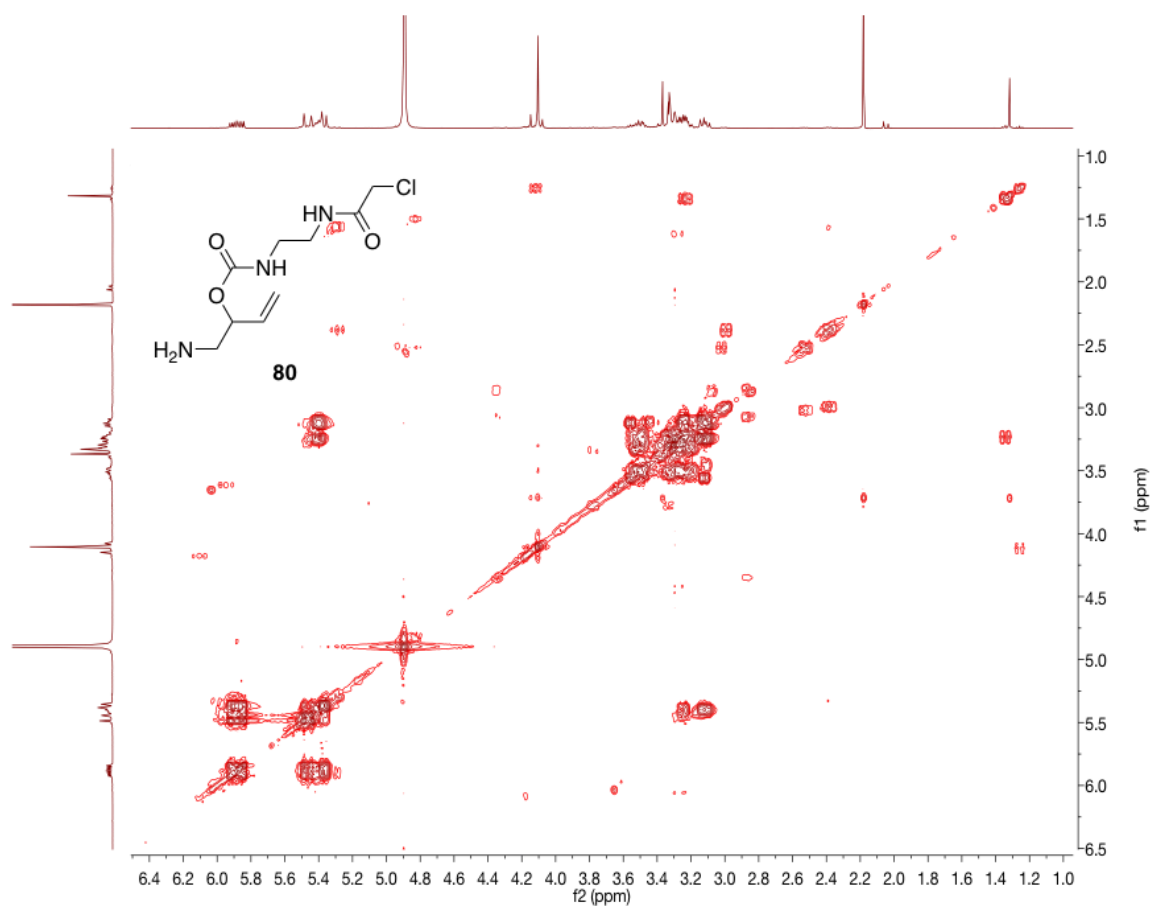
(C) COSY NMR spectrum of 1-aminobut-3-en-2-yl (2-(2-
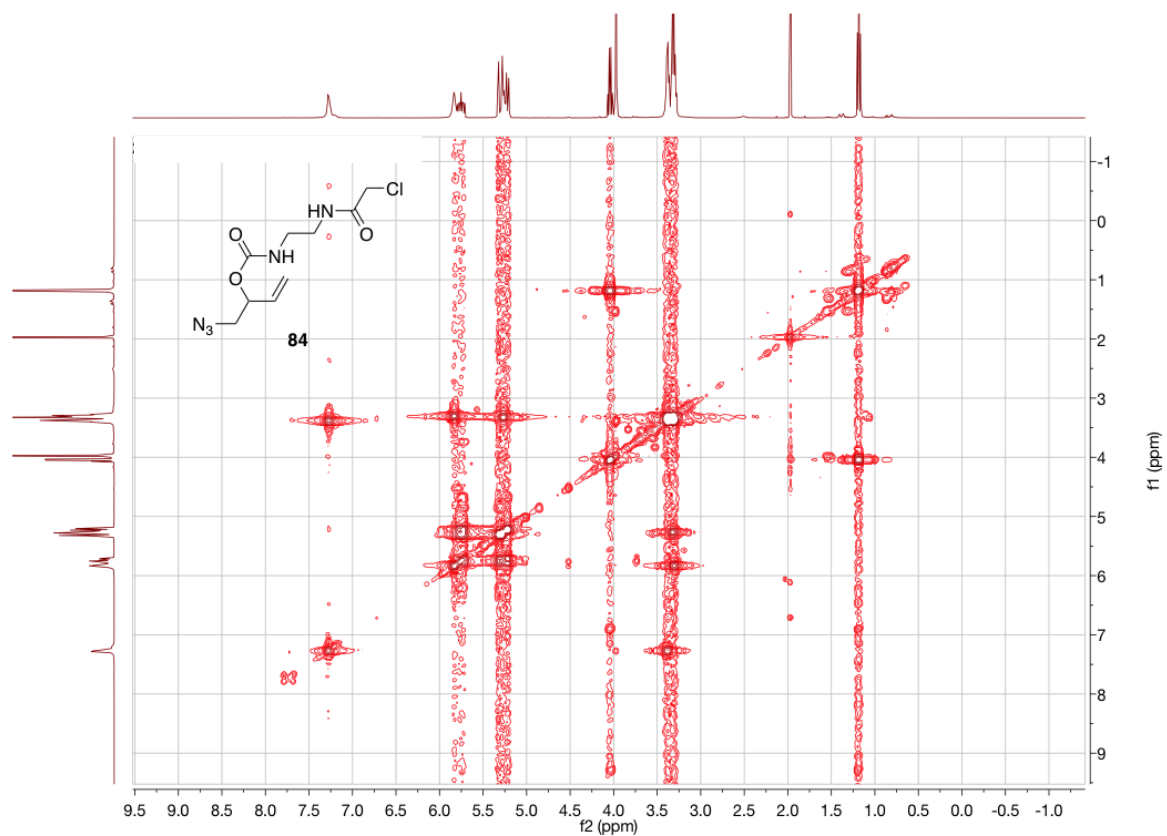
chloroacetamido)ethyl)carbamate **80**.

Figure 109: NMR spectra of 1-aminobut-3-en-2-yl (2-(2-

chloroacetamido)ethyl)carbamate **80**.
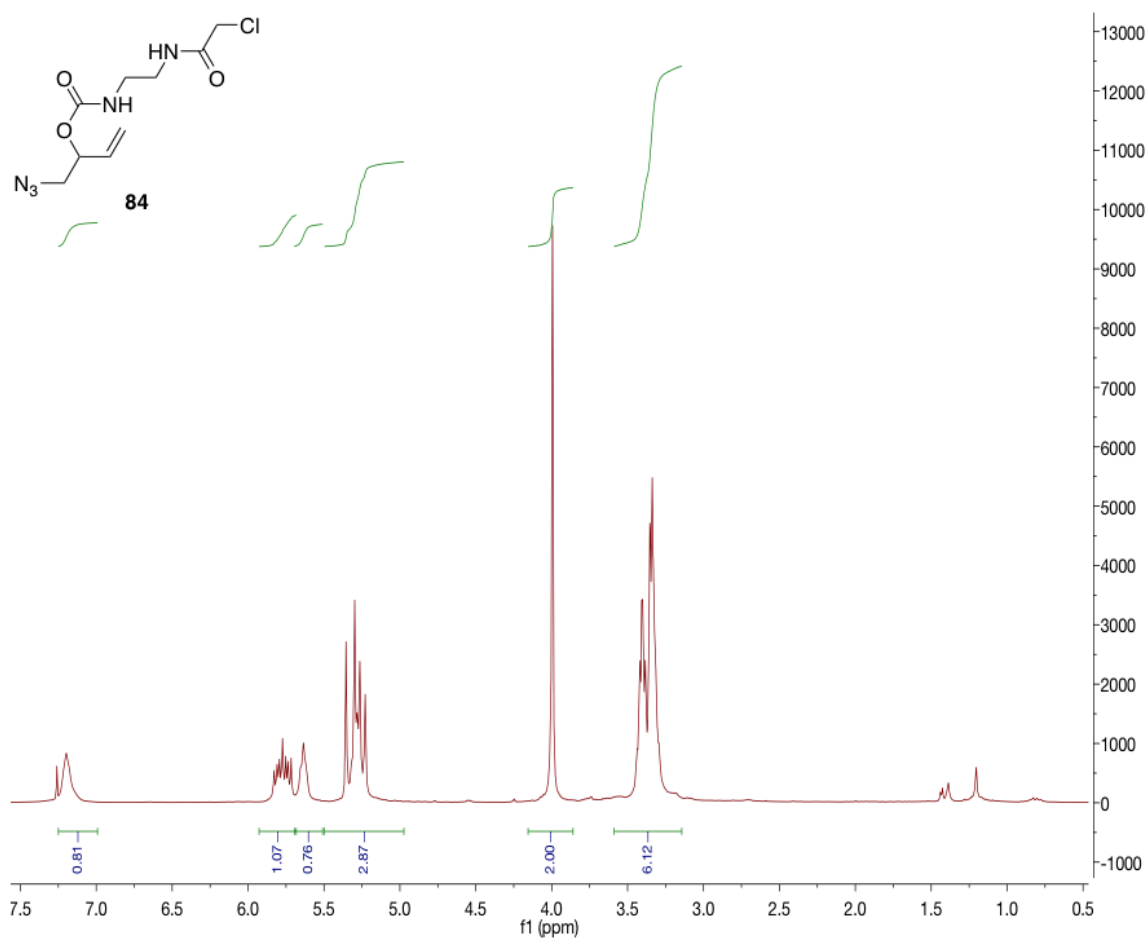
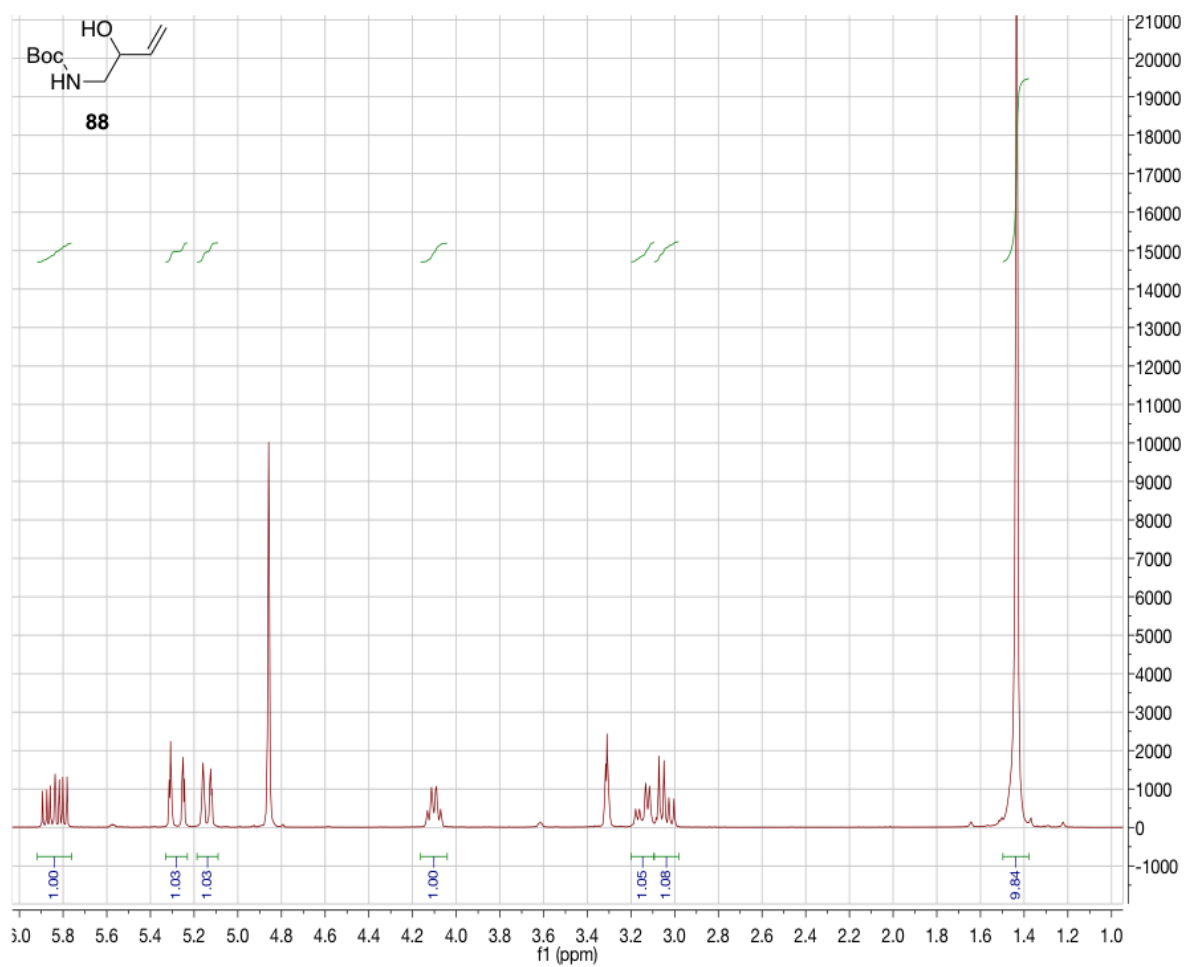(A) ¹H NMR spectrum of 1-azidobut-3-en-2-yl (2-(2-chloroacetamido)ethyl)carbamate **84**.

(B) ^{13}C NMR spectrum of 1-azidobut-3-en-2-yl (2-(2-chloroacetamido)ethyl)carbamate **84**.
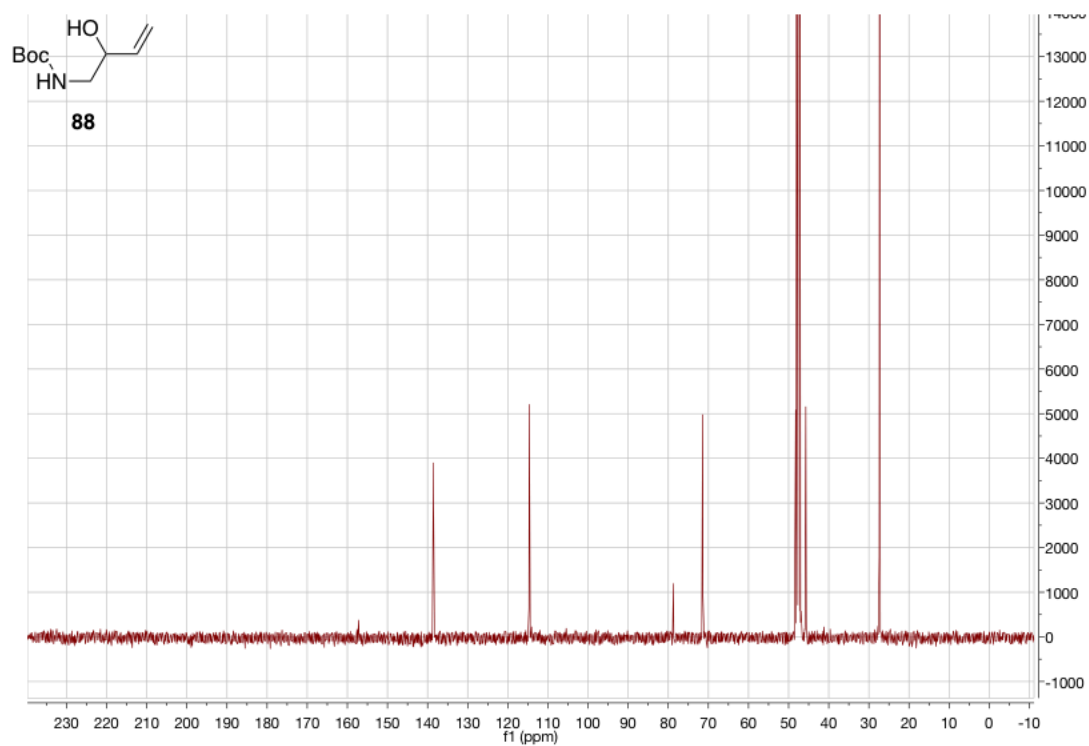
(C) COSY NMR spectrum of 1-azidobut-3-en-2-yl (2-(2-chloroacetamido)ethyl)carbamate **84**.
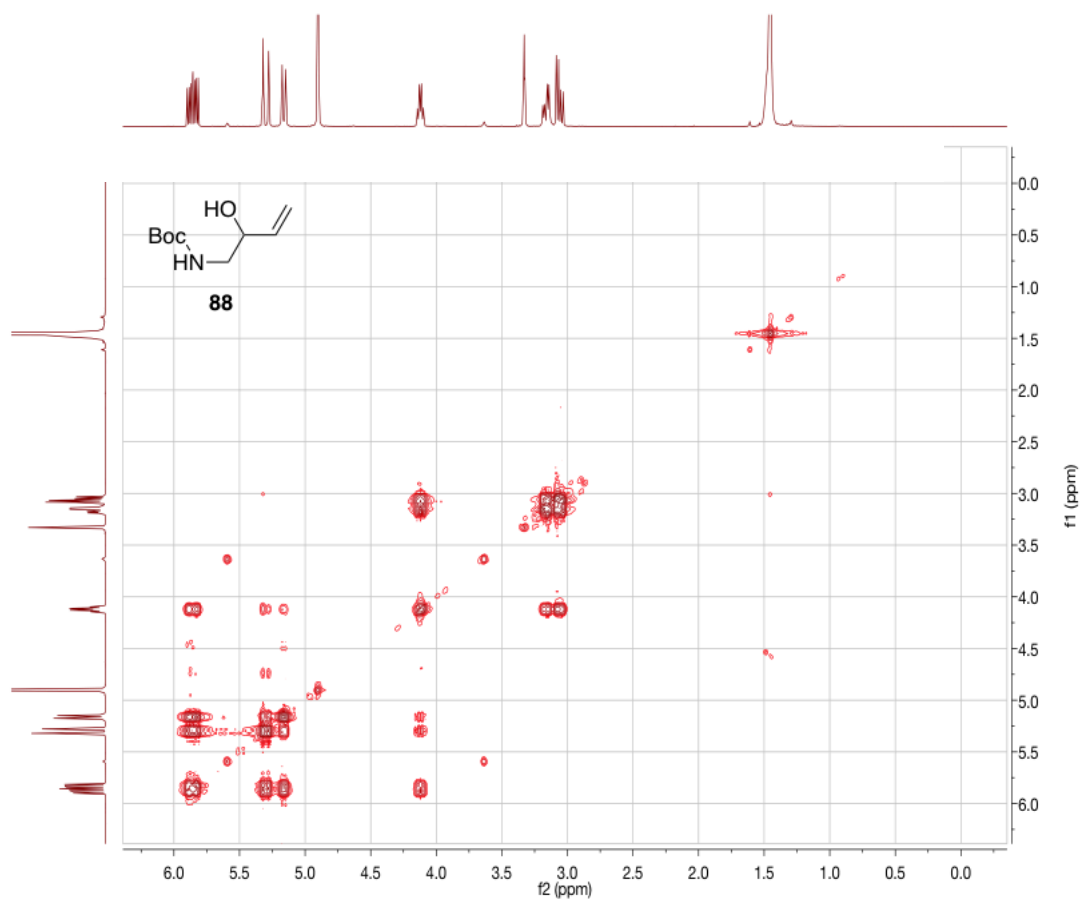
Figure 110: NMR spectra of 1-azidobut-3-en-2-yl (2-(2-chloroacetamido)ethyl)carbamate **84**.

(A) ^{1}H NMR spectrum of *tert*-butyl (2-hydroxybut-3-en-1-yl)carbamate **88**.

(B) ^{13}C NMR spectrum of *tert*-butyl (2-hydroxybut-3-en-1-yl)carbamate **88**.

(C) COSY NMR spectrum of *tert*-butyl (2-hydroxybut-3-en-1-yl)carbamate **88**.

Figure 111: NMR spectra of *tert*-butyl (2-hydroxybut-3-en-1-yl)carbamate **88**.